

BIOMECHANICS OF THE HOMININ UPPER LIMB: ENTHESEAL
DEVELOPMENT AND STONE TOOL MANUFACTURE

by

Elen Maree Feuerriegel

School of Archaeology and Anthropology

College of Arts and Social Sciences

A thesis submitted for the degree of Doctor of Philosophy

The Australian National University

July 2016

© Copyright by Elen Maree Feuerriegel 2016

All Rights Reserved

DECLARATION

This thesis is submitted to the Australian National University in fulfilment of the requirement for the degree of Doctor of Philosophy.

I declare that the work presented in this thesis is the result of my own independent research, except where otherwise acknowledged in text or in the bibliography. Chapter 8 is included as a manuscript Under Review with the *Journal of Human Evolution* in collaboration with my supervisors at the University of Sydney. Individual contributions are indicated in the signed declaration immediately preceding that chapter.

I hereby declare that this material has not been submitted either in whole or in part, for a degree at this or any other university.

Signed *Elon Feuerriegel*

ACKNOWLEDGEMENTS

I would like to thank my supervisors, Prof. Colin Groves, Assoc. Prof. Karen Ginn, and Dr. Mark Halaki for their patience and support throughout the course of my Ph.D. Completing this project would not have been as trouble-free as it was without Colin's continual encouragement, advice, and the immense well of knowledge he manages to hold in his head. I am deeply honoured to have had the opportunity to study under him. Without Karen and Mark, I would not have been able to pursue the questions asked in this thesis and I am very grateful to them for taking me on as a student, despite coming from a field wildly different from their own and a prior decision not to take on more students. I would also like to thank Dr. Darren Reed for his assistance throughout the biomechanics project and the very valuable feedback he gave on innumerable drafts of manuscripts and conference presentations.

I would like to thank Dr. Debbie Argue for her comments and feedback on early drafts of the first chapters of this thesis, as well as her ongoing support and helpful discussions. My friends Julia Filkorn, Shaun Lehman, Gavin Perry, and Ashley Jensen also deserve my praise and my thanks for every sanity-preserving conversation, morning tea, and lunch we shared, and for listening to me complain about my frustrations or talk out a problem with a sympathetic ear and a helpful suggestion.

My thanks are owed to the many institutions and curators that assisted me with getting access to fossil hominin material in both east and southern Africa: Kenya National Museum, National Museum of Ethiopia, National Museum of Tanzania, Ditsong National Museum of Natural History, and the University of Witwatersrand. My special

thanks go to Dr. Bernhard Zipfel and Ms. Stephany Potze in South Africa for their repeated assistance.

Finally, I would like to acknowledge my family. My parents, Carol and Robert, and my sister, Jehana, are the *sine qua non* for not just this project, but all my accomplishments to date. Their contributions to the success of this project are too numerous to recount, and if this is my achievement, then it is theirs also.

ABSTRACT

The close association of the advent of tool behaviours with changes to the upper limb morphology of fossil hominins has lead researchers to hypothesise that stone tool manufacture and use represents an important selective pressure for the upper limb, and yet the makers of the first stone tools, the Oldowan technological complex, remain obscure. Enteseal complexity studies have suggested that morphological changes to muscle attachment sites might be a fruitful means to investigate activity patterns in past populations. The aims of this study were therefore two-fold. First, upper limb kinetics, kinematics, and normal activation patterns of 15 shoulder and elbow muscles were investigated using electromyography (EMG) in 16 novices during Oldowan stone knapping to identify which muscles were highly and regularly recruited during this behaviour. Second, upper limb entheses in 10 species of fossil hominin were analysed using fractal analysis to score enteseal complexity. These results were then compared with the EMG analysis to determine whether patterns of enteseal complexity mirror muscle recruitment patterns in living subjects. If so, it may be possible to identify who made the first stone tools.

The results of the biomechanical study indicate that the motion of the knapping arm in stone tool manufacture is a dynamic three-dimensional flexion-extension motion. The shoulder and elbow musculature is active primarily to produce acceleration of the arm segments to generate the strike force. The segments of the upper limb moved in a coordinated proximal-to-distal sequence. This motion originated with the shoulder proximally in the up-swing or “cocking” phase and was transmitted through to the distal limb segments (the wrist and hammerstone) in the down-swing phase. The principle strike force-generating muscles of the down-swing are *Mm. latissimus dorsi*, *teres major*, and *triceps brachii*. *M. pectoralis major* works during this phase to decelerate the

rapidly extending arm to improve strike accuracy. The wrist flexor and extensor musculature, rather than producing specific motion of the wrist, appears to be highly recruited to stabilise the elbow and wrist against reactive forces from hammerstone impact.

The enthesal complexity analysis indicates that potential members of the tool-making guild include *Australopithecus africanus*, *Australopithecus anamensis*, *Paranthropus robustus*, *Homo habilis*, and *Homo ergaster*. While patterns of enthesal complexity in the fossil hominin upper limb do indeed mirror muscle recruitment patterns during stone knapping, the data is nonetheless equivocal as morphological evidence in at least two candidate species (one of which occurs 1.5 Ma prior to the first evidence of the Oldowan technological complex) suggests strong commitment to arboreality, calling into question the efficacy of enthesal complexity studies for identifying activity patterns in fossil hominins.

TABLE OF CONTENTS

DECLARATION	ii
ACKNOWLEDGEMENTS	iii
ABSTRACT	v
LIST OF TABLES	xiii
LIST OF FIGURES	xv
CHAPTER 1: INTRODUCTION	17
1.1 Identifying the Tool Makers and the Importance of Enteseal Development	17
1.2 Definitions	20
1.3 Structure	22
CHAPTER 2: ENTESIS ANATOMY AND DEVELOPMENT	24
2.1 Introduction	24
2.2 Enteses - Anatomy, Biomechanics, and Biochemistry	24
2.2.1 What are Enteses?	24
2.2.2 Classification of Enteses	26
2.2.3 Natural Variation in Enteses and the Role of Mechanical Factors	34
2.2.4 Entesis Pathologies	39
2.3 Enteseal Development in Bioarchaeology	45
2.4 Summary	55
CHAPTER 3: TOOL MANUFACTURE AND USE	56
3.1 Introduction	56

3.2 Archaeological Evidence for Tool Manufacture and Use.....	57
3.2.1 The Oldowan Technological Complex	58
3.2.2 Skill and Expertise in Oldowan Stone Knapping.....	63
3.2.3 The Tool Use of <i>Pan</i> Compared	69
3.2.4 Summary	73
3.3 The Anatomy of Tool Use.....	74
3.3.1 A Show of Hands: The Morphological Correlates of Tool Grips.....	74
3.3.2 Put a Shoulder (Or an Elbow) Into It: The Morphological Correlates of Tool Use in Upper Arm	83
3.4 Fossil Evidence for Adaptation to a Novel Behaviour.....	89
3.4.1 Early Hominins: <i>Australopithecus</i> and <i>Ardipithecus</i>	89
3.4.2 The “Robust” Australopithecines (<i>Paranthropus</i> sp.)	98
3.4.3 <i>Homo naledi</i>	102
3.4.4 <i>Homo habilis</i>	107
3.4.5 <i>Homo ergaster</i>	110
3.4.6 <i>Homo antecessor</i>	114
3.4.7 <i>Homo heidelbergensis</i>	116
3.4.8 <i>Homo neanderthalensis</i>	117
3.5 Summary	121
CHAPTER 4: BIOMECHANICS OF STONE TOOL MANUFACTURE.....	123
4.1 Introduction.....	123
4.2 Wrist and Hand Biomechanics in Oldowan Stone Knapping	123

4.3 Biomechanics of the Shoulder in Stone Knapping	128
4.4 Summary	131
CHAPTER 5: A (LESS THAN) RANDOM WALK THROUGH FRACTAL	
ANALYSIS	133
5.1 Introduction	133
5.2 Theoretical Background	134
5.2.1 Box dimension estimation method.....	139
5.3 Summary	143
CHAPTER 6: MATERIALS AND METHODS	
6.1 Materials.....	144
6.1.1 Enteseal Complexity	144
6.2 Methods.....	145
6.2.1 Electromyographic and Kinematic Data Acquisition	145
6.2.2 Confounding Factors.....	155
6.2.3 Quantitative Data Acquisition on Enthesis Complexity in Fossil Hominins	157
6.2.4 Statistical Analyses	160
CHAPTER 7: EARLY HOMININ UPPER LIMB ANATOMY	
7.1 Introduction	164
7.2 Fossil Descriptions	165
7.2.1 <i>Australopithecus africanus</i>	165
7.2.2 <i>Australopithecus afarensis</i>	174
7.2.3 <i>Australopithecus sediba</i>	187

7.2.4 <i>Australopithecus anamensis</i>	200
7.2.5 <i>Australopithecus sp.</i> and the “Robust Australopithecines”	201
7.2.6 Non- <i>ergaster/erectus</i> early <i>Homo</i>	211
7.2.7 <i>Homo ergaster</i> (“early <i>Homo erectus</i> ”).....	213
CHAPTER 8: ELECTROMYOGRAPHY, KINEMATICS, AND KINETICS OF THE UPPER LIMB DURING OLDOWAN STONE TOOL MANUFACTURE	217
Contribution of Authorship Declaration	217
Abstract	220
Introduction	221
Methods.....	222
<i>Subjects</i>	222
<i>Instrumentation</i>	223
<i>Normalisation Tests</i>	224
<i>Kinetic Measures</i>	225
<i>Kinematic Measures</i>	225
<i>Stone Material</i>	226
<i>Procedure</i>	227
<i>Statistical Analysis</i>	228
Results.....	228
<i>Motion Patterns</i>	228
<i>EMG Activity</i>	229
<i>Timing of Peak EMG Activity</i>	230

Discussion	230
Conclusion	236
Acknowledgements	237
Competing Financial Interests.....	237
References	243
CHAPTER 9: FRACTAL ANALYSIS RESULTS	248
9.1 Introduction	248
9.2 Modal Levels based on EMG Results.....	248
9.3 Results of Fractal Analysis	250
9.3.1 Entheses for Analysis.....	250
9.3.2 Generalised Linear Mixed Models Analysis of <i>D</i> -values	251
9.4 Summary	262
CHAPTER TEN: DISCUSSION	264
10.1 Candidate Tool-Makers: Comparison of the Fractal Data with the EMG Data	264
10.2 Interrogating the Candidates: The Morphology and Archaeology of Tool Use Compared	265
10.2.1 <i>Australopithecus africanus</i>	266
10.2.2 <i>Australopithecus anamensis</i>	269
10.2.3 <i>Paranthropus robustus</i>	270
10.2.4 <i>Homo habilis/Homo aff. habilis</i>	273
10.2.5 <i>Homo ergaster</i>	277
10.3 Interpretation of the Results: Limitations and Caveats	279

10.4 Summary	281
CHAPTER 11: CONCLUSION.....	282
11.1 Summary of Findings	282
11.2 Directions for Future Study.....	285
LIST OF REFERENCES	287
APPENDICES	319
APPENDIX 1: GLOSSARY OF TERMS	319
APPENDIX 2: FRACTAL DIMENSION VALUES	325
APPENDIX 3: RAW FRACTAL AXES.....	346

LIST OF TABLES

Table 1. Metabolic diseases known to affect entheses	40
Table 2. Species and specimen numbers for the fossil material included in the enthesal complexity study.	144
Table 3. Location of electrode placement for intramuscular and surface electrodes. ..	148
Table 4. Fractal dimension (<i>D</i>) values for each clavicle across each trial day for observer.	161
Table 5. Fractal dimension (<i>D</i>) values for each clavicle across each trial day for observer.	161
Table 6. Results of one-way ANOVA for intra-observer tests of <i>D</i> -values.....	162
Table 7. Results of one-way ANOVA for inter-observer tests of <i>D</i> -values.....	162
Table 8. Muscle activity in the up-swing phase of stone knapping according to modal level.	248
Table 9. Muscle activity in the down-swing phase of stone knapping according to modal level.	249
Table 10. Entheses included in fractal analysis.....	251
Table 11. Tests for fixed effects between levels of the model (Enthesis, Species, Genus).	252
Table 12. Predicted means for <i>D</i> -value and standard errors for Enthesis	253
Table 13. Predicted means and standard errors for Species.	255
Table 14. Table of predicted means and standard errors for Genus.....	255
Table 15. LSD calculations for enthesal comparisons between <i>Mm. biceps brachii</i> (1), <i>brachialis</i> (2), and <i>deltoid</i> (3).	256
Table 16. LSD calculations for species comparisons between <i>Au. afarensis</i> (1), <i>Au. africanus</i> (2), and <i>Au. anamensis</i> (3).	258
Table 17. LSD calculations for genus comparisons.	259

Table 18. Calculation of significant differences in enthesis-level PMs for <i>D</i> -values. .	260
Table 19. Calculation of significant differences in species-level PMs for <i>D</i> -values. ..	261
Table 20. Calculation of significant differences in species-level PMs for <i>D</i> -values. ..	262
Table 21. Entheses and muscles that exhibit high fractal complexity and muscle recruitment values.	264

LIST OF FIGURES

Figure 1. Indirect fibrous enthesis and its interface.	27
Figure 2. Histological section of a normal fibrocartilaginous bone-tendon interface (human supraspinatus insertion)	30
Figure 3. Normal development of the M. brachialis direct fibrous insertion on the anteroproximal diaphysis of the ulna, inferior to the coronoid process.	35
Figure 4. Superior view of the proximal olecranon process of the ulna; the bottom of the image is anterior	36
Figure 5. Healthy entheses (a, c) and enthesopathies (b, d–f) on the proximal humerus and radius.	42
Figure 6. Proliferative woven bone formation occluding many of the entheses for the posterior femoral musculature in a chimpanzee (<i>Pan troglodytes schweinfurthii</i>), sex uncertain.	43
Figure 7. Radiograph of coracoacromial ligament ossification in a 68-year-old woman, scapular view.	44
Figure 8. Superior view of a left scapula exhibiting lytic lesions (black arrow) and osteoblastic activity (white arrow) at the junction of the acromion and suprascapular fossa (origin of the M. supraspinatus) in a probable male individual in his early 40's from the post-Medieval Cross Bones burial site in Southwark, England	45
Figure 9. Oldowan stone tools from East Gona early Pleistocene (2.5-2.6 million years) assemblages EG10 and EG12	59
Figure 10. Fracture features of a flake produced by conchoidal fracture. Illustration reproduced with permission of the Trustees of the British Museum.	65
Figure 11. Human hand grips. (a) The 'power' (squeeze) grip of a cylindrical object - in this case a torch. (b) Two versions of the 'precision' (pinch) grip.	77

Figure 12. Proximal view of a right modern human humerus with ends superimposed.	85
Figure 13. Range of motion in hominin shoulders as dictated by scapula position and degree of humeral torsion.....	88
Figure 14. The Mandelbrot set	135
Figure 15. Electrode and wireless inertial sensor placement	151
Figure 16. Example of a disigitised enthesal “curve”	160

CHAPTER 1: INTRODUCTION

1.1 Identifying the Tool Makers and the Importance of Enteseal Development

The variety and complexity with which modern humans use and make tools makes them unique amongst life on Earth and the emergence of these behaviours represents one of the most significant turning points in human evolutionary history. The capacity for this behaviour is tied closely to the morphology of the shoulder and hand of early hominins (Churchill, 2001, Churchill and Trinkaus, 1990, Marzke and Shackley, 1986, Susman, 1998, Larson, 2007, Larson, 2013) and correspondingly a great deal of time and scholarly effort has been dedicated to identifying based on these features which members of the human lineage produced the first stone tools, the Oldowan technological complex (Semaw et al., 1997). The shoulder is one of the most extensively studied regions in comparative anatomy, yet the exact biomechanical behaviour of the shoulder girdle and, to a lesser extent, elbow during stone knapping remains largely a grey area in evolutionary studies. Significant unanswered questions are:

- What is the role of the shoulder and upper arm muscles in stone tool behaviours?
- What are the skeletal markers of stone tool manufacture at the shoulder girdle, if any?
- Can these markers be readily identified in fossil hominins?
- What does this reveal about the functional morphology of the shoulder in fossil hominins?

The purpose of this study is to identify the shoulder and elbow muscles strongly and repeatedly recruited during stone knapping in order to test whether patterns of development at muscle and ligament attachment sites on bone (also called entheses, singular: enthesis) may be fruitful predictors of tool manufacture behaviours in fossil hominins.

The reconstruction of past behaviour forms an important part of research on archaeological populations (Kennedy, 1989, Larsen, 1997, Larsen, 2000). These studies seek to reconstruct behaviour based on analyses of morphological changes in entheses as these changes are believed to reflect *in vivo* muscular activity (Chapman, 1997, Dutour, 1986, Eshed et al., 2004, Hawkey and Merbs, 1995, Kennedy, 1989, Kennedy, 1998, Lai and Lovell, 1992, Mariotti et al., 2004, Mariotti et al., 2007, Molnar, 2006, Robb, 1994, Steen and Lane, 1998). Changes in enthesis morphology that have been proposed to reflect habitual behaviours that are mechanically demanding and/or repetitive include: stress or fatigue fractures, osteoarthritic/degenerative joint lesions, and postural stress indicators such as squatting and kneeling accessory facets (Bouille, 2001, Capasso et al., 1999, Kennedy, 1989, Larsen, 1997, Ubelaker, 1979).

While the bulk of this research has focused on relatively modern archaeological populations, enthesal development in fossil hominin assemblages has only been studied minimally and in some anatomical regions more than others. There have been many extensive studies of the muscular and bony architecture of the hominoid hand and wrist as it relates to tool use (Almécija et al., 2010, Diogo et al., 2012, Leakey et al., 1964b, Lewis, 1977, Marzke, 1997, Marzke, 2005, Marzke and Marzke, 1987, Marzke and Marzke, 2000, Marzke and Shackley, 1986, Marzke et al., 1998, Marzke et al., 1992, Napier, 1962b, Skinner et al., 2015, Susman, 1988a, Susman, 1991, Susman, 1994, Susman, 1998, Tocheri et al., 2008, Tocheri et al., 2005, Toth and Schick, 2009).

Most either examine the lower arm morphology of a particular species only (whether it be extant or extinct) or compare and contrast the arm of modern humans with extant primates and a few with fossil hominin material. Some functional analyses of hominin hand morphology focused on manipulation of modern human tools or unspecified objects of varying shape (Lewis, 1977, Wolfe et al., 2006), while others investigated the morphological correlates of particular grips during Palaeolithic stone tool use (Marzke and Shackley, 1986). Other investigations utilised a broader approach that attempted to discern adaptive changes to hand morphology across different stages in the evolution of tool behaviour (i.e. stone and non-stone related) in hominins, with an emphasis on the importance of both the precision and power grips (Marzke, 1997, Marzke, 2005, Marzke and Marzke, 1987, Marzke and Marzke, 2000, Marzke et al., 1992).

The mechanical context of the hominin shoulder has been studied in less detail and the exact muscular recruitment patterns of the shoulder during stone knapping remain unknown. Given that strongly recruiting muscles generates bony changes at the enthesis and might therefore provide an indicator of the activity patterns (Benjamin et al., 2002, Drapeau, 2008b) such information would be invaluable for investigating the activity patterns of our fossil ancestors. In the absence of clear archaeological associations between fossil remains and Oldowan tools (Susman, 1991, Napier, 1962b), it would potentially enable us to answer one of the most elusive questions in palaeoanthropology: who made the Oldowan stone tools?

As there is presently no study detailing either the specific muscular recruitment patterns of the human shoulder during stone knapping behaviours, the aim of this dissertation will be to conduct an electromyographic (EMG) and kinematic study of the shoulder and upper arm in Oldowan stone knapping. By using these techniques to look at the biomechanical behaviour of this anatomical region in stone knapping, I hope to create a

clearer picture of which muscles are highly and repetitively recruited at hammer stone strike and flake removal. This dissertation investigates the hominin shoulder through the lenses of comparative anatomy and functional morphology, and presents a novel technique for the quantification of enthesal development in skeletal material. These data will then be used to explore whether these skeletal features may be used to identify those fossil hominins likely to have created Oldowan stone tools.

1.2 Definitions

The study of activity-related enthesal changes is a field of research that suffers from a dearth of consensus regarding key terminology. A review of the literature reveals a lack of consensus on certain important terminology and as such I define the following terms which will be discussed in greater detail in the following chapters. A more general glossary of anatomical terms is also included at the end of this dissertation (Appendix 1).

Enthesal development A spectrum of normal (i.e. non-pathological) osseous changes at the site of attachment for a muscle or ligament (cf. Hawkey and Merbs, 1995). They are the physiological responses of the bone to mechanical loading and the transmission of forces during movement by the muscle or ligament which in turn engender a bony response at the enthesis. The extent of this response (i.e. degree of development) varies between individuals resulting in different morphologies that occur across a spectrum of expression. This is unlike enthesopathies which are either present or absent. Used synonymously in this dissertation with “enthesal complexity”.

Entheseal robusticity	“Entheseal robusticity” is occasionally and confusingly used in the bioarchaeological literature to denote enthesal <i>rugosity</i> or development. Robusticity in biology generally or morphology specifically refers to a pattern of generalised skeletal strength relative to a mechanically relevant measure of body size.
Enthesis	The site of attachment, either origin or insertion, between muscle, tendon, or ligament and bone (pl. entheses). Entheses can be recognised on skeletal elements as irregularities in the bone surface ranging from rugosity to marked ridges or grooves. They may also appear completely smooth and indistinguishable from the surrounding non-insertion bone depending on the degree of development. There are two types of entheses: fibrous and fibrocartilaginous.
Enthesopathy	Any pathological change/s to the appearance or biochemistry of an entheses arising through the work of an abnormal condition. The aetiology of these changes may include trauma, hormonal, degenerative/age-related, genetic, disease, or dietary factors. This is the most common term in the clinical literature used for the description of these changes. Osseous markers of enthesopathy include enthesophytes or eroded areas and are characterised as a binary state. That is, unlike enthesal development/robusticity, enthesopathies are either present or absent and do not occur across a continuum of development (cf. Mariotti et al., 2007).

Enthesophyte	Pathological bony projections at an enthesis. They are differentiated from osteophytes, which are abnormal bony projections in joint spaces.
MSM	Musculoskeletal stress markers. This term appears in the bioarchaeological literature to describe activity-related changes to entheses in archaeological populations.

1.3 Structure

In order to explore the questions outlined in the introduction, this dissertation begins with a review of the theoretical and methodological approaches to studying enthesal development in bioarchaeology, as well as enthesis anatomy and histology as it relates to enthesal development (Chapter 2). This is followed by a discussion of the archaeological evidence for the first tool use, the links between particular morphological features and tool behaviours (Chapter 3), and the theoretical aspects of the two main methodologies used in this project, electromyography (EMG) and fractal analysis (Chapters 4 and 5 respectively). The materials and methods of the project are discussed in Chapter 6. The fossil hominin material is described, paying special attention to the shape and location of entheses, in Chapter 7.

In the second section I conduct the EMG, kinetic, and kinematic study (Chapter 8), as well as perform the fractal analyses of the enthesal curves from the fossil material to determine the degree of complexity/rugosity for each enthesis being examined (as determined by the *D*-value – see Chapter 5). The results of these investigations are then statistically analysed and compared in Chapter 9. The results of this study and their utility for determining tool use/manufacture behaviours in fossil hominins are discussed in relation to the fossil and archaeological records and the literature in Chapter 10. The

final chapter summarises the findings, along with the limitations of this study and suggestions for future research.

CHAPTER 2: ENTESIS ANATOMY AND DEVELOPMENT

2.1 Introduction

This chapter is the first part in a three-part critical review of the literature spanning five major topics. Specifically, this chapter concerns the anatomy, biomechanics, and biochemistry of entheses as well as the uses of entheses in bioarchaeology to infer behaviour of past populations. I will critically evaluate the evidence for using enthesal development as a tool for identifying and investigating behaviour in past populations, developing and providing justification for certain key terminology, with a view to determining how enthesal development can be better understood in relation to activity.

2.2 Entheses - Anatomy, Biomechanics, and Biochemistry

In order to understand their role in activity, it is first important to understand the anatomical and histological context of entheses. Entheses are clinically significant for a number of reasons, most notably because they are a common source of overuse injuries, they are targeted by seronegative spondyloarthropathies (a class of degenerative joint diseases that target the vertebral column), and surgical reattachment requires reconstitution of these areas. The following sections will place entheses within the context of the musculoskeletal system and review their anatomy and mechanisms for functional adaptation.

2.2.1 What are Entheses?

Entheses are the interface between soft tissues and the skeleton; they are the sites of insertion for tendons, ligaments, and fasciae to bone. Their primary function is to dynamically distribute forces applied to the skeleton in order to enable skeletal loading and execute movements while concomitantly maintaining joint integrity. Entheses must

also be able to limit the possibility of damage in the face of substantial mechanical loading, primarily by transferring the forces smoothly between the soft and hard tissue interface (Benjamin et al., 2006). They are therefore thought to represent the regions of the skeleton most likely to undergo remodelling triggered by muscular action (Judex and Carlson, 2009), as the interface is more likely to experience greater stress concentrations than the tendon or ligament itself. Nevertheless, researchers have shown that, in some animal test subjects, most – but not all – of the force generated by a muscle is transferred to the skeleton via the tendon. Myofascial continuity is a concept that describes the close association of some muscles, suggesting that force can be transmitted through fascial connections between closely associated muscles (Myers, 2001). Rijkelijhuizen et al. (2005) have demonstrated, in line with myofascial continuity, that force can be transferred to the skeleton even when the tendon is severed, providing that the epimysium (the fibrous sheath surrounding the muscle) and epitendinous tissue remain intact. While such connects are observed in the lower limb, they are not observed in the upper limb where musculoskeletal connections are separate and tendinous, which in turn facilitates the intricate and discrete nature of movements of the upper limb (Jones, 1982).

There is a mechanical mismatch at the tendon-bone interface arising from the attachment of flexible, compliant tissue (tendon/ligament) to a rigid scaffold (bone) and this presents a fundamental engineering challenge for diffusing potentially injurious biomechanical stress at the enthesis. The biological solution (and similarly one used commonly by engineers) has been to develop an enthesis that is functionally graded to cope with both the macroscopic and microscopic mismatch of materials and minimise the consequent stress concentrations. It is these stress concentrations that make the enthesis vulnerable to injury, either through overuse or as acute damage. Mechanical load influencing the structure of musculoskeletal tissue is a well-recognised

phenomenon (Benjamin et al., 2002, Benjamin and McGonagle, 2009, Benjamin et al., 2006) and it is this phenomenon that forms the basis of the ‘form follows function’ principle underpinning Wolff’s law (more on this later).

2.2.2 Classification of Entheses

The first studies on enthesis histology were conducted by German anatomists. Schneider (1956) and Dolgo-Saburoff (1929) provided amongst the first useful models for epiphyseal tendon entheses, defining four zones for these features: 1) tendon; 2) fibrocartilage; 3) calcified fibrocartilage; 4) bone. Biermann (1957) and Knese and Biermann (1958) went on further to identify three types of muscle attachments.

1. Muscles attached by tendons to cartilaginous outgrowths such as the attachment of the iliopsoas to the lesser trochanter of the femur. These are equivalent to the epiphyseal tendons of Schneider (1956).
2. Diaphyseal attachments which fall into two types:
 - a. Fleshy attachments to periosteum such as the origin of the supra- or infraspinatus, and;
 - b. Those with circumscribed tendinous attachments to bony crests, ridges, and prominences, such as the humeral insertion of the deltoid.

Cartilage may be present at the second sub-type but not as much as seen in tendons at cartilaginous outgrowths.

More recently, Benjamin and colleagues (Benjamin et al., 2002, Benjamin and McGonagle, 2009, Benjamin and Ralphs, 1998, Benjamin et al., 2006) have made additional efforts in the classification of entheses and their model has been widely adopted in the literature (e.g. Doschak and Zernicke, 2005, Zumwalt, 2005, Thomopoulos et al., 2010, Genin et al., 2009, Zumwalt, 2006, Lu and Thomopoulos,

2013). They recognised two categories of attachment site based on the structure and type of tissue present: fibrous and fibrocartilaginous entheses. Fibrous entheses are characterised by the tendon or ligament attaching either directly to the bone or indirectly via the periosteum, as well as the presence of Sharpey's fibres (perforating mineral fibres responsible for anchoring tendons, ligaments, and periosteum to bone)¹. Indirect attachments (Fig. 1) have dense fibrous tissue connecting the tendon/ligament to the periosteum which in turn attaches to the bone.

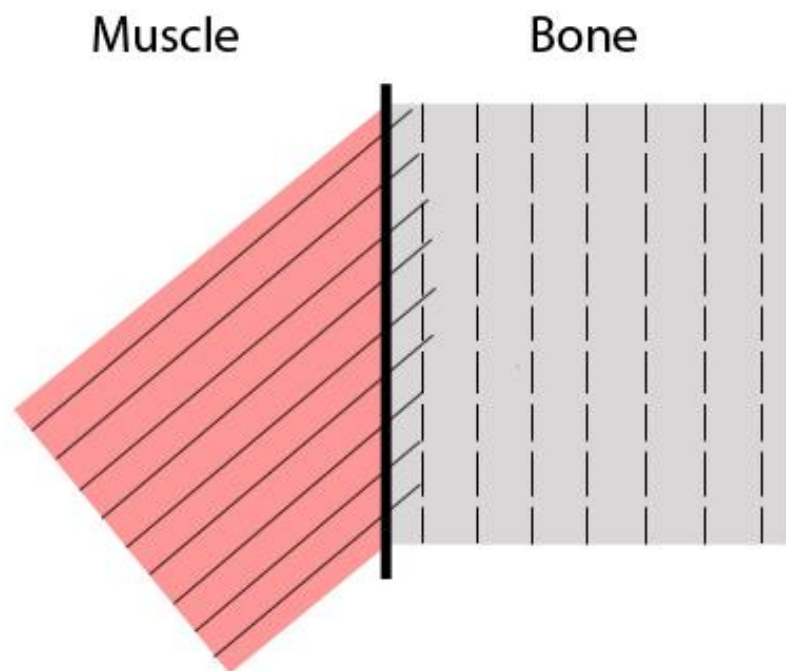


Figure 1. Indirect fibrous enthesis and its interface. Muscle joins directly to the bone by collagen fibres (the unbroken diagonal lines) inserting into the periosteum layer of the bone (the solid vertical line between bone and muscle). Modified from Paxton et al. (2012).

¹ Sharpey's fibres are a source of some debate in the literature. In the original publication, Sharpey (1867) was unclear what specifically he denoted by referring to "fibres", including whether they are present at fibrocartilaginous entheses or not, and correspondingly there has been considerable discussion in the literature on the topic without much clarification. Benjamin et al. (2002) recommend that Sharpey's fibres should be restricted to describing fibrous entheses.

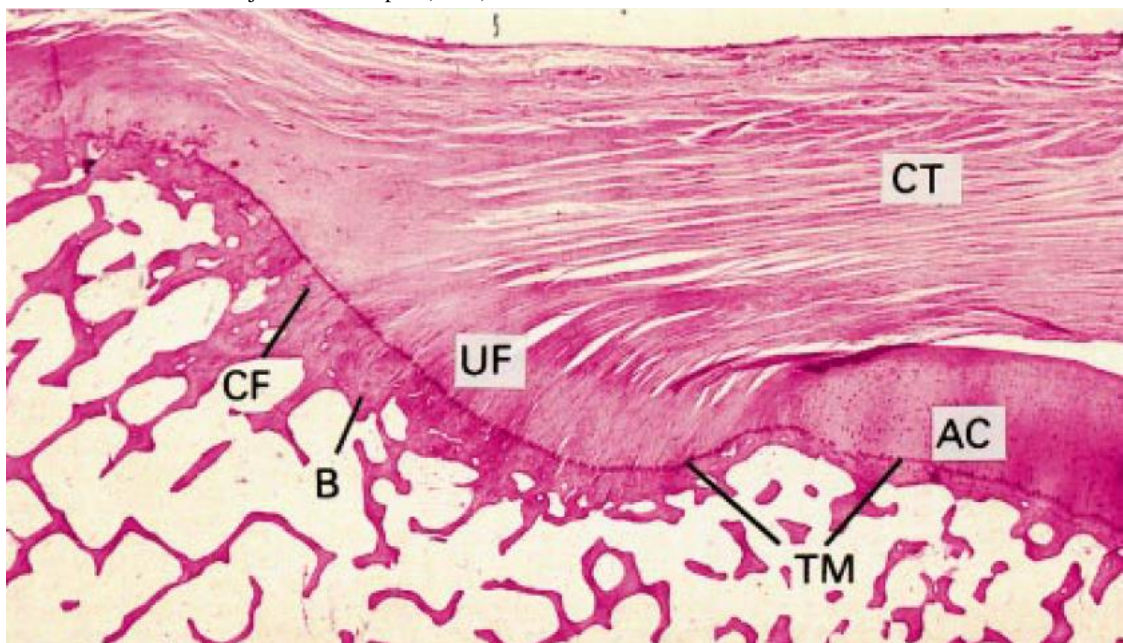
This is contra the terminology proposed previously by Woo et al. (1988) who used “indirect attachments” to refer to both fibrous and fibrocartilaginous entheses. There is no evidence of fibrocartilaginous differentiation in either case. Fibrous entheses are generally broad insertions that disperse forces over large areas and include the humeral insertion of the deltoid and the insertion of the medial collateral ligament on the tibia. In fibrocartilaginous entheses, on the other hand, chondrogenesis has occurred and the tissue is thus able to be divided into four zones:

1. Tendon; zone is populated by fibroblasts and Type I collagen fibres
2. Fibrocartilage; zone is populated by fibrochondrocytes and is composed primarily of Types I, II, and III collagen as well as proteoglycan aggrecan.
3. Third zone is also populated by fibrochondrocytes and mineralised fibrocartilage. Collagen Type II is the most common fibre though Type X collagen also occurs in significant concentrations in addition to aggrecan.
4. Bone; populated by osteoblasts and osteoclasts, comprised predominantly of Type I collagen.

The different zones of tissue and their continuity with one another can make defining the limits of fibrocartilaginous entheses difficult. Similarly, the bone of an enthesis grades imperceptibly with the bone of the rest of the skeleton. The periosteum is absent in fibrocartilaginous entheses and as such the attachment of tendon/ligament to the bone is direct without the membranous interface (Fig. 2). They tend to be characterised by short “footprints” and leave a characteristic marking on dry bone which Benjamin et al. (1986) described as a fibrocartilaginous plug. The surface of these entheses are smoother than the surrounding non-enthesis bone, though not necessarily flat, and lack vascular foramina. The colour and texture of these sites more closely resemble articular surfaces than areas of bone covered by periosteum.

Benjamin et al. (1986) suggested that this occurs for two reasons. First, that the zone of fibrocartilage at the enthesis is associated with a tidemark (or the junction between soft and hard tissue) that is smoother than the underlying osteochondral junction. Second, the tidemark separates uncalcified and calcified fibrocartilage regardless of the proximity of the fibrocartilage to the bone surface. While it is not certain whether the tissues are separated through the tidemark or immediately above it, or whether there are multiple tidemarks so closely spaced that they give the appearance of a singular tidemark, the regularity of the tidemark is what lends the enthesis its smooth appearance on the dry bone. This is further aided by the separation of the uncalcified area of the articular cartilage from the deeper stratum of calcified fibrocartilage at the tidemark. That calcified cartilage persists in dry bones to create a hard layer capable of smoothing out the rougher underlying lamellar bone has also been observed by other researchers (Haines and Mohiuddin, 1968).

Figure 2. Histological section of a normal fibrocartilaginous bone-tendon interface (human supraspinatus insertion). The tendon transitions through fibrocartilage regions before reaching the bone: connective tissue (CT), uncalcified fibrocartilage (UF), calcified fibrocartilage (CF), and bone (B). Bisecting the calcified and uncalcified fibrocartilage zones is the tidemark (TM) which in this case is continuous with articular cartilage (AC) adjacent on the humeral head. Modified from Benjamin and Ralphs (1998).



Fleshy attachments are smooth, featureless, and generally difficult to distinguish from areas of bone only overlaid by periosteum. In contrast to this, tendinous, aponeurotic, fibrous septa attachments have distinct markings in the form of tubercles, ridges, pits, or fossae. When fibrocartilage is present in high concentrations at the latter attachments,

the entheses are smooth and clearly differentiated from the surrounding non-articular bone. If there is very little fibrocartilage, the markings are rough and similar in appearance and texture to lamellar bone (Benjamin et al., 1986).

Benjamin and colleagues' classification differs from the classification of Biermann (1957) and Knese and Biermann (1958) above, who based their classification of entheses on their location, i.e. whether the enthesis occurs at the epiphyses of long bones (chondral-apophyseal) or on the diaphysis (periosteal-diaphyseal). These are fibrocartilaginous and fibrous entheses, respectively. The advantage of the Benjamin model compared to others is that it acknowledges the functional grading of the tissues at entheses and their role in the biomechanics of stress dispersion at the attachment site. The fibrous and fibrocartilaginous classification of Benjamin and Ralphs (1995) and Benjamin and McGonagle (2001) has been criticised by Hems and Tillmann (2000) as being too simplistic to capture the range of variation in enthesis morphology that they have observed; they suggested instead distinguishing between periosteal, bony, and fibrocartilaginous attachments based on their study revealing variation in human masticatory muscle attachments (Hems and Tillmann, 2000). These authors assumed that tissue composition in limb entheses is uniform and therefore the regional variation in the concentration of fibrous versus fibrocartilaginous tissues across the entheses of the masticatory muscles is indicative of a greater diversity of enthesis types in general. While there is almost certainly more regional variation within the chewing muscles than in tendon attachments in the appendicular skeleton, limb tendon entheses also vary regionally in their composition with fibrocartilaginous entheses consisting of one part that is fibrocartilaginous and another (usually the most superficial/distal part) being largely fibrous (Benjamin et al., 2002). The 'bony' and 'periosteal' subdivisions recognised in the Hems and Tillmann (2000) classification could further be considered

subsets of the fibrous enthesis type defined by Benjamin and Ralphs (1995) and Benjamin and McGonagle (2001, 2009).

While there are recognisable zones, the transitions between the biomechanical, compositional, and structural properties are continuous, which has the effect of reducing stress at the tendon-bone interface. Mechanical models of enthesis microstructure have shown that collagen fibres are orientated in such a way as to reduce stress concentrations across the enthesis and to protect the outward splay of the enthesis from the strongest stress concentrations. In one study of the femoral insertion for the medial collateral ligament, it was shown that the orientation of the collagen fibres aligns with the direction of the highest tensile stresses (Matyas et al., 1995). In another, cell shape was found to correlate with mechanical stresses (Genin et al., 2009). This suggests a direct relationship between cellular activity and the distribution of stress across the enthesis. In yet another study, collagen fibre orientation and mineral content was demonstrated to grade the mechanical properties of the tendon-bone transition so as to functionally grade the tissue. Increasing mineral content of the collagen fibres increased the rigidity of the fibres which was further reinforced by altering their orientation, effectively varying the stiffness of the tissue across the length and breadth of the bone-tendon insertion. These results align with what has been described in other experimental studies regarding how functional gradation of the tissue is achieved in the enthesis (Stouffer et al., 1985, Thomopoulos et al., 2003).

Animal models have shown that the functional grading of the enthesis only develops post-natally (Thomopoulos et al., 2007, Galatz et al., 2007, Fujioka et al., 1997, Bland and Ashhurst, 1997). Using in situ hybridisation, mouse studies studying Type I, II, and X collagen fibres have shown that at 15.5 days post-conception, the rotator cuff tendon precursors were juxtaposed to the humeral head and that it wasn't until after birth that a

transition zone between the developing tendon and bone developed. The only collagen fibre consistently expressed until 14 days postnatal on the tendon side of the insertion was Type I, while Type II was consistently expressed on the humeral side. The collagen fibre types effectively mirrored one another during these early periods of development. By 14 days, collagen Type X was expressed in association with hypertrophic chondrocytes. As would be predicted, collagen Type I (the main type of collagen found in mature bone) was expressed in greater concentrations as the humeral head began to mature and mineralise. By 21 days post-natal, a fibrocartilaginous insertion had developed which corresponded in timing to the complete mineralisation of the cartilaginous humeral head. These results coincide with results found for the Achilles tendon in humans (Shaw et al., 2008) and rats (Fujioka et al., 1997).

Parathyroid hormone-related protein (PTHrP) can be found in the insertion sites of both tendons and ligaments where it plays an important role in maintaining the population of cells that are available for growth and providing protection against untimely or inappropriate mineralisation (Chen et al., 2006). It is found in proliferating chondrocytes in the growth plate as well as being an integral part of the negative feedback loop that prevents their maturation into hypertrophic chondrocytes and eventually mature bone. PTHrP plays a similar role in providing a barrier between mineralised and unmineralised tissues at the tendon to bone interface. PTHrP also works in conjunction other factors such as IHH (Indian Hedgehog homologue, a protein coded by the IHH gene), both of them occurring in the developing tendon insertion site in the first 14-21 days postnatal, corresponding with the mineralisation of the humeral head. IHH is secreted by proliferative chondrocytes and binds to cell membrane receptor Patched 1, leading transmembrane protein smoothed to accumulate, and eventually to the production of PTHrP. These factors are also particularly sensitive to mechanical

loading and their expression has been found to decrease in the absence of loading (Chen et al., 2007).

2.2.3 Natural Variation in Enteses and the Role of Mechanical Factors

In enteses, much like any other part of skeleton, there is a natural range of variation in how and the degree to which they are expressed and these are related to factors such as age and body size (al-Oumaoui et al., 2004, Alves-Cardoso and Henderson, 2010, Henderson et al., 2012, Lieverse et al., 2009, Mariotti et al., 2007, Milella et al., 2012, Niinimäki, 2011, Stirland, 1998, Weiss, 2003, Weiss, 2004, Weiss, 2007, Wilczak, 1998, Churchill and Morris, 1998). Enteseal complexity has been demonstrated to increase with age through the cumulative effects of life-long activity through to the age of 40-50 years, after which the changes plateau and stabilise (Mays, 2000). Body size also factors into the expression of enteses (Weiss, 2003, 2004, 2007), as does muscle insertion size (Churchill and Morris, 1998). In non-human primate, entesis size has also been found to correlate with body size (Zumwalt et al., 2000). Other studies have argued that enteseal development can be sexually dimorphic (Churchill and Morris, 1998, Weiss, 2003, Weiss, 2004, Weiss, 2007, Weiss et al., 2012, Wilczak, 1998) and that these sex-related differences may be attributed to greater weight and overall size in males, or the sexual division of labour (Robb, 1998, Weiss, 2007, Weiss et al., 2012). These issues will be discussed in greater detail in Section 2.3.

Generally speaking, enteses are readily observable on dry bone, and the entesis type dictates the type of expression a healthy entesis takes (that is, how it looks on the bone). Variation in the degree of expression – how robust or complex the entesis appears – is thought to represent normal adaptation of the entesis to the distribution of stressors at the soft and hard tissue interface that occurs during habitual loading (Hawkey and Merbs, 1995, Mariotti et al., 2004). For instance, healthy direct fibrous

attachments are present on the diaphyses of long bones and are generally characterised by roughened sections of bone at the point of attachment. This can also include ridges (Fig. 3).



Figure 3. Normal development of the M. brachialis direct fibrous insertion on the anteroproximal diaphysis of the ulna, inferior to the coronoid process. This ulna is in the collection of the ANU biological anthropology labs. Photo by E. Feuerriegel.

Healthy indirect fibrous entheses, on the other hand, are smoother in appearance and poorly circumscribed as the presence of the periosteum acts as an interface between the surface of the bone and the muscle (Hems and Tillmann, 2000). Fibrocartilagenous entheses differ again in having well-delineated margins and an inner section that is smooth, devoid of vascular foramina, and somewhat depressed (Fig. 4). In fibrocartilagenous entheses, the margins are subject to greater cyclical forces than the inner sections, as the margins are where collagen fibres integrate with the periosteum (Nakama et al., 2005). The presence of a pad of calcified fibrocartilage is what gives these entheses their characteristic appearance (Benjamin et al., 2002, Benjamin et al., 2006).



Figure 4. Superior view of the proximal olecranon process of the ulna; the bottom of the image is anterior. This photo illustrates normal development of the fibrocartilagenous enthesis for the M. triceps brachii common tendon which is outlined in red. The anterior lip of the olecranon is non-insertional. This ulna is in the collection of the ANU biological anthropology labs. Photo by E. Feuerriegel.

As enthesis morphology is hinged to a certain extent on mechanical loading, function dictates structure, and these mechanical influences can account for differences in fibrocartilage quantity both within and between entheses as well as the presence of enthesophytes (see Section 2.2.4). For instance, Schneider (1956) observed how the structure of the biceps brachii insertion was notably different in an individual who had spent his life window cleaning (habitually pronated forearm) from another individual who had spent a significant portion of his working life milking cows (supinated forearm).

There is also a significant body of experimental evidence supporting the importance of mechanical loading in enthesis fibrocartilage development. Gao et al. (1996) studied the femoral attachment for the medial collateral ligament (MCL) in rat knees. Initially the tendon/ligament attaches to the hyaline cartilage of the bone anlagen in the rat foetus or neonate. During ossification, where bone replaces hyaline cartilage, not all cartilage at the attachment sites is eroded, resulting in a cartilage disc at the incipient enthesis. This hyaline disc is eventually reabsorbed and replaced with enthesis fibrocartilage which develops by metaplasia in the tendon/ligament. Rather than the cells continuing to differentiate into fibroblasts, they become fibrocartilage cells. Benjamin and Ralphs (1998) and Benjamin and McGonagle (2009) have proposed that the signal for metaplasia is mechanical loading, particularly elevated levels of compressions and/or shear stresses. Significantly, in the rat knee this change from hyaline cartilage to enthesis fibrocartilage occurs between 30-45 days post-partum, that is, at a time corresponding with an increase in physical activity and therefore an increase in the mechanical strength of the MCL. Thomopoulos et al. (2007) similarly conducted experimental work on mouse supraspinatus entheses. The left shoulders of newborn mice were paralysed using intramuscular injections of botulinum A toxin to simulate a neonatal brachial plexus injury and remove muscle load from the humeral head. The

contralateral shoulder was injected with a saline solution only. The authors observed that the development of enthesis fibrocartilage was markedly delayed in the left shoulder compared to the right, due to the decreased loading of the paralysed shoulder. The authors observed marked changes in muscle mass, bony development, muscle force generation, and soft-tissue contracture, but the most dramatic were the changes observed to the bone-tendon junction at the entheses, characterised by significantly decreased amounts of bone mineral, attributed to the greatly reduced loading of the shoulder. Further, when compared to the controls, the mice with botulinum toxin-injected shoulders exhibited a much greater number of osteoclasts lining the bone, indicating that the decreased mineral content resulted from decreased mineral deposition in addition to increased bone resorption.

Zumwalt (2006) studied the relationship between muscle action/size and enthesis morphology at six clearly differentiated tendons in adult sheep. Zumwalt endurance trained the sheep by exercising them for 90 days to mimic habitual behaviour with a view to investigating the validity of archaeologists/anthropologists using enthesal development as a gauge of likely activity levels in human skeletal populations. Her evaluations of enthesis complexity did not involve histological analysis and were restricted to macroscopic features on macerated bone. She concluded that the trained sheep did not display any notable changes in macroscopic enthesis morphology from the control group. This differs markedly from the results of Thomopoulos et al. (2007) and Gao et al. (1996). There are two possible explanations for this. First, it is uncertain to what extent the type of muscle fibre activity promoted by endurance training differs from other activity patterns and whether it influences the enthesis at the molecular, cellular, or tissue level. Nevertheless, it has been noted by Magnusson and Kjaer (2003) that the cross-sectional area of the Achilles tendon in distance runners is greater than those of non-runners, potentially indicating region-specific hypertrophy in response to

habitual loading, but it is unknown whether this extends to the size of the attachment of the Achilles tendon to the calcaneus. Second, Zumwalt used adult rather than juvenile animals in her investigation and it is not clear how much more responsive growing bone is to mechanical stresses compared to mature bone in the context of enthesal development.

2.2.4 Enthesis Pathologies

While entheses evolved to withstand high stress concentrations and may therefore be considered less likely to fail mechanically during loading compared to other components of the musculoskeletal system, they are nonetheless vulnerable to overuse injuries in addition to being associated with a variety of metabolic and inflammatory conditions. Collectively these pathological changes to the enthesis are referred to as ‘enthesopathy’. This category of change includes osteolytic and osteophytic activity within the enthesis or the formation of enthesophytes at the margins of the enthesis (Fig. 5; Mariotti et al., 2004, Villotte, 2006, Villotte et al., 2010). Pathological alteration can occur in any part of the enthesis. Enthesopathy in the context of studies on enthesal change will be discussed in the following Section 2.3.

Pathologies that are well-known as resulting from over-use include epicondylitis (‘tennis elbow’), proximal patellar tendinopathy (‘jumper’s knee’), a variety of Achilles insertional disorders and plantar fasciitis (‘fasciitis’) (Khan et al., 1996, Niepel and Sit'aj, 1979, Resnick and Niwayama, 1983). Other enthesopathies, such as enthesal tendinopathies at the rotator cuff, occur without underlying disease or overuse injury as their aetiology and may instead be attributable to traction forces or ischemia (Claudepierre and Voisin, 2005). Some quadri- or paraplegic individuals develop enthesopathy associated with calcification (Claudepierre and Voisin, 2005). A number of metabolic diseases are known to cause abnormalities in enthesal morphology and are

listed in Table 1, though the mechanism underlying enthesal pathology in these diseases remains obscure.

Table 1. Metabolic diseases known to affect entheses (from Niepel and Sit'aj, 1979).
Ochronosis Chondrocalcinosis Gout Apatite arthropathy Hyperparathyroidism Primary hypoparathyroidism Osteomalacia Familial hypophosphatemia Fluorosis Acromegaly

Seronegative spondyloarthropathies are a category of chronic, rheumatic autoimmune diseases that also target entheses (Benjamin and McGonagle, 2001) including ankylosing spondylitis, reactive arthritis, psoriatic arthritis, arthritis associated with inflammatory bowel disease, and undifferentiated spondyloarthropathies (Peloso and Braun, 2004). Diffuse idiopathic skeletal hyperostosis (DISH) is another cause of pathological changes to entheses; it is characterised by excessive bone deposition at entheses, leading to the development of bony spurs (Nascimento et al., 2014).

Pathological changes to entheses fall into a number of types which can be identified macroscopically on skeletal material. These include enthesophytes, cysts, foramina, bony production, and pitting. Enthesophytes (occasionally confused in the literature with osteophytes which occur on the margins of articular surfaces) are irregular bony projections, spikes, spurs, spicules, or ridges that occur at the enthesis (Fig. 5e). While the aetiology of enthesophytes can include inflammation, disease, or advanced age, they can also occur as a result of habitual activity (Mann and Hunt, 2005) and must therefore be considered on a case-by-case basis when assessing potential enthesal pathology on their presence alone. This will be discussed further in Chapter 6. At the upper limb, the

supinator crest of the ulna and radial tuberosity are particularly vulnerable to enthesophytic involvement (Mann and Hunt, 2005).

Bone formation at the enthesis may also occur in the form of woven bone. In woven bone, the collagen bundles are arranged irregularly, which differentiates it from the highly-organised, parallel structure of lamellar bone. The irregular structure of woven bone occurs as a result of rapid deposition; the chief purpose of woven bone is providing the body with a means to quickly respond to skeletal changes, either through growth, activity, fracture, or disease processes, although its disorganised structure means that it is mechanically weak compared to lamellar bone and unsuited as long-term solution to damage (Brickley and Rachel, 2008). Typically, woven bone is replaced over time by lamellar bone in a process referred to as bony substitution. Woven bone appears fibrous compared to the smooth, dense appearance of lamellar bone (Fig. 6).



Figure 5. Healthy entheses (a, c) and enthesopathies (b, d–f) on the proximal humerus and radius. Photo (a) shows a normal humeral insertion of Subscapularis. Compare this to (b) from a pathological specimen illustrating a cyst (white arrow), foramina (black arrow), and bony production (grey arrow) at the same enthesis. Photo (c) shows a normal radial insertion of *M. biceps brachii*, (d) irregular margin, and (e) enthesophyte. Photo (f) is of the humeral origin of the common tendon of the elbow extensor muscles (lateral view) exhibiting significant hyperostotic alteration and vascular foramina (black arrow) over much of its surface. The white arrow illustrates the irregular crest formed by the bony alteration. From Villotte et al. (2010).



Figure 6. Proliferative woven bone formation occluding many of the entheses for the posterior femoral musculature in a chimpanzee (*Pan troglodytes schweinfurthii*), sex uncertain. Normal lamellar bone is visible at the femoral neck and greater trochanter. While the cause of this reactive bone growth is unclear, it is probable that inflammation of the periosteum has led to widespread bilateral deposition of woven bone. Specimen No. 730 from the Royal Museum of Central Africa in Brussels, Belgium. Photo by E. Feuerriegel.

Tendon ossification may also obscure and change the appearance of entheses, and it is

caused by bone formation within the enthesis itself. The aetiology of tendon ossification is poorly understood in the absence of conditions such as fluorosis or DISH, though it has been linked to repetitive microtrauma and trauma resulting from surgery (Schweitzer and Karasick, 2000). While less common in the shoulder elements, ossification of the coracoacromial and coracoclavicular ligaments has been known to occur in modern populations (Chen and Bohrer, 1990, Reichmister et al., 1996) (Fig. 7).

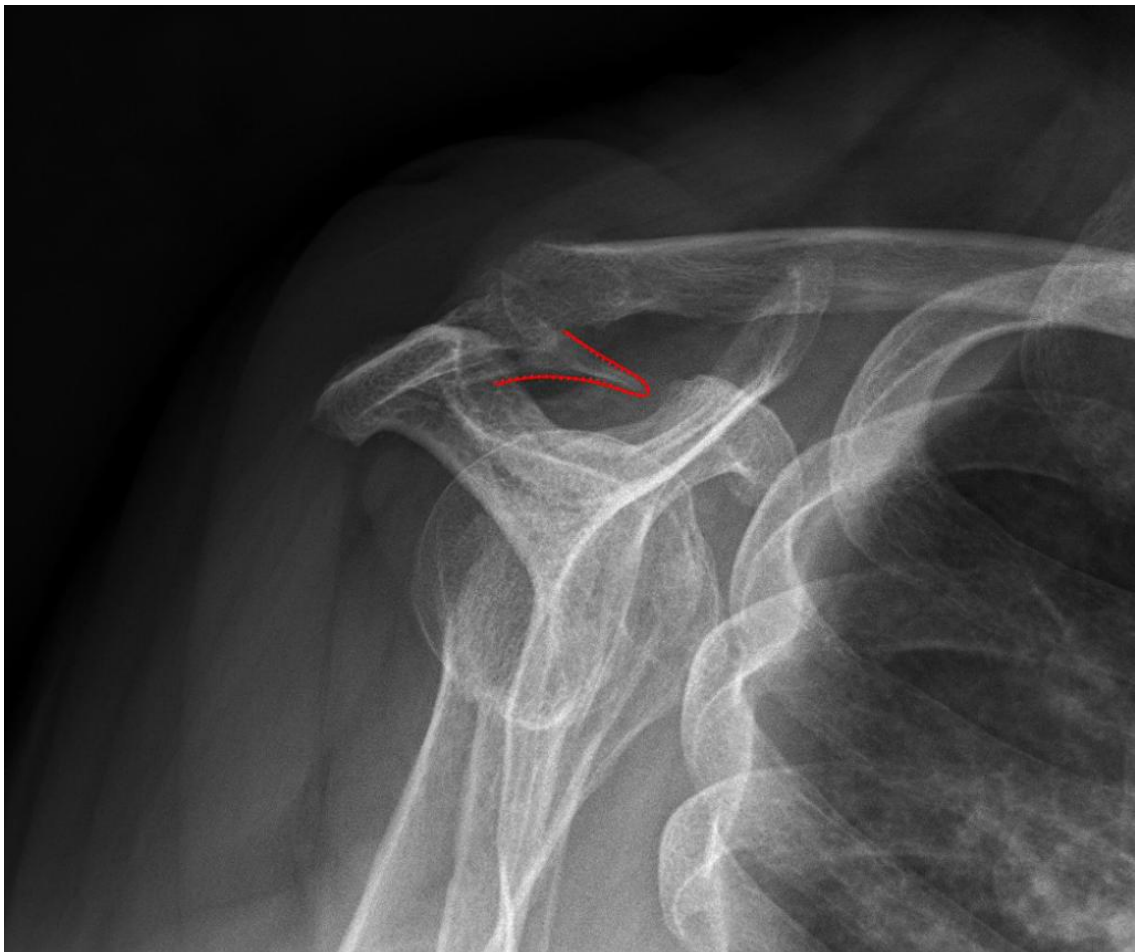


Figure 7. Radiograph of coracoacromial ligament ossification in a 68-year-old woman, scapular view. A large osseous projection is observed extending from the inferior surface of the acromion, angled towards the coracoid process. The ossified ligament is outlined in red. Radiograph courtesy of Dr Matt Skalski, Radiopaedia.org.

Bony changes at the enthesis may also be destructive, such as in lytic lesions, cysts, pitting, or erosion. Lytic lesions are characterised by destruction or loss of bone as a result of a disease process and can present as an area of porosity or erosion at the attachment site (Mann and Hunt, 2005, Henderson, 2008) (Fig. 8). Enthelial cysts can present as scooped-out concavities, pits, or depressions (Fig. 5b – white arrow) (Mann

and Hunt, 2005). Inflammatory pitting might also occur as a result of infection or other inflammatory disease which presents as clusters of fine pits on the bone surface (Brickley and Rachel, 2008). The presence of these features at the entheses in any investigation of muscle attachment site development must necessarily act as an exclusion criterion if normal variation is to be appropriately quantified.

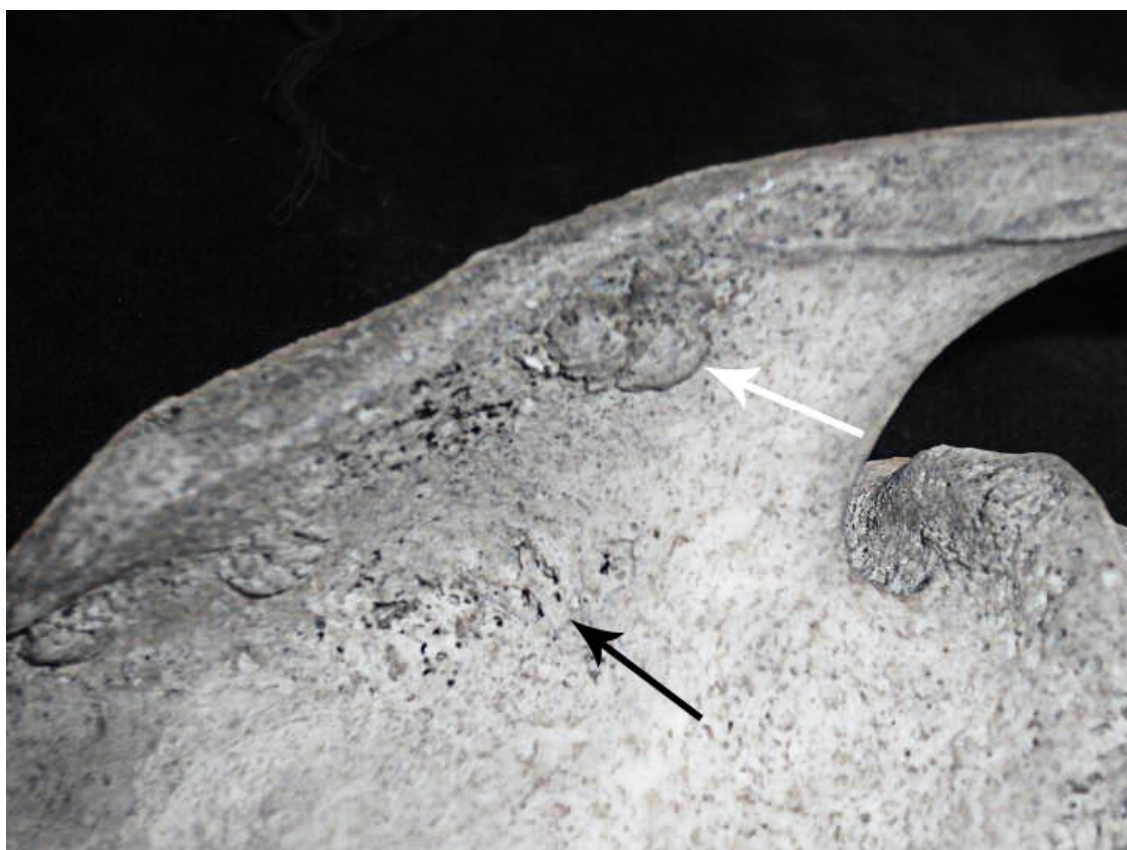


Figure 8. Superior view of a left scapula exhibiting lytic lesions (black arrow) and osteoblastic activity (white arrow) at the junction of the acromion and suprascapular fossa (origin of the *M. supraspinatus*) in a probable male individual in his early 40's from the post-Medieval Cross Bones burial site in Southwark, England. This individual is a suspected case of metastatic carcinoma. Photograph courtesy of the Museum of London, Wellcome Osteological Research Database.

2.3 Enteseal Development in Bioarchaeology

Studies of enteseal development are based on principles of bone remodelling in response to mechanical loading, known as Wolff's Law or bone functional adaptation (Ruff et al., 2006). The physiological processes involved in bone remodelling and the

biomechanical effects of stress on bone are well-documented in the literature (see Section 2.2). When force is applied to bone, deformation of the bone tissues is induced and bone remodelling (i.e. deposition or reabsorption) occurs in order to prevent these tissues failing under the strain and to maintain optimal strain levels on the active surfaces of bones, such as the trabeculae, the margins of entheses and joints, and periosteal and endosteal surfaces (Frost, 2001, Ruff et al., 2006). In this case, greater levels of biomechanical stress will lead to bone deposition whereas lowered levels of stress will induce bone reabsorption (Frost, 2001, Ruff et al., 2006). All of these regions have been subjects of interest in studies of activity patterns at one time or another.

A number of studies have investigated trabecular orientation to infer patterns of directional loading and, in doing so, reveal function and positional behaviour in fossil hominins, modern humans, and non-human primates (Skinner et al., 2015, Maga et al., 2006, Ryan and Shaw, 2012, Ryan and van Rietbergen, 2005, Tsegai et al., 2013). Researchers have utilised both quantitative and qualitative data infer a causal relationship between muscle insertions and particular patterns of behaviour, suggesting that the size and complexity of entheses are related to the intensity of stress diffused by the enthesis during physical activities (al-Oumaoui et al., 2004, Alves-Cardoso and Henderson, 2010, Capasso et al., 1999, Churchill and Morris, 1998, Kennedy, 1989, Molnar, 2006, Weiss, 2003, Weiss, 2004, Weiss, 2007, Wilczak, 1998, Steen and Lane, 1998). This observation, naturally, has led to the suggestion that specific behaviours may be inferred from skeletal material and indeed it is a logical conclusion that contractile forces generated through muscular activity engenders bony remodelling at the enthesis. There is in fact some evidence that suggests a functional relationship between enthesal complexity and activity patterns (Drapeau, 2008b, Niinimäki, 2011, Woo et al., 1981, Chamay and Tschantz, 1972), although a number of studies have questioned this relationship (Alves-Cardoso and Henderson, 2010, Milella et al., 2012,

Weiss et al., 2012) and it is unclear which types of stress lead to functional adaptation of the enthesis (Zumwalt, 2006).

Osseous and dental modifications produced by habitual patterns of behaviours are referred to commonly in the literature as “markers of occupational stress” (MOS) and include both musculoskeletal stress markers (MSM) and robusticity markers (RM). Two categories of modification are generally recognised in bioarchaeological studies of enthesal development: 1) complexity/robusticity and; 2) enthesopathy. Changes in enthesal complexity are generally taken to indicate normal adaptation of the skeleton to regular mechanical loading of the musculoskeletal system (Hawkey and Merbs, 1995, Mariotti et al., 2007) and enthesopathy is occasionally studied in this context. Complexity and enthesopathy are distinct phenomena and are not necessarily related to one another (Drapeau, 2008b, Mariotti et al., 2004, Mariotti et al., 2007, Milella et al., 2012); this is contrary to the view propounded by Hawkey and Merbs (1995) in their seminal paper in which they argued that enthesopathy and complexity should collectively be referred to as “stress lesions” and occur on a continuum. This is similar to Robb (1998), who considered all enthesopathies to be on a continuum with complexity (robusticity). Nevertheless, no study has been conducted into the relationship between enthesal complexity and enthesopathies, and no strong evidence illustrating the progression of development from “complexity” to “enthesopathy” has been presented in the literature.

To further complicate the subject, no clear definition for complexity exists in the literature and the term is consequently used variably to refer to a suite of features relating to muscle/tendon attachment sites, including the size, shape, and rugosity (Hawkey and Merbs, 1995, Mariotti et al., 2004, Mariotti et al., 2007, Niinimäki, 2011, Villotte, 2012, Villotte et al., 2010, Zumwalt, 2006). There is also a variety of analytical

techniques used to study entheses arising out of these definitions. Hawkey and Merbs (1995), Mariotti et al. (2007) and Robb (1998) have all developed qualitative methods for scoring the development of entheses that rely solely on visual assessment of entheses surface features such as the presence of pitting, depressions, ridges, and crests or the definition of the entheses margins. Quantitative methods have also been proposed and involve more precise measures to assess entheses complexity.

Zumwalt (2005, 2006) used three-dimensional surface area controlled for body mass as an indicator of entheses size, and then calculated the fractal dimension of profiles extracted from the entheses to indicate surface complexity. In this scheme a fractal dimension value closer to 1 is indicative of a “smooth” profile and a value closer to 2 indicated an “infinitely complex” profile. Wilczak (1998), on the other hand, used two-dimensional surface areas. The problem presented by the variety means of studying entheses complexity and the definitions of what constitutes “complexity”, as well as the seemingly disparate results, is one of comparison. Without a standardised definition of entheses development and similarly standardised means of quantifying this, it is difficult to properly compare the results and draw conclusions about entheses complexity. Other issues potentially affecting the comparability of studies include inter-observer error in identifying and delimiting features and entheses, and issues arising from many of these studies failing to account for other mechanical and systemic factors, such as body mass and genetic factors, that may influence the responsiveness of entheses to loading (Robb, 1994, Weiss, 2003, Wilczak, 1998, Zumwalt, 2006).

Two concerted efforts have been made to summarise the “state of the art” in entheses development studies and redress some of the primary issues concerning them. The first was a symposium titled *Activity Patterns and Musculoskeletal Stress Markers: An Integrative Approach to Bioarchaeological Questions*, held during the 66th annual

meeting of the American Association of Physical Anthropologists in 1997. A special volume published by the *International Journal of Osteoarchaeology* documented this symposium in the form of select papers presented at the meeting (Peterson and Hawkey, 1998). The focus of the symposium was to standardise the methodology of the field so that collection processes and analyses could be comparable across all future enthesal development studies. Participants in the symposium assessed the utility of entheses in reconstructing behaviour and activity in past populations, including their statistical and methodological limitations. Key issues identified by the contributors included the limited understanding of rates of bone remodelling, the role of hormones, and other biomechanical factors in the aetiology of enthesis development. They maintained that studies of this type nonetheless have value in investigating sex-specific differences in activity patterns providing that such studies were supported by appropriate data from archaeological and ethnographic sources, a factor that is not always reliable for archaeological populations. The need for well-established biocultural context is a recurring sentiment in studies of archaeological populations generally, especially since the publication of Wood et al.'s (1992) paper on the "osteological paradox" and problem of interpretation in palaeopathological studies. These issues notwithstanding, enthesal development studies continued (and still continue) to be conducted on musculoskeletal stress markers.

In 2009 a second symposium/workshop, titled *Workshop in Musculoskeletal Stress Markers (MSM): Limitations and Achievements in the Reconstruction of Past Activity Patterns* and held at the University of Coimbra, Portugal, was undertaken to review the field and address the emergent issue of methodological subjectivity (Santos et al., 2011). The workshop served to highlight the major methodological and interpretive contributions made to the field as well as the associated limitations of using tendon and ligament enthesis morphology to reconstruct past behaviour. Notably, the workshop

attempted to standardise the terminology used in used in these studies (Jurmain and Villotte, 2010), suggesting that MSM is an inappropriate descriptor for these features as it presupposes aetiology when in fact a number of factors have been implicated in enthesal development. They suggested instead that “enthesal change” be adopted which refers neutrally to both pathological and non-pathological changes. The Coimbra workshop also provided significant advances in qualitative methodologies for assessing entheses via 3D laser surface scanning which has the potential to facilitate statistical correlations between activity and skeletal morphology, as well as more meaningful macroscopic methodologies.

The Coimbra terminology is similar to the terminology adopted in this dissertation, although for further clarity I have chosen to adopt the term “enthesal development” to further distinguish the category of possibly activity-related change from pathological alterations of the enthesis (i.e. “enthesopathy” which, confusingly, has also been used in the literature to refer to enthesal development). In this dissertation, “enthesal development” is defined as a spectrum of normal (i.e. non-pathological) osseous changes at the site of attachment for a muscle or ligament (cf. Hawkey and Merbs, 1995). These changes are normal physiological responses of the bone to mechanical loading and the transmission of forces during movement by the muscle or ligament which in turn engender a bony response at the enthesis. The extent of this response (i.e. degree of development) varies between individuals resulting in different morphologies that occur across a spectrum of expression. This is unlike enthesopathies which are either present or absent, and the terms “enthesal development” or “enthesal robusticity” are used synonymously in this dissertation with “enthesal complexity”. Enthesopathy, in this case, is defined as any pathological change/s to the appearance or biochemistry of an enthesis arising through the work of an abnormal condition. Enthesopathies are either present or absent and do not occur across a continuum of

development (cf. Mariotti et al., 2007), unlike enthesal development. The aetiology of these changes may include trauma, hormonal, degenerative/age-related, genetic, disease, or dietary factors. This is the most common term in the clinical literature used for the description of these changes. Osseous markers of enthesopathy include cysts, lytic lesions, or eroded areas, and are characterised as a binary state (see Fig. 5).

Regardless of the advances, there remains a dearth of comprehensive research exploring the aetiology of enthesal development as it relates to activity. Weiss (2003, 2004, 2007) conducted a series of studies that found significant correlations between robusticity and geometrical properties of long bone muscle attachments, which led her to suggest that mechanical influences can be considered at least partly responsible for enthesal development at these sites as cross-sectional structure is indicative of such a relationship (Ruff et al., 2006). Using the criteria developed by Hawkey and Merbs (1995), Drapeau (2008b) analysed enthesal complexity in skeletal collections of pre-industrial modern humans, chimpanzees (*Pan troglodytes*), and gorillas (*Gorilla gorilla*), predicting that handedness in humans will lead to the upper limbs displaying bilateral asymmetry in enthesal complexity compared to African apes, which participate in locomotor behaviour involving bilateral use of the upper limbs. Drapeau's prediction was supported and she concluded that there was in fact some evidence that enthesal morphology provides information on activity patterns and that greater enthesal development may be associated with habitual behaviours. Mariotti et al. (2007) developed a standardised scoring method for assessing enthesal development and used it to compare a skeletal collection of human males of known occupations, finding evidence of variation in robusticity scores and mean functional complexity. Junno et al. (2011) performed a cross-sectional analysis of the radial tuberosity in a collection of known-occupation (heavy physical labour) human males and compared them with a control group. Junno et al. found that the radial tuberosity projected to a greater degree

in the group that had regularly participated in heavy physical labour, and that the prominence of the tuberosity aligned with the direction that the biceps muscle fibres pull.

Niinimäki (2011) conducted a study investigating the effects of labour intensity, age, and size on enthesal development using a skeletal collection of individuals of known age, sex, and occupation/labour intensity. Niinimäki found that age and size are the major confounding factors for interpreting labour intensity data and that enthesal development scores were unable to differentiate labour intensity in older individuals, likely due to the cumulative effects of age on enthesal complexity. She further found that sex was not a significant factor in enthesal development and enthesal complexity appeared to increase at a similar rate in both males and females such that differences in complexity were no longer significant after adjusting for muscle size. Contra to other studies, it appears as though sex-related differences in enthesal complexity may in fact be attributable to body and therefore muscle size, males on average having greater body size compared to females (Niinimäki, 2011). In terms of labour intensity, heavy labour has not been found to increase complexity as much as light labour, suggesting that some form of thresholding is occurring at the enthesis whereby the bone is no longer able to remodel after a certain level of strain has been reached (Milella et al., 2012, Niinimäki, 2011, Robb, 1998). However it should be noted that two of these studies measured enthesal development on a spectrum with enthesopathies (Niinimäki, 2011, Robb, 1998) and as such this pattern may actually reflect the presence of enthesopathy as opposed to complexity, an observation that has been made for upper limb enthesopathies independent of complexity (Villotte et al., 2010). Weiss (2012) has argued persuasively for the use of fibrocartilaginous entheses over fibrous entheses in activity reconstructions based on her research on hunter-gatherer California Amerinds, demonstrating that the confounding factor of body size is absent for these entheses.

While many of these studies have not distinguished between fibrous and fibrocartilaginous entheses in their efforts to understand enthesal development and its relationship to behaviour, some investigators (e.g. Alves-Cardoso and Henderson, 2010, Henderson, 2013, Villotte, 2006) have highlighted the importance of the types of entheses when recording and analysing complexity data. Alterations to fibrocartilaginous entheses have long been acknowledged in the clinical literature to be related to specific diseases such as seronegative spondyloarthropathies and diffuse idiopathic skeletal hyperostosis (DISH) (Henderson, 2008, Jurmain et al., 2012, Kacki and Villotte, 2006), and fibrous entheses have been demonstrated to be affected by calcific tendinitis and cortical erosion, though these are less common than fibrocartilaginous entheses pathologies (Henderson, 2013). Further there is normal variation between entheses types in terms of how they present on the skeleton, most likely representing variations in loading characteristics both within and between entheses. As mentioned in Section 2.2.1, fibrous entheses have a larger surface area than fibrocartilaginous entheses and occur predominantly on the long bone diaphysis where there is little shifting of the soft tissues during joint movements. Fibrous entheses can be harder to define macroscopically as their margins can be ambiguous. The surface of fibrous entheses are also typically rough in texture due to the presence of Sharpey's fibres which physically anchor the soft tissue into the bony matrix (François et al., 2001). Fibrocartilaginous entheses on the other hand are limited to the epiphyses and joints where they are constrained by space much more than fibrous entheses and are subject to greater bending loads at the interface during movement (Benjamin and Ralphs, 1998). The mediating layers of mineralised and unmineralised fibrocartilage at these entheses tend to leave smaller "footprints" on the bone that are well-delimited compared to fibrous entheses. In addition to this, the periosteum is absent in the deep part of fibrocartilaginous entheses, meaning that the soft tissues only insert into the

periosteum in the superficial parts of the enthesis. Consequently, changes in enthesal complexity are more likely to occur at the margins of these entheses (Hawkey and Merbs, 1995). Pathological changes to fibrocartilaginous entheses may be identified by the presence of vascular foramina and bony spurs (Weiss, 2012). Consideration of pathological conditions likely to affect the different types of enthesis, as well as their normal appearance and mechanical properties, is therefore essential in enthesal development studies. Scoring methods like those proposed by Hawkey and Merbs (1995) or Mariotti et al. (2007) score fibrous and fibrocartilaginous entheses on the same scale and do not acknowledge this normal variation.

Age has also been found to be a contributing factor to enthesal development and this relationship has been established in a number of studies (al-Oumaoui et al., 2004, Alves-Cardoso and Henderson, 2010, Henderson et al., 2012, Lieverse et al., 2009, Mariotti et al., 2007, Milella et al., 2012, Niinimäki, 2011, Stirland, 1998, Weiss, 2003, Weiss, 2004, Weiss, 2007, Wilczak, 1998, Churchill and Morris, 1998). Older individuals tend to be scored higher for enthesal complexity than younger individuals (but see below). These studies suggests that age-related increases in complexity may be attributed to the cumulative effects of long-term activity patterns or changes in bone structure like cortical thinning due to decreased osteoblast activity (Mays, 2000). Enthesal complexity has been found to increase progressively with age until 40-50 years old when the processes of development appear to level off, possibly as a result of a self-limiting process or changes/decreases in activity regime (Robb, 1998). These studies make clear the importance of controlling for size and age in study populations and this will be discussed further in the context of fossil hominins in Chapter 6 (Methods).

2.4 Summary

Ideally, any study on specific activities in past populations would be paired with evidence from historical, ethnographic, and archaeological sources in addition to evidence gleaned from skeletal remains. For fossil hominins, however, this is only possible in a limited fashion. Archaeological assemblages of stone tools and tool-marked bone are some of the only additional lines of evidence palaeoanthropologists have to explore these behaviours in early fossil hominins. Complicating this further is the lack of associations between tool evidence and skeletal remains. Common research questions include activity-level differences within populations (e.g. al-Oumaoui et al., 2004, Larsen, 1997) and temporal and spatial comparisons between populations (e.g. Larsen, 2000). While these are valuable questions for exploring past populations, circular logic is a common flaw for many of these studies. Bioarchaeological evidence is used to strengthen archaeological arguments while archaeological evidence is used to confirm the interpretation of the bioarchaeological data (Jurmain, 1999). Issues like this undermine the potential deductive strength of combining data sources. Nevertheless, while the research discussed above tends towards the equivocal, it does highlight the potential merits of quantifying enthesal morphology and complexity. If enthesal development is indeed indicative of patterns of skeletal strain and biomechanical loading, then it is possible to devise a macroscopically reproducible methodology to investigate them.

CHAPTER 3: TOOL MANUFACTURE AND USE

3.1 Introduction

This chapter is part two of a three-part critical review of the literature on topics pertinent to this dissertation. The aim of this chapter will be to explore the archaeological and anatomical evidence for tool manufacture and use, focusing on the technical aspects of these behaviours on both levels. Questions that will be addressed include: what are Oldowan stone tools and how are they diagnosed archaeologically and technologically? What kind of skill is required to produce them? What is the anatomical evidence for tool manufacture and use? What are the anatomical and cognitive requirements for this skill and what does anatomy tell us about the biomechanics of stone tool manufacture in fossil hominins?

It is appropriate to define precisely what is intended by the use of the term ‘tool use’ in this dissertation. Hall’s (1963) paper on this subject used a definition that in effect encompasses almost all social behaviour, including things such as using other animals in order to achieve a goal. Others maintain that the use of natural objects “as if they were tools” does not equate to true tool using, restricting this behaviour entirely to the human species on the assumption that only humans purposefully and skilfully alter objects for tools (e.g. Gruber, 1969). Further behaviours offered as potential tool-using behaviour include string-pulling and nest building by birds (Thorpe, 1963) and web and net building by spiders and caddis fly larvae (Wheeler, 1930). van Lawick-Goodall (1970), on the other hand, argued that behaviour such as string-pulling only constitutes the skilful manipulation of objects and does not equate to tool-using at all. Recognising the fact that no one definition is likely to satisfy every scholar, this dissertation will adopt one similar to that of Alcock (1972) and van Lawick-Goodall (1970), excluding all social behaviour. Tool-using, in this context, will thus be defined as the manipulation

of an inanimate object and having the effect of altering the position or form of a separate object. Tool manufacture is thus the modification of an objective material (stone or otherwise) through the processes of detachment, subtraction, recombination, or reshaping in order to alter the position or form of a separate object. In the case of the latter definition, I follow Beck (1980) in the definition of the “creative acts”. Detaching is separation of the incipient tool from substrate or other object (e.g. a twig from a branch), subtraction involves the removal of some part of the object to make it more effective as a tool (e.g. removing leaves from a twig to increase its efficacy for extracting ants termites), recombination entails combining one or more objects to make a tool (e.g. attaching two sticks to one another to make a longer stick), and reshaping is the reformation of an object for a particular use. Stone tool manufacture falls into both the categories of subtraction and reshaping.

3.2 Archaeological Evidence for Tool Manufacture and Use

Tool behaviours have assumed a central role in narratives about the evolutionary origins of human cognition and have been identified as one of the selective pressures driving many of the important morphological changes that lead to the modern human body plan. Their significance, both in the wider context of this narrative and to the anthropologists and archaeologists who study them, is manifold. For investigators, stone tools as physical objects are convenient for their physicality and durability in that they can be collected, quantified, and compared well after they were created and their creator has died. But the true import of stone tools lies in what they imply about the cognitive capabilities of their creators. The study of stone tools allows researchers to investigate questions about the abilities that governed tool behaviours and their anatomical foundations.

3.2.1 The Oldowan Technological Complex

The first evidence for hominin tool behaviour comes from Lomekwi, West Turkana, Kenya, and dates to 3.3 million years (Harmand et al., 2015). Called the Lomekwian, this complex is typified by flakes and cores created through passive hammer and bipolar reduction similar to the hammer and anvil techniques used by some extant primates during nut-cracking (Harmand et al., 2015); that is, the techniques used to produce the tools are poorly controlled and characterised by a greater proportion of “knapping accidents” than later traditions. The Oldowan Technological Complex represents the first archaeological evidence for an understanding of rock fracture mechanics, “grammars of action” (Hovers, 2012), and the importance of conchoidal fracture (see below) in the production of efficient stone tools. It is named for Tanzania’s Olduvai Gorge where Mary and Louis Leakey excavated a remarkable assemblage of cores, chopping tools, and flakes from the mid-1930’s on (Leakey, 1971b). It is characterised by modified tools such as flakes, flaked cores, and hammer stones, and required a fair degree of skill to produce; they demonstrate selectivity of raw material and in some cases up to 70 flakes have been recorded as having originated with a single core (Panger et al., 2002, Roche et al., 1999, Schick and Toth, 1993, Susman, 1991, Susman, 1994, Toth and Schick, 2009, Braun et al., 2009b, Semaw, 2000, Stout et al., 2005, Stout et al., 2010).

The earliest Oldowan assemblages date to 2.6 – 2.5 million years ago, originating in Gona, Ethiopia (Semaw et al., 1997, Semaw, 2000, Semaw et al., 2003), and the industry continued throughout East and Southern Africa until 1.7 – 1.6 million years ago when the Developed Oldowan and Acheulean industries became prevalent (Fig. 9). Major localities for Oldowan sites in Ethiopia include Gona (Semaw, 2000, Semaw et al., 1997, Semaw et al., 2003), Middle Awash (de Heinzelin et al., 1999), Hadar

(Kimbel et al., 1996), and the Omo basin (Howell et al., 1987). Olduvai Gorge is the major locality for Oldowan sites in Tanzania (Leakey, 1971b, Blumenschine and Peters, 1998). In Kenya, major sites are Kanjera (Plummer et al., 2009), West Turkana (Roche et al., 1999, Delagnes and Roche, 2005) and East Turkana (Isaac and Isaac, 1997). In South Africa, Swartkrans and Sterkfontein (Kuman, 1998) and Drimolen (Backwell and d'Errico, 2008) are the three primary tool sites.

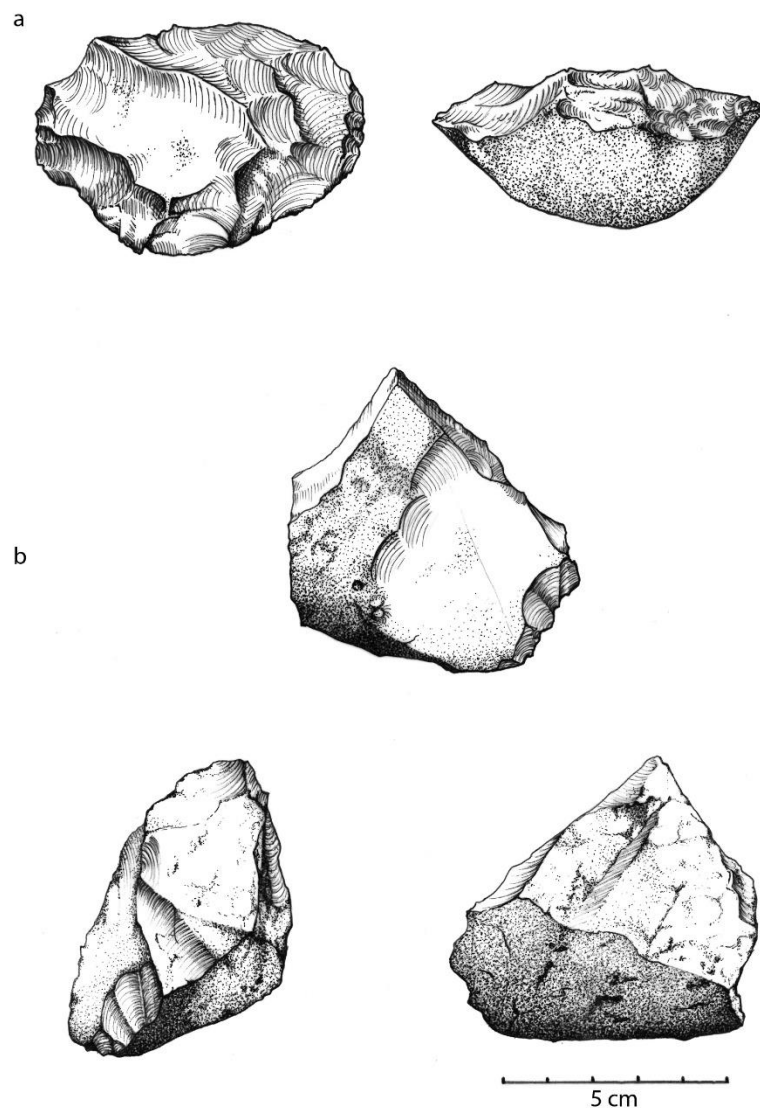


Figure 9. Oldowan stone tools from East Gona early Pleistocene (2.5-2.6 million years) assemblages EG10 and EG12. (a) Two views of unifacial centripetal tool; (b) Three aspects of a core tool (middle and bottom). Illustrations by E. Feuerriegel.

These assemblages consist predominantly of stone artefacts primarily because they are able to withstand the destructive taphonomic processes at work at these sites over millions of years. It is probable, based on the sophistication of the Oldowan tools, that the hominins who created them also maintained a tool repertoire involving organic materials, although of course due to their ephemeral nature those tools remain largely invisible in the archaeological record, barring the occasional reported instance of bone that may have been used as digging tools (Backwell and d'Errico, 2008, Brain, 2007, Backwell and d'Errico, 2001, Dart, 1961, d'Errico and Backwell, 2009, d'Errico and Backwell, 2003, d'Errico et al., 2001, d'Errico and Henshilwood, 2007).

Oldowan stone tools are largely the product of one of two techniques: simple percussive flaking (called hard-hammer percussion) or bipolar percussion (Schick and Toth, 1993). In the first technique, a hammer stone is held in one hand and used to strike another stone, generally held in the other hand, using a strong percussive blow in order to remove a flake or create a sharp edge. Bipolar percussion, on the other hand, involves the placing of the objective tool stone – called a core – on an anvil stone and striking it from the top using a hammer stone. This latter technique is less controlled than hard-hammer percussion as it is more likely to shatter the tool stone/core and create many flakes at once, rather than one or two at a time as in hard-hammer percussion. The raw material used for these tools tended to be what was immediately available in the vicinity, and rock types varied from igneous rocks such as basalt, rhyolites, and trachytes, flint, chert, quartz and quartzite, or limestone depending on what was locally available.

Nevertheless, a pattern that has been observed at some Oldowan sites is resource transport. This includes evident resource selectivity (i.e. a preference for some types of rock over others for use as stone tools) and transportation of fairly large quantities of flaked stone through the palaeolandscape (Blumenschine et al., 2008, Braun et al., 2009a, Braun et al., 2009b, Harmand, 2009, Stout et al., 2005). The longest documented distance for raw material transport comes from Kanjera, Kenya, where stone tool materials have been reported as originating as far as 13 km away (Braun et al., 2009b). These are impressive distances to travel but it would be erroneous to suggest that these transportations occurred as a singular event or special excursion for the express purpose of collecting stone. The more likely scenario is that fossil hominins were moving the raw materials for their tools shorter distances between sites on separate occasions as a part of complex foraging patterns, a scenario which is supported by analyses of artefact assemblages demonstrating that the cores were flaked prior to transportation, reduced further at the new site, and then transported again (Blumenschine et al., 2008).

Oldowan sites are often notable for the concentration of stone artefacts that they can contain – many sites are documented as including hundreds or even thousands of artefacts. Typically, they comprise of four main categories of artefacts:

1. Core tools (scrapers, choppers, polyhedrons, discoids)
2. Percussors (hammerstones)
3. Retouched artefacts (scrapers and awls)
4. Debitage (flakes and miscellaneous fragments)

Some authors have gone further and instituted much more granular category systems for flakes, such as Toth's (1985) Technological Flake Categories which assigns flakes to a particular category based on the presence or absence of cortex on the platform and dorsal surface. The aim of this system is to reconstruct patterns of artefact manufacture

(for an implementation of this system on assemblages from Olduvai Gorge, Tanzania, see Kimura, 1999, 2002). In addition to the products of stone tool manufacture, Oldowan sites and assemblages also contain a significant component of faunal skeletal material bearing the marks of stone tool-assisted processing in the form of cut marks and deliberate percussive smashing and/or fracturing (e.g. Blumenschine and Peters, 1998, Bunn, 1983, Pickering and Domínguez-Rodrigo, 2006). Whether this butchery represents secondary access to animal carcasses through scavenging carnivore kills (confrontationally or otherwise; Blumenschine and Peters, 1998) or the products of deliberate hunting efforts (Bunn, 1983, Bunn and Kroll, 1986, Pickering and Domínguez-Rodrigo, 2006, Pickering et al., 2007, Domínguez-Rodrigo, 2009, Pickering, 2013) is a matter of some considerable debate.

Determining the function and use of Oldowan tools is one of the enduring challenges for palaeoanthropologists and Palaeolithic archaeologists. Oldowan artefacts are often sorted into typologies or functional groupings based on features like size and shape and their inferred purpose based on these features (e.g. scrapers, blades, choppers). It has become increasingly clear with the advent of experimental studies on the Oldowan Technological Complex that this practice is highly problematic, as the creation of such *ad hoc* categories may not truly reflect the intentional and functional end-products of the tool makers themselves (Toth, 1985). As a consequence, much of the evidence for Oldowan tool functionality comes from indirect lines of evidence drawn from archaeological context (Braun et al., 2006), experimental studies (Toth, 1985, Toth, 1987, Jahren et al., 1997, Sahnouni et al., 1997, Braun et al., 2005, Diez-Martín et al., 2009, Lemorini et al., 2014), and ethnographic comparisons with modern human societies (Stout, 2002, Bril et al., 2005, Roux and Bril, 2005). For some tools, their function is more or less clear just by observing the marks on their surfaces, as is the case for hammer stones and spheroids whose battered surfaces attest to their use as

percussors. Similarly, the presence of cut marks and percussive fractures on animal bones speaks to the use of flakes and hammer stones in the processes of skinning, defleshing, dismemberment, and marrow extraction (e.g. Diez-Martín et al., 2009, Domínguez-Rodrigo, 2009). Nevertheless, not all Oldowan sites bearing both faunal remains and stone artefacts show clear evidence of carnivory and stone tool-assisted processing, calling into question the function of the tools themselves if they were not used to process meat. Usewear analyses on Oldowan artefacts from Koobi Fora and Kanjera, Kenya, has indicated the use of some flake tools in the processing of plant foods such as grasses, sedges, and tubers (Keeley and Toth, 1981, Lemorini et al., 2014). Lemorini et al. (2014) particularly identified wood cutting and scraping as a potentially important activity carried out by the Oldowan tool makers, specifically in the extraction of food items like larvae from tree trunks and limbs, similar to what has been observed in wild chimpanzees, and in the production and maintenance of wooden tools. These studies and others like it highlight the importance of considering the use of stone tools in the processing of materials other than meat, despite the lack of direct evidence in the fossil record.

3.2.2 Skill and Expertise in Oldowan Stone Knapping

Ostensibly, the manufacture of Oldowan stone tools is a simple process. At its most basic, it could be characterised as smacking two stones together to detach a flake and create a sharp edge through the mechanism of conchoidal fracture. Nevertheless, the Oldowan technological complex represents a significant cognitive leap taken by the human lineage. Experimental studies have demonstrated that mastering Oldowan knapping requires skill and practice, especially with regard to learning to predict the required angle, placement, and force of the percussive strike to produce a flake.

Oldowan stone tools are manufactured through the controlled production of a phenomenon called “conchoidal fracture”. Conchoidal fracture occurs when percussive force is applied to an objective piece of stone until the compressive loading stress exceeds the tensile and compressive strength of the rock, propagating a cone of force through the stone and leaving a recognisable bulb of percussion (Fig. 10) on the fracture plane (Pelegriin, 2005). Typically, conchoidal fracture occurs in stone types that share the properties of being isotropic (i.e. the quality of responding to load equally in any direction) and brittle. This includes silicate rocks like flint and chert with a homogeneous cryptocrystalline structure, and igneous glasses like obsidian with no preferred planes of fracture. Split-breaking fracture is the more common mechanism of fracture and it is not controllable in the same manner as conchoidal fracture, meaning that the stone can fracture in an unpredictable manner (Cotterell and Kamminga, 1987, Pelcin, 1997). Thus the production of workable flakes with sharp edges is inextricably tied to the understanding of fracture mechanics which would have required practice and skill to control (Roche, 2005), as well as considerable fine motor control (Bril et al., 2010). Understanding how these factors relate to one another may therefore provide insight into the technical competency of the first stone tool-making hominins.

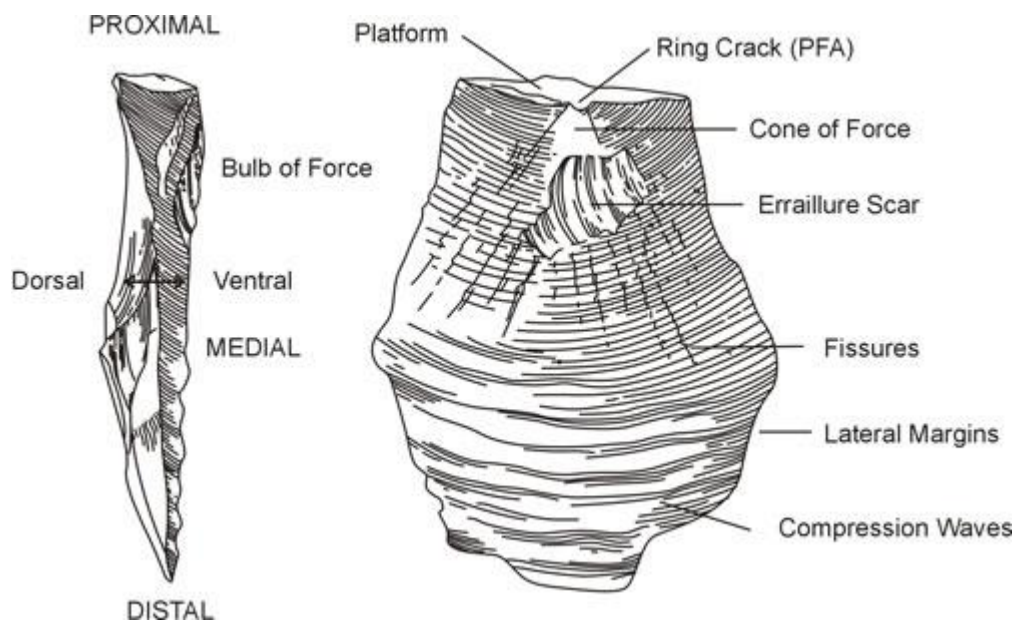


Figure 10. Fracture features of a flake produced by conchoidal fracture. Illustration reproduced with permission of the Trustees of the British Museum.

At present, only a handful of studies investigate the skill required to control the process of conchoidal fracture and these are worth exploring at length. Many of these studies are compiled in a single volume titled *Stone Knapping: The Necessary Preconditions for a Uniquely Hominin Behaviour* (Roux and Bril, 2005) geared towards clarifying the various dimensions of the ability of our earliest ancestors to develop and master systematic stone knapping, as well as addressing the cognitive aspects of skill acquisition in this context. In the first of these, Pelegrin (2005) discussed the distinction between the stone tool artefacts produced by fossil hominins and the flakes produced by some extant primates (e.g. Kanzi the Bonobo and his tool-making exploits) as an incidental product of other tool behaviours, recognising conchoidal fracture as the primary identifier of hominin tool behaviour. This is an important point that underpins many of the other studies in the volume. In the case of Kanzi, his technique for creating splinter stone tools was more comparable to the technique used in nut-cracking (i.e. split breaking) than conchoidal fracture (see Section 3.2.3 for further discussion).

Three studies (Bril et al., 2005, Biryukova et al., 2005, Roux and David, 2005) detail experimental knapping studies using stone bead makers of different skill levels from Khambhat, India, as an analogue for fossil hominin knapping behaviours. Stone bead knapping utilises the same principles of conchoidal fracture and provides a means to investigate the behavioural and biomechanical dimensions of knapping and skill acquisition. Bril et al. (2005) investigated how skill is expressed in the kinematics of the knapping armswing, using video tracking and accelerometers to capture arm segment movements, testing how both skilled and unskilled knappers responded biomechanically to changes in variables such as raw material. Their results strongly indicate that expertise lies with an individual's mastery of the "elementary action", i.e. flake removal, rather than on how knowledge of methods is implemented. High-level experts demonstrated more adaptability and flexibility in variables such as hammer acceleration to the objective material compared to low-level experts. In effect, high-level experts adapted to task constraints better than other skill levels through command of task dynamics, or technique. Expertise, then, is achieved by learning to manipulate the properties of the system – the dynamics between the knappers, stone, hammer, and the anvil – to their best advantage to achieve a particular outcome.

Biryukova et al. (2005) investigated how elementary movement kinematics and movement control varies between skill levels, using motion sensors attached to the dominant arms of knappers. The observation underpinning their study is that the human arm is kinematically redundant, meaning that, for any given task, there are a number of possible ways to perform the same movement using different combinations of rotations in the joints. This led the authors to hypothesise that differences in kinematic synergies may reflect individual-level peculiarities of motor control strategies depending on skill level. Biryukova et al. therefore compared kinematic synergies in knappers from different skill levels (low- and high-level learners, low- and high-level experts), finding

that the synergies of low-level experts were characterised by more stereotyped kinematic patterns, both in terms of joint and hammer trajectories. This differed from high-level expert synergies which demonstrated flexibility in the kinematic aspects of synergies (e.g. large number of degrees of freedom) and in the diversity of their motor synergy repertoire. Significantly, the findings of Biryukova et al. highlight the importance of control in technique and over elementary movements.

Roux and David (2005) investigated the relationship between course of action and control of elementary movements by studying the courses of action taken by skilled and unskilled bead makers. They found that there is a disjunction between knowledge of methods and high-quality bead roughouts in unskilled bead knappers such that knowledge is not sufficient for high-quality end results. Knowledge is only useful in as far as being guidelines. Skill, in this case, is characterised by the ability to effectively adapt and manage sub-goals in the process of efficiently making flake removals and rectifying failed ones. Expert bead knappers therefore shared an understanding of the sub-goals or technique necessary for producing a high-quality bead roughout, as well as flexibility in the use of those techniques. Novices, on the other hand, were rigid in their ordering of sub-goals. Roux and David concluded that efficient courses of action originate in the command bead knappers have of technique and this conclusion was borne out the variability observed within and between skill levels.

Ivanova (2005) also investigated the role of skill in stone tool manufacture through what she termed the “complex coordinated stroke”, and using experimental data derived from studies of stroke control in novice and expert tennis players, as different motor strokes share many biomechanical features in their organisation. A stroke is a biomechanically complex suite of movements involving multiple body segments and a successful stroke is characterised by the consecutive, organised movement of all these segments to

achieve the final desired velocity. This is achieved through control of impulse transmission between segments and the coordination of appropriate muscle groups. When a discontinuity occurs in this organisational sequence, the stroke fails. Ivanova (2005) concluded that flexibility in linking gestures is the main difference between expert and novice knappers, as well as humans and other primates. Expert tennis players have the most stable stroke kinematics, employ the greatest number of joints, and demonstrate the highest degree of segment coordination, compared to novices who are characterised by their stereotyped and inflexible movement patterns. This is true also for stone knappers of varying skill levels (Biryukova and Bril, 2008, Rein et al., 2014, Bril et al., 2010, Biryukova et al., 2005, Biryukova et al., 2015). Flexibility, then, is key.

Smitsman et al. (2005) broached the question of how flexibility is acquired. They argued that the present tendency to attribute the ascendancy of tool use in human evolutionary history to the development of a computational brain oversimplifies the contribution of the body to learning and skill acquisition. The authors used a dynamical approach to account for the interplay between the brain, sensory, and motor variables in the execution of actions, arguing that flexibility can only be acquired in a social context where it is possible for a novice to observe the verbal and non-verbal cues of more expert knappers during lithic production. Put differently, the ability to observe and imitate more skilled knappers at work is fundamental to improving the efficiency of action dynamics and ultimately to the acquisition of flexibility and skill in stone tool manufacture. Intention, communication, and the ability to link observed behaviour to conceptual goals are fundamental to human knapping behaviours.

Six studies from the *Stone Knapping* volume (Roux and Bril, 2005) all identified the importance of fine coordination and control of elementary movements as the defining feature of technical expertise in knapping. Stone knapping, and therefore control of

conchoidal fracture (Pelegriin, 2005), necessitates the ability to fine-tune the coordination of bimanual elementary movements in order to acquire and develop appropriate courses of action. These studies provide valuable insight on the process of skill acquisition and how it is conceptualised and expressed in a modern population. The results of Smitsman et al. (2005) and others (e.g. Minar and Crown, 2001, Morgan et al., 2015, Rein et al., 2014) indicate that learning stone knapping is inextricably linked with its social context and the socially-constructed scaffolds that enhance learning. This, in turn, has implications for how archaeologists and palaeoanthropologists conceptualise stone tool manufacture in prehistoric populations, especially with regard to questions of cognitive capabilities.

3.2.3 The Tool Use of *Pan* Compared

Wanting as we are for modern representatives of the earliest tool-makers, chimpanzees and bonobos (genus *Pan*) have become the oft-cited modern analogue for these behaviours, as they are perhaps the only species of extant primate with tool-making and tool-use abilities comparable to those of the first tool-making hominins. A comparison of cranial capacities between *Pan* and species of putative tool-makers supports this comparison. *Pan* has a cranial capacity in the range of 282-500 cc. (Tobias, 1971), which is comparable to the cranial capacities of several species of *Australopithecus* suggested to have manufactured stone tools: *Au. garhi* at ~450 cc. (Asfaw et al., 1999), *Au. africanus* average 459 cc. (Carlson et al., 2011), *Au. afarensis* average 481 cc. (Carlson et al., 2011), and *Au. sediba* (MH1) at 420 cc. (Berger et al., 2010). Thus stone tool behaviour emerged prior to the encephalisation suggested to be a pre-requisite for its manufacture, and indeed parsimony supports similar anatomical and cognitive constraints between modern *Pan* and early fossil hominins (Tocheri et al., 2008, Wynn et al., 2011). The propensity of *Pan* to make and use tools, and comparisons of their tool

behaviours with those of fossil hominins, may therefore provide insight into the behavioural innovations that may have contributed to the evolution of the human lineage.

Tool use by chimpanzees in the wild can be extraordinarily varied, ranging from clubbing prey/threats/competitors (Whiten et al., 2009) to using sharp sticks to wound prey or extract food items (Pruetz and Bertolani, 2007); stone tool behaviours occur less frequently and intentional stone flaking has never been observed in wild *Pan*. Chimpanzees in West Africa have been observed to use a hammer-and-anvil technique in nut cracking by placing a nut on an anvil (wood or stone) and, using one or both hands, striking it with a hammerstone in a manner that closely resembles bipolar percussion (Nishida, 1987, Matsuzawa, 1994, McGrew, 2004, Boesch and Boesch-Achermann, 2000, Anderson et al., 2002). The chimpanzees of the Taï Forest in particular use different kinds of stone to crack different species of nuts depending on the hardness of the nut (Boesch and Boesch, 1983). Mercader et al. (2002) have suggested that material found at a nut-cracking site frequented by chimpanzees falls within the range of variation seen for, and are therefore comparable to, Oldowan stone tools. This material nonetheless does not exhibit morphological features expected of intentional hard-hammer percussion, i.e. conchoidal fracture, and instead may only represent an unintentional by-product of nut-cracking.

A number of experimental studies have been conducted to explore the ability of captive bonobos (*Pan paniscus*) and chimpanzees (*Pan troglodytes*) to manufacture Oldowan stone tools by deliberate knapping (Toth et al., 1993, Roffman et al., 2012, Schick et al., 1999, Foucart et al., 2005). One of the first bonobos to be studied, Kanzi, learned to manufacture flakes through observation of a human knapper using freehand hard-hammer percussion to flake cobbles of chert, basalt, and quartzite. Notably, it was

difficult for Kanzi to understand the relationships between platform angles and strike success (e.g. acute angles on the core are better targets for a strike as the force is transmitted obliquely through the stone, shearing off a flake), or consistently generate enough force to produce flakes. Kanzi also defaulted to a direct projectile percussion technique for producing many flakes very quickly as a more efficient means of imparting enough force to the rocks than he was able to generate via hard-hammer percussion (Toth et al., 1993). Roffman et al. (2012) has similarly found that bonobos continue to use projectile percussion or hammering techniques for extracting food items from logs despite being trained in hard-hammer percussive knapping.

Toth et al. (2006) compared the tools manufactured at Gona by fossil hominins, an experienced bonobo (Kanzi), and a very experienced modern human knapper, all using the same raw materials. Their aim was to investigate the nature of skill in each of these assemblages based on morphological characteristics of the stone tools themselves. With regard to these characteristics, Toth et al. (2006) found that the Gona artefacts grouped variously with the modern human sample or as intermediate between the human and bonobo assemblages. The bonobo artefacts clustered as an outgroup in most analyses, tending to be larger than modern human and early hominin tools with a notable hammerstone battering from failed strikes. Bonobo-produced artefacts also tended to be less heavily-reduced than their fossil hominin and human counterparts. Morphological analyses of the flakes and cores indicate that the bonobo tools were produced with a lower impact velocity and less strike accuracy (Toth et al., 2006). In contrast, the Gona assemblage demonstrates a greater degree of skill in terms of reduction; battering scars were less evident than in bonobo tools, and cores were reduced to a greater degree. Bonobo tools were reduced less by comparison. Interestingly, the authors noted that the velocity of the arm swing is lower than what is typically observed in human knappers (Toth and Schick, 2009) and, indeed, modern human knappers can achieve a final

hammerstone velocity of up to 32 km/h (Dapena et al., 2006). Skill in knapping is then clearly predicated on both biomechanical (force generation, hammerstone velocity) and cognitive constraints (strike accuracy, understanding of fracture mechanics).

Until recently (Harmand et al., 2015), the presence of the earliest known complex stone tool tradition at 2.6 million years ago in the archaeological record implied both a cognitive and technological leap but it did not necessarily represent the moment of the leap, merely the first enduring evidence for it. Indeed, the discovery of the Lomekwian technological complex demonstrates that an earlier technological phase preceded the use of conchoidal fracture, where the benefits of a sharp edge were recognised by fossil hominins as useful but the mechanisms to create one effectively remained obscure. Prior to this discovery, this hypothetical preceding technological stage was anticipated to most likely resemble the stone tool assemblages generated by our closest extant relatives, chimpanzees and bonobos (Putt, 2015), and the technological stage preceding to the Lomekwian may yet do so. Chimpanzees and bonobos utilise hammerstones and anvils to crack nuts (Biro et al., 2003, Biro et al., 2006, Boesch and Boesch, 1990, Boesch and Boesch-Achermann, 2000, Kortlandt, 1986, Matsuzawa, 1994, Matsuzawa et al., 2001, Nishida, 1987), and alternative lithic reduction strategies like direct projectile percussion (throwing the objective stone against a hard surface) to split-fracture rocks (Beatty, 1951, Boesch and Boesch, 1990, Goodall, 1964, Nishida et al., 2009, Roffman et al., 2012, Schick et al., 1999, Toth et al., 1993, Whiten et al., 2001). While certainly capable of learning conchoidal fracture techniques, most captive apes will default back to these types of projectile percussive methods to fracture stones as the most expedient means to generate a lot of sharp flakes very quickly. The principle of parsimony supports the notion that the cognitive abilities of early hominins prior to the invention of freehand knapping would be similar to modern chimpanzees and bonobos (Wynn et al., 2011). Nevertheless, the level of cognitive sophistication evinced by

extant non-human primates is still not sufficient for the understanding, control, and implementation of conchoidal fracture to create sharp flakes (Toth et al., 1993, Rein et al., 2014, Roche et al., 1999, Toth et al., 2006).

3.2.4 Summary

To summarise, skill in the production of Oldowan stone tools is characterised by control of bimanual elementary movements, combining precision and force with fine coordination, the ability for which appears to be absent in extant ape tool-users on both a cognitive and a motor level. It is in this way that true stone knapping can be considered to be a uniquely hominin behaviour. While modern experimental research cannot reveal the social arrangements of fossil hominin populations, they can provide insight about the necessary cognitive pre-conditions. At the most basic, Oldowan stone tool technologies would have required social investment in the acquisition of skill beyond simple expedience (e.g. the “smash and grab” methods of lithic reduction used by wild and captive apes) and, by extension, the development of culture and proto-language. Fundamental to this is the development of inter-subjectivity, or the awareness of others as intentional agents (Quine, 1960). Inter-subjectivity provides a means for joint attention and action, through the lens of which simple social interactions are transformed into meaningful communications and connections. It is out of these meaningful interactions that the facility for intentional teaching and learning arise (Rogoff, 1990), revealing one of the impetuses for the development of hominin proto-culture and -language. The shift to knapping from more expedient forms of lithic reduction may consequently reflect a change in dexterity, food resource exploitation/diet, or social structure where tool functionality may have been more important than speed and convenience of production (Morgan et al., 2015). Oldowan stone tool manufacture may have pushed this process one step further by creating

selective pressure in favour of increasing complexity in the mechanisms of social transmission of knowledge (Wynn et al., 2011). The following section will explore the anatomical underpinnings for manipulatory behaviours and the anatomical evidence for stone tool behaviours in fossil hominins.

3.3 The Anatomy of Tool Use

Central to modern human dexterity in the manufacture and use of tools is the suite of morphological features that characterise our hands, arms, and shoulders. We are uniquely suited to these behaviours and unique again for the extensiveness of our tool repertoires. It is unsurprising then that questions of tool competence and proficiency have occupied the majority of investigations on fossil hominin upper limb anatomy, and it presents a particular challenge given the paucity of complete manual and arm remains. The earliest fossil evidence for the first stone tool maker has consequently been difficult to determine unequivocally. Nevertheless, if the release of the upper limb from locomotion is a prerequisite of complex manipulatory behaviours (Corbetta, 2005), then the presence of human-like derived morphology in the shoulder and hand of fossil hominins may be used to infer their manipulatory capabilities (and, inferentially, their degree of bipedality).

3.3.1 A Show of Hands: The Morphological Correlates of Tool Grips

The fossil remains of *Homo habilis*, specifically the Olduvai Hominid 7 (OH 7) manual remains, have historically been associated with Oldowan stone tools, which has bolstered the impression that *H. habilis* was the first stone tool maker as early as 2.4 million years despite the associations being problematic (Napier, 1962b, Leakey, 1960). The first evidence for a generalised human hand, however, appears in the fossil record with only *Homo antecessor* at 0.8 million years (Lorenzo et al., 1999) and a full suite of human-like hand characteristics with *Homo neanderthalensis* at approximately 0.2

million years (Tocheri et al., 2008). Traditionally, approaches to studying hand morphology have fallen into two categories: those that investigate hand grips and biomechanics compatible with tool manufacture and use, and those that look at the morphological correlates for those behaviours (Marzke, 2013). There are many extensive studies of the muscular and bony architecture of the primate hand and lower arm which have demonstrated a close correlation between structure and function in these anatomical regions (Ciochon and Corruccini, 1976, Leakey et al., 1964b, Marzke, 1997, Marzke et al., 1992, Tocheri et al., 2003, Tocheri et al., 2008, Tocheri et al., 2005, Napier, 1962b, Rolian and Gordon, 2014, Rolian and Gordon, 2013, Alba et al., 2003, Almécija and Alba, 2014, Almécija et al., 2010, Moyà-Solà et al., 2008). These studies have demonstrated that the features fully consistent with the requirements of tool behaviours are distinctly human but that aspects of the morphology that facilitates these behaviours are present in certain species of extant non-human primates and fossil hominins.

Comparative studies of tool manufacture in modern humans with comparable behaviours in extant primates (e.g. chimpanzee feeding behaviour) have illustrated the distinctiveness of human grips and their efficacy in the fine control of hammerstone trajectories and strike patterns. Napier's (1956, 1960, 1962a, 1962b) seminal comparative studies of primate hand morphology and prehensile behaviour concluded that the capacity to make and use stone tools is facilitated by our ability to make 'power' and 'precision' grips and to compensate for the large internal and external forces exerted on the hand during bimanual percussion. The power grip is characterised by a clamp being formed by the flexed fingers and palm and counter pressure applied by thumb as it lies approximately in the palmar plane, such as one might observe while grasping a cylindrical object (Fig. 11a). The precision grip, on the other hand, pinches the object between the flexor aspects of the fingers and thumb (Fig. 11b). Marzke

(1997) further broadened these categories to include subtypes of these two grips to what she called *forceful* precision grips (see also Marzke and Wullstein, 1996). This included the “three-jaw chuck” grip, in which the thumb, index, and third finger cup the object which is then supported by the flexed fourth and fifth fingers (Fig. 11c), and the “cradle grip” in which the thumb and finger pads cup the object – generally the tool stone – allowing for the working edges of the tool to remain exposed while resisting the large external forces exerted during the hammerstone strike (Fig. 11d). A final grip is the pad-to-side flake grip, where the flake is held between the pad of the thumb and the side of the index finger (Fig. 11e).

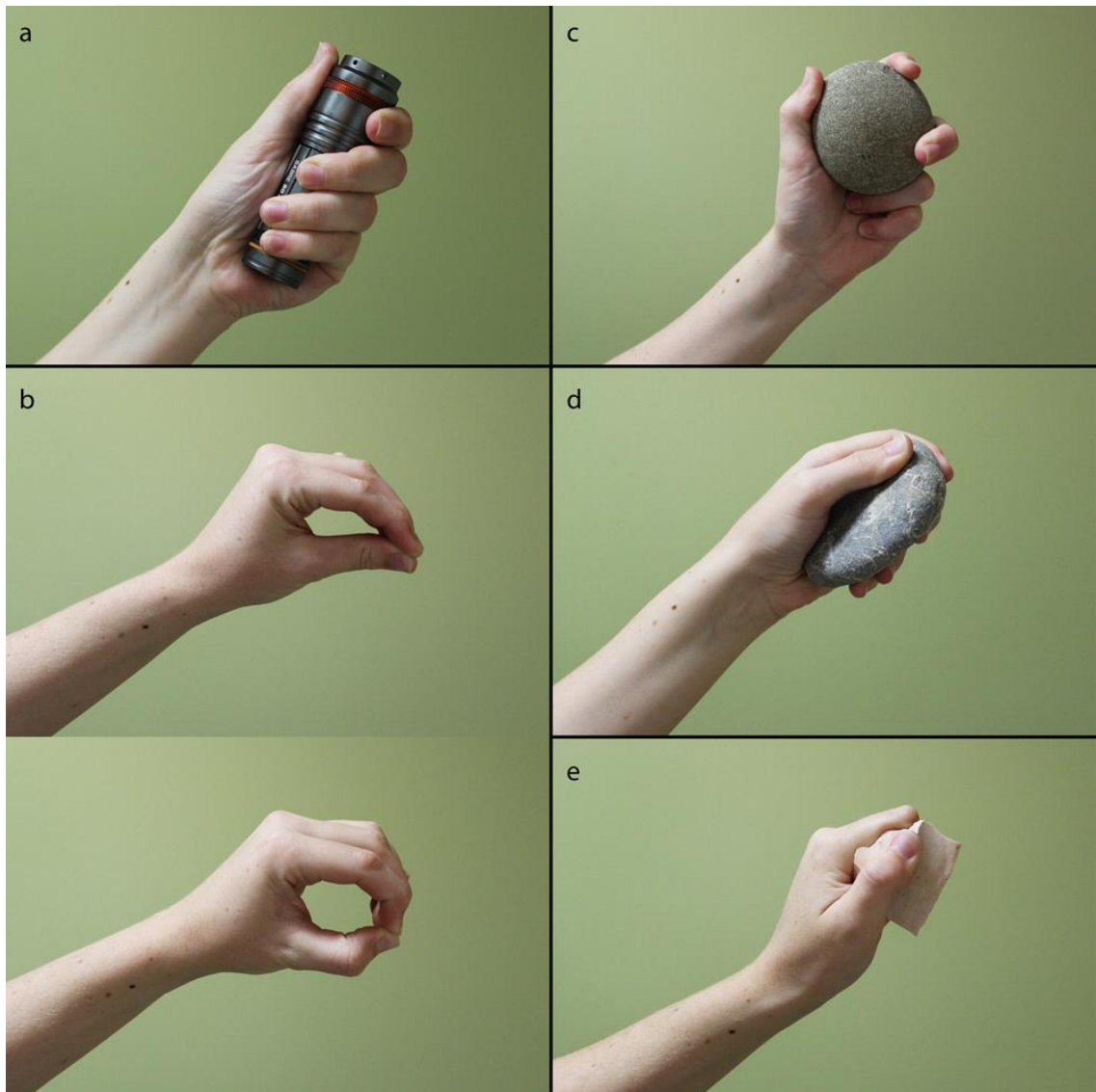


Figure 11. Human hand grips. (a) The ‘power’ (squeeze) grip of a cylindrical object - in this case a torch. (b) Two versions of the ‘precision’ (pinch) grip. Top: Pad-to-pad pinch grip. Bottom: Tip-to-tip pinch grip. (c) Three-jaw chuck grip of a hammerstone. (d) Cradle grip. (e) Pad-to-side pinch grip. Photos by E. Feuerriegel.

A number of studies have attempted to discern adaptive changes to hand morphology across different stages in the evolution of tool behaviour (i.e. stone and non-stone related) in hominins, with an emphasis on the importance of both the precision and power grips (Marzke, 1997, 2013b, Marzke and Marzke, 2000, 1987, Marzke and Wullstein, 1996, Marzke et al., 1992, Alba et al., 2003, Almécija and Alba, 2014, Rolian and Gordon, 2014, Rolian and Gordon, 2013). Modern humans are distinctive in the morphology and orientation of the carpometacarpal joints for digits 2-5 which facilitate cupping behaviours. The second and fifth metacarpal heads in particular

demonstrate marked asymmetry, such that the radial side of the articular surface on the second metacarpal on the volar aspect projects radially and bevels dorsally in an ulnar direction (Marzke, 1997). A similar pattern is also observable on the ulnar side of metacarpal V. These features cause tension in the adjacent collateral ligament during flexion of the proximal phalanx, pronating the index finger and supinating the fifth finger, and bringing the palm into full contact with the surfaces of the held object no matter how irregular the shape (Marzke, 1997, Marzke, 2013, Marzke, 2005).

The orientation of the second metacarpal joint surface of the trapezium in particular is distinctive in modern humans, lying in more of a transverse/coronal plane compared to chimpanzees and gorillas (Tocheri et al., 2003), as is the presence of a continuous articular facet between the second metacarpal and capitate that is convex (Lewis, 1977, McHenry, 1983). This contrasts to extant apes in which the capitate articular facet on the second metacarpal is discontinuous, aligned in a sagittal plane, and bisected by the carpometacarpal ligament, all of which serve to limit axial rotation of the second metacarpal in extant apes (Lewis, 1973, Lewis, 1977, Drapeau et al., 2005). Modern humans have relatively large and robust joint sizes at the thumb and fifth finger (Marzke et al., 1992) which are consistent with the strong muscle contraction in power grips reported by Chao et al. (1976). According to Marzke et al. (1998), the first and fifth digits are subject to strong loading from repeated powerful recruitment of both the extrinsic and intrinsic muscles during stone knapping. The prediction may therefore be made that early tool makers would also have been subject to similar patterns of loading and may also have proportionately robust first and fifth digit architecture as an adaptation to these manipulatory behaviours.

Tocheri and colleagues (Tocheri et al., 2003, Tocheri et al., 2008, Tocheri et al., 2005) have conducted a series of comparative three-dimensional analyses of the carpals and

metacarpals of modern humans, extant apes, and fossil hominins and found that the derived configuration of the modern human distal carpal row compensates for the radioulnar stresses exerted by strong pressures from the thumb. Modern humans also have relatively larger joint surface areas for the articular facet of the first metacarpal and scaphoid on the trapezium which accommodates the large axial loads from the thumb during manipulation (Tocheri et al., 2005). Great apes, conversely, have larger relative joint surface areas for the articular facets for the second metacarpal and scaphoid which is related to the loading of the second finger during locomotion. Another uniquely derived feature in modern humans is the morphology of the third metacarpal; the head is radially orientated towards the thumb in humans (Susman, 1979), and when flexed, this allows the third digit to be brought in opposition to the thumb which, along with the second digit, facilitates cupping of the hand around tool objects like hammerstones. The broad boot shape of the trapezoid, the proportionally larger, volar-positioned joint surface between the trapezoid and capitate, and presence of a third metacarpal styloid process on the radiodorsal aspect, all serve to stabilise the palm against the volar forces that accompany hard-hammer percussion (Tocheri, 2007, Marzke and Marzke, 1987).

Manual proportions play an important role for control of tools in precision grips. Having a proportionately longer thumb relative to the rest of the hand allows for the terminal pad of the thumb to control objects through digit tip-to-tip opposability, especially during rotation, translation, and pinch grips (Marzke, 1997, Rolian and Gordon, 2013). The medial digit-to-thumb ratio in modern humans is the lowest of the great apes but comparable to that observed in baboons (Napier, 1993) - and baboons have also been observed to be highly proficient in manual feeding behaviours, and particularly precision gripping (Etter, 1973). The reason for this similarity is convergence; a long thumb in baboons is likely an adaptation to frequent weight-bearing during digitigrade locomotion where the thumb contacts the substrate regularly

in the touchdown phase (Almécija et al., 2010). Consequently, the manipulative proficiency of baboons may actually represent an exaptation resulting from adaptation of the baboon hand to digitigrade locomotion rather than positive selection for pad-to-pad opposability and precision grips in these species. Other similarities between baboons and modern humans include broad apical tufts and distal finger pads, a large palmar fossa, and equivalent ratios for bone versus long flexor tendon dimensions (Almécija et al., 2010), and these convergences may indeed be related to enhanced manipulatory behaviours (Etter, 1973, Jolly, 1970). Notably, however, and unlike modern humans, thumb-to-second digit precision gripping has not yet been observed in any baboon species (Jude, 1993, Marzke, 2013), likely due to the flatter trapeziometacarpal joint in baboons (Marzke et al., 2010). In the context of hominin tool behaviour, the presence of a long thumb is significant because it speaks to the manipulatory capabilities of fossil species and their ability to effectively control stone tools with the volar aspect of the fingers when extended or partially flexed. In this case the length of the thumb is directly proportional to the degree of control the individual has over the object being manipulated. For fossil hominins participating in behaviours that require strong precision or pinch grasping of tools, fully modern or near-modern manual proportions would have been necessary.

The strength of human hand grips is an integral factor in the success of the stone knapping strike – that is, the ability of the hand to resist displacement of the tool by the large external forces associated with it – which in turn is dependent on the musculature of the hand. Marzke, Napier, and others have conducted a number of studies into the hand during stone knapping that identify particular musculoskeletal features of the thumb, including a well-developed and independent M. flexor pollicis longus (FPL) (Napier, 1962a, Tuttle, 1992), that enable power and precision grips. In addition to this, Marzke and colleagues have conducted a series of electromyography (EMG)

experiments monitoring muscle recruitment in the hands during stone knapping and comparing the mechanics of the muscles strongly recruited by hard-hammer percussion across a number of primate species.

Both Marzke et al. (1998) and Hamrick et al. (1998) used EMG to study the behaviour of the FPL, concluding that a powerful FPL muscle functioned to stabilise the terminal pollical phalanx in early hominins during frequent and forceful use of unmodified stone tools. Other muscles found to be highly recruited in these grips during stone knapping include *Mm. opponens pollicis*, *flexor pollicis brevis*, *flexor digiti minimi*, *abductor pollicis (transverse)*, and *first palmar interosseous* (Marzke et al., 1998). These muscles aid in the cupping of the radial and ulnar sides of the hand to accommodate the stones as well as stabilising the fifth finger and thumb to prevent displacement of the stone. While not reported in the Marzke et al. (1998), *M. flexor pollicis longus* has been reported as highly recruited during the power and three-jaw check grips in the experiment conducted by Hamrick et al. (1998). *M. flexor pollicis longus* is distinct in humans in the asymmetry of its attachment to the pollical distal phalanx (Shrewsbury et al., 2003). The insertion is marked on the distal phalanx of the thumb and described by Shrewsbury et al. (2003) as an asymmetrical “gable-shaped projection” that is longer on the distal aspect, reflecting the emphasis on the fibres of the FPL that pronate the thumb during flexion.

One of the most interesting findings of the Marzke et al. (1998) study was the strong recruitment of the muscles that rotate and flex the fifth digit to place it in opposition to the thumb in postures that “cup” the hand, i.e. the cradle and the power squeeze grips. Typically, the fifth digit has not been deeply considered in evolutionary studies of hominin hand morphology. The intrinsic muscles of the first and second digits are also highly recruited, in particular the three muscles that move and stabilise the

trapeziometacarpal joint during opposition of the thumb with the fingers. These are Mm. adductor pollicis, flexor pollicis brevis (superficial head), and the first dorsal interosseous. M. first dorsal interosseous also functions to abduct and pronate the second digit. Similar to Hamrick et al. (1998), Marzke et al. (1998) found that the FPL is primarily recruited in power squeeze grips.

Comparisons of human and chimpanzee muscle potential for exerting torque at the hand and wrist have shown that humans have larger thumb tendon moment arm lengths in both flexion/extension and parasagittal abduction/adduction than chimpanzees (Marzke et al., 1999). Modern humans, therefore, were more efficient in generating muscle torque which is advantageous in manipulatory behaviours as repeated contraction of the thumb muscles at high levels is energetically demanding. Marzke (2006) suggested that the reason for this muscular advantage may lie with the intrinsic muscles at the trapeziometacarpal joint which move and stabilise the thumb. The lateral belly of the first dorsal interosseous muscle in humans attaches to the first and second metacarpals as well as the base of the proximal phalanx on the lateral aspect. In this way the first dorsal interosseous counterbalances the pull of the intrinsic muscles across the trapeziometacarpal joint during flexion and extension of the distal thumb by the extrinsic muscles. The origin of the lateral belly of M. first dorsal interosseous muscle in humans differs from non-human primates in the large muscle scars associated with it and the length of the distal extent on the first metacarpal. Thus the presence of a large, human-like scar for this muscle, as well as human-like insertion morphology for the FPL, in fossil hominin manual remains may be indicative of strong recruitment of this muscle in stone tool behaviours. These features and the movements they facilitate (i.e. pronation and supination) are fundamental to the ability of the human hand to securely grasp and accommodate a variety of object shapes essential to the human precision and power squeeze grip grips as well as the skilful manipulation of tools.

3.3.2 Put a Shoulder (Or an Elbow) Into It: The Morphological Correlates of Tool Use in Upper Arm

Naturally, there has been an almost overwhelming focus on the hand during tool manufacture and use, and consequently the shoulder has been studied in more limited detail. The shoulders of modern humans are characterised by dorsally placed scapulae with laterally-orientated glenoid fossae, relatively long clavicles, and a high degree of humeral torsion. A proximally orientated olecranon process has been identified as one trait associated with the elbow of modern humans that enhances the manipulatory performance of the upper limb. The primary extensor of the elbow is *M. triceps brachii* muscle which has its sole insertion on the proximal aspect of the olecranon process of the ulna, and it is one of the largest and strongest muscles of the arm in both modern humans and chimpanzees (Amis et al., 1979, Thorpe et al., 1999). A short olecranon is suggested to be the primitive condition for the hominoids as it is observed in all extant ape species with the exception of modern humans, and it is generally interpreted as an adaptation arboreal climbing behaviours (Aiello and Dean, 2002b, Aiello and Dean, 2002a, Aiello et al., 1999, Tuttle and Basmajian, 1974, McHenry et al., 1976). In comparison to other apes, modern humans have a relatively long olecranon process proximodistally which has been interpreted as a derived character state associated with tool manufacture and use (Tuttle and Basmajian, 1974, Aiello and Dean, 2002a).

The bony lever of the triceps is formed by the olecranon process and as such its length and orientation has been used widely in the literature to infer upper limb functional specialisation in primates (e.g. Drapeau, 2008a, Drapeau, 2004, Oxnard, 1963, McCrossin et al., 1998, Jolly, 1966, Jolly, 1972). A superiorly orientated olecranon provides the maximal amount of leverage to *M. triceps brachii* during flexion of the forearm, whereas a posteriorly orientated olecranon confers greatest leverage during full

forearm extension, such as is seen in knuckle-walkers where the triceps muscle is active in preventing elbow collapse during locomotion (Drapeau, 2004, Tuttle and Basmajian, 1974). In modern humans (with their superiorly orientated olecranon), this means that greatest mechanical advantage is conferred to the triceps during behaviours such as hammering and scraping. So the orientation and length of the olecranon process may be an important indicator of tool capabilities in fossil hominins.

Humeral torsion is another feature of the upper limb that is potentially informative about the manipulatory capabilities of fossil hominins. Humeral torsion (HT) refers to the orientation of the humeral head relative to the long axis of the distal humeral articular surfaces (Fig. 12) and it is widely considered to be an important component of increased mobility in the glenohumeral joint (and thus the development of suspensory postures, locomotion, and manipulatory capabilities). Modern humans, on average, have some of the highest angles of torsion (that is, more medially orientated humeral heads) ranging between 141° – 178° (Krahl and Evans, 1945, Larson, 1988). Humeri with posteriorly oriented humeral heads (that is, low torsion) have torsion values between 90° – 120° , with 90° being equivalent to 0° in the clinical literature (e.g. Pieper, 1998, Reagan et al., 2002). The higher the torsion value, the more medially directed the humeral head: a torsion value of 180° indicates a humeral head orientated directly medially.

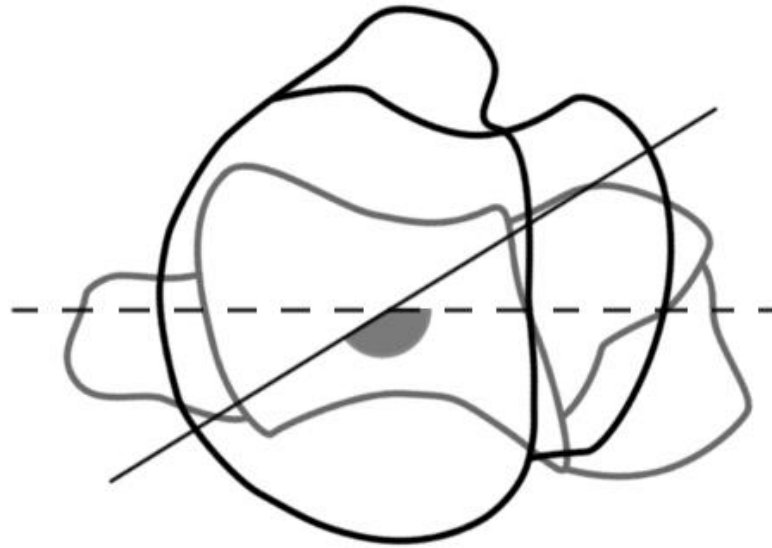


Figure 12. Proximal view of a right modern human humerus with ends superimposed. The horizontal dashed line represents the mediolateral axis of the distal articular surface; the solid line represents the long axis of the proximal epiphysis. Humeral torsion is measured as the angle (marked in grey) between the two axes. Illustration by E. Feuerriegel, modelled after Krahl (1947).

The degree of humeral torsion and scapula position has a significant effect on the range of motion available at the shoulder (Larson, 2007) (Fig. 13). In shoulders characterised by laterally positioned scapulae with anterior facing glenoid fossae and low humeral torsion (Fig. 8a), elevation of the arm is primarily limited to forward flexion. Low torsion also influences the plane in which the elbow functions, creating a lateral set to the elbow that constrains the ability of the arm to be placed directly in front of the torso in shoulders with laterally-orientated glenohumeral joints. This, by extension, would impact markedly on the manipulatory capabilities of any individual possessing such a shoulder, as greater flexibility and range of motion in this area would be beneficial for the performance of manipulatory behaviours: stone knapping, for example. In shoulders with dorsally positioned scapulae (such as those in Neanderthals and modern humans), the glenoid fossa is reoriented so that it faces laterally, permitting true abduction and

horizontal extension at the shoulder and dramatically increasing the range of glenohumeral mobility. The range of possible motion available at the shoulder will vary depending on the degree of humeral torsion. In humeri with modest torsion (Neanderthals, for instance; Fig. 13b anatomical right side), the arm has a greater range of external rotation but somewhat less internal rotation, while in humeri with high torsion (e.g. modern humans; Fig 13b anatomical left side) a much greater degree of internal rotation may be achieved, but at the cost of less external rotation. Modest to high torsion allows for a parasagittal set to the elbow (as opposed to a lateral set as with humeri with low torsion). This allows the hands to be positioned closer to the body, a condition that would clearly be advantageous for tool manufacture and use.

As high humeral torsion is a condition we share with African apes (Krahl and Evans, 1945, Krahl, 1947, Evans and Krahl, 1945), it is often cited as being a shared derived feature of both apes and humans (e.g. Martin, 1986, Le Gros Clark, 1959, Andrews, 1985). Larson (1988) put forward the hypothesis that HT in African apes is directly related to knuckle-walking. As a medially orientated humeral head is important for maintaining a parasagittally operating elbow and quadrupedal postures such as those involved in knuckle-walking require that the elbow operate in a parasagittal plane, knuckle-walking apes must necessarily have high degrees of torsion; a lateral set to the elbow would be mechanically inefficient in these circumstances. High torsion in modern humans, in this case, is somewhat of an anomaly. It has been suggested previously (most notably by Washburn, 1971, 1974, 1978) that knuckle-walking is a shared derived feature of hominins and African apes. This, however, seems unlikely as early hominins do not display the requisite amount of torsion necessary for such habitual postures (see Section 3.4.1 and 3.4.2). A possible explanation for human HT, then, is as an independently acquired characteristic that evolved as an accommodation to tool manufacture and use (Larson, 1996). While it is impossible to test this

hypothesis, it is evident that a high degree of humeral torsion nonetheless improves the range of motion available at the shoulder and elbow in a parasagittal plane.

The presence of high humeral torsion is also associated with dorsal repositioning of the scapula and lowering of the scapula glenoid fossa orientation from cranial to lateral (Larson, 2013). Significantly, high humeral torsion is only a functional requirement of a laterally-orientated glenoid fossa if it is necessary that the elbow to operate in a parasagittal plane (Inman et al., 1944). Thus a lowering of the scapular glenoid orientation in fossil hominins may also be inferred to reflect further morphological commitment of the upper limb to manipulatory behaviours over locomotion.

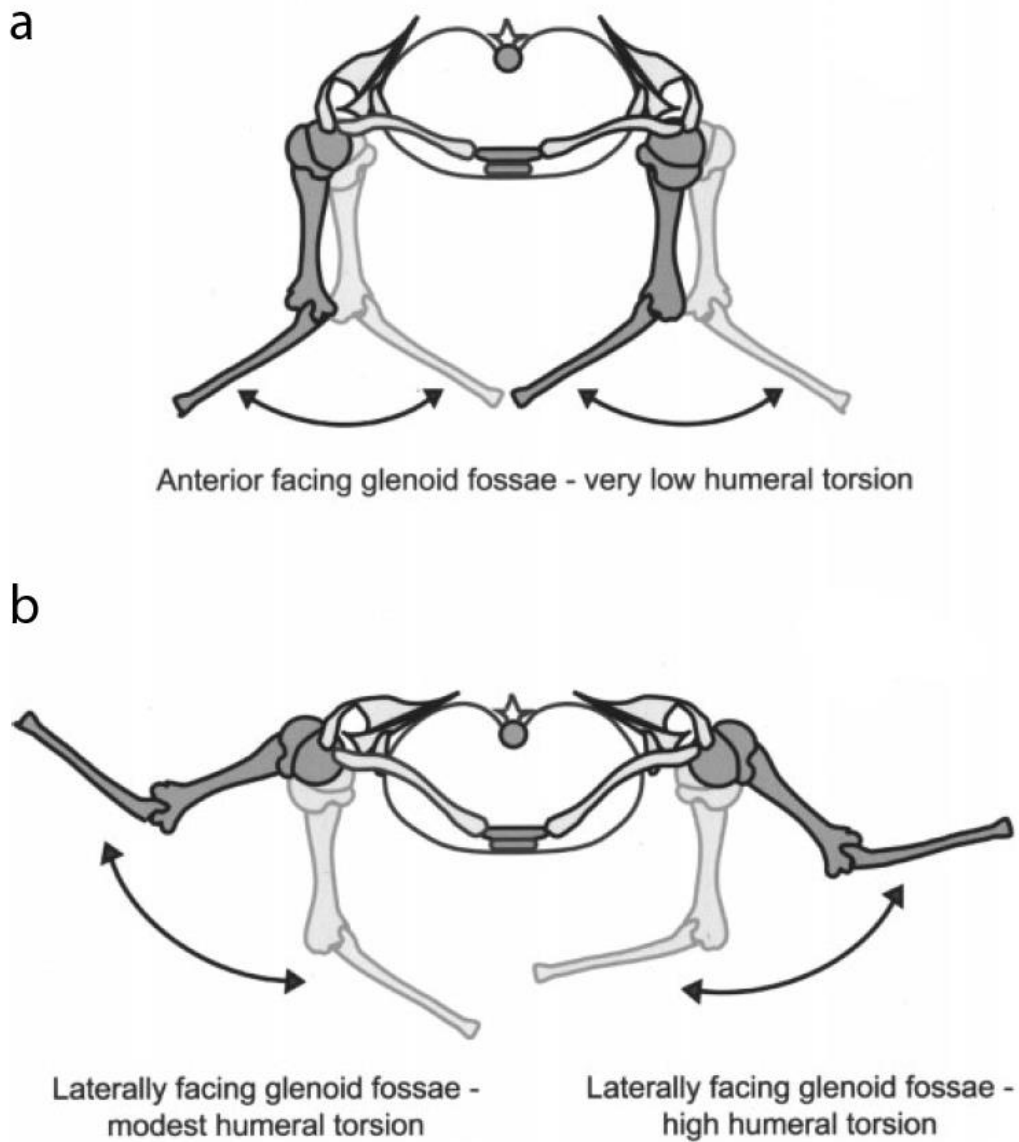


Figure 13. Range of motion in hominin shoulders as dictated by scapula position and degree of humeral torsion. The semi-transparent limb images illustrate the suggested range of motion due to humeral rotation at the shoulder. **(a)** Hominin thorax in superior view with laterally positioned scapulae and low torsion. **(b)** Hominin thorax in superior view with dorsally positioned scapulae and different degrees of humeral torsion per side. Right side: modest humeral torsion; left side: high humeral torsion. The humeral heads are in the same position relative to the glenoid on both sides but the right arm with less torsion has a comparatively greater range of external rotation but at the cost of a decreased range of internal rotation. The left arm is able to achieve greater internal rotation but less external rotation due to its greater degree of HT. Modified from Larson (2007:180).

3.4 Fossil Evidence for Adaptation to a Novel Behaviour

As the previous section highlights, the upper limb anatomy of modern humans is both unique and compatible with functional requirements – both in terms of manipulatory capabilities and managing the resultant biomechanical stressors – for stone tool behaviours. It is important to note, however, that this uniqueness arises out of the presence of these features as a complex rather than just as individual features. The upper limb of modern humans is armed and engined for the use of the arm as a manipulatory organ (as opposed to locomotion or even a compromise between the two behaviours) and this encapsulates a suite of features. When this pattern is broken down into its component parts, isolated morphological features or certain combinations thereof are revealing of grip and range of motion proficiencies in the human lineage. The following section presents a review of the fossil material and the possible evidence for commitment to tool behaviours in these species.

3.4.1 Early Hominins: *Australopithecus* and *Ardipithecus*

The species discussed in this section include *Australopithecus sediba* (known from Malapa, South Africa; Berger et al., 2010), *Australopithecus africanus* (known from Taung (Dart, 1925), Gladysvale (Berger et al., 1993), Sterkfontein (Broom et al., 1950, Vrba, 1979, Toussaint et al., 2003, Clarke, 2013), and Makapansgat (Reed et al., 1993, Dart, 1948)), *Australopithecus afarensis* (known from Hadar (Taieb et al., 1975, Drapeau et al., 2005, Johanson et al., 1982, Bush et al., 1982), Dikika (Alemseged et al., 2006), Maka (White et al., 2000), and Woranso-Mille (Haile-Selassie et al., 2010) in Ethiopia, and Koobi Fora (Kimbel, 1988) and possibly Lothagam (Kramer, 1986) in Kenya), *Australopithecus anamensis* (Kanapoi and Allia Bay, Kenya (Ward et al., 2013, Leakey et al., 1995, Leakey et al., 1998) and Fejej (Ward, 2014), Ethiopia), and *Ardipithecus ramidus* from Aramis, Ethiopia (White et al., 1994)

Shoulder material for early species of hominin tends to be fairly fragmentary. Three important scapula fossils are the MH2 *Australopithecus sediba* scapula (Berger et al., 2010, Churchill et al., 2013), Sts 7 (Broom et al., 1950) attributed to *Australopithecus africanus*, and A.L. 288-11 (Johanson et al., 1982) attributed to *Australopithecus afarensis*. In these three fossils, the orientation of the glenoid fossa has been of greatest interest to paleoanthropologists as it is considered to be the feature capable of revealing most about the functional anatomy of the australopithecine shoulder. In most hominoids the glenoid faces cranially which is indicative of an emphasis on overhead limb postures, whereas the glenoid of modern humans is oriented more laterally, reflecting the characteristically lowered position of the arm (Larson, 2009, Oxnard, 1969a). In all three specimens, the glenoid fossa faces more cranially than in modern humans indicating that *Au. sediba*, *Au. africanus*, and *Au. afarensis* likely retained some commitment to arboreal locomotion and climbing (Oxnard, 1968, Vrba, 1979, Arias-Martorell et al., 2015, Churchill et al., 2013, Stern and Susman, 1983). A recent find from Dikika, Ethiopia, of the juvenile *Au. afarensis* scapula DIK-1-1 similarly has a cranially directed glenoid (Green and Alemseged, 2012, Alemseged et al., 2006) which supports the characterisation of *Au. afarensis* as having a cranially-directed scapular glenoid. Of the coracoid process, the dorsolateral tubercle is quite projecting and placed more laterally than in modern humans, which has been interpreted by Vrba (1979) in *Au. africanus* to reflect a scapula positioned high on a funnel-shaped thorax with an oblique clavicle – a configuration very similar to that of extant apes and *Au. afarensis*.

Two clavicle specimens are known from *Au. sediba*, one each from the adult individual (MH2) and the immature individual (MH2; Churchill et al., 2013). In terms of length, Churchill et al. (2013) describe the right clavicle of MH2 as short both relatively (compared to humeral length) and absolutely in comparison to larger-bodied specimens such as *Au. afarensis* clavicle KSD-VP-1/1f from Woranso-Mille (Haile-Selassie et al.,

2010) and *Homo*. Both the MH2 and MH1 clavicle shafts inflect inferomedially with, in the MH2 specimen at least, joint surfaces at the sternoclavicular joint that imply an oblique orientation to the clavicle, the combination of which Churchill et al. (2013) interpret as reflecting a scapular positioned high on the thorax. The oblique positioning of the clavicle in early hominins supports the interpretation of the early hominin shoulder as more primitive than that of modern humans, indicating some stabilising selection for competence in postures that placed the arm habitually overhead (Ward, 2013).

While the fragmentary nature of most early hominin humeri makes interpretation difficult, the humeral heads appear to be elliptical with an intertubercular, or bicipital, groove that is relatively shallow – unlike African apes with their spherical humeral heads and deep, tunnel-like bicipital groove. The Sts 7 humerus has been described by Broom et al. (1950) as similar in most respects to modern humans, though the tubercles were distinct in that the lesser tubercle is more prominent than typical of modern humans and extant apes. The KNM-BC 1745 and the A.L. 288-1r proximal humeri have also been described as possessing projecting lesser tubercles (Johanson et al., 1982, Pickford et al., 1983). As all known early fossil humeri are incomplete or damaged, accurate measurement of humeral torsion had presented a significant obstacle in evolutionary studies, but Larson (1996) devised two methodologies for estimating the degree of humeral torsion on incomplete fossil humeri using sets of alternative reference axes and multiple regression analyses. The results of Larson's (1996) study of proximal fossil humeri established torsion measurements of 124° for AL 288-1r, 126° for Sts 7, and 130° for Omo 119-73-2718 (attributed by Howell and Coppens (1976) to *Au. cf. africanus*). Larson also measured torsion on the distal humerus KNM-ER 739 (assigned to *Paranthropus cf. boisei*; Howell and Coppens, 1976) gaining a measurement of 111°. Contrary to previous expectations of high torsion as a shared derived feature, all Plio-

Pleistocene hominin humeri display low to modest amounts of humeral torsion. Larson (1996) concluded that the shared high degree of torsion in great apes and modern humans is an independently acquired characteristic, and that its similarity in hominoids is due to convergence. These results are further reinforced by torsion measurements from *Au. sediba*: MH2 has an estimated humeral torsion value of 117° and the MH1 juvenile specimen a value of 112°, both which suggest more posteriorly-directed humeral heads than most other australopiths (Churchill et al., 2013).

Moving down the arm, most early hominins exhibit a proximal ulna morphology similar to modern humans (Drapeau, 2004, Drapeau et al., 2005). Drapeau (2004, 2005) quantified olecranon process orientation in four fossil hominin ulnae: A.L. 438-1 and A.L. 288-1 (both attributed to *Au. afarensis*; Drapeau et al., 2005, Johanson et al., 1982), L40-19 ascribed to a robust australopith of uncertain species (Howell and Coppens, 1976, McHenry et al., 1976), and the OH 36 ulna whose taxonomic status remains uncertain. This latter fossil has previously been attributed to *Paranthropus boisei* (Walker and Leakey, 1993, Aiello et al., 1999) and *Homo erectus* (= *Homo ergaster*) (Day, 1978, Leakey, 1978, Day, 1986) but see Section 3.4.2 for a more in-depth discussion of this fossil. Drapeau found that early hominins – exclusive of *Ardipithecus ramidus* which reportedly maintains a retroflexed olecranon much like great apes (Lovejoy et al., 2009) – have a *M. triceps brachii* lever arm that is more proximally orientated than the condition found in great apes, the former falling outside the sample ranges for apes and more closely aligning fossil hominins with humans near the mean (L40-19) and higher end of sample ranges (A.L. 438-1, A.L. 288-1, and OH 36). Proximal ulna orientation has not been studied in *Au. sediba*, although Churchill et al. (2013) do report a metric called triceps mechanical advantage (TMA), calculated as olecranon process length divided by the articular length of the ulna (from proximodistal midpoint of trochlea notch to distal-most articular surface of head). While it is unclear

how comparable this metric is to those reported by Drapeau (2004, 2005), it does appear that *Au. sediba* falls within the ranges reported for other australopiths and early *Homo* (Churchill et al., 2013), evincing a broadly similar morphological pattern. A proximally orientated olecranon, then, would appear to be the condition for hominins. This morphology, as mentioned previously, derives its advantage in providing greater mechanical leverage to the triceps brachii during 90° arm flexion, maximising the power the flexed forearm. Given that it appears unlikely that quadrupedalism involving forearm flexion was a significant selective pressure in *Australopithecus* species (Ward, 2013), it is probable that the proximally orientated olecranon of early fossil hominins arose through directional selection for manipulatory behaviours, if not necessarily tool manufacture.

Prior to the australopiths, *Ardipithecus ramidus* displays a continuous facet for the capitate on the second metacarpal (Lovejoy et al., 2009), indicating an early origin for this trait. According to Lovejoy et al. (2009), the terminal phalanx of the first ray in *Ar. ramidus* exhibits a prominent marking for *M. flexor pollicis longus* and digit proportions more similar to the condition observed for Old World monkeys and *Proconsul*, both features they attribute to arboreal quadrupedalism. Notably, what *Ar. ramidus* does *not* exhibit is any of the derived morphologies of the second, third, or fifth metacarpals associated with cupping of the hand in forceful precision grips. *Ardipithecus*, it would seem, was not a tool maker though selection for enhanced manipulation was likely well under way based on the continuous capitate facet.

Australopithecus afarensis is one of the better represented species in terms of the manual remains available for study (Bush et al., 1982, Drapeau et al., 2005), which has allowed, through 3D reconstruction techniques and mirroring, the construction of a nearly complete hand (Marzke, 2005). Significantly, with a temporal range of 3.6 – 3.0

million years ago (Brown et al., 2007), *Au. afarensis* pre-dates the first appearance of the Oldowan technological complex over a million years but falls within the temporal period attributed to the Lomekwian at 3.3 million years. Perhaps unsurprisingly then, aspects of the *Au. afarensis* hand morphology are primitive. According to Marzke (1997, 1983, Marzke et al., 1992), the fifth metacarpal lacks the robusticity and saddle-shaped joint topography of modern humans, the latter of which would have limited rotation/supination at this digit and thus reducing the efficacy of any grip involving flexion, abduction and rotation of the fifth metacarpal (e.g. the squeeze grip, precision grip between the thumb and four fingers). In addition to this, the trapeziometacarpal joint of *Au. afarensis* has a decidedly chimp-like topography and curvature (Marzke, 2005). While this morphology would have stabilised the thumb during opposition with the second digit, it is purchased at the price of the cradle grip – an integral grip for controlling large objects – by limiting excursion of the thumb to oppose it with the fifth digit. Nevertheless, there is evidence for an origin for the first dorsal interosseous muscle on the first metacarpal, though it is smaller than observed in modern humans (Marzke, 2005). Such a diminutive origin for this muscle in *Au. afarensis* is indicative of less internal stress exerted on the thumb by the extrinsic and intrinsic muscles of the medial hand than in modern humans (Marzke, 2005). All second metacarpals attributed to this species also exhibit continuous capitulate facets, a human-like condition that implies a missing carpometacarpal ligament as well as a human-like capability for pronation of the second digit (Bush et al., 1982, Drapeau et al., 2005, Marzke, 2005, Marzke and Shackley, 1986, Tocheri et al., 2003). Thus the absence of the carpometacarpal ligament (observed in apes) appears to be apomorphic hominins. *Au. afarensis* also exhibits a transversally and coronally orientated facet for the trapezoid which is, again, similar to humans (Tocheri et al., 2003). Unlike humans, the third metacarpal does not exhibit the proximal styloid process but it is probable that *Au.*

afarensis maintained a palmar stabilising ligament based on the presence of a conducting groove on the hamate similar to humans (Marzke and Marzke, 1987). Finger lengths were reduced in *Au. afarensis* meaning that the thumb was relatively long and human-like in terms of its proportions (Almécija and Alba, 2014).

Based on these features, it would appear that *Au. afarensis* had a basically human-like capability for grasping if not a human-like grasp strength or ability to resist the large loads exerted across the thumb and wrist during hard-hammer percussion. The topography of the first and second carpometacarpal joints would have facilitated cupping postures of the hand and fine control of objects by the thumb, as well as the three-jaw chuck grip and the side-to-side pinch grip, and these grips would have been stabilised by the primitive trapeziometacarpal joint morphology. The overarching morphological pattern exhibited by *Au. afarensis* is suggestive of a hand that could be effectively used in tool behaviours like nut or bone pounding (i.e. controlling a spherical hammerstone) or gripping a flake in a side-to-side pinch grip. While the evidence for tool-assisted meat processing presented by McPherron et al. (2010) is problematic (see Domínguez-Rodrigo et al., 2011, Domínguez-Rodrigo et al., 2010), there is little doubt that *Au. afarensis* possessed the manipulative prerequisites for these behaviours.

A nearly complete hand and wrist from a single individual, MH2, represents the most complete manual remains presently known for *Au. sediba* though MH1, the immature individual, does have an isolated third metacarpal associated with it (Kivell et al., 2011). The MH2 hand is complete and undistorted barring only the four distal phalanges of the fingers and the trapezium, trapezoid, and pisiform, which are absent. MH2 has a long thumb relative to finger lengths and shares many hand features with *Au. afarensis* including asymmetrical metacarpal heads and primitive carpometacarpal joint orientations. The base of the fifth metacarpal is particularly robust which Kivell et al.

(2011) associate with well-developed intrinsic and extrinsic musculature for this digit (i.e. Mm. flexor carpi ulnaris, abductor digiti minimi), which is compatible with supination of the fifth finger used in most tool grips discussed above as well as acceleration and stabilisation of the wrist during hammerstone strike (Marzke et al., 1998). Of the thumb, MH2 appears to have a well-developed M. flexor pollicis longus, a human-like palmar pad, a broad apical tuft, and a tall and gracile first metacarpal shaft which, in combination, are suggestive of an effective mechanism at the thumb to accommodate stressors incurred during flexion (e.g. during a forceful pinch grip). Nevertheless, the insertions for Mm. opponens pollicis and dorsal interosseous tendons in MH2 are only weakly developed (Kivell et al., 2011). As M. opponens pollicis is integral to opposition of the fingers with the thumb particularly during manipulation of objects, and the dorsal interosseous is strongly recruited during hammerstone grasping (Marzke et al., 1998), this suggests that these muscles were poorly developed in *Au. sediba* and would not have stabilised the trapeziometacarpal joint with the same effectiveness as modern humans. The overall gracility and apparently reduced musculature of the thumb in *Au. sediba* suggests that the thumb was not subject to the large intrinsic and extrinsic stressors exerted on it during Oldowan stone tool manufacture. Nonetheless, MH2 maintains a long thumb, a well-developed M. flexor pollicis longus, expanded apical tufts, and robust fifth finger musculature, all of which are associated with the ability for tool manufacture. The picture, then, is contradictory. The MH2 hand exhibits a mosaic of derived versus australopith-like features that are compatible with the use of the hand in forceful precision grips and resisting the forces generated during stone tool manufacture in some respects but crucially not in others. *Australopithecus sediba* at the very least highlights that many of the features associated with tool behaviours had evolved by at least 1.977 Ma, whether or not *Au. sediba* itself was not a tool-maker.

The *Australopithecus africanus* hand is less well-represented in the fossil record: by a collection of unassociated phalanges and metacarpals (representing digits one through four; see Green and Gordon, 2008, and Ricklan, 1987 for a summary) and potentially three unassociated carpals including a capitate (Broom and Schepers, 1946), scaphoid (Kibii et al., 2011), and triquetrum (Susman, 1988b, Kivell, 2011). Though the taxonomic status of these carpals remains unclear, they have been attributed to *Australopithecus* and appear to have originated from *Au. africanus*-bearing stratigraphic levels at Sterkfontein in South Africa. Another specimen of uncertain taxonomic standing from Sterkfontein, Stw 573 (Clarke, 1999, 2002), is a fairly complete skeleton including a hand and arm attributes to *Australopithecus*. Much like *Au. afarensis*, while *Au. africanus* is not associated with stone tools, aspects of its hand morphology speaks to manipulation being an increasing selective pressure. Ricklan (1990, 1987) analysed the manual remains from Sterkfontein Member 4 and concluded that the increased relative length of the Stw 418 first metacarpal would have provided this hominin with an enhanced ability for precise pad-to-pad grips. He also highlighted other human-like features of the *Au. africanus* hand, such as a saddle-shaped trapeziometacarpal joint that would have been able to flex and abduct the thumb during thumb-to-finger opposition, a marked insertion for M. extensor carpi radialis on the second metacarpal, and a styloid process on the third metacarpal which would have stabilised the palm during hard-hammer percussion (Marzke and Marzke, 1987, Ricklan, 1990).

In terms of manual proportions, *Au. africanus* exhibits a basically human-like pattern of length proportions but differed markedly from humans in terms of relative metacarpal breadth toward a more ape-like condition (Green and Gordon, 2008). This suggests that *Au. africanus* maintained a relatively long thumb suitable for a wide range of tool grips, although the potential complicating effects of pleiotropy on forelimb to hind limb proportions are difficult to rule out; selection for toe shortening related to locomotion

(i.e. bipedalism) may concomitantly shorten finger lengths as a consequence of a shared genetic basis (Galis et al., 2001), rather than direct selection for manipulatory behaviours such as tool manufacture and use. Recent work by Skinner et al. (2015) has shown that *Au. africanus* exhibits a pattern of trabecular bone structure and distribution consistent with forceful precision grips typical of habitual tool-makers and -users, and these results support and interpretation of the *Au. africanus* manual proportions as being at least partly driven by selection for these behaviours. Nevertheless, the primitive morphology of the Stw 618 scaphoid evinces a wrist not habitually subject to the large internal and transverse loading typical of a dedicated tool-using hand (Kibii et al., 2011), as does the maintenance of phalangeal curvature (Ricklan, 1987) and ape-like limb proportions (McHenry and Berger, 1998). Taken together, the hand and shoulder features of *Au. africanus* describe a locomotor regime that was predominantly arboreal but not inconsistent with a hand used regularly for tool use.

3.4.2 The “Robust” Australopithecines (*Paranthropus* sp.)

The robust Australopithecines refers to material attributed to the genus *Paranthropus*. *Paranthropus boisei*, known from Olduvai Gorge (Leakey, 1959, Domínguez-Rodrigo et al., 2013) and Peninj (Leakey and Leakey, 1964) in Tanzania, the Omo region (Coppens, 1978, Coppens, 1980, Coppens and Sakka, 1983, Alemseged et al., 2002) and Konso in Ethiopia, and Koobi Fora (Wood, 1991, Brown et al., 1993), west Lake Turkana (Leakey and Walker, 1988, Prat et al., 2003), and Chesowanja (Carney et al., 1971, Gowlett et al., 1981) in Kenya. *Paranthropus robustus* is known in South Africa from Kromdraai (Thackeray et al., 2001), Swartkrans (Susman, 1988b, Susman, 1989, Pickering et al., 2012, Grine and Susman, 1991), Sterkfontein (Kuman and Clarke, 2000), Gondolin (Menter et al., 1999), and Drimolen (Keyser et al., 2000). Few examples of well-associated craniodental and postcranial remains are attributed to

robust australopithecines. This poses a problem as diagnoses of fossil hominin species are typically conducted on the basis on craniodental material and much of the postcranial material attributed to *Paranthropus boisei* or *Paranthropus robustus* occurs in isolation from these diagnostically critical fossils. Only one skeleton from Level 4 in Bed II, Olduvai Gorge, Tanzania, thus far represents a well-authenticated example of a dentally-associated partial skeleton attributed to *P. boisei* (OH 80; Domínguez-Rodrigo et al., 2013). Dated to 1.34 million years, OH 80 preserves very little of the upper limb: only a distal humeral diaphyseal fragment and a partial radius preserving the head, proximal metaphysis, and a portion of the proximal diaphysis. In terms of diaphyseal shape, the OH 80 distal humerus appears to fit well with specimens attributed to *P. robustus* from Swartkrans, being more rounded in cross-section than the angular humeral diaphyses of *Homo* (Domínguez-Rodrigo et al., 2013). Very few functional inferences can be made from this specimen, especially about the morphology of the shoulder. The radius is very large and robust, but not notably different in morphology from other known australopithecine radii aside from its size (Domínguez-Rodrigo et al., 2013). Principle components analysis of the OH 80 radius reaffirms previous interpretations of *P. boisei* as having large, powerful forearms and a proximal articular morphology similar to that of climbing hominoids. It is noteworthy, then, that the manual remains attributed to *P. robustus* from Swartkrans do not appear to preserve morphology indicative of regular climbing or suspensory behaviours (Susman, 1988b). While the phylogenetic relationship between *P. boisei* and *P. robustus* is unclear, Domínguez-Rodrigo et al. (2013) argue that regular climbing behaviours may be a possible explanation for this radial similarity.

Much of the remaining robust australopiths' post-cranial material is highly fragmentary, undiagnostic, and tenuously attributed (Wood and Constantino, 2007). Two largely complete ulnae are of further interest with regard to the potential tool-making abilities

of robust australopiths as inferred from the upper arm: OH 36 and Omo L40-19. Omo L40-19 is a complete right ulna, lacking only the styloid process recovered from Member E of the Omo Shungura formation in Ethiopia which has been dated to 2.04 million years and referred to as *Paranthropus boisei* by Howell and Wood (1974). OH 36 is an almost complete right ulna from Upper Bed II, Olduvai Gorge, Tanzania, dated to 1.1-1.2 million years which has been attributed to both *Homo erectus* (= *H. ergaster*; Leakey, 1978, Day, 1986) and *Paranthropus boisei* (Walker and Leakey, 1993). Aiello et al. (1999) performed a comparative analysis of the OH 36 and Omo L40-19 ulnae, and concluded that they are significantly different, precluding their attribution to the same species. Consequently they recommended that OH 36 be tentatively assigned to *P. boisei* and Omo L40-19 to Hominini gen. et sp. indet. (Aiello et al., 1999). McHenry et al. (2007) agreed with this attribution of OH 36 but instead ascribed Omo L40-19 to *Paranthropus aethiopicus*. Drapeau (2004) analysed olecranon process orientation in both of these specimens (and two others, A.L. 288-1 and A.L. 438-1, attributed to *Au. afarensis*) and found that both have a human-like proximally orientated olecranon which is consistent with the habitual use of the arm in a flexed position such as in manipulatory behaviours. The orientation of the SKX 8761 proximal ulna from Swartkrans, while attributed to a robust australopith (Susman, 1988b), has yet to be analysed in this way.

The only manual remains that might be attributed to robust australopiths come from Member 1 at Swartkrans (Susman, 1988a, Susman, 1988b), and these include a fairly complete pollical metacarpal, a complete pollical distal phalanx, and an assortment of proximal, intermediate and distal phalanges. Member 1 is dated to 1.8 million years (Vrba, 1982). According to Susman (1988a), the hand of *P. robustus* is largely human-like. The pollical metacarpal is robust with a broad articular surface for the carpals. The musculature of the thumb is also appears well-developed: *Mm. opponens pollicis* and

flexor pollicis longus have clearly developed insertion sites on the metacarpal shaft and pollical distal phalanx. These muscles are integral to the ability to bring the thumb into opposition with the fingers and forceful precision gripping respectively (see Section 3.3.1). The distal pollical phalanx is broad and flat much like OH 7 (Napier, 1962b) and *Orrorrin* (Almécija et al., 2010) with an expanded apical tuft reminiscent of modern humans. This is functionally significant as it has the effect buttressing a correspondingly enlarged fleshy finger pad – *P. robustus* thus appears to have had a large fleshy pad on the tip of the thumb. Moving to the rest of the hand, the *P. robustus* manual remains exhibit short and straight proximal phalanges (Susman, 1988a) which differentiates them from the curved phalanges of earlier hominins (e.g. *Au. afarensis*, *Au. sediba*; see Section 3.4.1). Susman (1988a) concluded that together this suite of features indicated enhanced ability for precision grip but a limited potential for power grasping ability. The apparent straightness of the phalanges does indeed suggest that climbing behaviours were not as strong a modifying force in the morphology of the *P. robustus* hand.

Susman's interpretation of the fossil evidence has been called into question by some authors (see Hamrick and Inouye, 1995, Marzke, 1997), especially in light of how little material is available and how few characters he really examined (e.g. Susman makes no attempt to mention, describe, or infer carpometacarpal joint orientations for the first digit based on the proximal metacarpals available). Asserting that a particular species manufactured stone tool on the basis of a single grip type is problematic, especially when experimental workers have manufactured stone tools without utilising that grip (Krantz, 1960, Napier, 1962a). In addition to this, two different taxa are suggested to be present at Swartkrans – *Homo gautengensis* (see Curnoe, 2010) and *P. robustus* – and the species attributions for the Swartkrans manual material have also been called into question (Trinkaus and Long, 1990). Thus it is unclear how concretely this morphology

can be linked to stone tool manufacture in robust australopiths from Swartkrans rather than, for instance, other specialised manual feeding behaviours.

3.4.3 *Homo naledi*

Homo naledi is a recently discovered fossil hominin species from South Africa with reasonably well-preserved upper limb and hand remains associated with it (Berger et al., 2015, Feuerriegel et al., [Submitted], Kivell et al., 2015). The fossils were recovered from the Dinaledi Chamber of the Rising Star system in the Cradle of Humankind, approximately one kilometre from the well-known site of Sterkfontein. While the temporal position of this species is currently unknown, it is still possible to investigate its potential as a tool-using species based on its morphology.

No complete clavicles are currently known for *H. naledi*, but a composite clavicle was constructed using 3D laser surface scans from three clavicular fragments of similar size (Feuerriegel et al. [Submitted]). Though the fragments are from three different individuals which limits the deductive strength of the composite model, the Dinaledi model is short relative to modern humans but exhibits a very human-like sigmoid curvature in superior view. In dorsal view, the clavicle shows slight superior curvature medially and inferior curvature laterally, together suggesting a more superiorly oriented clavicle that articulates with a scapular positioned high on the thorax (Voisin, 2008, Voisin, 2006a, Voisin, 2004).

The scapula is poorly represented in *H. naledi*, although one fragment (U.W. 101-1301) does preserve much of the glenoid fossa, infraglenoid tubercle, and portions of the lateral border and spine. We were able to estimate the ventral bar/glenoid angle and scapular spine orientation for this specimen. The ventral bar/glenoid (VBG) angle of U.W. 101-1301 is estimated to be 121.1°, indicative of a more cranially oriented glenoid fossa than *Au. africanus*, A.L. 288-1 (132.2°), MH2 (131.2°), and even modern great

apes (Feuerriegel et al., [Submitted]). Highly obtuse ventral bar/glenoid (VBG) angles represent more laterally oriented GH joints, as in *Homo*, while *Hylobates* joints are cranially oriented with more acute VBG angles, and *Pan*, *Gorilla*, and *Pongo* are all similar to one another and significantly more cranially oriented than *Homo*. The spine projects dorsally from the scapular blade in lateral view as in australopiths and *Pan*, but unlike modern *Homo*; the overall size and morphology of U.W. 101-1301 is remarkably similar to that of A.L. 288-1 (*Au. afarensis*). Scapular spine orientation (measured as the angle between the spinal base and axillary border) was estimated at 26.8° in *H. naledi*, which suggests a markedly oblique orientation of the spine similar to Sts 7 and intermediate between *Pan* and *Gorilla*.

The most notable humeral fossils of *H. naledi* include a nearly complete adult humerus (U.W. 101-283) and four fragmentary specimens preserving variable amounts of the distal shaft and articular end (Feuerriegel et al., [Submitted]). The humerus combines prominent greater and lesser tubercles, bounding a deep bicipital groove, with a small, non-projecting humeral deltoid tuberosity and brachioradialis crest. Humeral torsion was estimated for U.W. 101-283 at 91°, which is the lowest recorded torsion value for any adult fossil hominin yet and meaning that the humeral head faces almost completely posteriorly in this species. A nearly complete immature humerus (U.W. 101-948) likewise displays low torsion (105.0°). No sufficiently complete ulnae have been recovered for *H. naledi* thus far, hence the orientation of the proximal ulna in this species is unknown. The Dinaledi radius and ulna diaphyses exhibit little curvature. The radius has a globular radial tuberosity, prominent pronator quadratus crest, and reduced styloid process.

Functionally, the shoulder and upper limb region of *H. naledi* fits within the pattern that characterises the upper limb of *Australopithecus*, though it differs notably in its overall

gracility. The upper thorax of *H. naledi* is narrow (Williams et al., 2016) and the glenohumeral joint is cranially directed, much as inferred for *Australopithecus* (Green, 2013, Green and Alemseged, 2012, Schmid, 1983, Stern and Susman, 1983) but *H. naledi* distinguishes itself in having substantially lower humeral torsion than either *Au. afarensis*, *Au. africanus*, or *Au. sediba*. In combination with the apparently primitive clavicular morphology, this suggests that the Dinaledi scapula was positioned superiorly and laterally about the thorax. In this way *H. naledi* approaches the primitive pectoral girdle morphology proposed by Larson (2007) and aligns closely with highly arboreal species such as *Pan* and *Pongo*, which corresponds with similarly apelike features in the scapula. Though based only on tentative estimates, the clavicle curvature values support the interpretation of the *H. naledi* pectoral girdle as being adapted for climbing rather than manipulation (Feuerriegel et al.[Submitted]).

The holotype of *H. naledi* (DH1) preserves a nearly complete adult right hand. Kivell et al. (2015) describe the hand as possessing many derived features of the palm, thumb, and wrist shared with both modern humans and Neandertals but nonetheless maintaining morphological features typical of climbing behaviours. (Much of the following description is derived from personal correspondence with the researchers and the up-coming paper on the material – see previous reference.) Thumb-to-finger proportions indicate that the thumb is long relative to the other digits, although the fingers themselves are long again relative to the palm and exhibit marked phalangeal curvature, more so than even that seen in australopiths (Kivell et al., 2015). Phalangeal curvature is biomechanically significant as it has been demonstrated to reduce the strain experienced by the hand in flexed-finger grasping postures because the curvatures align the bone with the joint reaction forces (Richmond, 2007, Nguyen et al., 2014). The trapezium-first metacarpal articulation is also relatively small compared with humans. Given the high degree of curvature exhibited by *H. naledi*, it is clear that the hand and

fingers experienced strong loading during grasping typical of climbing or suspensory behaviours. Other human-like features of the thumb include marked attachments for *Mm. opponens pollicis* and first dorsal interosseous (important for opposition of the thumb with the fingers and forceful precision grips, respectively), a large, robust pollical distal phalanx, a well-developed attachment for *M. flexor pollicis longus*, and a distinct ungual fossa (Kivell et al., 2015). Taken together, these latter features suggest a broad palmar pad with a mobile proximal pulp, as in humans and Neandertals, all of which facilitate forceful opposition of the thumb with the fingers.

Of the non-pollical metacarpals, the DH1 hand does preserve a largely-complete second metacarpal, although the capitate facet is damaged beyond being able to determine whether it was continuous or non-continuous. Nevertheless, the capitate-second metacarpal joint appears to be more radioulnarly orientated based on the angle of the capitate's second metacarpal facet, which is more similar to australopiths and *Homo floresiensis* (Orr et al., 2013, Tocheri et al., 2007). Another primitive feature is the absence of the third metacarpal styloid process. The DH1 metacarpal heads are similar to australopiths, modern humans, and Neandertals in overall robusticity, though the *H. naledi* fifth metacarpal (of which there are two) are particularly notable for their robusticity and for the pronounced crest for the attachment of the *M. opponens digiti minimi* tendon, which is similar to australopiths and the Swartkrans specimens (Kivell et al., 2015). The fifth metacarpals also display a hamate articulation that is saddle-shaped which, as noted previously, is an important feature for fifth digit supination/rotation towards the second digit and thumb. In sum, the metacarpal morphology of *H. naledi* is most similar to modern humans and therefore consistent with a well-developed ability to cup the hand, as in many of the aforementioned tool grips, and to manipulate large objects held in one hand.

Moving to the wrist, the overall shape of the carpals and articular morphologies are similar to modern humans and Neandertals (Kivell et al., 2015). The trapezoid is boot-shaped and has a non-articular palmar surface which is expanded relative to apes and some other hominins. The trapezoid-capitate articulation is enlarged and expanded palmarly, and the trapezium-scaphoid joint extends onto the scaphoid tubercle. These are all derived features and would have probably have functioned as a complex to disperse the large axial pollical loads and transverse carpal forces that occur at the wrist during forceful precision and pinch grips, while the absence of the third metacarpal styloid process, the small trapeziometacarpal joint, and the radioulnarly orientated second metacarpal-capitate articulation may have meant that this complex was less stable than in modern humans.

Over all, the picture formed by the *H. naledi* upper limb and hand is one of compromise. The marked phalangeal curvature and primitive pectoral girdle morphology indicate that climbing or some form of suspensory behaviour remained a substantial part of the locomotor repertoire for this species. On the other hand, the presence of a derived thumb, wrist and palm, a human-like ability for fifth digit supination, and the well-developed thenar musculature represent appreciable adaptation to manual manipulatory behaviours. Curiously, the morphology of the leg and foot of *H. naledi* is that of an obligate biped (Harcourt-Smith et al., 2015, Marchi et al., 2016). Corbetta (2005) has argued that the upper limb must be freed from the requirements of locomotion in order for complex manual manipulatory behaviours to develop. The presence of a sizeable complex of derived manual morphologies in the hand and an irrefutably bipedal lower limb in *H. naledi* might then suggest that the upper limb played little role in locomotion, and that the arboreal features of the hand and shoulder represent primitive retentions. On the other hand, reduced phalangeal curvature in one immature proximal phalanx from *H. naledi* negates this conclusion. Phalangeal

curvature has been demonstrated by Richmond (1998, 2003) to be strongly influenced by mechanical loading during ontogeny such that curvature is a functional response of the bone to behaviour. Thus the evidence from *H. naledi* suggests that climbing behaviours comprised a large component of the locomotor repertoire in this species well into adulthood.

3.4.4 *Homo habilis*

Homo habilis is known from Olduvai Gorge, Tanzania (Leakey et al., 1964a, Tobias, 1965, Susman and Creel, 1979, Johanson et al., 1987), Koobi Fora in Kenya (Leakey et al., 1989), Hadar in Ethiopia (Kimbel et al., 1997), and possibly Sterkfontein and Swartkrans in South Africa (Clarke, 1985, Grine et al., 1993).

There is very little shoulder material known for *Homo habilis*. The most complete specimen is OH 48, a nearly complete clavicle described by Napier (1965a) as being essentially humanlike with the exception of the cross-sectional shape of the medial end. Based on the orientation of the long axis of the cross-section of this area, Napier (1965a) concluded that the clavicle would have been rotated around its longitudinal axis and the shoulder positioned higher than in modern humans. Oxnard (1969b) measured significantly higher torsion in the clavicle than what typically occurs in modern humans, agreeing with Napier (1965a) that the clavicle would have been twisted cranially and the shoulder positioned superiorly. It is this superiorly positioned shoulder and cranially twisted clavicle that Oxnard (1969b) interpreted as reflecting some ability for suspension in the upper limb. Also attributed to *H. habilis* is the KNM-ER 3735 partial skeleton dated to 1.9 million years (Leakey et al., 1964b, Tobias, 1989, Wood, 1991, Leakey et al., 1989), of whose shoulder material, the lateral portion of the clavicle and a small section of scapular spine survive. Leakey et al. (1989) interpreted the thickness of the remaining scapular spine (in conjunction with the thickness of forelimb features

from KNM-ER 3735) as evidence of a considerable aptitude for climbing in this hominin. Despite the limited sample size, it is probable that *H. habilis* maintained a shoulder similar to that of earlier hominins and *H. naledi*, and therefore likely possessed a relatively low degree of humeral torsion.

The most notable manual remains attributed to *H. habilis* are hand bones from a single individual from Bed I at Olduvai Gorge, OH 7, which include, amongst others, a pollical distal phalanx and a trapezium (Napier, 1962b). The presence of the trapezium is important as it provides us with some idea of the manipulatory capabilities of the thumb and second digit. Most notably, the articular facet for the first metacarpal on the trapezium has a relatively level topography that differentiates it from modern humans and even more so from chimpanzees and *Au. afarensis* whose curvature for this facet is marked (Marzke et al., 2002, cited in Marzke, 2013). The flatness of this articular facet suggests that while the thumb in OH 7 would have capable of excursion to the fifth digit, it would have been less stable in forceful pinch grips between the first and second digits (Marzke, 2013). The articular facet for the second metacarpal is orientated sagittally, much as in African apes (Napier, 1962b), and as such would not have facilitated the kind of axial rotation of this digit necessary for cupping of the hand around objects. Again, this feature differentiates the hand of *H. habilis* from *Au. afarensis* which more closely approaches the human condition (Tocheri et al., 2003). The morphology of the carpometacarpal joints in these two digits could potentially distribute the large internal stressors associated with the pad-to-side pinch, cradle, and three-jaw chuck grips. Unfortunately, the fifth digit metacarpal is not preserved in OH 7 so it is impossible to know how this trapeziometacarpal morphology is complemented in the rest of the hand to the extent of speculating on the ability of *H. habilis* to cup large objects in the hand.

The pollical distal phalanx of OH 7 exhibits a mediolaterally expanded apical tuft similar to modern humans (Napier, 1962b). The diagnostic strength of this feature alone in relation to tool manufacture capabilities is limited however, as it is shared with modern baboons (Shrewsbury et al., 2003). This fossil may also have been misidentified, and may instead represent a hallucal phalanx (Susman and Creel, 1979). The intermediate phalanges of OH 7 are robust and exhibit marked curvature as well as well-defined groves for *M. flexor digitorum superficialis*, features that are consistent with climbing as an important part of the locomotor repertoire for *H. habilis* (Moyà-Solà et al., 2008, Napier, 1962b, Susman and Creel, 1979). Susman and Stern (1982) in particular argued that the robusticity and phenotypic plasticity of the bones are not simply vestiges of a suspensory heritage but rather reflect actual arboreal behaviour. Ruff (2009) similarly concluded that, while bipedal when terrestrial, *H. habilis* engaged in frequent arboreal behaviour, based on analysis of relative limb strength and locomotion in *H. habilis*. The powerful grasping capabilities and curved phalanges of the hand of OH 7 support the interpretation of the shoulder girdle as reflecting frequent climbing behaviour (Susman and Creel, 1979, Susman and Stern, 1982, Susman and Stern, 1979, Tocheri et al., 2003).

These conclusions are interesting because, despite being eponymously “handy” and contemporaneous with stone tools (if not associated with them), it would appear as though the *H. habilis* hand was better suited to use in climbing than manipulation or tool manufacture. While *H. habilis* is now well-accepted as a species, the erection and validity of this taxon has historically been fraught with controversy and it is unclear to what extent the postcranial remains can be associated with the cranial material from which the species was largely described (Moyà-Solà et al., 2008). The OH 7 cranial remains were assigned to *Homo* based primarily on craniodental evidence, including encephalisation beyond that of *Australopithecus* (Leakey et al., 1964a, Tobias, 1989),

which naturally made this hominin a fitting candidate for the manufacturer of the Olduvai stone tools. While they originated from the same locality, the manual remains were associated rather tenuously with cranial material based on their shared immature status rather than any strong taphonomic associations between the two (Robinson, 1965b, Robinson, 1965a, Tobias, 1965). Moyà-Solà et al. (2008) performed morphometric and morphological comparisons of the OH 7 hand with modern humans, *Australopithecus*, and robust australopiths, concluding that the OH 7 hand is better attributed to *P. boisei* and that the human-like features of the hand are better explained by specialised manual feeding techniques rather than tool manufacture. Though it is not the objective of this dissertation to resolve these taxonomic quandaries, it is nonetheless noteworthy that hand assigned to *H. habilis* does not appear well-suited to the kind of precise manipulation required to skilful Oldowan stone tool manufacture, especially in light of alternative taxonomic attributions.

3.4.5 *Homo ergaster*

Homo ergaster (also referred to as African or early *Homo erectus*) is best known from KNM-WT 15000 (or Nariokotome boy), a nearly complete skeleton of a juvenile male from Lake Turkana, Kenya, whose shoulder elements include both clavicles, one nearly complete and one partial scapula, and a humerus missing only its proximal epiphysis and part of the medial epicondyle (Walker and Leakey, 1993). The Dmanisi, Georgia, fossils also provide good examples of the shoulder morphology of *H. ergaster*², consisting of one juvenile partial skeleton and some adult postcranial material originating from one large individual (Lordkipanidze et al., 2007). The juvenile shoulder material includes a nearly complete clavicle (D2724), an incomplete right

² Recent work by Dembo and colleagues (2015) highlighted problems in referring to KNM-WT 15000, the Dmanisi, and the Asian *Homo* fossil material collectively as either *H. ergaster* or *H. erectus*. As the debate is ongoing and exact taxonomic positions have yet to be clarified, I refer to both KNM-WT 15000 and the Dmanisi material as *H. ergaster*.

humerus (D2715) and a nearly complete left humerus missing only its proximal epiphysis (D2680); the adult shoulder comprises incomplete right and left clavicles (D4162 and D4161 respectively), part of the right scapula (D4166) and the left humerus, lacking only its proximal epiphysis (D4507).

The clavicles of the Nariokotome boy and the Dmanisi hominins have a sigmoid curvature typical for both modern humans and great apes (Voisin, 2008, Larson, 2007, 2013, Jashashvili, 2005). However, KNM-WT15000 also exhibits an increased inferior curvature in dorsal view which evinces a more superiorly positioned scapula on the thorax (Voisin, 2006a, Voisin, 2006b). Interestingly, Lordkipanidze et al. (2007) report that, in terms of mid-shaft and conoid tubercular cross-sectional shape, the Dmanisi clavicles are less like those of KNM-WT 15000 and more comparable to modern humans. While the clavicles of both KNM-WT 15000 and the Dmanisi hominins are human-like in shape (Lordkipanidze et al., 2007, Walker and Leakey, 1993), they appear to be unusual in their length in that both have low relative clavicular length in comparison to modern human groups based on the claviculohumeral ratio (Larson, 2013, Larson, 2009). Accordingly, Larson (2009, 2007) suggested that the relatively short clavicles of *H. ergaster* are representative of the primitive condition for hominoids. Roach and Richmond (2015), however, argue that claviculohumeral ratios are a poor indicator of relative clavicle length and shoulder position and instead suggest the use of the claviculocostal ratio which they found better normalised clavicle length. In their analysis, KNM-WT 15000 was found to fall at the edge of the human ranges for claviculocostal ratios which is indicative of a short clavicle but perhaps not to the extreme that Larson (2007) implied. Regardless, Nariokotome boy is immature and it remains uncertain how this affects the claviculocostal ratio.

From what can be gleaned from the scapula KNM-WT 15000E, the glenoid fossa of *H. ergaster* no longer faced cranially as in earlier hominins. Other human-like features of this fossil include the scapular spine orientation (more horizontal than transverse) and human-like proportions of the supra- and infraspinous fossae (Green and Alemseged, 2012). In the D4166 scapular fragment the picture is a little less clear. Lordkipanidze et al. (2007) concluded that the glenoid faced more cranially than in modern human populations based on an axillo-glenoid angle of 129° ; note, however, that much of the axillary border in this specimen is missing, making reliable measurement difficult.

As the humeri from Nariokotome and Dmanisi are all missing their proximal epiphyses, it is not possible to determine the condition of the tubercles. The intertubercular groove of KNM-WT 15000 is wide and relatively shallow, and the shaft is straight much like those of the Dmanisi hominins (Lordkipanidze et al., 2007, Walker and Leakey, 1993). Humeral torsion in *Homo ergaster* is low: KNM-WT 15000F has a torsion value of 111.5° (Larson, 2007), though it is again worth noting that KNM-WT 15000 is a juvenile, and so it is likely that his adult torsion value would have been somewhat higher. Larson et al. (2007) put his maximum adult value at only about 120° based on equivalence to human growth patterns, though this is problematic as KNM-WT 15000 probably followed a more chimpanzee-like growth trajectory (Ruff and Burgess, 2015). Similarly, the Dmanisi hominin remains have low torsion values – 110° for the adult proximal humerus D4507 and 104° for the juvenile D2680 (Lordkipanidze et al., 2007). These values are well below those for modern humans: KNM-WT 15000 sits below the lower ranges of human variation in torsion values, while the Dmanisi individuals are more comparable in torsion to that of the Australopithecines – with the exception of the Omo 119-73-2718 individual – and *H. naledi* (Larson, 1996, Feuerriegel et al., [Submitted]).

While torsion involves a certain amount of developmental plasticity (Reagan et al., 2002), the lack of lateralisation in the Dmanisi subadult supports the interpretation of reduced HT as part of a plesiomorphic shoulder configuration that includes a more cranially orientated glenoid, more protracted scapular position, and a perhaps short clavicle (Larson, 2007). If this line of argument is to be followed, *H. ergaster* would have had a more australopith-like than human-like upper limb morphology (Stern and Susman, 1983). Contrary to this, Roach and Richmond (2015) reconstructed the *H. ergaster* shoulder girdle as following a more human-like pattern in terms of scapula position on the thorax as Nariokotome falls within the lower ranges of variation for modern humans. They argued that the anterior rotation of the scapula to articulate with a short clavicle predicted by Larson is unnecessary as this does not occur in modern humans in the low ranges of clavicular length. Regardless, KNM-WT 15000 maintains a fairly modern-looking scapula, with a glenoid that no longer faced cranially and sat on a more barrel-shaped rib cage than earlier fossil hominins (Jellema et al., 1993) and *H. naledi* (Williams et al., 2016). The clavicle is short compared to modern humans and appears to have been somewhat obliquely orientated such that the scapula was positioned higher on the thorax, which may explain the short clavicle through constriction of the upper thorax.

The hand of *H. ergaster* and *H. georgicus* is poorly represented in the fossil record. From Dmanisi, only two distal manual phalanges (D3480 and D2679) have been recovered so far (Lordkipanidze et al., 2007). More recently a single third metacarpal, KNM-WT 51260 attributed to *H. erectus sensu lato* (= *H. ergaster*), was recovered from sediments dating to 1.42 Ma in Kenya (Ward et al., 2014). A styloid process is present in this fossil, though it is less prominent and the capitate-second metacarpal joint less obliquely orientated than seen in Neandertals. *H. ergaster* has been associated with Acheulean stone tools (Beyene et al., 2013) which represents a significant

technological advance over the Oldowan. While a single morphological feature cannot be unambiguously linked to a particular behaviour, the basically human-like appearance of KNM-WT 51260 suggests that the complex of features characteristic of the modern human hand had already arisen with *H. ergaster*. The association of this species with complex forms of tool manufacture places this morphology in the context of increased reliance on sophisticated manipulatory behaviours.

Whether you adhere to Larson's (2007) or Roach and Richmond's (2015) model of *H. ergaster*'s shoulder, the it seems that the first major departure from the australopith pattern of shoulder morphology took place with *H. ergaster*. The shoulder was in the process of lowering from the high position seen in australopiths, the glenoid was no longer orientated cranially and may have faced more laterally than anteriorly (as hypothesized for australopiths). There are indications, both behavioural and morphological, that the hand was being used in the production and use of stone tools and the structural reorganisation of the shoulder supports this conclusion. It would appear then that, while not fully-modern, *Homo ergaster* was almost certainly a tool-maker.

3.4.6 *Homo antecessor*

The lower Pleistocene site of Gran Dolina, Sierra de Atapuerca, Spain, is dated to 0.8 Ma and has yielded postcranial remains attributed to *Homo antecessor* (Carretero et al., 1999), the hominin proposed to represent the last common ancestor of *Homo sapiens* and *Homo neanderthalensis* (Bermúdez de Castro et al., 1997). The remains include a complete adult clavicle (ATD6-50) and one complete and one partial subadult clavicle. The clavicle ATD6-50 has a very long absolute length, falling at the upper limits of size ranges for modern *H. sapiens* (Carretero et al., 1999). Given that *H. antecessor* is ostensibly ancestral to modern humans and Neanderthals, it is possible that ATD6-50

exhibits the necessary clavicular elongation for the shoulder configuration seen in both later taxa. While no humeri have yet to be recovered from this site, a reasonable prediction is that they will likely display a degree of humeral torsion more comparable to later hominins as the lengthening of the clavicles would reposition the scapula more dorsally, consonantly increasing HT so that the humeral head could articulate with a more laterally facing glenoid. This configuration would be comparable to modern humans in terms of range of range of motion facilitated by the glenohumeral joint and therefore perhaps manipulatory capabilities.

Manual remains attributed to *H. antecessor* have also been recovered from Gran Dolina, including a capitate, a second metacarpal, four proximal phalanges, and four intermediate phalanges (Lorenzo et al., 1999). The assemblage also contains a palmar fragment of a left hamate and an additional isolated metacarpal distal epiphysis. The second metacarpal facet on Gran Dolina capitate is continuous and distally orientated much like modern humans, and also exhibits a proximo-ulnar concavity similar to modern humans and Neandertals (Lorenzo et al., 1999). These features would have permitted pronation of the second digit such as that required by cupping of the hand in certain tool grips (Marzke, 1997). The capitate also preserves a primitive orientation of the distodorsal pillar which is more perpendicular to the longitudinal axis and lacks radial bevelling for the third metacarpal as in modern humans. From this Lorenzo et al. (1999) infer that the third metacarpal would likely have had a somewhat reduced styloid process relative to modern humans. The metacarpal heads are asymmetrical, again similar to Neandertals and modern humans, and functionally important in tool manufacture and use as it is linked with the ability to accommodate to an object via the metacarpal phalangeal joints (Marzke, 1997, Susman, 1998). The intermediate phalanges from *H. antecessor* appear straight and human-like in their dimensions (Lorenzo et al., 1999).

Overall, the morphology of *Homo antecessor* appears human-like. The clavicle has undergone elongation which is indicative of a low, wide shoulder and a dorsally positioned scapula important for enhanced range of motion at the glenohumeral joint. The hand is one of a committed stone tool-maker without evidence of adaptation to arboreal or climbing behaviours and this interpretation is supported by the association of *H. antecessor* with stone tools (Carbonell et al., 2008).

3.4.7 *Homo heidelbergensis*

Fossil remains of *Homo heidelbergensis* from the middle Pleistocene (325 – 205 Ka) site of Sima de los Huesos, Sierra de Atapuerca in Spain include fifteen clavicular fragments, seventeen scapular fragments, and thirty-three humeral fragments, including one complete humerus – Humerus II (Carretero et al., 1997). This humerus is very long, falling well above means for humeral length in both *H. neanderthalensis* and modern humans (Carretero et al., 1997). Broadly though, this humerus displays many features very similar to that of later Neandertals: the humeral head is wider than it is long and has a torsion value of 142°. In the same way, the Sima proximal humeri exhibit very large lesser tubercles, again contrasting to modern humans who tend to have very small lesser tubercles and demonstrating the similarity of these humeri to those of Neandertals (Arsuaga et al., 1997). Carretero et al. (1997) view the enlarged lesser tubercles as a shared derived feature of *H. heidelbergensis* and *H. neanderthalensis*, but Larson (2007) posits that it may instead represent a retention of the primitive condition for hominins as an enlarged lesser tubercle is reminiscent of the condition in early hominin proximal humeri Sts 7, KNM-BC 1945 and A.L. 288-1r. Taken as a whole, the shoulder region of *H. heidelbergensis* most closely resembles that of later Neandertals, so much so that their similarities are viewed by Carretero et al. (1997) and Trinkaus (1983) as

evidence that *H. heidelbergensis* is ancestral to *H. neanderthalensis*. No manual remains for *H. heidelbergensis* have been described.

3.4.8 *Homo neanderthalensis*

The Neandertal shoulder is characterised by long clavicles (Carretero et al., 1997, Vandermeersch and Trinkaus, 1995) and scapulae with unique axillary border morphology, horizontal scapular spine and a tall narrow glenoid fossa (Churchill and Trinkaus, 1990, Trinkaus, 1977, Vandermeersch and Trinkaus, 1995). The humerus has a prominent lesser tubercle, a head that is wider than it is long and only modest levels of humeral torsion, averaging at 138.5° (Churchill, 1994, Churchill, 1996, Carretero et al., 1997). While this measurement puts torsion in Neandertals (and also *H. heidelbergensis*) at the lower end of HT ranges for modern humans, it does not come close to the extremely low levels of torsion seen in *H. ergaster* or *H. naledi*. Vandermeersch and Trinkaus (1995), as well as Churchill (1996), relate the modest levels of torsion in Neandertals to an enlarged chest adapted for a cold climate. According to Larson (2007), low torsion suggests a scapula placed more laterally about the thorax, and thus an anteriorly orientated glenoid, necessitating that the humeral head be directed more posteriorly to maintain a sagittally functioning elbow (see also Larson, 1988). It would follow from this that the long clavicles seen in Neandertals are also a product of cold climate adaptation, as longer clavicles would have been needed to bridge the expanded distance from sternum to acromion resulting from large chest size.

Trinkaus (1989) has associated the apparent differences in pectoral girdle morphology in Neandertals and Upper Palaeolithic humans with tool use. He concluded that Neandertals possessed a suit of traits (including highly muscular shoulders, broad scapulae, and an expanded superior rib cage) typically associated with forceful use of the upper limbs. This morphological pattern is distinct from that found both in *H.*

ergaster and in Upper Palaeolithic humans who exhibit much more gracile and less muscular pectoral girdles. These changes, particularly the reduction in muscular strength of the upper limb, may be related to shifts in the frequency with which particular manipulative behaviours are performed as well as changes in articular proportions, orientations and shapes indicating shifts toward more glenohumeral rotation, arm loading in an extended position, and use of the hand in precision grips (Churchill and Trinkaus, 1990, Trinkaus, 1989, Churchill et al., 1996, Niewoehner, 2000). The Shanidar sample provides further evidence of the habitual use of the forelimb in certain activities (Trinkaus, 1983). Trinkaus (1983) notes the development of a dorsally orientated sulcus on the axillary border of the scapula and hypertrophy of the muscular attachments of deltoid and pectoralis major. These are features associated in some Neandertals with powerful and precise adduction of the humerus such as that in throwing (Trinkaus, 1989). In contrast, as noted earlier, the pectoral girdles of earlier fossil hominins appear to be better adapted for climbing rather than tool use (Larson, 2009, Larson, 2013, Leakey et al., 1989, Oxnard, 1969a, Oxnard, 1968, Oxnard, 1969b, Churchill et al., 2013, Schmid et al., 2013, Vrba, 1979, Feuerriegel et al., [Submitted]).

The morphology of *H. neanderthalensis* thus resembles what has been suggested for *H. ergaster* in some respects and may be argued to be a retention of the primitive condition with an additional increase in chest size. If this is so, then one would expect to see the last common ancestor (LCA) of Neandertals and modern humans to display the primitive condition also; if *H. antecessor* truly does represent LCA of both later taxa, clavicular elongation had occurred well before the appearance of Neandertals. As *H. antecessor* is unlikely to have been cold-adapted (cold-adapted taxa are virtually absent from the Spanish lower and middle Pleistocene; van der Made, 1999) and thus have a large chest, the initial clavicular increase seen in lower Pleistocene hominins is not associated with increased breadth in the upper body. Another possible interpretation is

offered by Larson (2007): that the increase in clavicle length that occurred subsequent to *H. ergaster* arose by the dorsal repositioning of the scapula, consonantly increasing the degree of HT, in order to increase the range of motion available in the upper limb. By positioning the scapula onto the dorsal thorax, the range of potential motion is dramatically increased, allowing for true abduction and horizontal abduction of the humerus. In Larson's interpretation, the LCA of modern humans and Neandertals had a derived pectoral morphology including dorsally positioned scapulae, laterally facing glenoid fossae and longer clavicles; the Neandertal shoulder only required the additional increase in clavicle length necessary to maintain the dorsal position of the scapula on an enlarged chest. Of course, Roach and colleagues (Roach and Richmond, 2015, Roach et al., 2013) reconstruct the *H. ergaster* shoulder girdle as more human-like to begin with, but whatever the case, the Neandertal shoulder girdle is unequivocally that of a creature fully capable of fine manual manipulation and tool manufacture.

The hand of *H. neanderthalensis* is almost completely human-like in terms of morphology and proportions, reflecting tool-making capabilities, with a few exceptions (Niewoehner et al., 1997, Trinkaus, 1983, Trinkaus and Villedieu, 1991). Much of the following information has been drawn from Trinkaus's (1983) volume on the Shanidar Neandertals unless stated otherwise. The overall proportions and muscular anatomy of the hand are indistinguishable from modern humans. The carpals are also human-like, barring very well-developed tubercles on the trapezium, scaphoid, and hamate which are inferred by Trinkaus (1983) to represent well-developed ("hypertrophied") intrinsic flexor musculature of the hand. The attachment of *M. flexor pollicis longus* is similarly extremely prominent in Neandertals which may represent an adaptation to slightly increased phalangeal proportions which decrease the effectiveness of *M. flexor pollicis longus* during grasping at the fingertip by alteration of the load arms at the fingertip, interphalangeal, and metacarpophalangeal joints. The proximal articular surface on the

first metacarpal is radioulnarly curved and dorsopalmarly straight, which sets the Neandertal carpometacarpal joint apart in not having the typical “saddle” shape that characterises modern humans and indeed most other hominins (see Section 3.3.1). Somewhat surprisingly, Neandertal trapezia are more human-like than the first metacarpal articular morphology would suggest in being more saddle-shaped (radioulnarly concave and dorsopalmarly convex) though perhaps not as curved as modern humans. This morphology has been suggested to have inhibited the full degree of axial rotation and therefore capacity for precision grips (Musgrave, 1971, Vlček, 1975) but, as Trinkaus (1983) highlights, it is the fully-interlocking saddle shaped carpometacarpal joint of African apes that inhibits rotational range of motion at this joint and thus a full precision grip. Indeed the more condyloid and open surface of both the first and fifth carpometacarpal articulations would have still permitted three degrees of freedom at these joints much like modern humans (Riley and Trinkaus, 1989, Stoner and Trinkaus, 1981, Trinkaus, 1983, Trinkaus and Villemeur, 1991). The Neandertal second metacarpal-capitate facet is unique compared to humans in being more parasagittally orientated but otherwise falling within modern human ranges for shape and size of the facet (Riley and Trinkaus, 1989), which indicates that the ability to pronate the second digit was fully-developed in Neandertals. Similarly, the third metacarpals of Neandertals have a styloid process which is small relative to modern humans but nonetheless present, indicating that their hands were able to resist oblique mid-carpometacarpal joint reaction forces. Cupping grips and forceful precision grasping were therefore not beyond the realms of capability for Neandertals, and their proficiency in the production of complex Mousterian stone tools would support these conclusions. While the anatomical differences between modern humans and Neandertals may reflect performance differences in tool behaviours (i.e. specific biomechanics, grip

strength, and force trajectories; Niewoehner, 2000, Niewoehner, 2001), they do not represent capability differences.

3.5 Summary

The earliest stone tools (the Oldowan Technological Complex) is characterised by modified tools such as flakes, flaked cores, and hammerstones and, despite their apparent simplicity, considerable skill is required in their manufacture. Things like control of bimanual elementary movements, and precision and force coupled with fine coordination are vital to the execution of conchoidal fracture and these skills have a dual basis in cognition and skeletal morphology. In this regard, the upper limb anatomy of modern humans is both distinctive and compatible with functional requirements of stone tool behaviours. Our morphology is uniquely suited to complex manipulatory behaviours in terms of its strength and dexterity, as well as in its ability to manage the resultant biomechanical stressors across the hand, wrist, elbow, and shoulder. This uniqueness arises out of the presence of a suite of features and, when this pattern is broken down into its component parts, isolated morphological features or certain combinations thereof are revealing of grip and range of motion proficiencies in the human lineage.

Evidence from morphology remains largely equivocal with regards to the tool behaviour of fossil hominins, but particularly in the early fossil hominins where associations between fossil material and stone tools are tenuous. The shoulder of early hominins remained largely primitive in comparison to modern humans and great apes, maintaining many features of the presumed ancestral condition. Generally speaking, the scapula was positioned high on a funnel-shaped thorax with a cranially directed glenoid fossa and a clavicle that was orientated obliquely. The humeral head was elliptical in shape, the bicipital groove relatively shallow and torsion levels that were modest at the

most. The hand remains largely mosaic in terms of morphology, exhibiting both derived and primitive features with exact combinations of features varying from species to species. Given that a completely human-like suite of hand morphology does not occur in the fossil record until *Homo neanderthalensis* at ~0.2 Ma and that the first archaeological evidence for tool behaviour occurs some 2.4 Ma prior to *H. neanderthalensis*, the evidence suggests that stone tool use and manufacture does not require a full complement of derived morphologies (either at the shoulder or hand). Indeed, the association of *Homo floresiensis* and its primitive hand and wrist morphology with Oldowan stone tools (Brumm et al., 2006, Orr et al., 2013, Tocheri et al., 2007) would indicate that anatomical/morphological criteria alone are insufficient to define the tool capabilities of our fossil ancestors. Thus we must look to other avenues to shed light on the issue of who made the first stone tools.

CHAPTER 4: BIOMECHANICS OF STONE TOOL MANUFACTURE

4.1 Introduction

This chapter will review the current tool use/manufacture biomechanics literature as it relates to functional morphology (rather than skill and cognition, as covered Chapter 3, Section 3.2.2) with a view to underlining and illustrating the importance of the research presented in this dissertation for placing the kinematic and kinetic data in its full biomechanical context.

4.2 Wrist and Hand Biomechanics in Oldowan Stone Knapping

Early experiments in stone knapping biomechanics focused on predominantly on the hand as the main site of selection and functional adaptation for tool behaviours in the hominin upper limb. Marzke and colleagues (Marzke and Shackley, 1986, Marzke et al., 1998) conducted some of the first analyses utilising biomechanics techniques to investigate functional morphological questions about fossil hominin upper limbs. Their work identified two capabilities of the modern human hand that are integral to proficient bimanual hard hammer percussion: the ability to control and stabilise stones (both hammerstone and objective/tool stone) in the hand during hammerstone strike, and the manual dexterity required to firmly grasp stones while still leaving their working edges exposed and avoiding the potential for crushing fingers (Marzke and Shackley, 1986, Marzke, 1997). A number of additional grip categories arose out of these studies to complement Napier's (1956) seminal study on tool use grips (See Chapter 3, Section 3.3.1 for further details). In one of the only electromyographic studies of stone knapping conducted to date, Marzke et al. (1998) monitored 17 muscles of the hand and wrist and found that the muscles most strongly and regularly recruited by these grips are the

intrinsic muscles of the thumb and fifth finger (including Mm. flexor carpi ulnaris, flexor pollicis brevis, flexor digitorum profundus 2 and 5, abductor digiti minimi, dorsal interosseous 1, opponens pollicis). These muscles work to cup the hand in order to accommodate and stabilise stones in the hand through forceful opposition of the thumb and fifth finger. Other grips elicit greater recruitment from the extrinsic muscles, such as M. flexor pollicis longus (FPL), though experiments differ in which grip specifically is attributed to generating strongest recruitment for this muscle. Marzke et al. (1998) reports the power (squeeze) grip as eliciting greatest activity from FPL whereas Hamrick et al. (1998) report this to be the three- and four-jaw chuck grips. Marzke (2013a) attributes this contradiction to differences in trial length and fatigue in subjects participating in behaviours requiring repeated strong recruitment of FPL, suggesting that compensatory alterations in thumb function may arise as a result. While Marzke does not remark on it, differences in skill and sample size may also play a role. Marzke et al. (1998) monitor more muscles per subject but their sample size is limited to three individuals across a range of knapping skill levels, including an expert and a proficient. This differs from Hamrick et al. (1998) who studied nine subjects participating in a variety of prehensile behaviours, not just stone knapping, all of an unknown skill level. Nonetheless, Marzke and colleagues relate the high recruitment of the intrinsic muscles of the thumb, index, and fifth finger regions to increases in first and fifth metacarpal robusticity, large tendon and muscle moment arms, and increased enthesal complexity in the hand bones.

More recently, Rolian et al. (2011) investigated the joint stresses and external forces present at the thumb during stone tool manufacture and use in order to test hypotheses associating a derived modern human hand morphology with the kinds of forceful precision grips required to effectively make and use tools. Rolian and colleagues found that digit length correlated with the amount of force required to stabilise digital joints

such that individuals with longer digits required less force and experienced lower joint contact stresses during stone tool use. They related this to relative robusticity of the metacarpals and carpals in modern humans compared to chimpanzees, concluding that increases in metacarpal robusticity, thenar muscle mass, and digit length are what enabled the genus *Homo* to tolerate higher joint stresses and produce more force in stone tool behaviours. Their results accord with the muscle recruitment findings of Marzke et al. (1998): the flexion and adduction/abduction forces recorded by Rolian et al. necessary to resist large extension moments at the proximal interphalangeal and metacarpophalangeal joints are likely the result of high recruitment of FPL and thenar muscles around the time of hammerstone strike. Key and Dunmore (2015) similarly investigated the role of the non-dominant hand (that is, the hand that holds the core rather than the hammerstone) and its influence on thumb evolution through frequencies of digit recruitment and forces experienced during stone tool production. These authors interpret their results to indicate that the robust thumb architecture of modern humans arose in part as a result of increased manipulative forces acting on the thumb compared to the fingers in the non-dominant knapping hand. While these findings also accord with the results of Marzke et al. (1998) in that the intrinsic muscles of the thumb are likely being strongly recruited to exert greater pressure on the tool stone, Key and Dunmore (2015) note that the fifth digit is comparatively gracile (compared to thumb and index finger) in modern humans, challenging Marzke et al.'s hypothesis that the higher recruitment of the fifth finger musculature is likely to result in increased robusticity in this digit. Fossil hominins may have more robust fifth digit than extant non-human apes (Marzke et al., 1992), but in modern humans at least it seems as though high recruitment of the muscles surrounding this digit may actually occur in order to compensate for the relative gracility of the modern human fifth digit and consequently less effective muscle moment arms. The significance of strong recruitment of the

intrinsic muscles of the fifth digit may then lie more in core repositioning than in core stabilisation (Key and Dunmore, 2015).

Williams et al. (2010, 2012, 2014) conducted a series of experiments investigating wrist and hand kinematics and their role in thumb robusticity and accuracy in stone tool manufacture. In one of the few studies on upper limb kinematics on stone knapping, Williams et al. (2010) performed a kinematic analysis of upper limb movements during stone tool knapping focusing on the role the wrist plays in the knapping arm swing. All the knappers in this study exhibited very similar motion patterns across the strike, including the timing of events within arm swing. Williams et al. (2010) divided the arm swing into distinct phases, an upswing phase and a downswing phase, and movements through the phases occurred in a proximal-to-distal fashion. The upswing phase is characterised by upward limb motion, flexion of the shoulder and elbow joints, and increasing wrist extension; the downswing phase is characterised by downward limb motion, extension at the glenohumeral joint, and continued elbow flexion and wrist extension, followed by rapid elbow extension. This downward action of the arm forms the largest and most important part of the arm swing in stone knapping – it is this phase that requires the most muscular activity from the shoulder and ultimately breaks away flakes from the core (Dapena et al., 2006). This proximal-to-distal joint sequence is significant because it facilitates a velocity summation effect whereby the distal joint segments (the wrist and hand) are able to achieve greater angular velocities than they would normally achieve. This occurs as a result of torque interactions in the more proximal joints. They further found that the wrist switched rapidly from extension to flexion immediately prior to hammerstone strike, though only minimally out of peak extension and rarely past the neutral position of the wrist. They suggest that wrist plays an important role in positioning the hand to confer maximum mechanical advantage to the forearm flexor muscles, as wrist position bears a positive second order polynomial

relationship to the moment arms of Mm. flexor carpi ulnaris (FCU) and flexor carpi radialis (Pigeon et al., 1996). Avoidance of higher degrees of wrist flexion by knappers may then allow for greater control and stability of the hammerstone against strong reaction forces as the digital flexors are weaker when the wrist is flexed. Nevertheless, the rapid switch to flexion prior to hammerstone strike – similarly noted by Marzke et al. (1998) as a wrist “flick” – is hypothesised by Williams and colleagues to increase acceleration and contribute to strike accuracy. Marzke et al. (1998) and Williams et al. (2010) contribute this flicking motion to the high recruitment of FCU immediately prior to hammerstone strike. It should be noted, however, that the flexor and extensor musculature of the wrist also crosses the elbow and it is unclear what role these muscles may also be playing further up the kinetic chain. The results of Williams et al.’s kinematic study also refutes Ricklan’s (1987) comparison of the knapping arm swing to the traditional hammering swing: rather than relying on radial and ulnar deviation, the knapping swing uses wrist extension and flexion while forearm is pronated and palm facing the tool stone. This configuration, according to Williams et al. (2010), allows the knapper to produce the “flick” prior to hammerstone strike and thus aim from the distal limb segments, increasing angular velocity at the wrist and potentially improving accuracy. Williams et al.’s study underlines the importance of *in vivo* studies of the kinematic, kinetic, and electromyographic patterns of modern human knappers; the knapping motion is biomechanically unique and use of EMG data from superficially similar actions like hammering or throwing is not appropriate for evaluating the mechanical forces involved in stone tool manufacture.

Focusing on the hand, Williams et al. (2012) measured the pressures and forces that occurred across the thumb, second, and third digits during Oldowan stone tool manufacture, finding that the thumb experienced reduced loading relative to the second and third digits, calling in to question that hypothesis of increased loading in the thumb

resulting in selection for greater thumb robusticity. These results are contra Rolian et al. (2011) and Key and Dunmore (2015). The dramatic differences between these studies are most likely attributable to the differences in the methods, measurements, and techniques employed by the authors in their respective analyses. The results of the hand pressure and kinematics studies by Williams and colleagues (2012, 2014) indicate that the thumb is being used to buttress against the side of the hammerstone in forceful precision grip identified by Marzke et al. (1998). In three-jaw chuck grip, the hammerstone is in direct contact with distal phalanges of second and third digits so that reaction forces through the swing and strike are directed to these regions – supporting Marzke and Shackley’s (1986) observations of finger position during stone knapping and further contradicting Napier (1956, 1965b) and Ricklan’s (1987) hypotheses that stone tool manufacture occurs with the hand in a traditional precision grip (that is, with the thumb fully opposed and flexed). When thumb buttressing is combined with the knapping swing, the thumb is abducted and slightly extended (Williams et al., 2012), agreeing with the muscle recruitment patterns documented in the Marzke et al. (1998) EMG study. Flexor pollicis longus was found not to be strongly recruited in the dominant hand, indicating that strong pinches were not occurring. This instead suggests that the low level FPL activity documented may be due to avoidance by knappers of grips likely to cause high levels of fatigue in FPL and extension (not flexion) of the pollical distal phalax in knapping.

4.3 Biomechanics of the Shoulder in Stone Knapping

Given the majority of past inquiry centres upon the role of the hand and wrist during stone tool production, the muscle recruitment patterns of the shoulder and elbow musculature remains something of an unknown. Studies such as these are vital for elucidating the functional demands that may have been acting on the upper limb during

early hominin evolution but do not provide a complete picture. Evidence from biomechanical studies on activities such as dart throwing (Wolfe et al., 2006), baseball pitching (Reagan et al., 2002, Debicki et al., 2004), and tennis serve (Ivanova, 2005) have demonstrated that gross movements of the upper limb consistently occur in a proximodistal sequence, and the work of Williams et al. (2010) demonstrate that the stone knapping arm swing conforms to this pattern. Only one study thus far has been conducted on the biomechanics and kinematics of the shoulder during stone knapping and, as a consequence, there is little quantitative information available for evaluating hypotheses about the mechanical context of stone tool production at this region. Dapena et al. (2006) looked specifically at shoulder and elbow torques of the arm swing in Oldowan stone knapping using one advanced knapper and kinetic chain analysis to analyse two trials. One trial was defined as lasting from the instant the hammerstone loses contact with the core until the instant before the hammerstone strikes the core on the next arm swing. The arm was modelled as a four-link kinetic chain consisting of upper arm, forearm, hand and hammerstone. This method allowed for forces and torques at the elbow to be understood as resulting from a combination of elbow musculature action and the forces exerted on the forearm by upper arm motion through the elbow joint. Joint torques are informative as torques can be caused by non-local muscular action and inducted via segment linkage, and thus can reflect the predominant muscular action at the joint. Hammerstone velocity was calculated throughout each trial in addition to torques. The results of this study are summarised as follows.

Hammerstone speeds were greatest just before impact at 8.3 and 9.0 m/sec for each trial. A combined impact speed was also calculated at 8.8 and 10.1 m/sec respectively as the subject also moved the core upward to meet the hammerstone. Archaeological evidence indicates that the hominins who made the Oldowan tools were capable of flaking basalt cobbles very efficiently and so probably achieved speed and kinetic energy values

similar to those documented in Dapena et al.'s (2006) study. Wireframe sequences and torque plots generated for the trials revealed the flaking motion as not just a simple planar flexion and extension, but rather a three-dimensional overarm motion driven primarily by the shoulder musculature with the elbow musculature also contributing. Movement across the wrist joint was revealed to be largely a flail action caused by muscular activity further up the kinetic chain (Dapena et al., 2006).

This study provides an indirect picture of the muscular forces involved in the arm motion during flaking. The torque plots indicate during the upswing phase of knapping the shoulder was flexing, externally rotating and abducting while the elbow was flexing. These muscle actions served to halt the downward motion of the core and accelerate the hammerstone upwards and were generated by the shoulder flexors and lateral rotator muscles. About .25 seconds before impact, the torques reverse direction as the knapper swings the hammerstone down toward the core and the elbow extends. During the downswing phase, the shoulder muscles became active in the directions of extension, internal rotation and adduction (positive S_1 , S_2 and S_3 torques respectively); during this time the elbow was extending (positive E_1 torque). This set of muscular actions, brought about by the extensor musculature of the arm and medial rotator muscles, halted the upward and outward motion of the upper arm and flexion of the elbow, before producing rapid downward and inward rotation of the upper arm and extension of the elbow. According to Dapena et al. (2006), the muscles of the wrist did not play a major role in producing the arm swing. Thus the muscular action during flaking motion may be characterised as follows: The muscles involved in producing the upward motion of the hammerstone were activated again immediately after impact in order to complete braking of the downward motion of the hammerstone and facilitate reversal of the stone's direction of travel. The muscles that produced the downward motion of the

hammerstone were activated to slow down the upward motion of the arm and subsequently to speed up the hammerstone's downward motion to the core.

4.4 Summary

The biomechanics of stone tool manufacture is an under-explored field and this is partly due to the invasive nature of electromyography (EMG) as a research tool. Intramuscular EMG at the very least requires advanced medical training and access to facilities that are not generally available to researchers in fields like palaeoanthropology. The difficulty is compounded by the complexity of the shoulder musculature. While surface EMG is non-invasive, its utility in answering biomechanical questions about tool use in the upper limb is limited by the way in which the muscles of the shoulder overlay one another; intramuscular electrodes are necessary to monitor these deep muscles as surface electrodes can only detect activity in superficial muscles. Thus the emphasis has been on techniques that are non-invasive and portable, such as kinematics, and the preponderance of research into stone knapping biomechanics reflects this.

The dearth of appropriate EMG studies for comparison with the kinematic data – the Marzke et al. (1998) study (and to a lesser extent, the Hamrick et al. (1998) study), while seminal, suffers from small sample sizes – does not allow researchers to place the activity of the wrist and hand musculature in its full biomechanical context. Studies such as those conducted by Marzke, Williams, and colleagues are necessary, but focus on the hand and wrist accounts for only one section of a complex larger mechanism. In addition to this, nearly all of these studies suffer from small sample sizes and only a few involved detailed statistical analyses of their results. Given that the upper limb operates in a co-ordinated fashion in the knapping strike with force originating in the proximal limb segments (shoulder and elbow), just looking at the hand and wrist muscles is not sufficient to understand the upper limb mechanism as a whole. Dapena et al.'s (2006)

study provides only a very indirect quantification of muscle recruitment patterns at the shoulder during the Oldowan knapping strike and does not speak to specific values of activation for particular muscle groups. The precise biomechanical context of stone tool production at the shoulder and elbow therefore remains a gap in the literature, one that this dissertation will contribute to amending. While muscles of the upper limb are strongly and regularly recruited in stone tool manufacture and can this information be used to infer stone tool behaviours in the hominin fossil record?

CHAPTER 5: A (LESS THAN) RANDOM WALK THROUGH FRACTAL ANALYSIS

5.1 Introduction

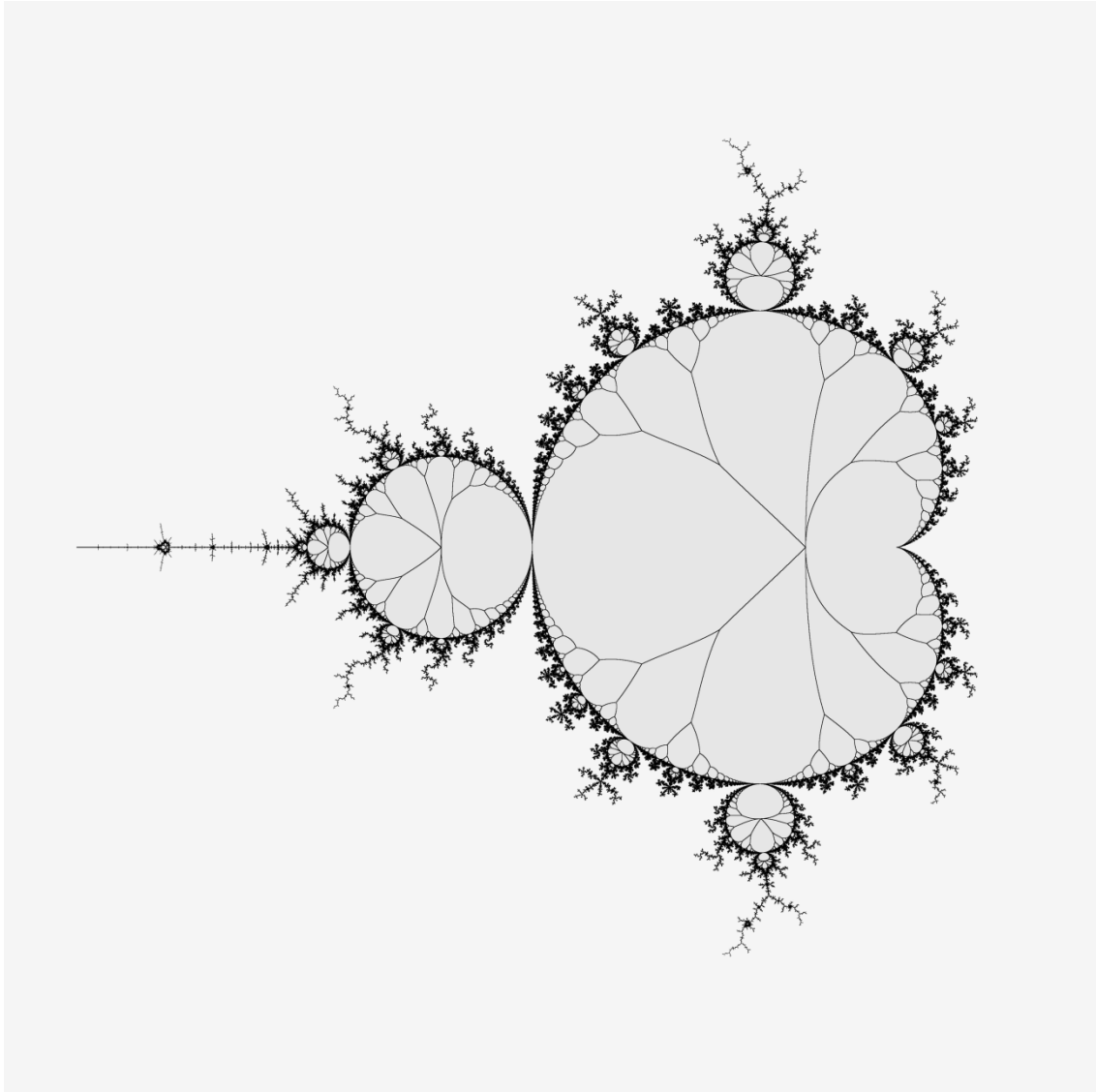
The fractals used to quantify entheses in this study are produced by using a contour gauge to replicate the contour of the enthesis at six rigidly defined axes: x- and y-axes as well as at two additional equidistant points along those two. The contours along those axes are then traced on to paper, scanned, scaled, and then cleaned digitally, ultimately producing a digital image of the contour. This procedure is undertaken for each enthesis of interest and while there is no numerical data associated with these “enthesal curves”, it is nonetheless possible to quantify their complexity using fractal analysis. The methods will be enumerated in greater detail in Chapter 6. The reasoning for using this method over readily available 3D laser scanning techniques is down to museum restrictions; not all the institutions where fossil hominin remains are kept will allow for the scanning of their specimens by third party researchers, and the costs associated with acquiring museum scans were beyond the resources available for this study. Using a contour gauge to quantify entheses has the advantage of being cheap, simple, reproducible, portable, and free from the above mentioned constraints.

This section details the theoretical background to fractal analysis and provides justification for its use as an analytical tool in studies such as the one presented in this dissertation. The properties of fractals will be described as well as how the complexity or roughness of a natural object may be quantified as a single value (fractal dimension or *D*-value).

5.2 Theoretical Background

The concepts of fractal geometry were originally presented by Benoit Mandelbrot in the mid-1970s and formalised in his publication *The Fractal Geometry of Nature* (Mandelbrot, 1983). Fundamentals of fractal geometry centre on the observation that natural objects are not well described by the ideal constructs of Euclidean geometry. That is, the natural world does not easily fit within an idealised Euclidean space defined by points, straight lines, and Platonic solids. The concept of a fractal dimension (D) was introduced as a necessary step to extending the concept of dimension to fractal objects and it differs from topological dimensions in that D -values may be non-integer. That is, the manner in which a fractal object occupies and fills space differs both qualitatively and quantitatively from ordinary geometrical objects. Analytic use of fractal geometry in real images and datasets (e.g. time series data and rescaled range analysis) has since been explored extensively in the literature, from finance to rock fracture mechanics.

Two fundamental properties characterise fractal objects: self-similarity or self-affinity, and fractal dimension (D). “Self-similarity” is the property of being exactly (mathematical objects) or statistically (natural objects) similar at all levels of magnification such that an object may be continuously subdivided into parts which approximate a reduced-scale replica of the original whole.



Mathematical fractals, such as the eponymous Mandelbrot set (Fig. 14), have a precise definition as possessing infinite length and exact self-similarity. For objects that are self-similar, the amount of detail is constant over an infinite range of scaled whether the fractal is generated theoretically or mathematically; this is exact self-similarity. An object (A) is said to be exactly self-similar if A comprises N individual subsets all of which are identical to $r(A)$ under translation and rotation (i.e. all the subsets are congruent to $r(A)$). In this equation, r is a scaling function that acts to scale all the

coordinates in the object to the same amount. Natural fractals (statistically self-similar objects), however, have a limited range of self-similarity that ranges between two and four decades (Peitgen and Richter, 1986), which is limited by the range over which a natural object may be magnified without breaking down into atomic structures. This also holds for empirical datasets. There is an element of randomness that prevents real data sets from being truly or exactly self-similar, in addition to finite size limits on measurements, calculations, and observations. An object (B in this instance) is said to be statistically self-similar if B is comprised of N distinct subsets which possess *statistical* properties identical to $r(B)$.

Fractals may also be “self-affine”, which is the property of being self-similar only when scaled or transformed anisotropically as self-affine sets are naturally scale differently along the x- and y-axes (Mandelbrot, 1985). This differs from self-similar fractals which scale isotropically but does not preclude fractal behaviour. Determining the fractal dimension of self-affine features is usually less straight-forward than self-similar fractals, limited to only a few methods which are applicable only to certain kinds of data and these will be discussed in the following sections. Determining whether an object is self-affine versus self-similar can be achieved simply interchanging the axes (x, y) of the coordinate system used to map the feature of interest; if the axes of the feature can be interchanged without fundamentally altering it, then it fulfils the basic requirements of self-similarity. Linear features such as topographic contours, for instance, are not altered substantially when the axes are switched as both contain the same information meaning that slices through topographic surfaces are self-similar and the fractal dimension of those slices bear a direct relationship to the original surface (Orey, 1970). The distinction between a self-affine profile and self-similar profile, however, is ambiguous (Mandelbrot, 1985, Klinkenberg, 1994). Traditionally, profiles generated by time-series data are considered to be self-affine because the axes encode different

information and the profile itself exists only in a self-affine/anisotropic plane. Topographic profiles/cross-sections are a more complicated issue as a profile of a topographic surface is a curve in an isotropic plane, and thus may be assessed mechanically – if not theoretically – as a self-similar fractals (Mandelbrot, 1985). Whether a profile can be considered self-similar or self-affine is ultimately a function of research objectives (Klinkenberg, 1994, Sakellariou et al., 1991, Carr and Wardner, 1987, Mandelbrot, 1985). Given that the enthesal profiles or curves generated by this study are analogous to topographic cross-sections and that this kind of binary data can only truly be assessed via one method (see below), their treatment as self-similar fractals is justified as a heuristic measure of relative complexity.

Mandelbrot's fractal dimension provides a measure of complexity whereby uncomplicated structures have small D -values and complex structures have large D -values (Mandelbrot, 1967, Mandelbrot, 1983). The Hausdorff-Besicovitch dimension provides a more granular approach to exploring this complexity. The Hausdorff-Besicovitch dimension (originally the Hausdorff dimension) was first introduced by Felix Hausdorff (Hausdorff, 1918) and further developed by Abram Besicovitch (Besicovitch, 1929). The Hausdorff-Besicovitch dimension was significant when it was introduced because it put forward a definition of dimensions with non-integer values such that the Hausdorff-Besicovitch dimension may be defined as an extended non-negative real number associated with any metric space. In this way a fractal may be formally defined as a set for which the Hausdorff-Besicovitch dimension or fractal dimension exceeds the topological dimension (i.e. for an n -dimensional inner product space, the D will equal n). While there is no one set way of defining the fractal dimension (it is dependent on the method used – see below), for our purposes D at its most basic can be calculated by the equation

$$D = \frac{\log N}{\log S} \quad (1)$$

Where N is the number of self-similar subsets into which the fractal object may be divided and S is the scaling factor needed to observe N . The D -value of an object is limited to the dimension in which it exists. This means, for instance, that an assemblage of single points will have a D -value of 0, lines a D -value 1, surfaces a D -value 2, and so on. At each level, as the dimension of an object moves from one integer to the next, the complexity of the object increases. Curves (such as the those generated in this project) have a dimension that lies between 1 and 2 which is related to the degree of information they contain and it is these non-integer D -values that are referred to as the Hausdorff-Besicovitch dimension. While the Hausdorff-Besicovitch dimension is of theoretical interest, it is largely included here for completeness. It is this theoretical basis that many fractal analysis methods stem and its discussion provides context for the following sections.

The formalism of fractal geometry is useful as a heuristic tool for quantifying morphological complexity in enthesal studies. The borders and topography of entheses can be fully specified as a series of Cartesian co-ordinates and this process can be fully automated through the use of three-dimensional laser surface scanning and other specialised processing software. The difficulty, as mentioned in previous sections, is the means of quantification; historically entheses have been assessed qualitatively (see Chapter 2). Further complications arise when fossil specimens are the subject of study as not all institutions allow the specimens that they hold to be laser scanned by third parties, which in turn limits sample sizes, which was a serious difficulty encountered during the data collection phase of this dissertation. Manual methods involving the generation of curves (binary images) using tools like profile gauges provide a simple and effective means to describe and quantify entheses by allowing them to be visualised

as curves in a topography. As a fractal dimension is an index of the space-filling properties of an object, it is possible to use D -values as a heuristic to describe the organisation of entheses surface complexity or roughness and indeed, in materials science roughness is directly related to fractal dimension (Pfeifer, 1984).

Many fields determine the fractal dimension of linear features – naturally occurring objects and features with a topological dimension of 1 – as a routine part of investigation, and a wide variety of methods have been developed to do this (Klinkenberg, 1994). These methods include – but are not limited to – box counting, line-scaling, variogram, power spectrum, Korack's law, divider relation, and area/perimeter relation. Some considerations must be made when selecting the right method for the type of feature being analysed. Some methods work well on certain types of objects (e.g. area-based methods require the target object be a closed loop) while others should only be used on one type of fractal (self-similar versus self-affine) or applied with particular considerations to the limitations and analytical power of the method. Fractal dimension may also be calculated for time series data which, while mono-dimensional, differ from binary images in having numerical values associated with the datasets (e.g. elevation and distance in topographies, co-ordinates in 3D scans, intensity and frequency data from seismograms).

5.2.1 Box dimension estimation method

The box dimension estimation method or box-counting dimension is a simple and flexible way to quantifying the fractal complexity of complicated self-similar, non-integer objects of any size, from the very small (e.g. dust) to the very large (e.g. the known universe). The greatest utility of the box dimension estimation method lies in its ability to be applied to sets of any dimension. It works by containing the object of interest with squares or boxes depending on whether the object occupies one-, two-, or

three-dimensional space, and performing a statistical analysis to determine the object's physical dimensions.

The basic procedure for calculating the fractal dimension involves overlaying the object with grids of varying sizes and then comparing how much space is occupied by the image at different grid scales. A grid square is counted only once if it encounters at least one pixel of the image. The fractal dimension of the image is then established by plotting the *log* of the number of tiles encountered against the *log* of the grid edge length. While the boxes are placed within a grid for mathematical convenience, it is theoretically possible to define a box dimension where boxes are placed at any position and orientation so as to minimize the number of boxes needed to cover the set. It should be noted however that finer grids generally produce a more accurate measured dimension due at least in part to amount of variation that can arise in counting regions dependent on how a grid is placed.

While this process produces accurate results, it is limited by the plane in which the object exists because a fractal's dimension cannot exceed the dimension of the units used to measure it (Falconer, 2003). For instance, if a two-dimensional grid is used to overlay the object, the fractal dimension calculated cannot exceed 2. An increase in the number of space coordinates means an exponential growth in the amount of computation and therefore the possibility of error. Regardless, within one- and two-dimensions the box dimension estimation method has been described as an exact way to calculate the fractal dimension of objects (Smith Jr et al., 1989). As the curves generated in this study exist only in one dimension (that is, $D_T = 1$), this method is considered to be an appropriate means by which to quantify the fractal complexity of the entheses curves used in this study.

The Hausdorff-Besicovitch dimension can be equivalent to the box-counting dimension however due to its subtlety it is generally used only in theoretical settings as it can be difficult to implement in practical settings (Skubalska-Rafajłowicz, 2005). Further there are several comparable definitions available for the box dimension, the most commonly used of which is the Minkowski–Bouligand dimension and the one discussed here (Falconer, 2003, Dubuc et al., 1989). In box dimension estimation method, the fractal dimension is given by the exponent Db in the relationship:

$$N(d) \approx \frac{1}{d^{Ds}} \quad (2)$$

In this power law, $N(d)$ represents the number of grid squares of linear size d required to enclose the set in a one- or two-dimensional plane. In this way equation (2) defines the fractal dimension of Euclidian objects. In order to cover a set of points distributed on a smooth line, a number of boxes proportional to $1/d$ are required, proportional to $1/d^2$ for points distributed on a plane (et cetera). As mentioned previously, Db is calculated by counting the number of boxes to cover the set for a range of values of d and then plotting $N(d)$ versus d within *log-log* space. Providing that the set is indeed a fractal, the plot will follow a straight line with a negative slope that equals $-Db$. Using box sizes that follow a geometric progression (e.g. $d = 1, 2, 4, 8\dots$) rather than an arithmetic progression (e.g. $d = 1, 2, 3, 4\dots$) gives points that are evenly distributed in *log-log* space. The box dimension method can and has been applied with equal effectiveness to sets of points, areas and volumes, curves, and linear features like contour lines (Klinkenberg, 1994).

The procedure for applying the box counting method to curves is slightly different compared to other objects (Klinkenberg, 1994, Klinkenberg and Goodchild, 1992). First the curve is divided lengthwise into a number of segments (e.g. four). Using a specified vertical value drawn from the section divides, the number of intersections are counted

for the curve along a horizontal line. The number of boxes/divisions is then geometrically increased and the number of intersections recounted, and this process continues until the minimum resolution of the data is reached. Box size is then plotted logarithmically against the number of intersections counted and the fractal dimension is calculated as the slope multiplied by minus one. For a one-dimensional curve contained in a two-dimensional space, the range of possible D values is from 1 to 2. Higher values of D (i.e. values closer to 2) indicate a more complex curve. Conversely, the closer D is to 1, the less complex the curve. The output allows for assessment of surface complexity within and between different entheses by calculating the total amount of space occupied by a self-affine curve (such as the curves generated in this study) within a grid.

In the past, problems associated with this method were predominantly computational; they required significant computer memory to implement (Liebovitch and Toth, 1989). With the advent of modern computing and exponential increases in computing power, this is no longer an impediment to its use. Nevertheless, resolution remains an important consideration to make before utilising this method. Dubuc et al. (1989) note that, for the box dimension method to return accurate results, there should be as many data points used as possible and that instabilities with the method are liable to occur when the number of data points used is small (i.e. the shape in question can be covered one or four boxes, which are always the first two iterations in the box count). Liebovitch and Toth (1989) defined the upper and lower boundaries for box size, finding that the first two counts should not be used and nor should cell sizes equal to the resolution of the data (i.e. when each data point falls within a single cell). A restriction common to methods which determine the slope within *log-log* space is cell size; the boxes should increase by a power of two in order for the boxes to be evenly spaced in *log* space.

However, if this occurs too rapidly, not enough data points fall within the *log-log* plot (Dubuc et al., 1989) and as such dyadic boxes should be avoided.

5.3 Summary

The box dimension method is the best analytical tool for quantifying the fractal complexity of the enthesal curves as it is easily accessible and reproducible. While fractal dimension values can vary according to the method used to quantify them in the case of real-world (that is, not exact mathematical) fractals (Klinkenberg, 1994), the use of the box dimension method as a heuristic tool for mechanically assessing the complexity of entheses as no other method is suitable for this kind of data. Directions for future studies with more funding might include conducting the same analysis using 3D laser scanning and other fractal methods, but until then this study may nonetheless be revealing of patterns in enthesal complexity in fossil hominins.

CHAPTER 6: MATERIALS AND METHODS

6.1 Materials

6.1.1 Enteseal Complexity

The fossil material spans ~10 species and includes 4 clavicularae, 3 scapulae, 20 humeri, 5 radii, and 13 ulnae, totalling 45 individual elements. The original fossil material was studied in all cases with the exception of A.L. 288-1 (“Lucy”, *Au. afarensis*), where a first-generation cast of the fossil was used instead. The fossil specimens included for analysis represent a variety of taxa, here provisionally classified as follows in Table 2:

Table 2. Species and specimen numbers for the fossil material included in the enteseal complexity study.		
Species	Specimens	Element type
<i>Australopithecus sp.</i>	Omo 119-73-2718	Humerus
	KNM-ER 739	Humerus
<i>Australopithecus sediba</i> (MH2)	U.W. 88-57, U.W. 88-101	Humerus
	U.W. 88-38	Clavicle
	U.W. 88-85	Radius
	U.W. 88-62	Ulna
<i>Australopithecus africanus</i>	STS 7, STW 150, STW 328, STW 339, STW 433	Humerus
	STS 7, STW 434	Scapula
	STW 437	Clavicle
	STW 380, STW 398, STW 432a, STW 571	Ulna
	STW 528	Radius
<i>Australopithecus afarensis</i>	A.L. 137-48A, A.L. 288-1M, A.L. 322-1, A.L. 333-107, A.L. 333-109, A.L. 438-1C	Humerus
	A.L. 288-1L	Scapula
	A.L. 333x-6/9	Clavicle
	A.L. 288-1T, A.L. 438-1A	Ulna
<i>Australopithecus anamensis</i>	KNM-KP 271	Humerus
<i>Paranthropus boisei</i>	KNM-ER 1504	Humerus
	OH 36, L40-19	Ulna
<i>Paranthropus robustus</i>	TM 1517f	Humerus
	TM 1517e, SKX 8761	Ulna

<i>Homo habilis</i>	OH 48	Clavicle
<i>Homo aff. habilis</i>	SK 24600	Humerus
	SK 24601	Radius
<i>Homo ergaster</i>	SKX 34805	Humerus
	SK 18b, KNM-BK 66	Ulna
	SK 2045	Radius

The sample of fossil material includes specimens from the Ditsong National Museum of Natural History, Kenya National Museum, National Museum of Ethiopia, National Museum and House of Culture, Dar es Salaam, and The Evolutionary Sciences Institute, University of Witwatersrand.

6.2 Methods

6.2.1 Electromyographic and Kinematic Data Acquisition

6.2.1.1 Subjects

Sixteen subjects (9 male, 7 female; age (mean \pm standard deviation: 26.8 ± 9.3 ; age range: 19-54 years); height: 1.70 ± 0.07 m; mass: 71.6 ± 16.9 kg; all right-handed), who had not had shoulder or elbow pain, for at least 2 years and had never sought treatment for shoulder or elbow pain were recruited from the student body of the University of Sydney and the general population. Each volunteer completed a questionnaire gathering basic data such as age, sex, weight, height, handedness, physical activity patterns, and previous history of shoulder surgery or injury. Basic functional testing was conducted to ensure normal shoulder and elbow range of motion and scapulohumeral rhythm in participants as well as no pain during isometric shoulder internal and external strength testing, confirmed visually and by self-report.

Prior to testing, subjects were given the opportunity to practice simple stone knapping so as to familiarise themselves with the task required. One-hour tutorials were run on an individual or group basis depending on individual availability in which the participants

had the basic principles of Oldowan stone knapping explained to them verbally by me (proficient at Oldowan flake production). This was followed by a demonstration of the process in which the participants were encouraged to mimic me as I knapped. The rest of the hour was spent practicing the task while being observed by me, and the participants' form corrected where necessary. Participants were given the opportunity for follow-up practice sessions on an elective basis. This fostered a satisfactory level of familiarity with the task, and participants were supplied with additional video and written material on the process to review at their leisure. Longest time between training and data collection was 4 weeks due to the constraints of scheduling for three participants, though most participants had a gap of a day or two between training and data collection. Those participants with the longer breaks were re-familiarised with the task immediately prior to data collection taking place.

The study was approved by the Australian National University's Human Research Ethics Committee (HREC) (Protocol number 2014/321). As the study has previously been approved by the ANU HREC, it was unnecessary to seek a second ethical approval from the University of Sydney HREC in accordance with the policy of that organisation. The Head of the School of Medical Sciences, Dr. Peter Knight, at the University of Sydney, was informed of the project, and the study proceeded under the authority of the ANU HREC. Participants were fully informed of the experimental protocol and provided their consent prior to commencing the experiment.

6.2.1.2 Instrumentation

EMG data were collected simultaneously from 15 shoulder and elbow muscles using both indwelling (intramuscular) fine wire and surface electrodes. Nine surface electrodes were used to capture EMG data from pectoralis major, biceps brachii, lower and upper trapezius, proximal and distal portions of triceps brachii, anterior deltoid, and

the superficial wrist and finger flexors and extensor muscle groups. Six intramuscular electrodes were used to record activity in subscapularis, teres major, latissimus dorsi, rhomboid major, infraspinatus, and supraspinatus. The wrist flexor and extensor muscles were measured collectively with one surface electrode each to give a broad indication of their activity; as these muscles are individually quite small and thin, and because of their close proximity to one another, the likelihood of crosstalk and intramuscular electrode displacement was considered high. Given that the flexor and extensor groups have their origins on the medial and lateral epicondyles and supracondylar ridges respectively, a more generalised view of their collective activity levels was considered sufficient to infer their individual role and recruitment patterns.

Before the placement of the surface electrodes, the skin of each participant was prepared with alcohol and an abrasive gel (NuPrep, DO Weaver and Co., Aurora, USA) to limit skin impedance. Excess hair was shaved where necessary. Electrode placement was determined via anatomical landmarks and the procedures outlined by Basmajian and DeLuca (1985) for surface electrodes. At each appropriate location, two surface electrodes (Red Dot, 2258, 3M, Sydney, Australia) were placed 2 cm apart in line with the direction of the underlying muscle fibres, and inter-electrode resistances were ensured to be $<10\text{ k}\Omega$ in all instances.

Indwelling electrodes were manufactured in the laboratory using the technique described by Basmajian and DeLuca (1985). These electrodes were used for muscles for which surface electrode recording has been shown to be invalid (latissimus dorsi, infraspinatus; Ginn and Halaki, 2015, Johnson et al., 2011), and which underlie superficial muscles (subscapularis, rhomboid major, supraspinatus), or shift with respect to the overlying soft tissue during shoulder movements (teres major). Correct indwelling electrode placement was determined. Indwelling electrodes were inserted

using a 23-gauge cannula needle with the subject lying down in the positions summarised in Table 3 (see also Fig. 15). Correct indwelling electrode placement was determined by visual inspection of the EMG signals as the participant performed standardised submaximal tests expected to elicit a large amount of activity from the muscle in question. This was compared with tests expected to activate surrounding muscles into which the electrode may have inadvertently been placed. Because of the difficulty in distinguishing rhomboid major activity from lower trapezius activity using this method, intramuscular electrodes were inserted into rhomboid major using ultrasound guidance (Mindray, DP-9900). A grounding electrode (Universal Electrosurgical Pad:Split, 9160F, 3M, Sydney, Australia) was placed on the acromion and scapular spine of the contralateral limb.

The signals were amplified (Iso-DAM 8 amplifiers, World Precision Instruments, Sarasota, FL; gain = 100-1000, input impedance $>10^{12}\Omega$, common mode rejection >100 dB), filtered (band-pass = 10-1000 Hz) and acquired on a PC with a 16-bit analogue to digital converter at a sampling rate of 2,564 Hz using Spike 2 software (version 4.00, Cambridge Electronics Design).

Table 3. Location of electrode placement for intramuscular and surface electrodes.

Electrode type	Muscle	Electrode placement
Intramuscular	Latissimus dorsi	Posterior axillary fold directly lateral to the inferior angle of the scapula
	Teres major	Posterior axillary fold 5 cm superior to the electrode for latissimus dorsi
	Subscapularis	5 cm below the medial edge of the scapular spine and directed perpendicular to the medial scapular border
	Supraspinatus	Medial one-third, immediately superior to the scapular spine
	Infraspinatus	Centre of the infraspinous fossa
	Rhomboid major	Midway between T3 or T4 and the vertebral border of the scapula
Surface	Pectoralis major	3.5 cm distal to the coracoid process of the scapula in line with the muscle fibres
	Biceps brachii	Centre of the muscle belly
	Lower trapezius	Midway between T7 spinous process and

		inferior angle of the scapula
	Upper trapezius	Superomedial and inferolateral to a point 2 cm lateral to one-half the distance between the C7 spinous process and the lateral tip of the acromion
	Proximal triceps	On the midline of the arm, approximately 25% of the distance between the acromion process and proximal olecranon
	Distal triceps	2 cm lateral to the midline of the arm, approximately 50% of the distance between the proximal olecranon and acromion process
	Anterior deltoid	3.5 cm below the anterior angle of the acromion
	Wrist/finger flexors	Centre of the muscle bellies 5 cm distal to the humeral medial epicondyle
	Wrist/finger extensors	Centre of the muscle bellies 5 cm distal to the humeral lateral epicondyle

6.2.1.3 Signal Normalisation

EMG data were normalised to maximum voluntary isometric contraction (MVIC) by having each participant perform the eight maximal tests in random order, the five shoulder normalisation tests (Boettcher et al., 2008, Ginn et al., 2011), and three elbow/wrist tests. These tests were:

- Self-resisted shoulder adduction at 90° flexion (“Palm press”)
- Resisted shoulder internal rotation at 90° abduction (“Internal rotation 90°”)
- Resisted shoulder abduction with the shoulder at 90° abduction and internally rotated (“Empty can”)
- Resisted shoulder flexion with the shoulder at 125° flexion (“Shoulder flexion 125°”)
- Resisted shoulder extension with the shoulder at 30° abduction and 0° flexion
- Resisted wrist, finger and elbow flexion at 90° elbow flexion with the shoulder at 0° abduction
- Resisted elbow extension at 90° flexion with the shoulder at 0° abduction

- Resisted wrist and finger extension at 90° elbow flexion with the shoulder at 0° abduction

These maximal shoulder tests have been shown to have a 95% chance of maximally activating the all the shoulder muscles investigated in this study (Boettcher et al., 2008, Ginn et al., 2011). Each test was performed in three repetitions with each repetition lasting for a duration for 5 seconds and a rest interval of at least 30 seconds between repetitions. The rest interval between normalisation tests was a minimum of 1 minute. During the testing process, subjects were given verbal feedback and closely monitored to ensure that compensatory movements of the shoulder and trunk did not occur during the MVICs. If compensatory movements did occur, those repetitions were noted to be disregarded later on that participant's data collection sheet or deleted from the EMG signal recordings if it occurred in the first repetition. Subjects were also able to observe the raw EMG signals on the computer screen in front of them during the testing phase.

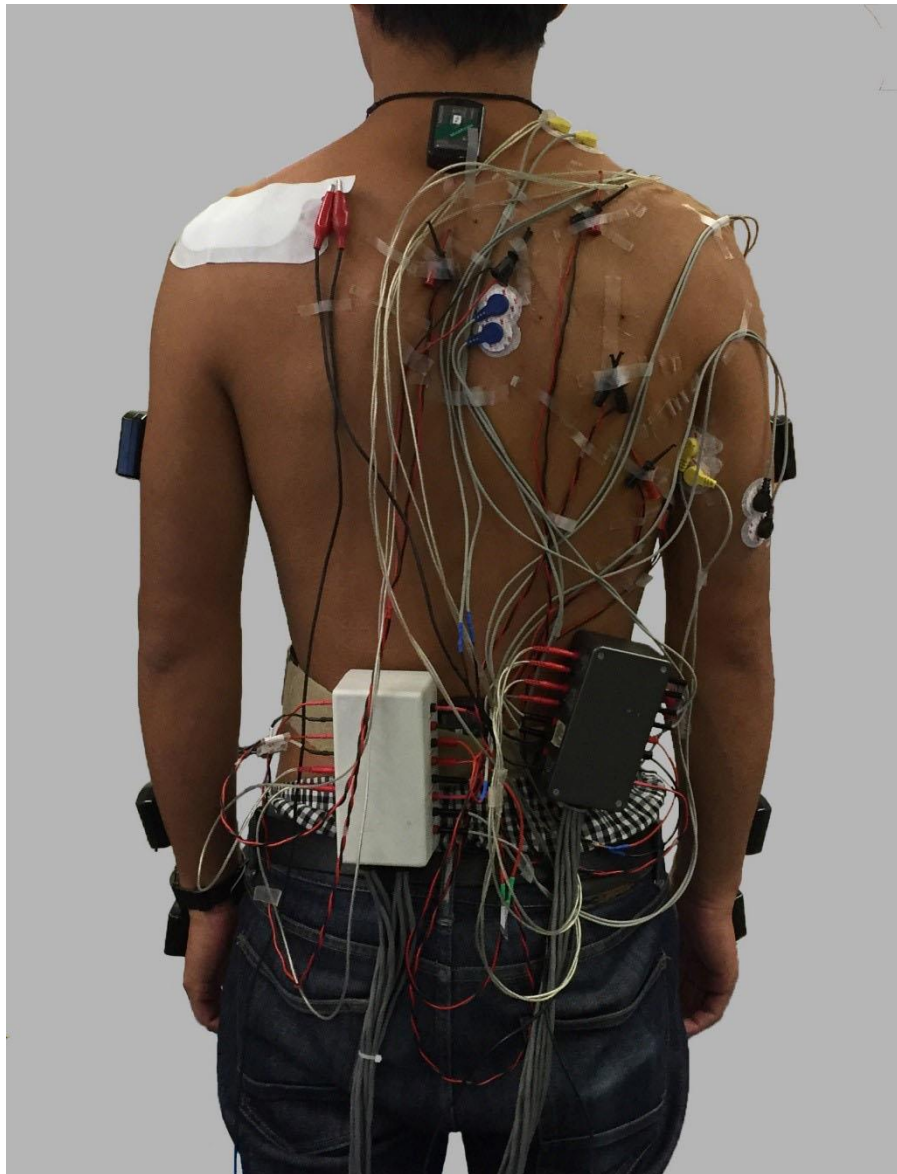


Figure 15. Electrode and wireless inertial sensor placement. The small black boxes are the inertial sensors. All electrode cables were taped in place and full range of motion ensured prior to data collection taking place.

6.2.1.4 Kinematic Measures

Wireless inertial measurement units (MyoMotion Research Sensors – Model 610, Noraxon, Scottsdale, AZ, USA) were attached to the hand, forearm, and upper arm of the striking arm, as well as to the upper and lower thorax of each participant using medical tape to measure joint kinematics of the striking arm during the knapping cycle. These sensors then transmitted data on the limb orientations to a receiver (MyoMotion

Research Receiver – Model 680, Noraxon, Scottsdale, AZ, USA) attached to the computer using the MR3 software (Version 3.6.20, Noraxon, Scottsdale, AZ, USA) at a sample rate of 100 Hz, where they were synchronised with the EMG and force signals during the strike (MyoSync, Noraxon, Scottsdale, AZ, USA).

6.2.1.5 Kinetic Measures

A force platform with four load cells (Kistler 9287B, Kistler Instrumente AG Winterthur, Switzerland) was used to record forces in the anterior-posterior (X), medial-lateral (Y), and vertical (Z). The force signals were collected using a 16-bit analogue to digital converter at a sampling rate of 1000 Hz (MP100A, Biopac Systems Inc., Santa Barbara, CA, USA).

6.2.1.6 Stone Material

Heat-treated Keokuk chert spalls, prepared by expert knapper Craig Razat at Neolithics.com, were used in the knapping experiment. Keokuk chert is a fine-grained, silica-rich sedimentary rock and was selected for three reasons. First, its lack of natural planes of separation, meaning that when struck with sufficient force conchoidal fractures occur; this process is predictable, which allows the knapper to control and direct the application of force so as to shape the material being worked. Secondly, the ease with which it is able to be worked by a beginner. Thirdly, its availability. All spalls are bifacial and broadly similar in dimensions (~12 cm in length). The angular protrusions make the cores suitable for the production of a sequence of flakes. This procedure ensured standardised initial conditions as much as possible.

Hammerstones consisted of a selection of ovoid water-worn basalt cobbles sourced from the North Island of New Zealand. The hammerstones provided were of a range of similar shapes and sizes so that participants could select the hammerstone that was most

comfortable for them to use during training, but were then limited to a single hammerstone of known mass during data collection to eliminate hammerstone weight as a variable.

6.2.1.7 Procedure

With all electrodes and sensors in situ and inserted according to the procedures outlined above, each participant was seated on the force plate during the experiment with the hammerstone and a supply of spalls. All subjects used the same hammerstone (weight: 500 g). Using their dominant hand, the subjects were then instructed to knap for at least 5 minutes or until a sufficient number of successful strikes had been produced for analysis.

To encourage the correct form during the knapping process, the subjects were observed closely by me and given the opportunity to observe me knapping along with them while they were under experimental conditions. In the event that the core became too reduced to allow for further detachment of flakes, the core was replaced with a new one.

6.2.1.8 Data Analysis

EMG signals were high pass filtered (10 Hz, zero lag 8th order Butterworth), rectified and then low pass filtered (5 Hz, zero lag 8th order Butterworth) using Matlab 2014b (The Mathworks). The maximum value of each muscle obtained during the MVICs was used to normalise the EMG recordings during stone knapping for that muscle. All signals were then resampled to 200 Hz. The start of the up-swing and down swing of the arm was identified using the elbow and shoulder flexion angles. The initiation of either angle in each direction was identified using their angular velocity traces. The strike of the hammerstone with the core was identified from the vertical force trace. A subject

specific threshold force was used to identify strikes and eliminate any movement artefact due to subject movements.

The peak EMG amplitude and the timing of the peak EMG during each up and down swing phases were calculated. All signals were then time normalised to 101 points for each phase and mean and 95% confidence intervals calculated across cycles for each subject as well as across subjects. The timing of the peaks were then converted to a percent of duration of each phase for each cycle.

6.2.1.9 Statistical Analysis

Peak EMG amplitudes and the timing of the peak EMG values were compared across muscles using a one factor (muscle: 15 levels) repeated measures analysis of variance (ANOVA) (Genstat 18th Edition, VSN International). Fisher's least significant difference post hoc analysis was used to identify specific differences when significant ANOVA results were obtained. Statistical significance was set at $p < 0.05$.

6.2.1.10 EMG Modal levels

Muscle activity in the knapping experimental was classified according to a modal level scheme, similar to what had been proposed by Marzke et al. (1998), in order to generalise muscle recruitment levels in knapping for comparison with the fractal data. Marzke et al. (1998) used a three-category system giving preference to data from one highly experienced knapper:

- Category 1: Muscles with maximum recruitment in one or both hands in the highly-experienced (Subject 1) and proficient knapper (Subject 2).
- Category 2: Muscles with high recruitment in Subject 1 and Subject 2.
- Category 3: Muscles with low levels of recruitment in Subject 1.

Marzke et al. (1998) used non-standard MVIC levels to allocate muscles to these categories. In order to make the results of this project more generalisable to the clinical literature and more accurately represent muscle activity magnitude, recruitment in this study will be categorised the following way:

- 0–20% MVIC: low muscle activity
- 21–40% MVIC: moderate muscle activity
- 41–60% MVIC: high muscle activity
- >60% MVIC: very high muscle activity

These percentage levels reflect typical procedure in the clinical literature for generalising EMG data (Escamilla and Andrews, 2009) and this approach will be used in this study.

6.2.2 Confounding Factors

In Chapter 2 Section 2.3, factors that have been found to confound analyses of enthesal development were discussed. Niinimäki (2011) found that age and body size, rather than sex, are the major confounding factors for interpreting labour intensity data in entheses. While it is not possible at this point to know precisely the nature of these scaling relationships in fossil hominin populations, it is nonetheless necessary to consider and account for these factors in this study.

6.2.2.1 Exclusion Criteria

Fossil material was excluded from analysis on the basis of a number of criteria: any fossils that were obviously immature (unusually small size, unfused epiphyses) or too old (degenerative joint changes, extreme wear on any associated dentitions), or exhibiting obvious signs of skeletal and enthesis pathology in line with the conditions and criteria discussed in Chapter 2, Section 2.2.4. For instance, KNM-ER 1808

represents a fragmentary partial skeleton attributed to *H. ergaster*, including upper limb material, which shows evidence of pathological apposition of bone. This has been attributed by Rothschild et al. (1995) to treponematosi s in the form of yaws which causes extensive bone destruction. Although enthesis involvement is unusual in such cases (Rothschild et al., 2000), the extensiveness of the pathology in KNM-ER 1808 excluded it from analysis.

6.2.2.2 Controlling for Body Size Bias

Weiss (2012) has demonstrated that the confounding factor of body size is absent for fibrocartilaginous entheses but it is factor in fibrocartilaginous entheses (that is, diaphyseal entheses). While excluding diaphyseal entheses would be the most expedient means by which to control this factor, doing so reduces sample size and removes potentially informative entheses such as that of pectoralis major from analysis. In order to control for body size effects, each fibrous enthesal curve was scaled to set (arbitrarily selected) pixel dimensions of 250 by 150 pixels.

6.2.2.3 Controlling for Age Bias

As increasing age has been found to be a confounding element in enthesal complexity studies (Niinimäki, 2011), fossil developmental age must be carefully considered on a case-by-case basis. Postcranial material offers a particular challenge in this regard as many fossil hominin postcranial specimens are not associated with craniodental material with which to make strong developmental age judgements. Further complications arise when the specimens lack epiphyses/metaphyses as a result of taphonomic processes (e.g. isolated diaphyseal fragments), limiting researchers to making educated guesses about the age of individual specimens based on size and rugosity.

In the context of this study, it was important to ensure that only adult specimens were used, and in the majority of specimens this was easily ascertained based on examination of associated skeletal (especially craniodental) material and patterns of epiphyseal fusion. By this criterion, well-known specimens such as KNM-WT 15000 (*H. ergaster*) and MH1 (*Au. sediba*) were excluded based on their young age and incomplete development. With more fragmentary specimens, aging becomes increasingly uncertain, particularly when trying to account for older individuals and whether pronounced enthesal complexity in one specimen is a peculiar activity-related morphology or simply the result of advancing age. Fortunately, studies of palaeodemography offer some insight. Caspari and Lee (2004) examined changes in longevity in fossil hominins from the Plio-Pleistocene (*Australopithecus*, early *Homo*) through to early Upper Palaeolithic (post-Neandertal Europeans) by assessing ratios of older to younger adults based on age determinations from dental wear seriation. They found that a greater proportion of young adults is represented by australopith assemblages, noting that the proportion of older adults doubles with Early/Middle Pleistocene *Homo* but nonetheless remains very low. As the purview of this study is limited to Late Pliocene and Early/Middle Pleistocene hominins, individuals of advanced age were not considered to be a significant confounding factor.

6.2.3 Quantitative Data Acquisition on Enthesis Complexity in Fossil Hominins

6.2.3.1 Enthesis Complexity Collection Procedure

A six-inch zinc-plated steel contour gauge with 1 mm pins was used to create curves of entheses in fossil hominin material following an adaptation of the method developed by Henderson (2012). A contour (or profile) gauge is a tool commonly used in woodworking or metalworking to record the cross-sectional shape of irregular surfaces. It consists of an array of steel or plastic pins aligned parallel to one another in a frame.

The frame maintains the pins in the same plane while allowing them to move freely perpendicular to the frame. The pins conform to the shape of the surface when pressed against it, and hold the shape so that the user may then trace an exact copy of the curve onto another surface. Contour gauges have also been used in archaeological illustration to record the shape of pottery. As the entheses of the muscles chosen for study display clear delineations, all were considered appropriate surfaces for analysis. In instances where, for reasons of preservation, the boundaries of the enthesis were not clear, a margin of surrounding bone was also included.

Two perpendicular chords of the entheses, mediolateral (x-axis) and proximodistal (y-axis), were measured using digital sliding callipers to define the shape of the enthesis. To facilitate fractal analysis, the mediolateral axis was taken from the exact midpoint of the proximodistal axis rather than, for instance, from the maximum width. The method used in this dissertation differs from Henderson (2012) in that surface roughness was recorded at two additional axes at equidistant locations along the proximodistal and mediolateral axes. The advantage of this method is that, as the intersection of the x- and y-axes occurs at the midpoint of the enthesis and the end point of each axis is further defined by the midpoint, this point is theoretically identical for all the individuals in the sample and is therefore comparable between individuals. This has the added advantage of eliminating most problems encountered in geometric morphometry which require size and shape scaling.

The contour gauge was placed along the length of all six axes on the surface of the enthesis and each resultant curve transferred to graph paper using a mechanical pencil using 0.5 mm lead. In both the qualitative and quantitative analyses of the attachment sites, it was important to define the limits of the entheses. The entheses of many of the muscles chosen for this study had the advantage of having clearly identifiable edges. As

such, delineation of the borders for the curves was uncomplicated in most instances and confirmed by repeated testing. The diagnostic sensitivity of this step was determined by my ability to differentiate insertion from non-insertion bone. Where preservation or the nature of the fossil did not allow this, a margin of up to 2 mm of non-insertion bone around the estimated shape and location of the enthesis was taken to ensure all available information about the complexity of the enthesis was extracted.

The curves were digitised using a flatbed scanner, and rotated to ensure that the left and right sides could be compared. The curves (Fig. 16) were then digitally transformed and cleaned in the image processing software Adobe Photoshop CS5 using the following procedure. This step eliminates “noise” within the raw curves and allows for the curve to be converted to a file type compatible with the Benoit 1.3 fractal analysis software.

The images were cropped to the end of the curves and converted to black and white by selecting the “Greyscale” option from the Image → Mode menu bar. From here the images were cleaned by selecting the Image → Adjustments → Threshold menu and the “Threshold” set to “170”. The threshold function determines which tones appear as black and which are dropped from the image altogether. Adjusting the threshold removes all intermediate tones and leaving only black and white tones. In the cases where a Threshold setting other than 170 was used, the file name was changed to specify the threshold level (e.g. “Rclavicle delt-ori x-axis BW [threshold number].bmp”). Once this process was completed, the resultant cleaned curve was scrutinised for extraneous marks which were removed where appropriate and scaled. The image was then saved as a bitmap (“.bmp”) file type to allow analysis in the Benoit 1.3 fractal analysis software.



Figure 16. Example of a disigitised enthesal “curve”. In this case, the curve represents the distal x-axis of the medial epicondyle of KNM-ER 1504.

6.2.3.2 Enthesis curve analysis and Fractal Dimension Calculation

The fractal dimension of the curves was calculated using the box dimension estimation method in the Benoit 1.3 fractal analysis software whereby larger fractal dimensions (D) are indicative of greater enthesal complexity (Falconer, 2003) (Chapter 5, Section 5.2.1). The output of these calculations was saved as both a graphics file (see Appendix 2) and as a text file. The fractal dimension (D) values were then exported to GenStat 18th Edition (Payne et al., 2015) for statistical analysis using a linear mixed models approach.

6.2.4 Statistical Analyses

6.2.4.1 Intra- and inter-observer error for enthesal curves

The enthesis for the clavicular origin of the Deltoid was tested for both intra- and inter-observer error (that is, tested for differences in fractal dimension values). This was achieved by extracting the curve for the x-axis of the Deltoid on 3 clavicae, using the same contour gauge on five consecutive days. These curves were then scanned and assessed as described above, and the fractal dimension (D) calculated and compared.

The D values for each trial are presented in Table 4 for observer 1 and Table 5 for observer 2.

Table 4. Fractal dimension (D) values for each clavicle across each trial day for observer.					
	Trial 1	Trial 2	Trial 3	Trial 4	Trial 5
D -value	1.90	1.91	1.92	1.91	1.90
	1.92	1.91	1.92	1.91	1.92
	1.93	1.91	1.91	1.93	1.91

Table 5. Fractal dimension (D) values for each clavicle across each trial day for observer.					
	Trial 1	Trial 2	Trial 3	Trial 4	Trial 5
D -value	1.90	1.92	1.91	1.92	1.91
	1.91	1.91	1.91	1.91	1.93
	1.90	1.91	1.91	1.91	1.93

The fractal dimension values were compared using a one-way ANOVA for both intra- and inter-observer error (Tables 6 and 7). For the intra-observer test, there were no outliers, as assessed by boxplot; D values were normally distributed for all five trials, as assessed by Shapiro-Wilk's test of normality ($p > .05$), and; a Levene's Test of Homogeneity of Variance proved there was homogeneity of variances ($p = .124$). Data is presented as mean \pm standard deviation.

For the inter-observer test, there were no outliers, as assessed by boxplot; D values were normally distributed for all five trials, again as assessed by the Shapiro-Wilks test of normality ($p > .05$), and, again, a Levene's Test of Homogeneity of Variance proved there was homogeneity of variances ($p = .132$). Data are presented as mean \pm standard deviation.

No statistically significant difference was found between the samples in either in intra- or inter-observer error tests at 95 percent confidence interval ($p= 0.05$). These results assure the robusticity of the method for use in this experiment.

Table 6. Results of one-way ANOVA for intra-observer tests of *D*-values.

	Sum of Squares	df	Mean Square	F	Sig.
Between Groups	0.000	4	0.000	0.553	0.702
Within Groups	0.001	10	0.000		
Total	0.001	14			

Table 7. Results of one-way ANOVA for inter-observer tests of *D*-values.

	Sum of Squares	df	Mean Square	F	Sig.
Between Groups	0.000	4	0.000	1.500	0.274
Within Groups	0.001	10	0.000		
Total	0.001	14			

6.2.4.2 Statistical analyses for enthesal curves

The fractal complexity of fossil hominin entheses were analysed using a generalised linear mixed models (GLMM) approach and the results of these analyses are presented in Chapter 9. A GLMM approach works in much the same fashion as an unbalanced ANOVA where the number of observations at each factor-level are unequal. The aim of both is the same: to determine which treatment effects differ significantly from a zero-value at which factor-level combinations and levels. GLMM has a number of advantages over unbalanced ANOVA, however, including treatment for effect not being dependant on the order the terms are entered into the model, as it already has its own explicit model structure (Seltman, 2015). GLMM is capable of modelling individual

change across time while being flexible enough that repeated measures are not required to have the same number of observations per subject (e.g. missing observations, or axes in this case, can be compensated for in the model), and time is modelled as continuous instead of as a set of fixed points. Further, GLMM has the ability to handle correlated clustered (individuals belong to a group of individuals, such as a species) data with unequal variances such as the fossil data presented in this dissertation. It can also be used for repeated observations within individuals within clusters while allowing for flexible specification of the covariance structure among repeated measures and contains methods for testing the specific determinants of this structure (Seltman, 2015). All statistical analyses were conducted in Genstat 18th Edition, VSN International.

CHAPTER 7: EARLY HOMININ UPPER LIMB ANATOMY

7.1 Introduction

The upper limb of early fossil hominins is represented by several species including *Australopithecus africanus*, *Australopithecus afarensis*, *Australopithecus sediba*, *Australopithecus anamensis*, *Paranthropus robustus*, *Paranthropus boisei*, *Homo habilis*, and *H. ergaster*. These fossils collectively allow for a relatively complete picture of the shoulder girdle and elbow to be developed. Descriptions of the *H. naledi* material are not included in the analysis as the state of surface preservation in those specimens precluded them from inclusion using the current methodology. The case was similar for specimens such as OH 62 (attributed to *H. habilis*) where upper limb material is preserved in fair overall completeness, but the quality of preservation was not sufficient for analysis. If a specimen is not included here, either it was not available for analysis at the time of visiting the relevant institution or the preservation did not allow for the collection of good quality data. The focus of this chapter will be describing the fossil remains used in this study and as such the chapter is organised by species which is further grouped by skeletal element for ease of assessment. The citations next to individual specimen catalogue numbers refer to the publication describing or attributing the specimen, where available.

7.2 Fossil Descriptions

7.2.1 *Australopithecus africanus*

7.2.1.1 Humeri

STS 7 (Broom et al., 1950)

The STS 7 humerus is a right proximal humeral fragment including the humeral head and a portion of diaphysis. The articular surface is almost completely intact, though both tubercles are slightly damaged and the shaft has been significantly deformed by crushing. Both tubercles are largely intact with the exception of the lateral/posterior surface of the greater tubercle below the level of the supra- and infraspinatus insertion facets as a part of the mediolateral crushing the diaphysis has undergone. The lateral margin of the bicipital groove is consequently eroded along its length. The medial margin of the bicipital groove and lesser tubercle are completely intact and free from distortion. Despite these defects, there does not appear to be any noticeable distortion to the shape of the humeral head. The mediolateral head diameter is 39.9 mm and the anteroposterior head diameter 35.1 mm. This yields a humeral head index of 88.0%.

STS 7 appears to be essentially human-like in morphology. The lesser tubercle is more pronounced than is generally seen in modern humans with a well-developed crest that bounds the bicipital groove. Greatest width of the intertubercular groove is approximately 6.0 mm. Broom et al. (1950) estimated the reconstructed length of the STS 7 humerus as between 290.0 mm and 310.0 mm. The greater tubercle by comparison is not as well-developed and does not project above the head of the humerus. The insertions for the Mm. supraspinatus and infraspinatus are rugose and separated from one another by a pronounced bony ridge. The insertion for the M. subscapularis is slightly damaged at its proximal-most extremity where small segments

of insertion bone have flaked away, obscuring the contour of the insertion surface. On the posterosuperior surface of the greater tubercle, there is a concavity that represents the insertion of *M. teres minor*. Insertions for the *Mm. pectoralis major*, *latissimus dorsi*, and *teres major* are completely indistinguishable. If there was a deltoid tuberosity, it has been damaged beyond recognition. The remainder of the specimen is too badly damaged to be of any utility in morphological assessments.

STW 328

STW 328 is a right proximal humeral fragment consisting of three-quarters of the humeral head, a section of the greater tubercle, most of the lesser tubercle, and a small portion of the diaphysis. Possible carnivore damage and weathering to the bone surface on anterior and posterior surfaces of head and lateral part of anatomical neck. This damage has exposed large portions of trabecular bone. Fossilisation cracks present in the bicipital sulcus speak to some distortion having occurred.

The mediolateral head diameter is approximately 34.0 mm, but the anteroposterior head dimension cannot be determined due to damage to the articular surface. Distally, the articular surface forms a ledge over the intracapsular non-articular area, which is slightly concave and flares anteriorly below the lesser tubercle somewhat. The lesser tubercle has a pronounced anterior projection with a roughened surface. In addition to this, there is a large area of complexity on the distal portion which likely represents the insertion for the subscapularis muscle. The crest of the lesser tubercle is most pronounced proximally before flattening out and becoming continuous with the insertion of *M. teres major* distally. Within the floor of the bicipital groove itself there is an area of rugosity that may mark part of the insertion for *M. latissimus dorsi*. The greater tubercle is large and globular, based on what can be determined of remaining segment. This segment is approximately 21.0 mm in length. The greatest breadth of the

bicipital groove is approximately 5.0 mm, but it is otherwise badly damaged due to weathering. Cortical bone thickness varies between 3.0-3.4 mm.

STW 433 (Toussaint et al., 2003)

STW 433 is the right distal humerus belong to the skeleton STW 431. Much of the shaft below the level of the midshaft is preserved including epicondyles and distal articular surfaces. Overall cortical surface preservation is good, though some damage has occurred to the condyles and the medial trochlea particularly, exposing trabecular bone. The medial pillar and medial supracondylar crest are absent distally. The trochlear and the capitulum are neatly divided into two segments near-equal in size by a prominent lateral trochlea crest. Both medial and lateral epicondyles are intact, the latter being pronounced. Cross-sectional diaphyseal shape distally is somewhat triangular and flattens quickly moving distally. Proximal to the olecranon fossa, the anteroposterior diameter of the shaft is 15.0 mm. The radial and coronoid fossae appear broad and shallow with only a slight crest delineating the margin between them. Biecondylar breadth is 59.3 mm.

7.2.1.2 Scapulae

STS 7 (Broom et al., 1950)

The STS 7 right scapular fragment preserves the lateral half of the scapular spine, a little over half of the superior axillary margin, a segment of the acromion, the coracoid process, most of the glenoid cavity, and supraglenoid tubercle.

The glenoid fossa of STS 7 has a pyriform shape with strong notching of the mid-costal margin and some superficial damage to the articular surface. Damage to the glenoid has meant that estimates of the dimensions vary widely between studies (see Broom et al., 1950, Robinson, 1978, Vrba, 1979). Vrba (1979) put the greatest length of the STS 7

glenoid cavity at approximately 38.0 mm. Assuming that the supraglenoid tubercle is largely intact through the superior surface and that anteroposterior distortion is minimal for the length of the tubercle, this is more or less in agreement with my estimate of 37.0 mm. Substantial damage to the dorsal margin of the glenoid, as well as minor damage to the costal glenoid along its lower margin, makes estimation of greatest breadth of the glenoid more difficult to ascertain. A number of authors have nonetheless attempted to estimate this; it should be noted, however, that this specimen underwent cleaning and reconstruction in the late 1970's (see Vrba, 1979), calling into question measurements of this dimension taken earlier (e.g. Broom et al., 1950, Robinson, 1978). This process removed breccia matrix and revealed considerably more of the bone surface for analysis. Vrba (1979) has estimated the articular surface breadth to be 19.5 mm and the greatest glenoid cavity breadth to be 22.0 mm. Berger (1994) estimated the articular surface breadth to be 19.0mm and the greatest breadth to be 23.0mm, based on his belief that the ridge along the costal margin of the glenoid at the point of greatest breadth is the attachment site for the glenoid labrum. This would therefore delineate the furthest extent of the articular surface. Berger's (1994) reconstructions and estimate of original greatest breadth also included an allowance for bone loss on both the lower dorsal and costal margins, hence its slight elevation in comparison to Vrba's (1979) estimates. I am in agreement with Berger (1994) as to the significance of the ridge on the costal margin of the glenoid as being the attachment for the glenoid labrum, and as such I have estimated a greatest articular breadth of c. 19.0 mm. Where I would differ is in the estimation of greatest cavity breadth; my estimate of 22.1 mm, since I considered the amount of bone loss to be too uncertain and I therefore measured only what could be observed. From these measures a glenoid index value of 59.7% was calculated which is comparable with those taken from the literature. The only exception would be Robinson (1972), whose estimated glenoid index of 51.4% is likely the result of his

underestimating greatest glenoid breadth when the specimen was still partially encased in breccia.

The supraglenoid tubercle is orientated costolaterally and well-developed. The infraglenoid tubercle is narrow and long with a well-defined superior projection resembling a tubercle. Vrba (1979) suggested that this projection may represent post-mortem alterations to the bone. The axillary margin is narrow with a total length of 71.0 mm. Along its length there is a slight costal curvature. The acromion, while lost, has been illustrated in Broom et al. (1950); from the illustration, it is clear that the acromion was incomplete but nevertheless apparently extended medially over the glenoid fossa. The scapular spine is absent except for a small portion remaining at its base medial to the spinoglenoid notch. Some thickening to the scapular spine can be observed here relative to the modern human condition despite some loss of bone surface laterally. Vrba (1979) hypothesised that this can be attributed to increased angle at which the scapular spine intersects with the scapular surface – at more of a right angle by Vrba's evaluation and dissimilar to *H. sapiens* in this way. Depth of the spinoglenoid notch is approximately 12.0 mm.

The coracoid process is partially complete. The dorsolateral tubercle is well-developed and laterally placed. It is likely that this represents a homologue of the attachment of the conoid ligament in other hominoids. If this is indeed the case, then the placement is more lateral than seen in *Homo*, more closely resembling *Pan* or *Pongo* but differing from the latter in that it does not markedly project dorsally. It is unclear to what extent the coracoid process extended laterally, and authors subsequently differ in their estimates. Ciochon and Corruccini (1976) interpreted the STS 7 coracoid as not projecting significantly over the glenoid laterally, while Vrba (1979) suggested that it

approaches the condition seen in *Pongo* but is not otherwise as pronounced as in other extant hominoids.

STW 434 (Toussaint et al., 2003)

This specimen is a right scapular fragment belonging to the partial *Au. africanus* skeleton STW 431 and comprises the axillary margin with part of infraglenoid tubercle and inferior angle attached. The supraspinous fossa, scapular spine and acromion, coracoid process, and glenoid cavity are entirely absent from this specimen. The infraspinous fossa is also missing with the exception of a small portion represented by the inferior angle of the scapula. There does not appear to be any noticeable distortion to the specimen. The length of the axillary margin is approximately 140.0 mm, though the original length was probably 2-3 mm longer given that much of the infraglenoid tubercle is absent. The infraglenoid tubercle is rotated costolaterally.

On the anterior surface, the ventral bar is orientated almost completely superoinferiorly with a slight costal curvature along its length. There is an axillary sulcus located inferomedially to the distal infraglenoid tubercle. The sulcus is transversely thin and expands laterally, possibly accommodating the scapular insertion for the long head of *M. triceps brachii*. Distally, the insertion for *M. serratus anterior* on the inferior angle is largely absent medially due to damage. Where present, the surface is complex with an ovoid depression toward the centre of the roughened area. The ridge for the attachment of the *Subscapularis* muscle is pronounced.

On the dorsal surface, the origin of *M. teres minor* is weakly developed and occupies the lateral-most edge of the axillary margin. Approximately 40.0 mm inferior to the superior breakage point there is a depression that may represent a groove for the passage for the dorsal scapular artery. The inferior attachment of *M. teres minor* and superior attachment for *M. teres major* lies in the distal one-third of the axillary margin with a

prominent ridge separating them. At the junction of Mm. teres major and teres minor there is a slight depression that crosses the ridge obliquely, which may denote a homologue of the oblique line; the ridge continues inferomedially and terminates close to the axis of the inferior angle. Inferior to this, there appears to be some overlapping of the serratus anterior muscle attachment with the ridge as well as with a small segment of the inferior-most part of the attachment for M. rhomboid major. There is also another small ridge near to the serratus anterior attachment. While it is unclear what this ridge may represent functionally, two possibilities are 1) a tuberosity created by the intersection of Mm. serratus anterior and teres major muscles, or 2) an attachment for M. latissimus dorsi. There is a laterally projecting protuberance located on the superior-most part of the M. teres major attachment on the axillary margin with a distinctive tubercle at the superolateral tip. The origin of M. teres major continues distally until it comes into contact with the superomedial projection of the serratus anterior attachment.

7.2.1.3 Claviculae

STW 437 (Toussaint et al., 2003)

The STW 437 right clavicular fragment is associated with the STW 431 partial skeleton. It is missing both medial and lateral articular ends, totalling 71.5 mm in length. At the medial end shaft dimensions are 8.7 mm superoinferiorly and 13.1 mm anteroposteriorly. Cortical bone thickness varies between 3.0 mm at medial end and 1.5 mm at lateral end. There is no observable distortion to the shaft of the clavicle. In cross-section, the STW 431 clavicle is flattened inferiorly with a rounded superior surface. As both articular ends are absent it is impossible to accurately determine the degree of clavicular torsion, but based on visual assessment it is clear that there would have been some degree of torsion present. Sigmoid curvature of the clavicle is low.

Overall the appearance of the clavicle is notably smooth with only a few areas of development at muscle attachment sites. The deltoid crest is present as an enlarged, sharpened ridge located anteriorly on the inferior surface approximately 23.5 mm from the lateral breakage point. The length of deltoid crest is approximately 20.0 mm; it terminates artificially with a medial breakage point. There is an area of rugosity present near the lateral point of breakage on posterior margin of inferior surface which possibly represents a medial continuation of the conoid tubercle. Toussaint et al. (2003) note that the conoid tubercle appears poorly developed. On the superior surface at the mediolateral breakage point there is a small area of development approximately 13.0 mm in length that constitutes part of the deltoid tuberosity. The clavicular site of attachment for M. deltoideus extends medially from tubercle across the superior surface before continuing inferiorly onto the anterior surface. Here it forms a well-developed deltoid crest.

7.2.1.4 Radii

STW 431 (Toussaint et al., 2003)

The STW 431 radius is a proximal right radius, broken at the approximate midshaft and preserving the proximal articular surfaces. This specimen is associated with the STW 431 partial skeleton. The radial head is markedly circular in form when viewed superiorly, with a distinct circumferential margin. The articular fovea is quite a bit smaller than the radial head. Moving distally, the neck of the radius appears long and robust, and the radial tuberosity is quite rugose and narrow. Inferior to the tuberosity, interosseous crest is relatively blunt and proximodistally short. The minimum circumference of the diaphysis is 41 mm and the diaphyseal cross-sectional shape at the midshaft is ovoid.

7.2.1.5 *Ulnae*

STW 432a (Toussaint et al., 2003)

STW 432a right proximal ulna associated with the STW 431 partial skeleton, preserving approximately two-thirds of the length of the ulna and proximal epiphysis in good condition. The coronoid process is largely missing. Maximum breadth of the olecranon is 25.8 mm. The trochlear notch is superoanteriorly orientated with slight elongation proximodistally. The supinator crest is present as a prominent tubercle which grades smoothly into the surrounding bone as it moves distally. On the medial aspect of the olecranon, the origin of *M. flexor carpi ulnaris* (as well as the attachment of the posterior and oblique bands of the ulnar collateral ligament) is evident as a distinct tubercle, distal to which is a marked concavity marking the origin of *M. flexor digitorum profundus*. The ulnar tuberosity maintains a shallow sulcus for the insertion of *M. brachialis*, the lateral margin of which is somewhat rounded compared to the medial margin. Midshaft diameters are 12.0 mm AP and 14.7 mm ML.

7.2.1.6 *Additional specimens*

The following specimens attributed to *Au. africanus* have also been included in the analysis but lack descriptions due to unrecoverable data loss in the course of developing this dissertation. The data loss resulted from a hard-drive failure and included the descriptions of the fossils and the photos used to document the specimens from a single day of work, but not the fractal data as this was non-digital. As these specimens have not been formally described outside of non-digitised Ph.D. theses, it has not been possible to supplement these descriptions for this chapter. These specimens are: STW

339 (humerus), STW 150 (humerus), STW 380 (ulna), STW 398 (ulna), STW 571 (ulna), STW 528 (radius).

7.2.2 *Australopithecus afarensis*

7.2.2.1 Humeri

A.L. 137-48A (Lovejoy et al., 1982)

A.L. 137-48a is a right distal humerus, 74.6 mm in length, and preserving the trochlea, capitulum, and both epicondyles. The lateral supracondylar crest is damaged along its length (subperiosteal bone missing), whereas the medial supracondylar crest is only mildly sharpened and otherwise smooth. Regarding the medial supracondylar crest, there is a nutrient foramen situated 20.4 mm superior to the superior-most point of the medial epicondyle. The lateral epicondyle is almost completely eroded in a circular patch, exposing trabecular bone. A section of the posterolateral trochlea wall has also been affected by this damage. The lateral supracondylar ridge is intact, nonetheless. There are a number of fossilisation cracks, only one of which has distorted the specimen somewhat on its medial aspect; the others largely do not affect the preservation of the morphology. The medial distortion has been caused by a large fracture passing through the centre of the trochlea (dividing it into roughly medial and lateral halves) in a superomedial direction, arcing over the medial epicondyle, and following much the same course on the posterior aspect as it did on the anterior aspect, passing through the posteromedial border. This medial fragment has been completely circumscribed by the fracture, separating it from the bulk of the specimen, and it has been subsequently posteriorly displaced somewhat though it remains affixed to the main fragment by matrix. Maximum breadth of the fracture is 1.5 mm. The medial lip of the trochlear is

abraded along its length and a large piece of bone is missing from it on the posterior aspect

The lateral epicondylar ridge has been damaged along its length to the level of the superior (missing) lateral epicondyle and appears weakly developed. The medial epicondyle is somewhat rugose and presents a relatively distinct margin separating the anterior and posterior aspects of the bone, though the origin of *M. pronator teres* is indistinct. Projection of the medial epicondyle from the medial margin of the trochlea is 15.0 mm. The area for the origin of the common flexor tendon is very rugose with a sharp margin circumscribing the limits of the attachment, the most pronounced of which is the posterior margin. On the posterior aspect, the olecranon has a strongly ovoid shape and is very deep, having a mediolateral breadth of 19.5 mm and 13.2 mm anteroposterior diameter. Moving anteriorly, there is a septal aperture perforating the coronoid fossa, approximately 6.1 mm in diameter at its widest point and 4.9 mm proximodistal height. The radial fossa has distinct margins and achieves its greatest depth immediately proximal to the centre of the capitulum though it is otherwise shallow. It is the same breadth (ca. 10.7 mm ML) as the coronoid fossa (ca. 10.8 mm ML).

The overall impression of the distal articular surfaces is of an essentially human-like condition proportionally, although the sulcus between the capitulum and lateral trochlea margin is very deep which is unlike modern humans, producing a marked trochlear/capitular keel. The biepicondylar breadth is 49.4 mm with an estimated distal articular breadth of 32.1 mm excluding the medial fossilisation crack (including the added 2.2 mm breadth from the fracture, this metric is 34.3 mm). The medial diameter of the trochlea measured anteroposteriorly is estimated to be 18.9 mm although damage to the medial trochlear margin makes this metric a very tentative estimate. The diameter

of the lateral trochlea measured anteroposteriorly is 19.8 mm. The trochlea has a deep waist, creating a distinct groove between the medial and lateral trochlea... crests. The estimated true trochlear breadth is about 17.9 mm mediolaterally (without the fossilisation crack; with the crack the actual breadth is 20.1 mm). The capitulum has a breadth of 12.5 mm, a superoinferior diameter of 14.7 mm. The AS-PI diameter of the capitulum (measured across the articular surface) is estimated at 15.7 mm, while the anterior projection (the AP diameter from the most projecting point on the anterior surface to the non-articular dorsal surface) cannot be determined.

A.L. 288-1R (Taieb et al., 1975, Johanson et al., 1982)

This specimen is a proximal left humeral fragment consisting of the proximal one-third of the humerus. The anatomical neck of the specimen has been internally expanded and the bicipital groove has been heavily damaged, along with the lesser and greater tubercles. What can be determined of the tubercles is that they are unlikely to have projected greatly over the articular surface. The articular surface is nearly completely preserved. While the humeral head has undergone some distal compression and posteromedial displacement, the mediolateral diameter does not appear to have changed appreciably. This gives a mediolateral head diameter of 31.0 mm. Compression damage does make accurate determination of the anteroposterior head diameter difficult, though an estimated measure of 26.9 mm was obtained by the author on a first generation cast, producing a humeral head index of 86.8%.

A.L. 288-1M (Taieb et al., 1975, Johanson et al., 1982)

AL 288-1m is a right humerus in two pieces with a reconstructed length of 237.0 mm. The first preserves much of the proximal shaft and portions of the humeral head; this segment is badly crushed and thus not very informative in terms of morphology. The articular surface is intact only in the central portion. Most of the lesser tubercle is

preserved, as is part of the greater tubercle. The bicipital groove is intact superiorly and appears free of deformation.

A.L. 322-1 (Lovejoy et al., 1982)

A.L. 322-1 is a left proximal humerus, 82.9mm in length. There is a fossilisation crack running mediolaterally just above the level of the coronoid fossa, with some slight (ca. 1 mm) posterior displacement of the distal articular section as a result. There is another crack moving inferiorly from the proximal breakage point on the anterior aspect, 23.0 mm in length. The lateral margin of the capitulum is eroded superiorly, exposing trabeculae. The superomedial margin of the trochlea, also on the anterior aspect, is damaged for a distance of 11.9 mm. On the posterior aspect, the medial and lateral margins of the trochlea are also slightly eroded with a proximodistally orientated fissure beginning 7.1 mm from the lateral margin. Cracking is also evident throughout the posterior aspect of the distal humerus, though no distortion is apparent. Both epicondyles are intact, as well as the articular surfaces of the capitulum and trochlea.

A.L. 322-1 is unfortunately broken too low on the diaphysis to estimate minimal shaft circumference. The lateral supracondylar ridge is only mildly sharpened, and there is some rugosity on the anterior surface. It extends from the superior-most point of the lateral epicondyle for the full length of the remaining diaphysis in this specimen (58.6 mm), suggesting development of *Mm. brachioradialis* and *extensor carpi radialis longus*. The lateral epicondyle is pronounced and rugose, and achieves its greatest lateral projection proximal to the superior-most point on the anterior capitulum (that is, the lateral epicondyle is proximally positioned). On the medial epicondyle, the origination site of the humeral head of *M. pronator teres* appears smooth and featureless, though it is somewhat obscured by the distal fracture. The biepicondylar

breadth is 45.8 mm mediolaterally and the medial epicondyle projects medially 12.0 mm from the medial trochlea margin.

The olecranon fossa is centrally located on the shaft with only slight development of the lateral distodorsal pillar. Its dimensions are 20.3 mm ML at its widest point by 13.5 mm PD. There is no septal aperture. The approximate depth, relative to the medial and lateral corners and measured to the centre of the fossa, is 8.5 mm. The lateral pillar is 12.3 mm thick and the medial pillar is 10.7 mm thick. The proximal edge of the olecranon fossa does not have a sharp apex superiorly and is mediolaterally elongate and rounded on its lateral margin. The capitulum has a breadth of 12.6 mm, a SI diameter of 16.2 mm. The AS-PI diameter of the capitulum is estimated at 15.7 mm, while the anterior projection is 17.9 mm. The radial fossa is broad but shallow, and is wider (ca. 13.8 mm ML) than the coronoid fossa (ca. 11.0 mm ML); both fossae appear tall (ca. 11.4 mm). The estimated trochlea breadth is about 17.3 mm mediolaterally. On the posterior surface, the lateral trochlear crest is oriented obliquely from proximolateral to distomedial.

A.L. 333-107 (Lovejoy et al., 1982)

AL 333-107 is a right proximal humerus preserving the humeral head and a portion of shaft whose surface is badly exfoliated. There are also a number of fossilisation cracks present in the shaft. The total length of A.L. 333-107 is 128.1 mm. The mediolateral dimension of the head is 39.5 mm and the anteroposterior dimension of the head is 34.0 mm, yielding a humeral head index of 86.3%. The specimen is robust with a wide and deep bicipital groove with a greatest width of 8.0 mm. The greater tubercle exhibits a large oval depression on the posterior surface for the insertion of the supraspinatus muscle. Just inferior and posterior to this is the insertion for M. teres minor which

presents as a small protuberance. The attachment of *M. teres major* on the proximal shaft is present as a well-developed ridge.

A.L. 333-109 (Lovejoy et al., 1982)

A.L. 333-109 is an extremely robust right humeral shaft. It is broken just inferior of the anatomical neck of the humerus and at the approximate point of the midshaft distally, giving the specimen a total length is 137.8 mm. The cortical bone appears thickest at the distal extremity of the specimen. There appears to be some degree of medial retroflexion to the shaft below the delto-pectoral junction, with the whole specimen curving medially along its length and flattening across the medial surface. Proximally, only the inferior 6.0 mm of the bicipital groove remains. This feature is wide and shallow, measuring 8.4mm wide at its greatest expanse, and exhibiting a well-developed ridge on its medial side indicating the insertion of *M. teres major* at this site. Moving distally, the deltoid tuberosity is extremely rugose and located approximately 100.0 mm from the proximal point of breakage. Located posteroinferiorly from the deltoid tuberosity is its junction with the similarly well-developed *M. pectoralis* insertion.

A.L. 438-1C (Drapeau et al., 2005)

A.L. 438-1c is a very large right humeral proximal diaphyseal fragment, preserved from the level of the surgical neck for a distance of 76.2 mm before terminating at the distal one-third of the insertion for *M. pectoralis major*. While this specimen does not preserve any diagnostic morphology, it does preserve the insertions for *Mm. pectoralis major*, *latissimus dorsi*, and *teres major*. There are a number of fossilisation cracks, orientated both transversely and longitudinally, are present in this specimen although no observable distortion has occurred to the specimen. At the proximal point of breakage, trabecular bone is exposed and some crystallisation has occurred in the fossilisation

process. Distally, the fracture plane has exposed the medullary cavity and cortical bone, the cavity itself having been infilled by crystallisation.

The insertion for *M. pectoralis major* begins approximately 10.0 mm inferior to the proximal breakage point and is expressed as a prominent crest on the anterolateral aspect of the diaphysis. This insertion grades into the proximal portion of the deltoid tuberosity. In the floor of the preserved portion of the bicipital groove, the insertion for *M. latissimus dorsi* is distinguished from the insertion for *M. pectoralis major* by a section of smooth non-insertion bone. There is depression on the anteromedial aspect of the diaphysis extending from the less tuberosity representing the insertion for *M. teres major*. Moving to the posterior aspect, the origin for the lateral head of *M. triceps brachii* is present as a low and rugose ridge running the full length of the fragment in an inferolateral direction. Measured at the surgical neck, mediolateral diameter of A.L.438-1c is 24.9 mm and 28.8 mm anteroposteriorly at the same point.

7.2.2.2 Scapulae

A.L. 288-1L (Johanson et al., 1982)

A.L. 288-11 is a right scapular fragment. It preserves the glenoid fossa, the base of the coracoid process, sections of the base of the scapular spine, and approximately 50.0 mm of the axillary margin. This specimen has been reconstructed from three large pieces that fit together in near perfect alignment. While A.L. 288-11 features a number of cracks, none of them appear to have caused any notable distortion to the specimen. This specimen is missing everything medial from the base of the scapula spine. Johanson et al. (1982) note a small subchondral defect on the articular surface of the glenoid fossa at the junction of cranial two-thirds and caudal one-third as being pre-mortem.

The preservation of the glenoid fossa is excellent. The ridge marking the attachment for the glenoid labrum is well-developed dorsally and in the superior one-half of the fossa. The supraglenoid tubercle is also well-developed and extends superolaterally to form a protruberance. This prominent rugosity marks the origin of the long head of the biceps brachii muscle and the coracohumeral ligament. The infraglenoid tubercle is less well-developed and presents as a slightly bulbous tuberosity at the distal rim of the glenoid fossa. Exact dimensions of the glenoid in A.L. 288-11 vary between authors. Johanson et al. (1982) measured glenoid length as 25.7 mm and glenoid breadth as 18.2 mm. Carretero et al. (1997) report values of 27.0 mm for glenoid fossa length and 18.1 mm for glenoid breadth. While I was not able to work on the original fossil material, measurements of the first generation cast held by the University of Witwatersrand produced values of 26.9 mm for glenoid length and 18.1 mm for absolute glenoid breadth, which are in close congruence with the literature. The resultant glenoid index is 67.3%. Also estimated from the cast was a spinoglenoid notch depth of approximately 10.0 mm.

Moving inferior of the glenoid, the axillary margin is narrow in the anteroposterior aspect with a deep ventral sulcus. Johanson et al. (1982) describe this as being “triangular ovoid” in shape. Dorsally, the axillary margin features a distinct groove just inferior of the glenoid rim. The significance of this is unclear. There are three possibilities: it could represent 1) the superior limit of the origin of *M. teres minor*; 2) the most inferior extent of the scapular origin of *M. triceps brachii*, or; 3) a groove for the circumflex scapula artery positioned more superiorly than is usually seen.

7.2.2.3 *Claviculae*

A.L. 333x-6/9 (Lovejoy et al., 1982)

This specimen is a right clavicular fragment missing both articular ends and preserving only the shaft. The total length of the fragment is 97.9 mm. Measurement taken at the midshaft of anteroposterior dimension gave a value of 12.2 mm, and 9.6 mm for the superoinferior dimension. Sigmoid curvature through the midshaft in this specimen is relatively mild compared to modern humans, though the missing medial articulation may account for this. Laterally, the clavicle flares markedly. Cross-sectional shape of the midshaft is ovoid in an anteroposterior direction and flattened more on the inferior surface. The superior surface is convex.

As noted by Lovejoy et al. (1982:638), the shaft is particularly nondescript with regard to muscular and ligamentous attachments. The superior surface features a ridge which forms the origin of the deltoid muscle. Inferiorly, the conoid tubercle is absent although an angular margin appears to have replaced it forming a discriminating line between the superior and inferior surfaces. The attachment of the costoclavicular ligament presents as a slight rugosity on the posterior surface of the specimen. In lateral aspect, the specimen has a rhomboidal shape.

7.2.2.4 *Ulnae*

A.L. 288-1T (Johanson et al., 1982)

A.L. 288-1t is a left proximal ulna. The proximal one-third of the bone is very well-preserved. Fossilisation cracks are present in a few places, and the surface of the bone has undergone some abrasion on the posterior aspect of the olecranon process, the margins of the articular surfaces, and at certain points on the diaphysis.

The olecranon process appears fairly human-like in its morphology. The insertion for *M. triceps brachii* on the superior surface is only slightly marked, and the area for the subtendinous bursa is not well-differentiated. The trochlear notch appears quite waisted, with a lateral border that is slightly concave. The radial notch is tear drop-shaped. The insertion for *M. brachialis* is marked as a deep depression on the anterior aspect of the proximal diaphysis, the distal extent of which is more marked than the proximal. The medial border of the insertion has a length of 30.2 mm and is notably sharp and crest-like. On the lateral border of the insertion, the ulnar tuberosity is 44.5 mm in length and presents as a fairly blunt bar of bone that grades smoothly into the diaphysis as it extends distally. Johanson et al. (1982) have suggested that *Mm. brachialis* and *pronator teres* find both their insertions in this depression, and I see no reason disagree with that assessment.

Moving laterally, the supinator crest is in fairly low relief, especially when compared to other crests in this specimen, and it forms a gentle parabola as it transmits distally toward the anterior aspect of the proximal diaphysis. Total length from the posterolateral border of the radial notch to its distal extremity is 18.5 mm, and the crest achieves greatest prominence just inferior to the radial notch. A slight rugosity extends from the distal extremity of the supinator crest, moving distally and posteriorly for some 24.0 mm before abruptly changing course to travel anteriorly and proximally where it grades into the proximal part of the interosseous crest. This rugosity, in addition to the supinator crest, likely circumscribes the full attachment of *M. supinator* on this specimen.

Moving further distal of the supinator crest proper, there is a second crest beginning at the midline (longitudinal axis) on the anterior aspect of the specimen, which spirals abruptly to the posterior aspect of the diaphysis, likely representing the inferior

extension of the M. anconeus insertion. The interosseous crest arises 30.0 mm from the inferior-most margin of the radial notch, and it is quite prominent and smooth in appearance. Total appearance of the diaphysis in this specimen is distinctly angular, more so than what is typically observed in modern human ulnae, and it compares well with other specimens from Hadar.

A.L. 438-1A (Drapeau et al., 2005)

A.L. 438-1a is a largely complete left ulna. Missing from this specimen are the anterior lip of the olecranon and a section of the articular surface of the semilunar notch immediately inferior to this, exposing trabeculae (dimensions 15.1mm ML by 9.1 mm PD). Some erosion has occurred to the inferomedial surface of the semilunar notch, measuring 4.2 mm in diameter mediolaterally. The radial facet is damaged along its inferior margin for a length of 10.6 mm anteroposteriorly and 1.8 mm proximodistally. The specimen is refitted from four large fragments though the pieces join cleanly and without distortion. The proximal break occurs 36.0 mm inferior to the inferior lip of the radial notch (at the level of the supinator crest). Some bone is missing here from the anterolateral and posteromedial aspects and no taphonomic rounding has occurred to the edges of the breaks. The dimensions of the missing section on the posteromedial aspect are 14.3 mm AP by 7.1 mm PD. On the anterolateral aspect, the missing section measures 12.0 mm ML by 6.4 mm AP at the point of greatest width. The second break is weathered, more or less completely transverse in orientation, and located 116.2 mm from the distal-most tip of the styloid process. The third break occurs 71.5 mm from the second weathered break and follows an irregular trajectory, the posterior portion of the break occurring 10 mm inferior of its anterior portion. On the lateral aspect of this break, a proximodistally orientated fossilisation crack is also present though it does not

appear to have caused any deformation of the fossil. A small segment of bone is also missing from the anterior surface of this break, 2.0 mm by 2.0 mm. Generally speaking, however, the cortical surface of the specimen is well preserved.

The morphology of this specimen, including muscle attachment sites, is in very good condition though there is some evidence of pathological activity. The semilunar notch is anterior-facing with only weak keeling. The articular surfaces of the semilunar notch are gently concave with mild lipping around its margins. Some vascularisation of the central non-articular area of the semilunar notch has occurred in the form of a cluster of foramina. The non-articular bone has a sharp margin and almost completely bisects the articular surface mediolaterally. The radial notch is tear drop-shaped, anteriorly tapered, and concave anteroposteriorly. The insertion for *M. triceps brachii* on the superior aspect of the olecranon process is pathological. There is a subchondral bone cyst located centrally on the enthesis, as well as enthesophytic development along the posterior margin clearly evident when viewed laterally. Cystic changes to the enthesis such as this can be indicative of either acute pathologies including infection or trauma, or chronic conditions like osteoarthritic, rheumatoid arthritis, and aseptic necrosis (Mann and Hunt, 2005).

The crest for *M. supinator* is strongly developed and extends inferiorly from the posterior margin of the radial notch for 29.0 mm before beginning to round and flatten out. Along this length, the crest is rugose with irregular ridging posteriorly. Inferior to the supinator crest, immediately below the proximal break (10 mm below the crest), a parabola of raised bone extends distally for 16.3 mm and curves anteriorly for 8.9 mm. This arc of bone may represent the distal extremity of the attachment for *M. anconeus*. The interosseous crest is rounded and continues the length of the diaphysis to the insertion of *M. pronator quadratus*. There is distinct rugosity to the posterolateral

margin of the crest indicating the attachments sites for Mm. abductor pollicis longus, extensor pollicis longus, and extensor indicis, though individual attachments cannot be determined.

On the posterior boarder of the proximal ulna and medial boarder of the olecranon, the attachment for M. flexor carpi ulnaris and ulnar collateral ligament is present as a distinct ridge that grades to a slightly concave surface just inferior to the ridge. On the lateral aspect, the insertion for M. anconeus also produces a salient ridge on the posterior boarder of the olecranon process. These two ridges combine to create a triangular section non-insertion bone that is somewhat vascularised (there are a number of small nutrient foramina dispersed across this area). The confluence of Mm. anconeus and flexor carpi ulnaris ridges occurs at the level of the radial notch, extending distally to meet the posterior boarder of the diaphysis. The posterior boarder is blunted but becomes rugose approximately 81 mm from the inferior margin of the radial notch.

Moving distally, the interosseous crest is blunt and extends to the origin of M. pronator quadratus. There is a pronounced sulcus for M. extensor carpi ulnaris on the posterior aspect of the styloid process bordered by a rugose margin, and this sulcus moves anteriorly toward the tip of the process. The overall appearance of the styloid is short, extending only 3.4 mm beyond the ulnar head. The head of the ulna has a mediolateral dimension of 17.6 mm and 8.8 mm anteroposteriorly, and some vascularisation of the space between the styloid process and ulnar head has occurred. Including the styloid and distal articular surface, the distal ulna has a maximum dimension of 20.0 mm measured anteroposteriorly.

7.2.3 *Australopithecus sediba* (Berger et al., 2010, Churchill et al., 2013)

Australopithecus sediba is presently represented by two largely complete individuals: an immature male (MH1) and adult female (MH2). As MH1 is not fully developed, it was excluded from use in this study as per the exclusion criteria outlined in Chapter 6, Section 6.2.3. The following descriptions therefore pertain only to upper limb material attributed to MH2. The MH2 complete scapula was not included in the analysis as the original fossil was not available for study at the time of visiting the institution.

7.2.3.1 Humeri

U.W. 88-57

This specimen is a right humerus in three pieces with surface morphology well-preserved. The proximal section preserves the humeral head and a portion of the diaphysis down to approximately the middle of the deltoid tuberosity, 110.3 mm in length. The central section, approximately 87 mm in length, preserves the distal remainder of the deltoid tuberosity. The distal-most portion includes a section of the distal diaphysis, epicondyles, and distal articular surfaces, approximately 92 mm in length. There is a transverse fracture, roughly perpendicular to the long axis of the diaphysis, which separates the proximal and central fragments. While the fracture surfaces appear to be congruous, some crushing is present on the posterolateral surface of the central fragment at the proximal break. The central and distal fragments are cemented together with matrix; the central fragment has undergone some anterior displacement such that its distal end overlaps the proximal end of the distal fragment. The effect is some angular displacement in the sagittal plane. Unlike the proximal break, this fracture is comminuted with diaphyseal fragments adhered to the remaining shaft with matrix. On the whole, preservation in this specimen is very good, with only minor exfoliation, abrasion, invertebrate damage, or fossilisation cracking present.

Maximum length of the humerus is difficult to determine due to the fractures. The humeral head is elliptical and clearly posteriorly directed, indicating that MH2 has a low humeral torsion value. Humeral head diameter values are 33.2 mm superoinferiorly and 32.7 mm mediolaterally³. Of the tubercles, the insertions for *Mm. supraspinatus* and *infraspinatus* are preserved on the greater tubercle and exhibit a moderate degree of development. The lateral lip of the bicipital groove is markedly developed with a maximum thickness of 5.2 mm measured mediolaterally at the top of the groove which is suggestive of a well-developed *M. pectoralis major*. The lip extends distally to form a pronounced, somewhat rounded ridge which narrows to a crest at the level of the surgical neck. The greater tubercle appears large relative to the humeral head and the lesser tubercle is prominent and medially projecting. This latter feature is unlike modern humans where the lesser tubercle projects more medially. The medial lip of the bicipital groove in MH2 is formed by the lateral margin of the lesser tubercle proximally and a crest that intersects the tubercle at the midline distally. The length of the lesser tubercle taken along the length of the insertion facet for *M. subscapularis* is 13.7 mm. The *M. subscapularis* insertion facet is rugose along the anteromedial margin but is largely smooth. Taken with the projection of the lesser tubercle, it appears as though *M. subscapularis* was well-developed in MH2. The intertubercular groove is narrow and deep proximally (6.2 mm in width measured proximolateral-anteromedial, 3.6 mm deep), although the medial lip of the groove deflects medially as it moves distally, widening the groove markedly.

The insertion for *M. pectoralis major* is pronounced. Inferiorly, it is present as a narrow but well-developed crest before becoming a rounded, prominent ridge as it moved proximally. The insertion site for *M. latissimus dorsi* is marked as a section of rugosity

³ This measurement is usually taken as the maximum anteroposterior breadth in modern humans and extant non-human primates with high torsion values as the humeral head faces more medially. In more retroverted species such as *Au. sediba*, this measurement is the maximum mediolateral breadth as the humeral head faces posteriorly.

on the medial margin of the distal bicipital groove, at the distal extremity of which it is overlapped slightly by the M. teres major insertion. A narrow sulcus borders this ridge on its medial aspect, possibly indicating significant development of M. teres major in *Au. sediba*. On the posterolateral aspect of the diaphysis, there is no development to indicate the origin of the lateral head of M. triceps brachii. The deltoid tuberosity is present only as a moderately developed rugosity, anterolaterally located, which extends toward the level of the midshaft but terminating approximately 2 mm prior to it. The anterolateral position of the deltoid tuberosity in *Au. sediba* is unlike the lateral positioning seen in modern humans. The cross-sectional diaphyseal shape of the humerus at the level of the tuberosity is triangular (cross-sectional shape at the level of the midshaft also appears triangular).

Moving distally, there is a nutrient foramen located on the medial diaphysis approximately 14 mm below the level of the midshaft. There is an area of slight rugosity just distal to the nutrient foramen on the medial aspect of the shaft, possibly marking the insertion for M. coracobrachialis, whereas the origin for M. brachialis is featureless. The origin for M. triceps brachii medial head on the posteromedial aspect of the distal shaft is also largely smooth with a low, narrow superoinferiorly-orientated ridge bisecting it. The origin for M. brachioradialis is a moderately-developed rugosity. The M. extensor carpi radialis longus origin is demarcated as a sulcus 14.9 mm superoinferiorly by 4.2 mediolaterally.

The lateral supracondylar crest is strongly developed and present as a marked and thick ridge extending proximally from the superior-most point of the lateral epicondyle. As it moves proximally, the ridge becomes a sharp margin between the anterior and posterior aspects of the diaphysis. The lateral epicondyle is marked, somewhat proximal in its position, and laterally projecting. The medial epicondyle is strongly projecting

(projecting 13.0mm from the medial trochlea margin) and has a superoinferior diameter of 13.0 mm. The origin for the humeral head of M. pronator teres is a mild rugosity and the origin for the common flexor tendon is similarly mild in its development. Biepicondylar breadth for U.W. 88-57 is 50.0 mm. Moving posteriorly, the olecranon fossa is round in shape, 19.7 mm at its widest point, and constrained in its lateral development by a broad lateral distodorsal pillar. The lateral distodorsal pillar is 14.1 mm thick and the medial pillar is 7.7 mm thick. The superoinferior diameter of the olecranon fossa is 16.0 mm. There is a large septal aperture in the fossa, 9.7 mm superoinferiorly and 6.8 mm mediolaterally.

First impression of the distal articular surfaces is of a large capitulum relative to the trochlea, such that the capitulum appears to be superoinferiorly expanded. This effect is likely the result of a relatively small trochlea. Trochlear/capitular keel is pronounced and produced by a moderately deep sulcus between the capitulum and lateral trochlea margin. The trochlea itself is deeply waisted with a breadth of 16.2 mm. Capitular breadth is 12.2 mm and height is 15.0 mm superoinferiorly. The AS-PI diameter of the capitulum is 16.9 mm. The radial fossa is very large compared to the coronoid fossa, though both are deep. Distal articular breadth is 32.4 mm.

U.W. 88-101

U.W. 88-101 is a left proximal humerus separated from the diaphysis at the anatomical neck, preserving only the articular surface and majority of both lesser and greater tubercles. Total superoinferior length of the fragment is 35 mm. The articular surface is complete and only minor abrasion has occurred to the anterior aspect of the lesser tubercle and superior aspect of the greater tubercle. Matrix is present on much of the fracture surface.

This specimen is morphologically similar in every respect to its antimere, the U.W. 88-57 right humerus. The humeral head is elliptical with a superoinferior diameter of 33.7 mm and mediolateral breadth of 32.2 mm. Viewed dorsally, the greater and lesser tubercles appear to project more laterally (greater tubercle) and medially (lesser tubercle) than the humeral head. Mediolateral bi-tubercular breadth across the most projecting points is 36.3 mm perpendicular to the long axis of the diaphysis. The greater tubercle appears large and the insertion sites for *Mm. supraspinatus* and *infraspinatus* are largely smooth with some moderately-sized ridges throughout. As in U.W. 88-57, the lateral lip of the bicipital groove is thick and rugose, suggesting a well-developed *M. pectoralis major*. The lesser tubercle is pronounced as in U.W. 88-57 but differs in projecting more medially than posteriorly. Its length, taken along the insertion for *M. subscapularis*, is 16.0 mm. The insertion facet for *M. subscapularis* is more rugose along the anteromedial margin and smooths out posteriorly, against suggesting a well-developed *M. subscapularis*. The bicipital groove is narrow and deep proximally (5.8 mm in breadth, approximately 4.0 mm in depth) before widening markedly as it moves distally as a result of medial deflection of the medial lip of the groove.

7.2.3.2 Claviculae

U.W. 88-38

U.W. 88-38 is the largely completely right clavicle of MH2, comprised of two congruous fragments representing the medial and lateral portions of the clavicle. The lateral fragment is approximately 64.2 mm in length and the medial portion is approximately 46.4 mm in length. The two fragments do not refit neatly, but visual inspection of the anteroinferior aspects suggest that there has been no more than 1-2 mm of bone loss at the fracture. The fracture surface of the lateral portion is unaffected by rounding due to taphonomic processes, although a small fragment of cortical bone

(approx. 1 mm by 1.5 mm) has been displaced from the anterior border of the acromial extremity of the lateral fragment. The dislocated fragment remains adhered to the lateral fragment by matrix and represents the only visible evidence of taphonomic damage to this portion. The fracture surface of the medial portion is more irregular than the lateral portion, missing a fragment of cortical bone on the posterior aspect in a broadly triangular shape approx. 6.0 mm at its base and 6.4 mm in height. The medial fracture surface also appears to have undergone some taphonomic rounding and abrading. The fracture surfaces of the two fragments are more or less continuous only on the anteroinferior aspects of the diaphysis. There is a crack which varies between 1-2 mm in width dividing the anterior and superior aspects of the U.W. 88-38 diaphysis.

Aside from the aforementioned issues, preservation of the specimen is good. The lateral fragment is in better condition than the medial fragment as the medial fragment has been exfoliated to a certain degree, obfuscating some of the morphology of the muscle attachment sites on the medial-most half of this fragment. Nonetheless, gross morphology is still clearly assessable, and the clavicular origin of *M. pectoralis major* is present as a line of rugosity on the anterior aspect of the medial clavicle, extending some 24 mm from the sternoclavicular joint margin. Similar to humans, the clavicle has a sigmoid curvature in the transverse plane. When the fragments are lined up, the estimated maximum length of the clavicle is 107.5 mm. At midshaft the specimen has a maximum diameter of 9.5 mm, a minimum diameter of 6.5 mm and a circumference of 26 mm.

The attachment for the costoclavicular ligament is a shallow sulcus with ambiguous margins on the inferior aspect of the medial diaphysis. It is largely smooth with a roughened margin anteriorly that extends approx. 29 mm laterally away from the articular margin. This roughened margin likely forms the inferior part of the origin for

M. pectoralis major. Moving superiorly, there is a section of gentle rugosity on the medial and anteromedial aspect of the superior surface which most likely represent the medial and anterior margins of the origin for *M. sternocleidomastoideus*. The clavicular origin for *M. deltoideus* is only weakly developed in this specimen. It is present as a mild rugosity only on the anterior aspect of the lateral shaft while the inferior aspect is relatively featureless. The deltoid scar is located on the anterior aspect of the lateral shaft curvature. U.W. 88-38 differs in this respect from the STW 431 clavicle and STW 582 where the scar is more anteroinferiorly located, and again from the condition seen in chimpanzees where the scar is positioned on the superoanterior surface. The insertion for *M. trapezius* is observable only as a pronounced ridge on the superoposterior margin of the lateral clavicle; there is no evidence of this attachment on the posterior surface. The lateral extremity of the *M. trapezius* insertion is a smooth, triangular-shaped area located posterior to the acromial articular facet, 9.5 mm wide superoinferiorly and 12.0 mm high anteroposteriorly. Here the inferior margin of the *M. trapezius* insertion is delineated by a pronounced crest which terminates in a distinct and rugose tubercle at its inferoanterior corner.

The subclavian groove is shallow with ambiguous margins that becomes more salient as it moved laterally toward the conoid tubercle. The conoid tubercle itself is prominent and projects posteriorly. There is a pronounced angular margin continuous with the tubercle medially and separating the inferior from the posterior surfaces, as also seen in A.L. 288-1, A.L. 333x-6/9, A.L. 438-1, and STW 606 (Partridge et al., 2003). Similar but perhaps less-developed angular margins are present in the STW 431 and STW 582. The shaft at the level of the conoid tubercle has an anteroposterior diameter of 12.7 mm and 7.8 mm superoinferiorly. Cross-sectional diaphyseal shape at the same level is rhomboidal, similar to A.L. 333x-6/9. The transition to the superior surface from the conoid tubercle is smooth and rounded and the trapezoid line is sharp, extending

approximately 4.7 mm anterolaterally before smoothing out into a rounded rugosity like in modern humans.

When viewed anteriorly, the acromial extremity of the clavicle has a mild inferior inflection when held in the horizontal plane and is anteroposteriorly expanded with a maximum anteroposterior diameter of 19.0 mm and maximum superoinferior diameter of 11.4 mm. The articular surface for the acromion is ovoid in shape (13.3 mm AP by 10.0 mm SI) and inclines gently from superoanterior to inferoposterior, with a sharp, anteriorly-projecting superior margin. As the superior margin moves posteriorly it widens into the aforementioned tubercle at the inferoanterior corner of the M. trapezius insertion. The inferior margin of the acromial articular surface is notably thick and rounded.

7.2.3.3 Radii

U.W. 88-85

U.W. 88-85 is a complete right radius, largely free of damage or distortion and preserving all surface morphology. One notable source of damage is a fresh transverse fracture at the midshaft that occurred during preparation. The radius has a maximum length of 226 mm and an articular length of 220 mm. In terms of overall appearance, the radial diaphysis is strongly bowed. The radial head, when viewed proximally, is very round with an anteroposterior diameter of 18.7 mm, a mediolateral diameter of 17.6 mm, and a circumference of 56 mm. The capitular fossa has an AP diameter of 12.2 mm, ML diameter of 12.2, and has a depth of 1.4 mm at the centre. The radial neck has an AP diameter of 11.4 mm and a ML diameter of 7.8 mm. There appears to be some mediolateral compression of the radial neck, a morphology more similar to the condition seen in *Pan* than *Homo*. Circumference of the radial neck is 32.5 mm. Radial head-neck length is 27.3 mm.

Proximally the diaphysis has a round cross-sectional shape. Its diameters are 10.3 mm AP and 10.1 mm ML, with a circumference of 32 mm. The bicipital tuberosity is orientated medially with very rugose markings for the insertion of *M. biceps brachii* on the posterior margin (the anterior margin is comparatively smooth). The dimensions of the tuberosity are 27.8 mm PD and 13.2 mm AP, and the diaphysis has a diameter of 13.6 mm measured anterolateral-posteromedial at the point of greatest development of the tuberosity. Immediately distal to the bicipital tuberosity, minimum shaft diameter is 10.0 mm. The insertion for *M. supinator* is marked only by an area of very mild complexity toward the lateral margin of the enthesis. The interosseous crest is weakly developed and mostly strongly in evidence at its proximal extremity. On the anterior aspect of the proximal diaphysis (inferior to the tuberosity), there is a low ridge, quite rounded in appearance, approximately 30 mm in length PD. Given its location, this likely represents the oblique line for *M. flexor digitorum superficialis*. Medial to this ridge, there is a shallow, somewhat rugose sulcus similarly most likely indicating the lateral origin of *M. flexor pollicis longus*.

Moving distally to the midshaft, the AP diameter is 9.9 mm, ML diameter 11.3 mm, with a midshaft circumference of 33 mm. Cross-sectional shape at the same point is ovoid. At the point of insertion for *M. pronator teres*, the bone is essentially featureless. The origin of *M. abductor pollicis longus* is marked as a rounded ridge of the dorsal aspect of the diaphysis that travels for a distance of approximately 24 mm from the level of the midshaft in a proximal direction. The origin for *M. extensor pollicis brevis* is absent. Distal minimum circumference is 33.6 mm.

The *M. pronator quadratus* insertion is similarly featureless. The brachioradialis crests are comparatively very developed, expressed as a crest 26.5 mm in length PD and 3.4 mm thick on the anterolateral aspect of the distal diaphysis. This crest is most salient at the distal extremity with a distinct sulcus for the tendons of *Mm. abductor pollicis*

longus and extensor pollicis brevis. Moving dorsally, there is a pronounced crest on the distal shaft that transmits proximally from the dorsal styloid process. This crest divides the sulci for the tendons of Mm. abductor pollicis longus and extensor pollicis brevis, and M. extensor carpi radialis longus. Lister's tubercle is well-developed. There is yet another low ridge that separates the M. extensor carpi radialis longus sulcus from the M. extensor carpi radialis brevis sulcus. There is a very shallow, poorly-delimited groove for Mm. extensor digitorum and extensor indicus.

Moving to the distal articular surface, the distal epiphysis has an anteroposterior breadth of 19.4 mm and a mediolateral breadth of 26.0 mm. The articular surface is somewhat concave in both the anteroposterior and mediolateral directions. Along the anterior margin, there is a distinct and somewhat sharp edge that delineates the articular surface from the non-articular surface, and this extends to the medial two-thirds of the posterior margin. The posterolateral margins are rounded by comparison.

7.2.3.4 Ulnae

U.W. 88-62

U.W. 88-62 is the complete right ulna of MH2. In terms of preservation, there is a green break to the lateral aspect of the olecranon process that has caused some angular (anteromedial) displacement of the olecranon process relative to the remainder of the diaphysis. This fracture travels in an arc beginning at the coronoid process and travelling dorsally through the trochlea articular surface. The fracture continues to the posterior aspect of the olecranon process, arcing in a roughly horizontal manner, before terminating as it meets the medial aspect. The fracture widens as it moves anterior to posterior through the process, reaching a maximum diameter of 5.5 mm proximodistally on the posterior aspect. Matrix occludes the fracture along its full length. There are three fresh (that is, post-fossilisation) transverse fractures: one at the level of the midshaft,

one approximately 45 mm distal of the midshaft, and another just proximal of the M. pronator quadratus crest (65 mm distal of midshaft). All of these fractures have refitted cleanly with no loss of bone or gross morphological detail. Aside from a few points of minor flaking and displacement of subperiosteal bone, this specimen is in remarkably good condition and preserves all surface morphology.

In the sagittal plane, the shaft of U.W. 88-62 is somewhat bowed and when viewed coronally is moderately deflected laterally at its distal extremity (ulnar neck and head). The maximum length of U.W. 88-62, without correcting for the angular displacement of the olecranon process, is 248 mm. The articular length is 240 mm and maximum length of the ulna excluding the styloid process is 240 mm. Shaft dimensions proximally are 11.7 mm mediolateral, 12.7 mm anteroposterior, with a circumference of 39.5 mm.

Proximally, the olecranon process has a breadth of 17.4 mm and appears mediolaterally narrow. The insertion for M. triceps brachii, present as a squarish raised pad on the proximal-most aspect of the process, is largely smooth with dimensions of 15.3 mm ML and 16.2 mm AP. The area for the subtendinous bursa for M. triceps brachii, semi-lunate in shape and somewhat distally inflected, gives the olecranon process its anterior lip. The olecranon process has a length of 16.7 mm, estimated depth of 14.4 mm, and height of 20.7 mm. Maximum and minimum breadths of the articular surface must be estimated due to the proximal olecranon fracture. Minimum mediolateral breadth of the semilunar notch is estimated at 15.2 mm; maximum mediolateral breadth of the articular surface is estimated at 17.4 mm; minimum mediolateral breadth of the articular surface is estimated at 12.0 mm. The semilunar notch appears waisted with only minimal development of the guiding ridge. The coronoid process has a maximum mediolateral breadth of 16.8 mm (as measured from the proximal margin of the radial facet to the medial margin of the semilunar notch) and a height of 24.8 mm. The articular surface of

the semilunar notch is divided into two unequal medial and lateral sections by the trochlear keel. The medial section has a maximum ML breadth of 12.0 mm and the lateral section has a maximum ML breadth of 5.1 mm. The semilunar notch appears to open anteroproximally as in modern humans and fossils from Sterkfontein (STW113 and STW 398; pers. obs.), although the distortion to the process confounds things somewhat.

Moving laterally, the radial notch has dimensions of 7.6 mm proximodistally by 12.0mm anteroposteriorly and is delineated from the semilunar notch by a sharp proximal margin that grows sharper as it moves posteriorly. The notch is tear drop-shaped, shallow, tapering anteriorly, and concave in both a proximodistal and anteroposterior direction. There is distinct rounding to the anterodistal margin on the notch, and while the notch as a whole is laterally-directed, there is a slight superior tilt along its proximodistal axis. The ulnar origin of *M. flexor carpi ulnaris* on the anteromedial aspect of the diaphysis is relatively large with a prominent tubercle bounding a shallow fossa proximoposteriorly. There are two additional crests, one located on the anterior aspect near the rim of the semilunar notch and another anterodistally near an additional crest for the anterior band of the ulnar collateral ligament and the ulnar head of *M. flexor digitorum superficialis*. These crests represent the attachments for the posterior and oblique bands of the ulnar collateral ligament, the latter of which transmits distally from the distomedial aspect of the coronoid process and forms the medial margin of the brachial tuberosity. The tuberosity itself is a shallow fossa, 20.0 mm proximodistally and 9.3mm mediolaterally, lying between two distinct crests. The lateral crest bordering the tuberosity is prominent and board and clearly demarcates the anterior and lateral aspects of the ulnar diaphysis, whereas the medial crest is low and comparatively undeveloped. The insertion of *M. brachialis* is an anteromedially-directed area of moderate rugosity. On the distomedial corner of the

coronoid process, there is an area of rugosity, triangular in shape that represents the ulnar origin of *M. flexor digitorum superficialis*.

The crest for the attachment of *M. supinator* on the lateral aspect of the ulna is short but continuous (not divided into superior and inferior portions) and strongly developed in U.W. 88-62, approximately 14 mm in length moving distally from the radial notch. Moving distally, there is a blunt crest that joins the *M. supinator* crest with the interosseous crest running at an oblique angle such that it is clear that the two crests reside in slightly different planes, the supinator crest most posteriorly-placed relative to the interosseous crest. Mediolateral diameter of the shaft at the level of greatest development of the *M. supinator* crest, including the crest, is 13.8 mm. Taken just posterior to the crest (that is, excluding the crest), this diameter is 12.8 mm. Cross-sectional diaphyseal shape distal to the *M. supinator* crest is D-shaped. The interosseous crest is sharp and more salient at its proximal extremity than anywhere else along its length. As the crest moves distally it becomes rounded before becoming more distinct below the level of the midshaft, providing a clear (though non-projecting) margin between the anterior and inferolateral aspects of the diaphysis. Shaft dimensions at the level of the midshaft are 8.8 mm mediolateral and 11.8 mm anteroposterior. Midshaft circumference is 34.0 mm. The midshaft is markedly flattened in a mediolateral direction and there is a nutrient foramen on the anteromedial aspect of the diaphysis. Minimum circumference of the distal shaft is 27 mm.

The *M. pronator quadratus* crest is prominent and thick, moving from the anteromedial to medial aspect of the distal ulna, approximately 30 mm in length. Maximum diameter of the shaft at the point of greatest development of the crest is 9.9 mm; minimum diameter at the same level is 7.9 mm and circumference is 28.5 mm. Moving to the ulnar head, the width of the head itself is 15.4 mm mediolateral with an anteroposterior

diameter (depth) of 16.4 mm, while the distal articular surface is a somewhat flattened kidney shape with a mediolateral breadth of 15.4 mm and 8.1 mm deep anteroposterior. The styloid process projects roughly 5.5 mm beyond the distal articular surface and has a breadth of 6.6 mm mediolateral (measured at the tip). Overall appearance of the styloid is prominent.

7.2.4 *Australopithecus anamensis*

7.2.4.1 Humeri

KNM-KP 271 (Patterson and Howells, 1967)

KNM-KP 271 is a fragment of left distal humerus, 57.6 mm in length, assigned to *Au. anamensis* (Patterson and Howells, 1967, Leakey et al., 1995). This specimen preserves the distal articular surfaces and is free from any significant taphonomic damage excluding the proximal break that severed the fragment from the original fossil. This break slopes mediolaterally such that a great portion of the diaphysis is preserved on the medial aspect of the specimen, with the fracture sheering in a markedly oblique manner to terminate at mid-lateral supracondylar crest.

The specimen is notably robust and large, and basically human-like in its morphology. The lateral supracondylar crest is damaged along its length and the medial supracondylar crest is present as a distinct sharp margin beginning 23.8 mm from the most projecting point on the medial epicondyle. The medial epicondyle is large and projecting, and the origin for the common flexor tendon is rugose. The area of the common extensor tendon on the lateral epicondyle is similarly rugose. The coronoid fossa is very deep relative to the radial fossa, and moreso medially than laterally. The mediolateral diameter of the coronoid fossa is 15.1 mm with a superoinferior height of

16.2 mm. The margin separating the two fossae is rugose and includes two small semi-contiguous projections orientated SM-IL. The radial fossa is very shallow with a mediolateral diameter of 11.5 mm. There is a septal small aperture with dimensions 5.6 mm mediolateral by 4.3 mm superoinferior.

Moving to the distal articular surfaces, the posterolateral margin of the trochlea is very sharp, somewhat projecting, and orientated almost completely superoinferiorly with a slight SM-IL tilt. The trochlea is also strongly waisted with a medial diameter of trochlear of 24.3 mm and a lateral diameter of 23.5 mm, both measurements taken anteroposteriorly. Trochlear width is 25.6 mm mediolaterally in the anterior aspect and 27.8 mm in the posterior aspect. The medial trochlea appears large compared to the capitulum. Capitular breadth is 16.0 mm and the AS-PI diameter of the capitulum (measured across the articular surface) is 20.1 mm. Anterior projection of the capitulum – measured as the anteroposterior diameter from the most projecting point on the anterior surface to the non-articular dorsal surface – is 22.6 mm.

On the posterior aspect, the olecranon fossa is strongly medially offset in its placement with a mediolateral breadth of 26.5 mm at its widest point and superoinferior height of 16.3 mm. The breadth of the lateral distodorsal pillar is 16.3 mm and the breadth of the medial distodorsal pillar breadth is 10.4 mm.

7.2.5 *Australopithecus sp.* and the “Robust Australopithecines”

7.2.5.1 Humeri

Omo 119-1973-2718 (Howell and Coppens, 1976)

The taxonomic attribution of Omo 119-1973-2718 is uncertain. This fossil has previously been attributed to *Au. africanus* or *Au. cf. africanus* by Howell and Coppens

(1976), Howell (1978), Senut (1980), Senut (1978), and McHenry and Temerin (1979). McHenry (1994) later described it as *Homo sp.* before it was reassigned it to *Australopithecus sp.* by Larson (2007). Consensus opinion indicates that Omo 11-1973-2718 is most likely a member of *Australopithecus*. This study will take the conservative view and also refer to this specimen as *Australopithecus sp.* following Larson (2007).

Omo 119-1973-2718 is a left proximal humerus comprising of the well-preserved humeral head, parts of both tubercles, and proximal shaft. Total length of the specimen is 146.9 mm with the shaft extending 115.0 mm below the humeral head to the distal point of breakage. While this specimen does not appear distorted, there are numerous sites of damage. It has been broken just below the surgical neck of the humerus. Some damage has occurred to the articular surface of this specimen where trabecular bone has been exposed on the superior surface and along the anterior and posterior rim. The damage to the rim, in particular, has somewhat altered the shape of the head, giving it a more ovoid appearance than may strictly be accurate. The greater tubercle is missing a large portion of the lateral surface although the superior muscle insertions remain intact. A fine fossilisation crack is also evident, originating from the inferior-most segment of the greater tubercle and extending distally to the point of breakage. The shaft exhibits a number of other fossilisation cracks.

Damage to the rim of the articular head gives it an irregular appearance. The mediolateral head diameter is approximately 40.6 mm and the anteroposterior head diameter is approximately 37.9 mm. This yields an estimated humeral head index of 93.3%. The tubercles are both pronounced, although the greater tubercle does not extend above the surface of the humeral head, lying instead approximately 4.0 mm below it and projecting anteriorly at the level of the insertion for M. teres minor. The insertions for Mm. infraspinatus and teres minor are both preserved on the greater

tubercle, being well developed. The bicipital groove is broad (approximately 8.0 mm at its superior-most point) but also appears to be somewhat deep, though the missing lateral/posterior margin makes this difficult to confirm. The medial border formed by the lesser tubercle curves somewhat over the groove, giving the impression of being tunnel-like. The point of greatest constriction to the bicipital groove occurs proximally at the superior-most point of the lesser tubercle. The tubercles themselves are large and somewhat globular in appearance, though the greater tubercle does not project past the superior surface of the humeral head, nor does the lesser tubercle project anteriorly. The inferior lip of the humeral head is weakly projecting. Foramina are present both in the floor of the bicipital groove and on the lesser tubercle. On the lesser tubercle, the insertion for *M. subscapularis* is rugose and extends along the length of the tubercle, orientated more or less completely superoinferiorly with a slight anterior projection inferiorly.

Muscle attachment sites on the diaphysis and on the tubercles are extremely well-developed. The insertion for *M. pectoralis major* is present as a pronounced and sharp ridge beginning at the inferior-most portion of the lateral bicipital margin and extending inferiorly before it merges with the crest of the greater tubercle superiorly, 72.9 mm in length. While the insertion begins as a sharp ridge superiorly, it broadens out inferiorly before migrating somewhat posteriorly on the diaphysis. On the anterior aspect, the insertion for *M. latissimus dorsi* is similarly well-developed, originating with the inferior extremity of the lesser tubercle and 45.6 mm in length and 10.7 mm at the point of greatest breadth. This insertion does not approach the sharpness of the insertion of *M. pectoralis major* but is nonetheless observable as a pronounced rugosity on the anterior aspect of the diaphysis originating within the floor of the bicipital groove. The insertion for *M. teres major* is a distinct rugosity situated parallel to the insertion of *M. latissimus dorsi* in the floor of the bicipital groove, 34.3 mm in length SI and 5.2 mm in breadth,

which blends with the crest of the lesser tubercle on the anterior margin of the bicipital groove. Moving to the posterior aspect of the shaft, the origin for the lateral head of *M. triceps brachii* is a large, protruding rugosity beginning on the posterior aspect before moving laterally as it continues inferiorly, 60.0 mm in length originating 25.8 mm from the neck crack and terminating prematurely at the inferior breakage point of the shaft. This feature is located approximately 51.7 mm inferior to the greater tubercle. It is broad, 8.9 mm at its greatest breadth, with a sulcus present in the centre of the attachment. The *M. triceps brachii* insertion is most projecting at its medial margin. The insertion for *M. teres minor* is obscured by the section of missing subperiosteal bone at the neck break on the posterior surface of the shaft. The extent of development at the entheses of this specimen would indicate that this individual was likely to have been exceptionally robust. The shaft itself exhibits little curvature.

KNM-ER 1504 (Leakey, 1973, Senut, 1980)

Originally attributed to *Australopithecus*, Lague (2015) has since reassigned this specimen to *P. boisei*. KNM-ER 1504 is a right distal humerus preserving both epicondyles and distal articular surfaces, 68.5 mm in length. Damage is present on the posterior aspect of this specimen in the form of fossilisation cracks and flaking of the sub-periosteal bone below the superior point of breakage. Similarly, the posterior aspect of the lateral epicondyle and medial and lateral margins of the trochlea have been damaged, exposing trabecular bone. This specimen is notably robust. The origins for the wrist and finger flexors and extensors are intact on the epicondyles. Both the medial and lateral epicondyles are pronounced. The capitulum has a mediolateral breadth of 16.6 mm and 17.0 mm superoinferiorly, appearing large relative to the strikingly waisted trochlea. The trochlea has a medial anteroposterior breadth of 19.6 mm, lateral anteroposterior breadth of 19.5 mm, and a mediolateral breadth of 21.4 mm. The radial fossa is board

but shallow, with a breadth of 11.9 mm mediolaterally. The coronoid fossa has a mediolateral breadth of 16.4 mm and a superoinferior diameter of 14.0 mm, and it appears very deep relative to the radial fossa. The olecranon fossa is located centrally on the shaft.

KNM-ER 739 (Leakey et al., 1972)

KNM-ER 739 is a right humerus preserving the majority of the shaft and the trochlea portion of the distal articular end. Proximally, the humeral head and a portion of the shaft are absent. While the exact taxonomic status of this specimen remains somewhat uncertain, a number of authors have assigned it to the genus *Australopithecus* (Leakey, 1971c, Leakey et al., 1972, Leakey et al., 1971, McHenry, 1973, Day and Leakey, 1974). Total length of the specimen is 130.0 mm. In cross-section, the shaft of KNM-ER 739 is triangular proximally before transitioning to a more ovoid shape distally. The shaft also appears to have a gentle curvature along its length. The bicipital groove is wide with a minimum width of 10.0 mm. The anterior and posterior borders of the groove are well-developed with a slight roughening in the floor of the groove to represent the insertion for *M. latissimus dorsi*. The insertion for *M. pectoralis major* is expressed as a prominent crest that represents what Leakey et al. (1972) describes as the “distal continuation of the crest of the greater tuberosity”. This crest continues distally to merge with the deltoid tuberosity.

TM 1517f (Broom, 1938, Broom and Schepers, 1946)

TM 1517f is a right distal humerus attributed to *Paranthropus robustus*, 54.8 mm in length. This specimen preserves both epicondyles and articular surfaces. The posterior aspect of the medial epicondyle is damaged with some bone missing where the specimen has incompletely fractured and stabilised/infilled with adhesive where bone loss has occurred. A central fracture divides the medial epicondyle from the body of the

specimen. This fracture continues anteriorly to divide the medial border of the trochlea, moving across the articular surface from the superomedial corner and arcing inferiorly to terminate at the midpoint of the medial border of the trochlea. Total length of the fragment delineated by this crack, including the medial epicondyle, is 19.0 mm SM-IP by 5.5 mm ML. There are a number of fossilisation cracks present on the anteromedial aspect of the remaining diaphysis. The superior aspect of the capitulum is also eroded, somewhat obscuring the superior contour of the capitulum.

There appears to be some anteroposterior flattening of the diaphysis in this specimen such that the distal section preserved is quite narrow and flattened in an anteroposterior direction. Overall, TM 1517f appears small but robust. There is a small depression 11.9 mm superior to the point of greatest projection of the medial epicondyle, 6.7 mm superoinferior by 3.5 mm anteroposterior, representing the humeral origin of *M. pronator teres* and this feature is located quite centrally on the epicondyle. The coronoid fossa is markedly deep relative to the very shallow radial fossa. The coronoid fossa has a breadth of 12.6 mm mediolaterally and superoinferior height of 7.7 mm, whereas the radial fossa has a mediolateral breadth of 6.6 mm. Height of the radial fossa is difficult to determine due to the indistinct margins of the fossa but it appears narrow. The area for attachment of the common extensor tendon on the lateral epicondyle is relatively smooth and featureless. The medial epicondyle and attachment for the common flexor tendon is comparatively rugose, although this is partly the result of damage to the entheses. Moving posteriorly, the olecranon is only very slightly medially-offset, indicating that the medial and lateral distodorsal pillars are of approximately equal widths.

7.2.5.2 *Ulnae*

TM 1517e (Broom, 1938, Broom and Schepers, 1946)

TM 1517e is a right proximal ulna, attributed to *P. robustus*, and preserving part of the olecranon process and semilunar notch. Preservation in this specimen is poor. The anterior lip of the semilunar notch is missing so it is difficult to accurately determine olecranon dimensions. The specimen is broken approximately at the midpoint of the semilunar notch such that the coronoid process is absent. While this specimen does not preserve much by way of morphology, the insertion for *M. triceps brachii* is intact as the anterior lip has fractured just at the border between the fibrocartilaginous pad and the area for the subtendinous bursa.

SKX 8761 (Susman, 1989)

SKX 8761 is a left proximal ulna, 108.5 mm in length, attributed to *P. robustus*. This specimen is generally poorly preserved in that much of the remaining diaphysis and articular surfaces have been badly damaged by the fossilisation process. A network of superoinferiorly orientated cracks are present on all aspects of the shaft, some of which gape and thereby disrupt the continuity of the cortical surface. The olecranon process has been refitted to the diaphyseal fragment with a large section of bone absent from the semilunar notch medially (10.1 mm SI by 8.9 mm ML with a depth of ca. 7 mm) and a smaller segment from the notch laterally (11.0 mm AP by 4.6 mm SI). On the medial aspect of the proximal end and following the contour of the insertion for *M. anconeus* is another missing fragment of bone, 15.5 mm SI by 4.6 mm AP. The same crack that causes these defects to the olecranon process also interrupts the posterior surface of the process, where some crushing is present. The proximal-most surface of the olecranon, and thus the insertion for *M. triceps brachii*, is intact. The coronoid process is present; however, some loss of bone has occurred to the anterior lip of the process. The radial

notch similarly has been eroded along its posteroinferior border though the notch itself remains largely intact.

The radial notch is tear drop-shaped, tapering anteriorly, and gently concave in an anteroposterior direction. The length of the superior margin of the notch is 13.4 mm and the proximodistal dimension of the notch is 8.5 mm. It is difficult to determine whether there is any tilt to the notch due to damage to the margins. Moving distally, the supinator crest is a rounded but distinct margin situated 2.3 mm posterior to the posterior margin of the radial notch which continues distally for some 27.6 mm, transmitting somewhat posteriorly as it reaches its distal extremity.

The posterior aspect of the specimen is relatively straight with only slight evidence of a proximodistally-orientated sinusoidal curvature. There is a smooth, round (previously fibrocartilaginous) mound/tuberosity on the medial margin of the coronoid process demarcating the ulnar origin of *M. flexor digitorum profundus*, just anterior to the section of missing bone described previously on the medial aspect of the proximal diaphysis. Buckling and distortion due to cracking of the diaphysis makes determination of the diaphyseal entheses morphology untenable.

L40-19 (Howell and Wood, 1974)

L40-19 is a complete right ulna attributed to *Paranthropus boisei*. Total length of the ulna is 312 mm. While largely intact, fossilisation cracks and crushing are present throughout the bone, distorting the shape of the diaphysis somewhat in the proximal one-third. The styloid process is absent along with a portion of the posterior aspect immediately superior to the process, 14.7 mm ML by 18.2 mm PD. Proximally, the coronoid process is largely absent and it is clear that crushing has displaced the proximal part of the ulna somewhat relative to the diaphysis. A crack runs through the neck of the ulna at this point. The olecranon process is otherwise completely intact,

though a small segment of bone has been excised from the posterior aspect inferior to the insertion for *M. triceps brachii*. The semilunar notch is intact, though the radial notch has been eroded around its margins.

This ulna is markedly robust with anteroposterior bowing to the diaphysis. The antebrachial musculature is very well-developed generally. The dimensions of the olecranon process are 28.0 mm mediolaterally by 28.2 mm anteroposterior and the mediolateral width of the semilunar notch including radial notch 27.6 mm. The insertion for *M. anconeus* is a sharp ridge adjacent the radial notch on the proximolateral aspect of the ulna. On the posterior aspect 12.7 mm from the proximomidshaft point of breakage, is a rugosity that represents the inferior most insertion for *M. anconeus*. Compared to *Australopithecines*, the radial notch is large and broad relative to the semilunar notch. While damage to the margins precludes exact measurement, the proximodistal dimension of the notch is estimated at 13.8 mm by 18.4 mm anteroposterior. There is a strong depression present on the proximomedial aspect of the specimen. The particularly sharp development of the superior margin of this depression may be attributed to the development of the *M. triceps brachii* insertion, though the exact cause is unclear. The insertion for *M. brachialis* on the anterior aspect is small relative to the breadth of the shaft, and medially displaced (as opposed to be centrally located as in modern humans and other fossil ulnae). On the lateral aspect, the supinator crest is damaged at its proximal extremity as a part of the damage to the radial notch, though the inferior section remains intact as a rounded crest 13.1 mm in length.

Moving distally, there is a foramen 15.6 mm superior from the proximomidshaft point of crushing. Adjacent and inferolateral to the nutrient foramen on the diaphysis, there is a strongly developed crest representing the ulnar origin of *M. flexor digitorum profundus*. The pronator quadratus crest is prominent and very rugose, approaching

bulbous, towards its superoanterior extremity. The crest moves from the medial margin of the anterior aspect, wrapping around the diaphysis to terminate on the posteromedial aspect of the distal shaft. The distal head of the ulna is kidney-shaped, with dimensions 21.2 mm mediolateral by 11.2mm anteroposterior. Midshaft dimensions are 14.5 mm anteroposterior by 17.7 mm mediolateral, with a circumference at the same point of 51.8 mm. Shaft dimensions at the point of greatest development of the pronator quadratus crest are 15.5 mm ML by 12.7 mm AP, and circumference at this point is 44.6 mm.

OH 36 (Aiello et al., 1999)

OH 36 is a largely complete right ulna attributed to *Paranthropus boisei*, 264 mm in length, and broken distally just inferior to the M. pronator quadratus crest. This specimen has been refitted from three fragments but is in reasonable overall condition. The olecranon and coronoid processes as well as the diaphysis have been abraded, and a segment of bone is missing from the proximal end of the middle fragment on the posterior aspect.

Muscle attachment sites in this individual are well-marked. On the superior surface of the olecranon process, the insertion for M. triceps brachii appears to be a distinct and relatively large platform, though damage to the medial and lateral margins of the process make its true shape and size difficult to determine. The extension of an area of rugosity from the superior surface of the olecranon onto the posterior aspect of the process indicates that the attachment for M. triceps brachii was sizeable. This entheses cannot be included in the analysis due to the damage. The trochlear notch has an anteroproximal orientation on visual inspection, with notable midline keeling. The radial notch is tear drop-shaped and orientated anteroposteriorly with slight concavity along its posteroanterior length. The interosseous crest is relatively rounded and not especially projecting. The ulnar tuberosity is pronounced and somewhat narrow, and

bounds a small depression for the insertion of *M. brachialis* laterally. The supinator crest is a distinct crest on the lateral aspect of the proximal diaphysis, originating at the posterolateral margin of the radial notch, before becoming more rounded and less prominent as it moves distally. The crest has a notable sinusoidal curvature to it. Distally, the diaphysis is relatively featureless barring the pronator crest, which presents as a sinuous rugosity 20.2 mm in length.

7.2.6 Non-ergaster/erectus early *Homo*

7.2.6.1 Humeri

SK 24600 (Susman et al., 2001)

SK 24600 is a left distal humerus previously attributed to *P. robustus* (Susman et al., 2001) but more recently reassigned to *Homo* aff. *habilis* by Lague (2015). This specimen is 57.8 mm in length and preserves both epicondyles, articular surfaces, and olecranon fossa. SK 24600 is in a good state of preservation with the exception of some minor erosion to the lateral margin of the capitulum, the medial border of the trochlea, and the posterior aspect of the lateral articular surfaces (posterior capitulum and lateral trochlea border). There is a very small septal aperture present only ca. 1.4 mm in diameter; this appears to be genuine morphology rather than taphonomic damage based on the complete cortical appearance of the aperture margins. The posterior aspect of the lateral epicondyle has also undergone some erosion in small segments adjacent the point of greatest lateral projection of the epicondyle. A fossilisation crack occurs on the posterior aspect beginning ca. 5.0 mm from the distal point of breakage and continuing distally to skirt around the superior contour of the olecranon fossa and terminating 12.6 mm from the point of greatest projection of the medial epicondyle.

This specimen is robust but small in size. Biepicondylar breadth is 44.3 mm. distal articular breadth is ca. 33 mm. The lateral supracondylar crest is only mildly developed compared to other *P. robustus* specimens and the medial supracondylar crest is only present as a slight rounded margin – both are incompletely preserved due to the distal point of breakage occurring low on the diaphysis. The olecranon fossa is located centrally on the diaphysis rather than being medially offset as in many *P. robustus* distal humeri. The trochlea and capitulum are in proportion with one another with the capitulum appearing slightly larger. The trochlea is strongly waisted.

7.2.6.2 Claviculae

OH 48 (Leakey et al., 1964a)

This left clavicular fragment, attributed to *Homo habilis*, is missing both articular ends, giving the shaft a total approximate length of 130.0 mm. The sigmoid curvature is marked. At the midshaft, its anteroposterior diameter is 14.8 mm and its superoinferior diameter 10.7 mm. Medially, these dimensions are 22.2 mm and 22.4 mm respectively with cortical thickness ranging between 2.5-3.5 mm. At the lateral point of breakage, the anteroposterior diameter is 16.8mm with a superoinferior diameter of 10.2 mm, and cortical thickness varying between 2.0-2.4 mm. Oxnard (1969b) measured the degree of torsion in the OH 48 clavicle and reported a value of 52-60°.

7.2.6.3 Radii

SK 24601 (Susman et al., 2001)

SK 24601 is a left proximal radius associated with the humerus SK 24600, both of which were previously attributed to *P. robustus* by Susman et al. (2001) but more recently reassigned to *Homo. aff. habilis* by Lague (2015). This specimen is 47.1 mm in length, preserving the radial head with damage along the medial margin and radial

tuberosity. The radial tuberosity and therefore the insertion for *M. biceps brachii* appears to be complete. There is a sharp margin on the posterior aspect of the radial shaft at the level of the tuberosity, though it is unclear what the significance of this feature may be. It may possibly represent a proximal extension of the radial origin of *M. abductor pollicis longus*, but if so, it is very proximal on the diaphysis; more probably the margin marks the posterior extremity of the *M. supinator* insertion. Laterally, the *M. supinator* insertion is marked only as a slight rugosity on the lateral aspect of the diaphysis level with the radial tuberosity. The radial tuberosity is low and projects only at the superior most extremity of the insertion for *M. biceps brachii*.

7.2.7 *Homo ergaster* (“early *Homo erectus*”)

As per the exclusion criteria, KNM-WT 15000 – arguably one of the most complete *H. ergaster* specimens – was excluded from analysis based on his developmental status. As stated in Chapter 6, the position and development of muscle attachment sites changes with growth and on this basis KNM-WT 15000 must be excluded from this study. The following descriptions refer to adult specimens only.

7.2.7.1 Humeri

SKX 34805 (Susman, 1989)

SKX 34805 is a right distal humerus, 78.3 mm in length, missing distal articular surfaces and both epicondyles. This specimen was originally attributed to *Paranthropus* by Susman (1989) based on similarity to TM 1517f, but subsequently reassigned to *Homo ergaster/erectus* by Susman et al. (2001) and Lague (2015) based on humeral diaphyseal cross-sectional shape. SKX 34805 preserves the epicondylar crests and the olecranon, radial, and coronoid fossae. The lateral epicondylar crest is damaged

inferiorly. Post-depositional damage to this specimen has resulted in the distal-most portions of the specimen being sheared off the shaft at the inferior margin of the coronoid fossa anteriorly and just inferior to the olecranon fossa posteriorly. The overall appearance of the specimen is relatively gracile compared to much of the other Swartkrans material.

The medial epicondylar ridge is present as a slight sharpened margin on the medial aspect of the diaphysis. The lateral epicondylar crest is very well-developed and is present as a projecting, slightly curling ridge on the lateral aspect of the diaphysis that extends for 39.4 mm before terminating just proximal to the lateral epicondyle, however the section of greatest development difficult to ascertain due to damage. What remains of the lateral epicondyle appears to be anteriorly deflected. The biepicondylar diameter is 47.1 mm. The radial fossa appears broad relative to the coronoid fossa, with a mediolateral dimension of 17.0 mm and approximately 6.8 mm proximodistally. The coronoid fossa has dimensions of 12.1 mm mediolaterally and approximately 5.8 mm proximodistally. The olecranon fossa is medially offset.

7.2.7.2 Radii

SK 2045 (Susman et al., 2001)

SK 2045 is a right proximal radius including radial head, radial tuberosity, and a portion of proximal diaphysis with interosseous crest, 123.7 mm in length. There appears to have been some buckling of the cortical surface of the specimen, but otherwise the specimen is in reasonable condition: morphology is preserved despite the cracks and manganese and ferrous oxide staining present throughout the fossil. The interosseous crest morphology is obscured by cracking at the remaining inferior extremity, while proximally it is clear that the crest was a rounded margin with a segment of rugosity at

its proximal-most extremity, delineating the radial head of *M. flexor digitorum superficialis*.

A depression is present on the medial aspect of the diaphysis immediately adjacent the interosseous crest, 42.7 mm superior to the distal point of breakage, 3.7 mm anteroposterior breadth. The depression's margins are more starkly defined in an anteroposterior direction than in a superoinferior direction, so that determining the length of this feature is difficult. Nevertheless, it is clear from its location on the shaft that this is the radial origin of *M. abductor pollicis longus*, and its conspicuousness may indicate some hypertrophy of this muscle or may just be due to the large size of the specimen. The radial head is strongly posterolaterally deflected. The radial tuberosity is moderately well-developed but the area of greatest projection is located at the superior extremity of the *M. biceps brachii* insertion. The radial insertion of the *M. supinator* is not so well-developed as to project the lateral border of the radial tuberosity.

On the lateral aspect, the distal extremity of the *M. supinator* insertion is marked by a rugosity 28.8 mm superior to the distal point of breakage. Approximately 9.6 mm inferior to this rugosity is another raised and roughened area that marks the radial insertion of *M. pronator teres* which terminates artificially with the distal break. The quite marked development of both these entheses is indicative of the overall pronounced development of the antebrachial musculature in this specimen.

7.2.7.3 *Ulnae*

SK 18b (Robinson, 1953)

SK 18b is a left proximal ulna, original described by Robinson (1953) as belonging to *H. erectus* (= *H. ergaster*) and more recent studies have been unable to differentiate this specimen from other Pleistocene radial specimens attributed to *Homo* (Grine and

Susman, 1991, Senut, 1983), thereby supporting this taxonomic assessment. This specimen preserves only the radial head and bicipital tuberosity, having been broken immediately inferior to the tuberosity, and as such there is very little to say about the gross morphology of this specimen. The insertion for *M. biceps brachii* is certainly complete enough for inclusion in this study. The insertion is somewhat rugose and oval-shaped in appearance.

KNM-BK 66 (Senut, 1981, Solan and Day, 1992)

KNM-BK 66 is a right ulna missing the distal articular surfaces broken just inferior to the pronator quadratus crest. The *M. pronator quadratus* crest is present but only moderately developed. The insertion for *M. triceps brachii* is completely preserved and overall enthesal rugosity is modest. There is a strongly flanging insertion for *M. supinator* beginning 6.6 mm posterior to the inferior margin of the radial facet. The radial facet is tear drop-shaped and tapers anteriorly with dimensions of 13.3 mm anteroposteriorly and 7.6 mm proximodistally. The supinator crest has a breadth of 6.9 mm at the point of greatest development and a length of 37.3 mm. A small rugose tuberosity, 10.8 mm proximodistally and 2.8 mm anteroposteriorly, is also present just anterior to the supinator crest and further highlights the development of this muscle. Keeling of the semilunar notch is minimal. The *M. brachialis* insertion occurs on the anteromedial aspect of the specimen, rugose ovoid depression on the proximal shaft. Superomedial to this and 5.0 mm inferior to the medial lip of the coronoid process, the ulnar origin of *M. flexor digitorum profundus* appears as a slight tuberosity that continues inferiorly to become continuous with the medial border of the brachialis insertion. The *M. anconeus* insertion is present as a rugosity on the medial aspect of the olecranon process.

**CHAPTER 8: ELECTROMYOGRAPHY, KINEMATICS, AND KINETICS OF
THE UPPER LIMB DURING OLDOWAN STONE TOOL MANUFACTURE**

Contribution of Authorship Declaration

The following chapter consists of a manuscript titled ‘Electromyography, Kinematics and Kinetics of the Upper Limb during Oldowan Stone Tool Manufacture’, co-authored by Dr. Mark Halaki, Dr. Darren Reed, Prof. Colin Groves, and A/Prof. Karen Ginn, Under Review for publication to the *Journal of Human Evolution*.

I attest that Research Higher Degree candidate Elen Feuerriegel contributed significantly in the conception of the project, experimental design, data collection and analysis, and drafting of the manuscript in the aforementioned publication.

Name:

Signature:

Date:

Name:

Signature:

Date:

Name:

Signature:

Date:

Name:

Signature:

Date:

Name of Candidate: ..Elen Feuerriegel

Signature of Candidate: *Elen Feuerriegel*

Date: ...15/06/2016

ELECTROMYOGRAPHY, KINEMATICS AND KINETICS OF THE UPPER LIMB
DURING OLDOWAN STONE TOOL MANUFACTURE

Elen M. Feuerriegel^{a*}, Mark Halaki^b, Darren Reed^c, Colin. P. Groves^a, Karen A. Ginn^c

Author Affiliations

^a School of Archaeology and Anthropology, College of Arts and Social Sciences,
Australian National University, Canberra, ACT 2601, Australia.

^b Discipline of Exercise and Sport Science, University of Sydney, Lidcombe, NSW
2141, Australia.

^c Discipline of Biomedical Science, Sydney Medical School, University of Sydney,
Lidcombe, NSW 2141, Australia.

***Corresponding Author:** Correspondence and requests for information should be
addressed to Elen M. Feuerriegel (elen.feuerriegel@anu.edu.au).

KEY WORDS: electromyography; kinematics; upper limb; Oldowan; shoulder; elbow

PAGES: 26

FIGURES: 5

Abstract

The close association of the advent of tool behaviours with changes to the upper limb morphology of fossil hominins has lead researchers to hypothesise that stone tool manufacture and use represents an important selective pressure for the upper limb. Nevertheless, little data is available for evaluating these hypotheses, particularly with regard to specific patterns of muscle recruitment in the shoulder and elbow. This study investigated the upper limb kinetics and kinematics, in addition to the normal activation patterns of 15 shoulder and elbow muscles using intramuscular and surface electromyography (EMG) in 16 novices during Oldowan stone tool manufacture. Results indicate that the stone knapping arm motion is a dynamic three-dimensional flexion-extension task with shoulder and elbow musculature primarily producing the acceleration of arm segments to generate the strike force. The segments of the upper limb moved in a coordinated proximal-to-distal sequence, originating with the shoulder proximally in the up-swing or “cocking” phase and moving through to the wrist and hammerstone distally in the down-swing phase. The major torque-generating muscles of the strike are the latissimus dorsi, teres major, and triceps brachii; pectoralis major works to decelerate the rapidly extending arm in the down-swing to improve strike accuracy. The wrist flexor and extensor musculature appears to be recruited to stabilise the elbow and wrist against reactive forces from hammerstone impact rather than producing motion of the wrist. Together these results present one of the first detailed investigations into upper limb muscle recruitment and kinematics in simple stone tool manufacture.

Introduction

Fossil hominin shoulders have undergone a number of shifts in the course of human evolution, many of which occurred in conjunction with or soon after the origins of the earliest forms of stone tool production (Larson, 2007; Roach and Richmond, 2015; Roach et al., 2013). These shifts included changes to the shape, height, and orientation of the shoulder and structure of its elements. The close temporal association of these changes with the advent of stone tool technology has led many researchers to hypothesise that stone knapping represents a significant selective pressure guiding the evolution of the hominin shoulder girdle and other aspects of the upper limb (Larson, 2007, 2015; Marzke and Marzke, 2000; Panger et al., 2002; Tocheri et al., 2008). Few studies have been conducted on the muscle recruitment patterns during stone knapping and consequently there is little quantitative information available for evaluating hypotheses about the mechanical context of stone tool production in this region. The majority of knapping biomechanics studies centre upon the role of the hand and wrist (Marzke et al., 1999; Williams et al., 2010; 2012; 2014) or elementary movements (e.g. Biryukova et al., 2005; Biryukova et al., 2015; Bril et al., 2012). Dapena et al. (2006) have conducted one of the only studies to look at muscle torques in the shoulder and elbow during stone tool manufacture. They looked specifically at the kinetics of the arm swing in Oldowan stone knapping using one advanced knapper with a view to inferring muscle activity patterns. The arm was modelled as a four-link kinetic chain consisting of upper arm, forearm, hand, and hammerstone, allowing for joint forces and torques at the elbow to be understood as resulting from a combination of elbow musculature action and the forces exerted on the lower arm by upper arm motion through the elbow joint. Dapena et al. (2006) used the joint torques to infer muscle recruitment patterns as torques are exerted exclusively by muscles and thus reflect the main muscular activity at the joint. The authors inferred that only low levels of muscle

activity are required for stone tool manufacture based on the small joint torques exhibited in one subject in two trials.

Studies such as these are vital for clarifying the functional demands that may have been acting on the upper limb during early hominin evolution but do not provide a complete picture. Many of these studies suffer from small sample sizes and provide only indirect evidence of muscle recruitment patterns at the shoulder during the Oldowan knapping stroke. As there is presently no study detailing either the specific muscular recruitment patterns of the human shoulder or elbow during stone knapping behaviours, the aim of the current study was to conduct an electromyographic (EMG), kinetic, and kinematic study of the shoulder, elbow, and wrist in Oldowan stone knapping to create a clearer picture of upper limb biomechanics during stone tool manufacture.

Methods

Subjects

Sixteen subjects (9 male, 7 female; age (mean \pm standard deviation: 26.8 ± 9.3 (range: 19-54 years); height: 1.70 ± 0.07 m; mass: 71.6 ± 16.9 kg; all right-handed) who had not had shoulder or elbow pain for at least 2 years and had never sought treatment for shoulder or elbow pain were recruited from the student body of the University of Sydney and the general population. Each volunteer completed a questionnaire gathering basic data such as age, sex, weight, height and handedness. Basic functional testing was conducted to ensure normal shoulder and elbow range of motion and scapulohumeral rhythm in participants as well as no pain during isometric shoulder internal and external strength testing, confirmed visually and by self-report. All participants were unfamiliar with knapping except for one who was proficient and trained in Oldowan stone tool production as a part of academic training and had been knapping sporadically for

several years since. Prior to the experiment, subjects were given the opportunity to practice the Oldowan stone knapping so as to familiarise themselves with the task required. The participants practiced in one-hour sessions until they were able to consistently produce flakes.

Participants were fully informed of the experimental protocol and provided their consent prior to commencing the experiment. The study was approved by the Australian National University's Human Research Ethics Committee (Protocol number 2014/321).

Instrumentation

EMG data were collected simultaneously from 15 shoulder, elbow and forearm muscle sites using both indwelling (intramuscular) and surface electrodes (Figure 1) in the dominant arm of each knapper. Nine surface electrodes were used to capture EMG data from pectoralis major, biceps brachii, lower and upper trapezius, proximal and distal portions of triceps brachii, anterior deltoid, and the superficial wrist and finger flexor and extensor muscle groups. Six intramuscular electrodes were used to record activity in subscapularis, teres major, latissimus dorsi, rhomboid major, infraspinatus and supraspinatus.

Before the placement of the surface electrodes, the skin of each participant was prepared with alcohol and an abrasive gel (NuPrep, DO Weaver and Co., Aurora, USA) to limit skin impedance. Electrode placement was determined via anatomical landmarks and the procedures outlined by Basmajian and DeLuca (1985) for surface electrodes. At each appropriate location, two surface electrodes (Red Dot, 2258, 3M, Sydney, Australia) were placed 2 cm apart in line with the direction of the underlying muscle fibres and inter-electrode resistances were ensured to be $<10\text{ k}\Omega$ in all instances.

Indwelling electrodes were manufactured in the laboratory using the technique described by Basmajian and DeLuca (1985) and consisted of two Teflon coated 0.14

mm in diameter stainless steel wires inserted into the muscle using a hypodermic cannula. These electrodes were used for muscles for which surface electrode recording has been shown to be invalid (latissimus dorsi, infraspinatus; Ginn and Halaki, 2015; Johnson et al., 2011), that underlie superficial muscles (subscapularis, rhomboid major, supraspinatus), or shift with respect to the overlying soft tissue during shoulder movements (teres major). Correct indwelling electrode placement was determined by visual inspection of the EMG signals as the participant performed standardised submaximal tests expected to elicit a large amount of activity from the muscle in question. This was compared with tests expected to activate surrounding muscles into which the electrode may have inadvertently been placed. Because of the difficulty in distinguishing rhomboid major from lower trapezius activity using this method, intramuscular electrodes were inserted into rhomboid major using ultrasound guidance (Mindray, DP-9900). A grounding electrode (Universal Electrosurgical Pad:Split, 9160F, 3M, Sydney, Australia) was placed on the acromion and scapular spine of the contralateral limb.

The signals were amplified (Iso-DAM 8 amplifiers, World Precision Instruments, Sarasota, FL; gain = 100-1000, input impedance $>10^{12} \Omega$, common mode rejection >100 dB), filtered (band-pass = 10-1000 Hz) and acquired on a PC with a 16 bit analogue to digital converter at a sampling rate of 2,564 Hz using Spike 2 software (version 4.00, Cambridge Electronics Design).

Normalisation Tests

EMG data were normalised to maximum voluntary isometric contractions (MVIC) by having each participant perform eight maximal tests in random order, five shoulder normalisation tests which have been shown to have a high likelihood of maximally

activating all the shoulder muscles investigated in this study (Boettcher et al., 2008; Ginn et al., 2011) and three elbow or wrist tests. These tests included:

- Self-resisted shoulder adduction at 90° flexion
- Resisted shoulder internal rotation at 90° abduction
- Resisted shoulder abduction with the shoulder at 90° abduction and internally rotated
- Resisted shoulder flexion with the shoulder at 125° flexion
- Resisted shoulder extension with the shoulder at 30° abduction and 0° flexion
- Resisted wrist, finger and elbow flexion at 90° elbow flexion with the shoulder at 0° abduction
- Resisted elbow extension at 90° flexion with the shoulder at 0° abduction
- Resisted wrist and finger extension at 90° elbow flexion with the shoulder at 0° abduction

Kinetic Measures

A force platform with four load cells (Kistler 9287B, Kistler Instrumente AG Winterthur, Switzerland) was used to record forces in the anterior-posterior (X), medial-lateral (Y), and vertical (Z) directions. The force signals were collected using a 16 bit analogue to digital converter at a sampling rate of 1000 Hz (MP100A, Biopac Systems Inc., Santa Barbara, CA, USA).

Kinematic Measures

Wireless inertial measurement units (MyoMotion Research Sensors – Model 610, Noraxon, Scottsdale, AZ, USA) were attached to the hand, forearm and upper arm of

the striking arm, as well as to the upper and lower thorax of each participant using medical tape to measure joint kinematics of the striking arm during the knapping cycle. These sensors then transmitted data on the limb orientations to a receiver (MyoMotion Research Receiver – Model 680, Noraxon, Scottsdale, AZ, USA) attached to the computer using the MR3 software (Version 3.6.20, Noraxon, Scottsdale, AZ, USA) at a sample rate of 100 Hz, where they were synchronised with the EMG and force signals during the strike (MyoSync, Noraxon, Scottsdale, AZ, USA).

Stone Material

Heat-treated Keokuk chert spalls and flint nodules were used in the knapping experiment. Keokuk chert and flint are fine-grained, silica-rich sedimentary rocks and they were selected for three reasons. First, its lack of natural planes of separation, meaning that when struck with sufficient force conchoidal fractures occur. This process is predictable, which allows the knapper to control and direct the application of force so as to shape the material being worked. Secondly, the ease with which it is able to be worked by a beginner. Thirdly, its availability. All spalls were bifacial and broadly similar in dimensions (~12 cm in length). The angular protrusions make the spalls suitable for the production of a sequence of flakes. This procedure ensured standardised initial conditions as much as possible. Hammerstones consisted of a selection of ovoid water-worn basalt cobbles sourced from the North Island of New Zealand. The hammerstones provided were of a range of similar shapes and sizes so that participants could select the hammerstone that was most comfortable for them to use during training, but limited to a single hammerstone of known mass (weight: 500 g) during data collection to eliminate hammerstone shape and weight as variables.

Procedure

With all electrodes and sensors in situ and inserted according to the procedures outlined above, each participant was seated on the force plate during the experiment with the hammerstone and a supply of spalls. All subjects used the same hammerstone during data collection. Using their dominant hand, the subjects were then instructed to knap for at least 5 minutes. In the event that the core became too reduced to allow for further detachment of flakes, the core was replaced with a new one.

EMG signals were high pass filtered (10 Hz, zero lag 8th order Butterworth), rectified and then low pass filtered (5 Hz, zero lag 8th order Butterworth) using Matlab 2014b (The Mathworks). The maximum value of each muscle obtained during the MVICs was used to normalise the EMG recordings during stone knapping for that muscle. All signals were then resampled to 200 Hz. The start of the up-swing and down swing of the arm and was identified using the elbow and shoulder flexion angles. The initiation of either angle in each direction was identified using their angular velocity traces. The strike of the hammerstone with the core was identified from the vertical force trace. A subject specific threshold force was used to identify strikes and eliminate any movement artefact due to subject movements.

The peak EMG amplitude and the timing of the peak EMG during each up and down swing phases were calculated. All signals were then time normalised to 101 points for each phase and mean and 95% confidence intervals calculated across cycles for each subject as well as across subjects. The timing of the peaks was then converted to a percent of duration of each phase for each cycle.

Statistical Analysis

Peak EMG amplitudes peak EMG values were compared across muscles and the up-swing and down-swing using a two factor (muscle: 15 levels, swing: up and down) repeated measures analysis of variance (ANOVA) (Statistica version 10, Statsoft).

Peak EMG timing were compared across muscles during each of the up-swing and down-swing phases using a one factor (muscle: 15 levels) repeated measures ANOVA.

Tukey post hoc test was used to identify specific differences when significant ANOVA results were obtained. Statistical significance was set at $p < 0.05$.

Results

Signals from subscapularis for one subject and from rhomboid major data for another (< 1% of total data) were lost due to dislodgment of the electrodes during the experiment.

Group averages were imputed for these missing data.

Motion Patterns

The mean (\pm 95% confidence intervals) of the time normalised kinetic and kinematic data are presented in Figure 2. Analysis of the kinematic and kinetic data indicate that the motion of the dominant arm during knapping is divisible into two phases: an up-swing phase (mean \pm standard deviation: 0.45 ± 0.06 s corresponding to approximately 70% of the knapping cycle) and a down-swing phase (0.18 ± 0.03 s representing the remaining approximately 30% of the cycle) terminating at the point of hammerstone impact. The end of the up-swing is identified with the vertical dotted line in Figure 2.

The largest contribution to the overall movement of the knapping arm in the sagittal plane came from the elbow joint which moved an average of 40° . Shoulder flexion/extension contributed an average of approximately 20° with small contributions

from shoulder abduction/adduction ($<5^\circ$) or wrist movement ($<10^\circ$). The forces generated during knapping were predominantly vertical forces.

The up-swing phase was characterised by elbow flexion, shoulder flexion and slight external rotation and abduction, and slight wrist extension. The down-swing phase was characterised by rapid elbow extension, shoulder extension with some internal rotation and adduction, and wrist extension and radial deviation followed by flexion and ulnar deviation. All subjects exhibited broadly similar patterns of upper limb motion during the up-swing and down-swing phases, particularly in terms of the consistency in the order of motion events within subjects (Fig. 2).

EMG Activity

The mean (\pm 95% confidence intervals) of the time normalised EMG data are presented in Figure 3. Peak EMG activity levels during the up-swing and down-swing phases are shown in Figure 4. Moderate to low average activity levels were generated during knapping, ranging from 3-26% MVIC during the upswing phase, and 12-36% MVIC during the downswing phase. ANOVA results indicated significantly greater mean activity levels during the downswing phase. Tukey post hoc analysis indicated that average activity levels between the upswing and downswing phases did not differ in only six of the muscles examined (upper and lower trapezius, infraspinatus, supraspinatus, anterior deltoid and biceps brachii). Anterior deltoid and biceps brachii were the only two muscles examined that recorded $<15\%$ MVIC in both upswing and downswing phases of the knapping cycle.

Muscles with the highest peak EMG values at the shoulder during the up-swing phase were lower trapezius (26% MVIC), infraspinatus (19% MVIC), and the wrist and finger extensors (18% MVIC). During the down-swing phase the following muscles recorded peak activity levels greater than 26% MVIC: lower trapezius (36% MVIC), teres major

(33% MVIC), the wrist and finger extensors (33% MVIC), pectoralis major (32% MVIC), the wrist and finger flexors (29% MVIC), proximal triceps brachii (29% MVIC), latissimus dorsi (28% MVIC), and infraspinatus (27% MVIC).

Timing of Peak EMG Activity

The timing of the peak EMG activity during the up-swing and down-swing phases are shown in Figure 5. There were significant differences in the timing of the muscles in both up-swing ($F(12,180)=7.92, p < 0.001$) and down-swing ($F(14,210)=12.10, p < 0.001$). Note, triceps brachii (proximal and distal) were not included in analysis of timing of activity during the upswing phase due to the low peak activity levels ($< 5\%$ MVIC) measured. During the upswing phase almost all muscles examined were recruited simultaneously. Latissimus dorsi was recruited significantly later than all other muscles except teres major. In general, the muscles producing extension torque at the elbow and shoulder, i.e. muscles causing downward acceleration of the knapping limb, were recruited early in the downswing phase with elbow and shoulder flexor muscles recruited closer to hammerstone strike.

Discussion

The results of this study indicate that all knappers exhibited a broadly similar pattern of upper limb motion during the up-swing and down-swing phases, particularly in terms of the consistency in the order of motion events. The motion of the knapping strike occurs in a proximodistal sequence through to hammerstone impact. The elements of the shoulder, elbow, and hand moved in a coordinated sequence, originating with the shoulder proximally in the up-swing and moving through to the wrist and hammerstone distally in the down-swing phase. This result is consistent with previous biomechanical

studies investigating stone knapping (Williams et al., 2010). A proximal-to-distal joint sequence is advantageous in activities requiring speed and accuracy as it increases the muscular efficiency of the strike and allows fine control of movements at the distal extremity (Furuya and Kinoshita, 2007; 2008). It does this by centralising muscular torques to the proximal joint (the shoulder, in this case), using them to accelerate the proximal limb segment and generate passive interactive torques at the distal joints of the limb. As the distal muscular torques are freed from a role in generating primary motion of the limb, they instead work to refine the motion patterns in the distal limb segments and thereby increase strike accuracy (Hirashima et al., 2003).

The up-swing phase acts as a “cocking” or preparatory phase in which the hammerstone is moved away from the objective tool stone to provide some range through which to generate acceleration and force during the down-swing. Stone knapping is a dynamic flexion-extension task: the arm is flexed in the up-swing, and then rapidly extended in the downswing to generate force for the strike. Upper limb muscle activity in the up-swing phase is low due to the comparatively slow movement that occurs. Pectoralis major and the anterior deltoid are recruited at similar times in the early stages to flex the shoulder, while biceps brachii flexes the elbow. Latissimus dorsi comes on significantly later than all other muscles in the late stages of the up-swing in order to initiate shoulder extension in preparation for the down-swing. Teres major is similarly activated in late up-swing to work synergistically with latissimus dorsi in this role.

Muscular force generation and acceleration in the knapping strike occurs as a result of the action of triceps brachii, teres major, and latissimus dorsi in the down-swing phase. The proximal and distal portions of triceps brachii peak the earliest of all muscles in the initiation stage of the down-swing to forcefully extend the elbow. Latissimus dorsi and teres major also peak early in the down-swing, at similar magnitudes, exhibiting the greatest peak activity of all muscles in either phase in the knapping arm swing.

Latissimus dorsi and teres major work with the triceps brachii to rapidly extend the shoulder and elbow during the down-swing to generate the force for hammerstone strike. A rapid deceleration phase occurs late in the down-swing phase. The flexor musculature of the shoulder (particularly pectoralis major) experiences some of its greatest activity in this part of the down-swing, and is recruited to decelerate the rapid shoulder extension in order to improve control of the distal limb segments, the hammerstone's direction of travel, and as a result, strike accuracy.

Rotator cuff muscle activity levels are greatest during the downswing phase of the knapping cycle as they function to stabilise the shoulder joint against potential humeral head displacement caused by the muscles accelerating and decelerating shoulder extension. Subscapularis (anterior rotator cuff) is activated earlier in the down-swing than infraspinatus (posterior rotator cuff) in order to stabilise the humerus in the glenoid fossa during shoulder extension against posterior humeral head displacement caused by strong extensor torques. As the shoulder flexor muscles decelerate shoulder extension infraspinatus and supraspinatus are recruited at their highest levels during the knapping cycle to stabilise against potential anterior humeral head displacement caused by these flexor muscles as well as to decelerate the shoulder internal rotation movement associated with downswing. During the two phases, the rotator cuff muscles, rather than contracting simultaneously, are recruited in a more direction-specific manner to provide dynamic stabilisation of the shoulder joint during dynamic flexion and extension activities like stone tool manufacture (Wattanaparakornkul et al. 2011).

Axioscapular muscles function during shoulder joint movement to rotate the scapula and to stabilise the scapula against potential translation forces created by scapulohumeral muscles (e.g. rotator cuff, deltoid, teres major, triceps brachii). In the up-swing/preparatory phase of the knapping cycle, upper and lower trapezius are recruited at low-to-moderate levels to produce the upward rotation of the scapula

required to correctly position the glenoid fossa for shoulder joint flexion in preparation for arm acceleration into the down-swing. Rhomboid major is recruited in the down-swing to produce the downward rotation of the scapula required during shoulder extension. Lower trapezius exhibited the highest peak activity of all muscles investigated in both the up-swing down-swing phases with significantly higher activity levels recorded during the downswing phase. This reflects the role of lower trapezius to stabilise the scapula against potential translation caused by the rotator cuff, teres major, and triceps brachii activity during the knapping strike.

In the present study, the wrist generally underwent slight flexion prior to hammerstone impact in all subjects. In addition, both wrist and finger flexor and extensor muscle groups demonstrated peak activity levels during the downswing phase of the knapping strike with the wrist and finger flexor group peaking earlier than the extensor group. Similar to the results reported by Williams et al. (2010), wrist flexion range of motion did not occur beyond a neutral wrist position. In a study on hand muscle recruitment during hard hammer percussion, Marzke et al. (1998) reported that flexor carpi ulnaris (FCU) in the dominant hand (i.e. the hand grasping the hammerstone) experienced peak activity immediately prior to impact, arguing that this sudden burst of activity from the FCU induced a “flicking” (wrist flexion) motion at the wrist.

While the knappers in this study exhibited very similar kinematic patterns in the shoulder and elbow during both up-swing and down-swing, the motion of the wrist was more variable particularly immediately prior to hammerstone impact. Though the muscles of the superficial wrist and finger flexors/extensors did not play a major role in producing the arm swing, their moderate-to-high activity and consistent activation pattern in the down-swing around the time of hammerstone impact suggests they play an important role in the knapping strike. The higher degree of inconsistency in wrist movement observed in this study is then surprising as their pattern of muscle

recruitment is highly consistent. If these muscle groups were important for producing the movements of the wrist and trajectory of the hammerstone (and consequently strike accuracy), it would be expected that wrist kinematics between subjects would be as consistent similar to the other upper limb segments. This suggests that these muscles are unlikely to be causing the “flicking” movement of wrist as suggested by Marzke et al. (1998).

The wrist and finger flexor musculature may instead be highly active to stabilise the elbow and wrist for hammerstone impact by producing a shunting force to compress the elbow joint during the loading and speed of the knapping strike and by stabilising the wrist joint in mid position to facilitate gripping of the hammerstone. The minimal flicking motion observed in this study and others (Marzke et al., 1998; Williams et al., 2010) is more likely the result of movement generated through a “summation of speed” effect (Putnam, 1993). According to this principle, velocity and force in each segment of the kinetic chain are transferred to the terminal segment by the action of the proximal segments. That is, the velocity and force generated by the shoulder is transferred down the kinetic chain to the wrist/hand in a proximal-to-distal sequence, where the distal segments begin movement when the proximal reaches maximum angular velocity. The smaller distal limb segments achieve greater angular velocity as they have a smaller moment of inertia, passively increasing the end point velocity of the distal segments and thus strike forces during stone knapping. In this way the upper limb acts as a flail or whiplash during the stone knapping arm swing. The high recruitment of the wrist flexor and extensor musculature during the knapping arm swing must not then be working to actively produce the wrist “flick” but instead to minimise and absorb reactive forces from the hammerstone impact that might be transferred to the proximal limb segments. This occurs through co-contraction to stabilise the elbow against centrifugal forces at the elbow from the speed of elbow extension, and stiffen the wrist to prevent greater

degrees of flexion that would lower the mechanical advantage of the digital flexor musculature and stability of the hammerstone in a forceful precision grip, as these muscles are weaker through greater degrees of wrist flexion (Pigeon et al., 1996).

Triceps brachii is the primary extensor of the elbow which has its sole insertion on the proximal aspect of the olecranon process of the ulna, and it is one of the largest and strongest muscles of the arm in both modern humans and chimpanzees (Amis et al., 1979; Thorpe et al., 1999). The bony lever of the triceps brachii is formed by the olecranon process and as such its length and orientation has been used widely in the literature to infer upper limb functional specialisation in primates (e.g. Drapeau, 2004; Drapeau, 2008; Jolly, 1966, 1972; McCrossin et al., 1998; Oxnard, 1963). Two features associated with the elbow of modern humans that are suggested to enhance the manipulatory performance of the upper limb are the length and orientation of the olecranon process. Olecranon length (measured from the rotational centre of the ulna to the posterior-most point of the triceps brachii insertion) reflects the maximum length of the bony lever of triceps brachii (Drapeau, 2004). A relatively short olecranon is suggested to be the primitive condition for the hominoids as it is observed in all extant ape species with the exception of modern humans, and it is generally interpreted as an adaptation to arboreal climbing behaviours (Aiello and Dean, 2002; Aiello et al., 1999; McHenry et al., 1976; Tuttle and Basmajian, 1974). Modern humans by comparison have a relatively long olecranon process which has been interpreted as a derived character state associated with tool manufacture and use (Aiello and Dean, 2002; Tuttle and Basmajian, 1974).

Olecranon orientation is the angle formed by the intersection of the long axis of the ulna with olecranon length, and this angle is related to the moment arm of triceps brachii. A more superiorly orientated olecranon (i.e., an olecranon for which this angle approaches 180°) provides the maximal amount of leverage to triceps brachii during flexion of the

forearm. A posteriorly orientated olecranon (i.e. an olecranon with an orientation angle closer to 90°) confers greatest leverage during full forearm extension, such as is seen in knuckle-walkers where the triceps muscle is active to prevent elbow collapse during locomotion (see Drapeau, 2004 for details; Tuttle and Basmajian, 1974). In modern humans (with their superiorly orientated olecranons), therefore, the greatest mechanical advantage is conferred to the triceps during behaviours such as hammering and scraping. The role of triceps brachii as one of the main strike force generators in Oldowan stone tool manufacture documented in this study supports hypotheses of olecranon process orientation and length as an important potential indicator of tool capabilities in fossil hominins.

Conclusion

Archaeological evidence indicates that the hominins who made the Oldowan tools were capable of flaking basalt cobbles very efficiently and so probably achieved speed, kinematic, kinetic, and muscle recruitment values similar to those documented in this study. The stone knapping arm motion is a dynamic three-dimensional flexion-extension task (rather than simple planar flexion and extension) wherein both the shoulder and elbow musculature play integral roles in the production of acceleration of arm segments, stability, strike force, and accuracy. The major torque-generating muscles of the strike (accelerating and decelerating the upper limb and producing force during down-swing) are triceps brachii, latissimus dorsi, teres major, and pectoralis major. The “flicking” action at the wrist joint noted in other studies of stone tool manufacture appears to be largely a passive action caused by muscular activity further up the kinetic chain. Instead, the high activity of the wrist flexor and extensor muscle groups during the knapping strike occurs primarily in order to stabilise the elbow and wrist against reactive forces resulting from hammerstone strike and greater degrees of

wrist flexion that would destabilise the hammerstone in a forceful precision grip. Future investigations would benefit from understanding how variations in joint anatomy influence muscle recruitment patterns and kinematics in stone tool manufacture in order to more precisely model the knapping behaviour of fossil hominins, and how skill affects muscle recruitment patterns by comparing novices and experts.

Acknowledgements

We would like to thank everyone who participated in the study and the anonymous reviewers for their helpful feedback on the manuscript.

Competing Financial Interests

The authors declare no competing financial interests.

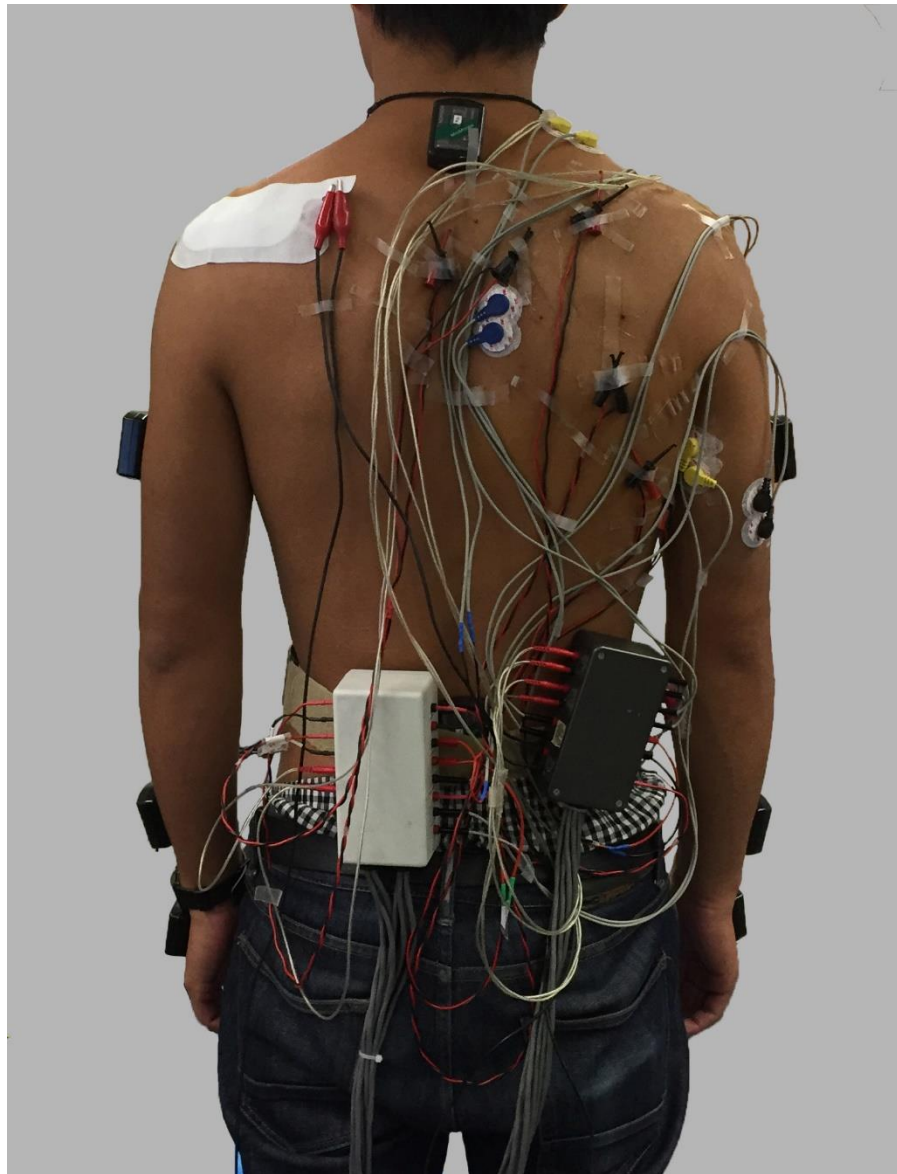


Figure 1. Electrode and wireless inertial sensor placement. The small black boxes are the inertial sensors. All electrode cables were taped in place and full range of motion ensured prior to data collection taking place.

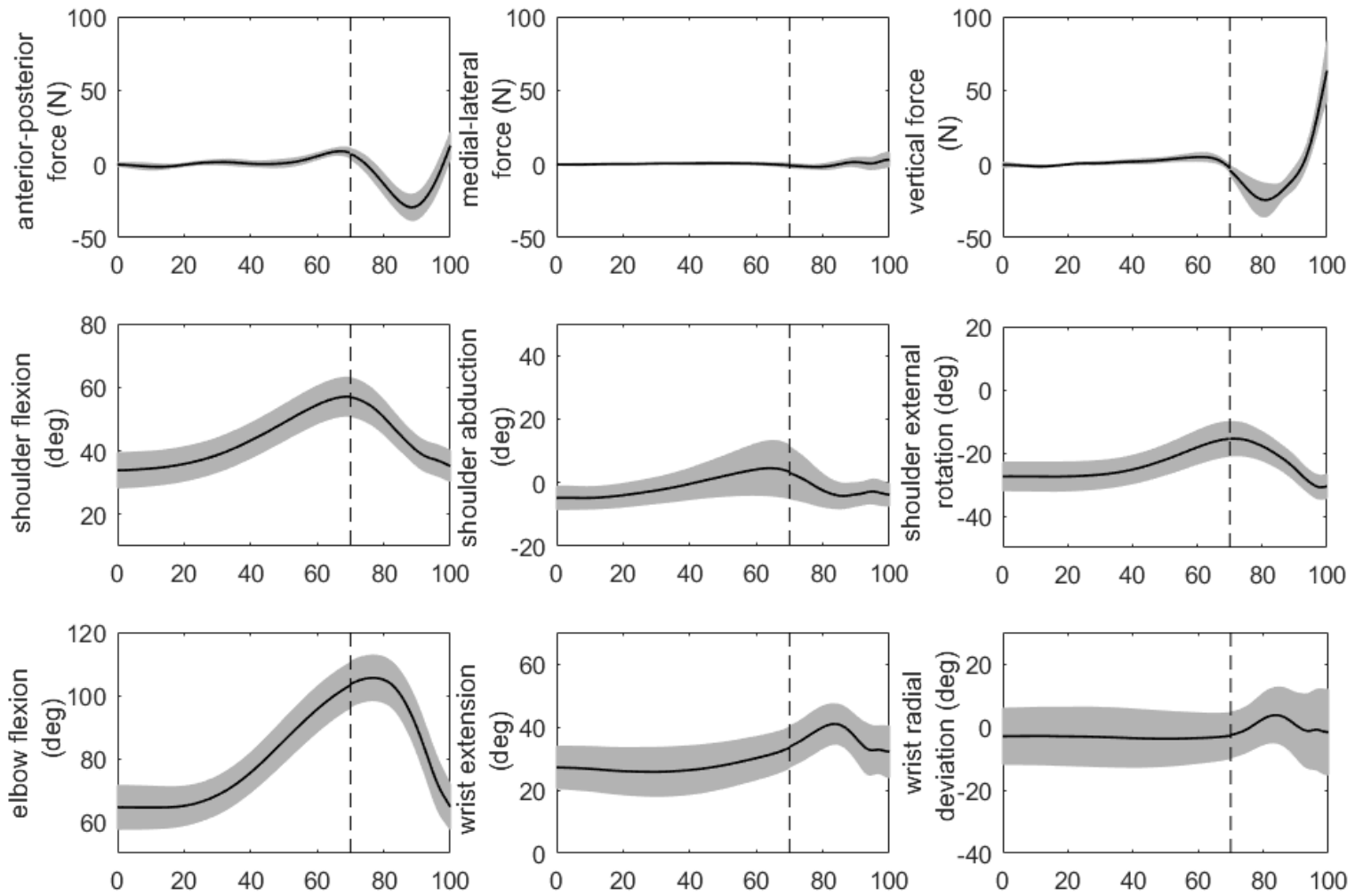


Figure 2. The mean \pm 95% confidence intervals (grey shaded area) of the time normalised kinetic and kinematic data vs time normalised to cycle duration. Up-swing is 0-70% cycle duration and down swing is 70-100% cycle duration. The vertical dotted lines indicate the end of the up-swing. Hammerstone impact occurs at point 100%.

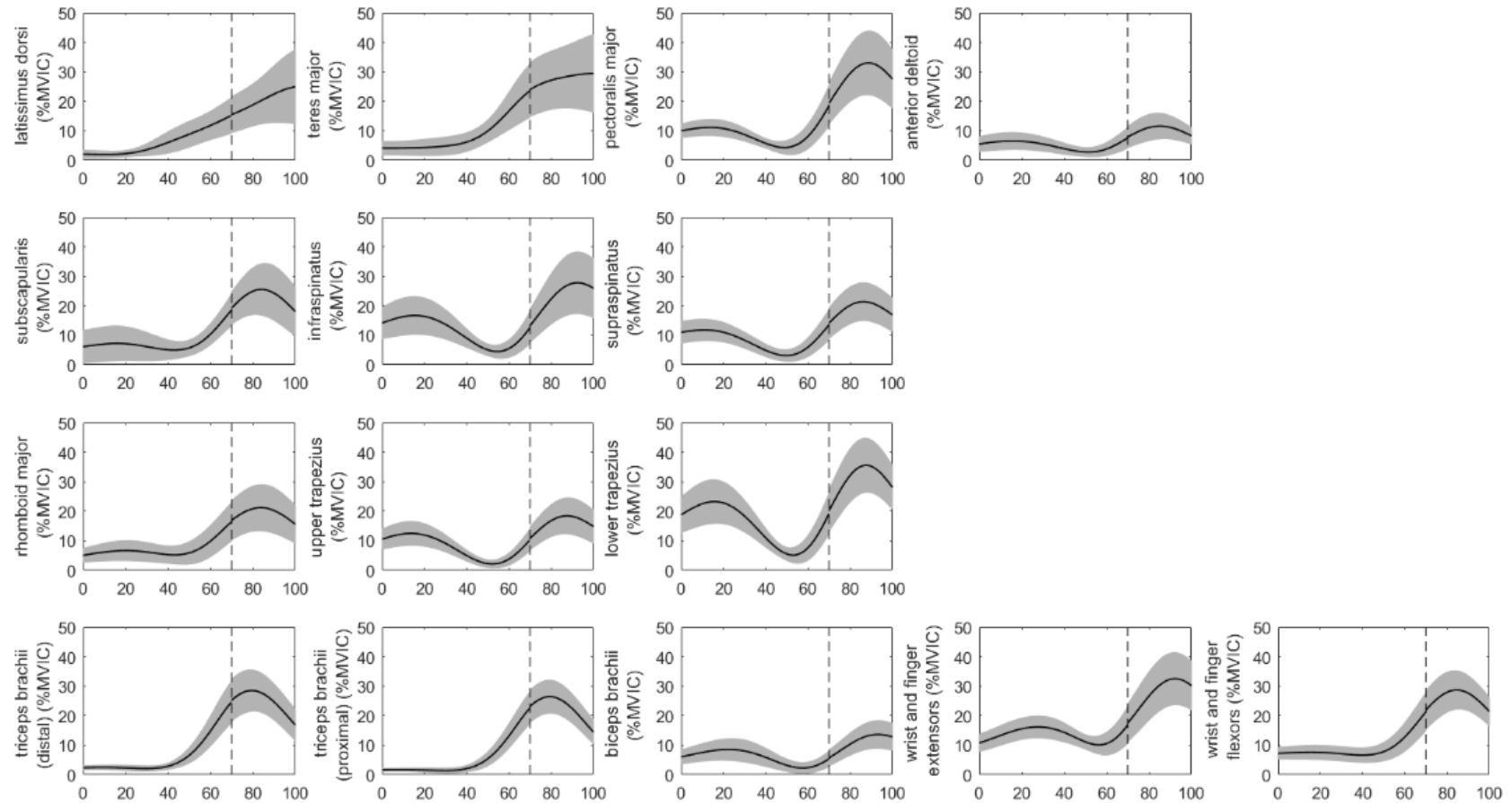


Figure 3. The mean \pm 95% confidence intervals (grey shaded area) of the time normalised EMG data vs time normalised to cycle duration. Up-swing is 0-70% cycle duration and down-swing is 70-100% cycle duration. The vertical dotted lines indicate the end of the up-swing. Hammerstone impact occurred at point 100%.

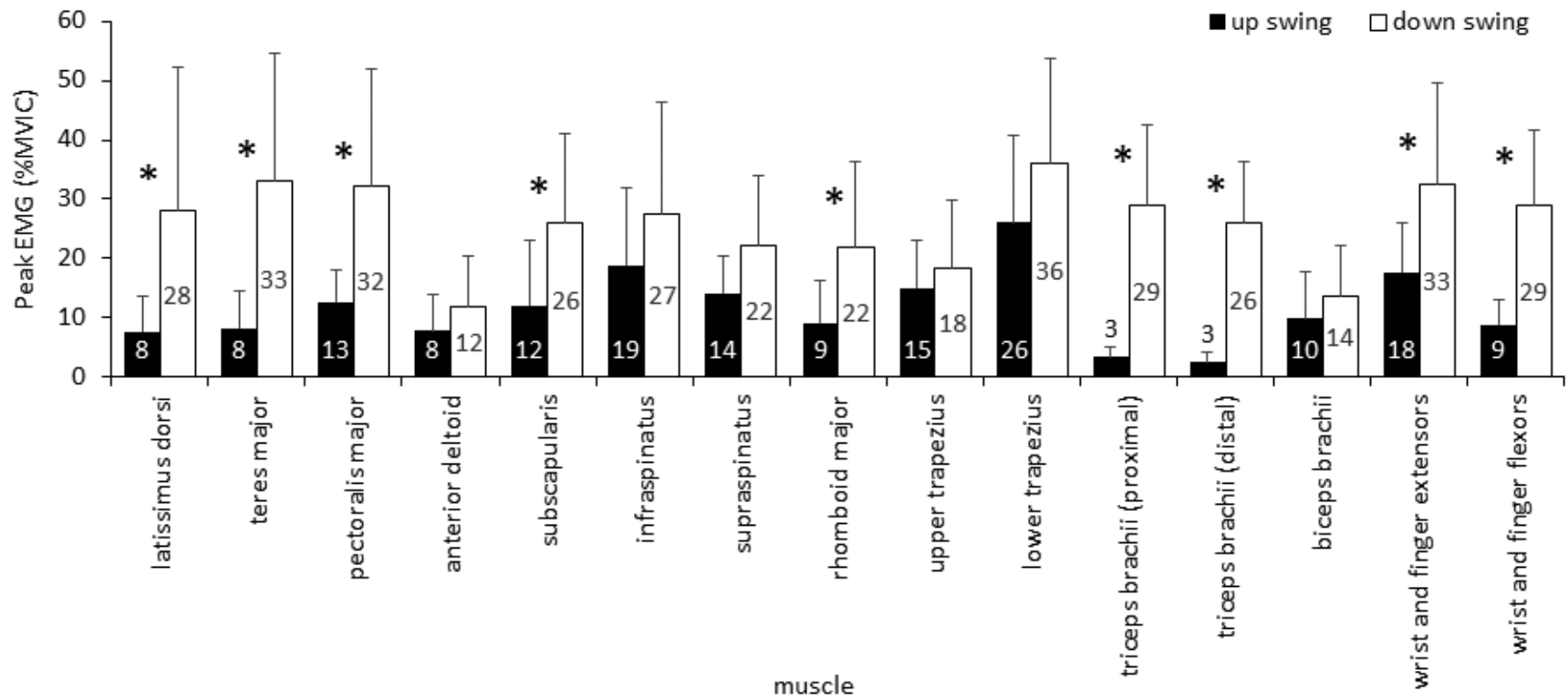


Figure 4. Mean and standard deviation of the peak muscle activation in the up-swing and down-swing phases of the knapping strike.

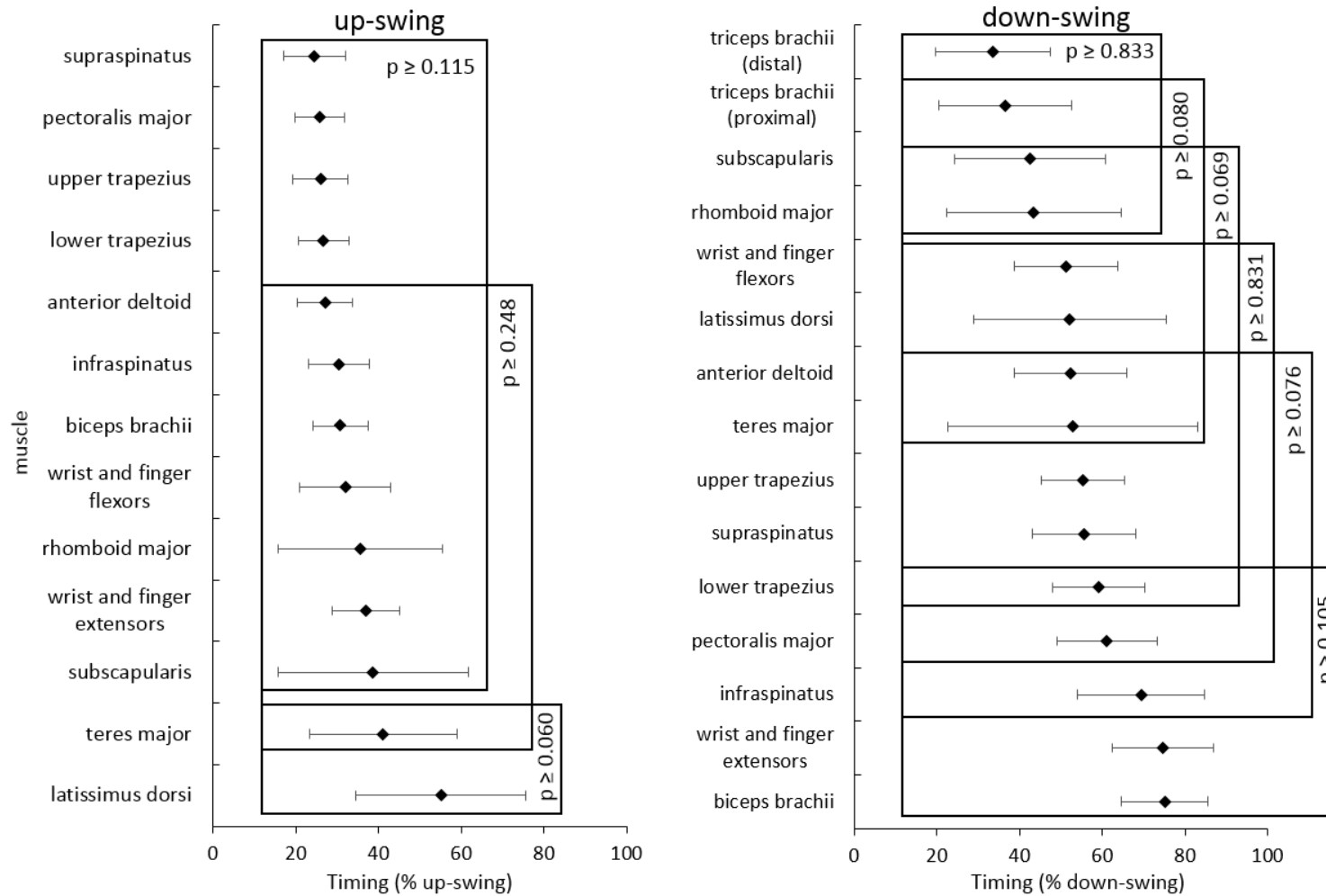


Figure 5. Mean and standard deviation of the timing of peak muscle activation in the up-swing and down-swing phases of the knapping strike (represented as a percent of swing duration). The boxes and *p*-values denote muscles whose peak activation timing were not significantly different to each other.

References

- Aiello, L., Dean, C., 2002. *An Introduction to Human Evolutionary Anatomy*. Academic Press, San Diego.
- Aiello, L.C., Wood, B., Key, C., Lewis, M., 1999. Morphological and taxonomic affinities of the Olduvai ulna (OH 36). *Am. J. Phys. Anthropol.* 109, 89-110.
- Amis, A.A., Dowson, D., Wright, V., 1979. Muscle Strengths and Musculoskeletal Geometry of the Upper Limb. *Journal of Engineering in Medicine* 8, 41-48.
- Basmajian, J.V., DeLuca, C.J., 1985. *Muscles Alive: Their functions revealed by electromyography*, Fifth ed. Williams & Wilkins, Baltimore.
- Biryukova, E.V., Bril, B., Dietrich, G., Roby-Brami, A., Kulikov, M.A., Molchanov, P.E., 2005. The Organization of Arm Kinematic Synergies: the Case of Stone-bead Knapping in Khambhat, in: Roux, V., Bril, B. (Eds.), *Stone Knapping: The Necessary Conditions for a Uniquely Hominin Behaviour*. McDonald Institute for Archaeological Research, Cambridge, England, pp. 73-90.
- Biryukova, E.V., Bril, B., Frolov, A.A., Koulikov, M.A., 2015. Movement kinematics as an index of the level of motor skill: the case of Indian craftsmen stone knapping. *Mot. Control* 19, 34-59.
- Boettcher, C.E., Ginn, K.A., Cathers, I., 2008. Standard maximum isometric voluntary contraction tests for normalizing shoulder muscle EMG. *J. Orthop. Res.* 26, 1591-1597.
- Bril, B., Smaers, J., Steele, J., Rein, R., Nonaka, T., Dietrich, G., Biryukova, E.V., Hirata, S., Roux, V., 2012. Functional mastery of percussive technology in nut-cracking and stone-flaking actions: experimental comparison and implications for the evolution of the human brain. *Phil. Trans. R. Soc. Lond. B Biol. Sci.* 367, 59-74.

- Dapena, J., Anderst, W.J., Toth, N., 2006. The Biomechanics of the Arm Swing in Oldowan Stone Flaking, in: Toth, N., Schick, K. (Eds.), *The Oldowan: Case Studies Into the Earliest Stone Age*. Stone Age Institute Press, Gosport, pp. 333-337.
- Drapeau, M.S.M., 2004. Functional anatomy of the olecranon process in hominoids and plio-pleistocene hominins. *Am. J. Phys. Anthropol.* 124, 297-314.
- Drapeau, M.S.M., 2008. Articular morphology of the proximal ulna in extant and fossil hominoids and hominins. *J. Hum. Evol.* 55, 86-102.
- Furuya, S., Kinoshita, H., 2007. Roles of proximal-to-distal sequential organization of the upper limb segments in striking the keys by expert pianists. *Neurosci. Lett.* 421, 264-269.
- Furuya, S., Kinoshita, H., 2008. Expertise-dependent modulation of muscular and non-muscular torques in multi-joint arm movements during piano keystroke. *Neuroscience* 156, 390-402.
- Ginn, K., Halaki, M., Cathers, I., 2011. Revision of the shoulder normalisation tests is required to include rhomboid major and teres major. *J. Orthop. Res.* 29, 1846-1849.
- Ginn, K.A., Halaki, M., 2015. Do surface electrode recordings validly represent latissimus dorsi activation patterns during shoulder tasks? *J. Electromyogr. Kines.* 25, 8-13.
- Hirashima, M., Kudo, K., Ohtsuki, T., 2003. Utilization and compensation of interaction torques during ball-throwing movements. *J. Neurophysiol.* 89, 1784-1796.
- Johnson, V.L., Halaki, M., Ginn, K., 2011. The use of surface electrodes to record infraspinatus activity is not valid at low infraspinatus activation levels. *J. Electromyogr. Kines.* 21, 112-118.
- Jolly, C.J., 1966. The evolution of the baboons, in: Vagtberg, H. (Ed.), *The baboon in medical research*. Texas University Press, Austin, Texas, pp. 23-50.

Jolly, C.J., 1972. The classification and natural history of *Theropithecus* (*Simopithecus*) (Andrews, 1916), baboons of the African Plio-Pleistocene. *Bulletin of the British Museum of Natural History. Geology.* 22, 3-123.

Larson, S.G., 2007. Evolutionary transformation of the hominin shoulder. *Evol. Anthropol.* 16, 172-187.

Larson, S.G., 2015. Humeral torsion and throwing proficiency in early human evolution. *J. Hum. Evol.* 85, 198-205.

Marzke, M.W., Marzke, R.F., 2000. Evolution of the human hand: Approaches to acquiring, analysing and interpreting the anatomical evidence. *J. Anat.* 197, 121-140.

Marzke, M.W., Marzke, R.F., Linscheid, R.L., Smutz, P., Steinberg, B., Reece, S., An, K.N., 1999. Chimpanzee thumb muscle cross sections, moment arms and potential torques, and comparisons with humans. *Am. J. Phys. Anthropol.* 110, 163-178.

Marzke, M.W., Toth, N., Schick, K., Reece, S., Steinberg, B., Hunt, K., Linscheid, R.L., An, K.N., 1998. EMG study of hand muscle recruitment during hard hammer percussion manufacture of Oldowan tools. *Am. J. Phys. Anthropol.* 105, 315-332.

McCrossin, M.L., Benefit, B.R., Gitau, S.N., Palmer, A.K., Blue, K.T., 1998. Fossil evidence for the origins of terrestriality among Old World higher primates, in: Strasser, E., Fleagle, J., Rosenberger, A.L., McHenry, H.M. (Eds.), *Primate locomotion: Recent advances*. Plenum Press, New York, N.Y. , pp. 353-396.

McHenry, H.M., Corruccini, R.S., Howell, F.C., 1976. Analysis of an early hominid ulna from the Omo basin, Ethiopia. *Am. J. Phys. Anthropol.* 44, 295-304.

Oxnard, C.E., 1963. Locomotor adaptations in the primate forelimb, *Symposia of the Zoological Society of London: The primates*. Zoological Society of London, London, pp. 165-182.

Panger, M.A., Brooks, A.S., Richmond, B.G., Wood, B., 2002. Older than the Oldowan? Rethinking the emergence of hominin tool use. *Evolutionary Anthropology: Issues, News, and Reviews* 11, 235-245.

Pigeon, P., Yahia, L.H., Feldman, A.G., 1996. Moment arms and lengths of human upper limb muscles as functions of joint angles. *J. Biomech.* 29, 1365-1370.

Putnam, C.A., 1993. Sequential motions of body segments in striking and throwing skills: descriptions and explanations. *J. Biomech.* 26, 125-135.

Roach, N.T., Richmond, B.G., 2015. Humeral torsion does not dictate shoulder position, but does influence throwing speed. *J. Hum. Evol.* 85, 206-211.

Roach, N.T., Venkadesan, M., Rainbow, M.J., Lieberman, D.E., 2013. Elastic energy storage in the shoulder and the evolution of high-speed throwing in Homo. *Nature* 498, 483-486.

Thorpe, S.K.S., Crompton, R.H., Gunther, M.M., Ker, R.F., McNeill Alexander, R., 1999. Dimensions and moment arms of the hind- and forelimb muscles of common chimpanzees (*Pan troglodytes*). *Am. J. Phys. Anthropol.* 110, 179-199.

Tocheri, M.W., Orr, C.M., Jacofsky, M.C., Marzke, M.W., 2008. The evolutionary history of the hominin hand since the last common ancestor of *Pan* and *Homo*. *J. Anat.* 212, 544-562.

Tuttle, R.H., Basmajian, J.V., 1974. Electromyography of brachial muscles in *Pan gorilla* and hominoid evolution. *Am. J. Phys. Anthropol.* 41, 71-90.

Williams, E.M., Gordon, A.D., Richmond, B.G., 2010. Upper limb kinematics and the role of the wrist during stone tool production. *Am. J. Phys. Anthropol.* 143, 134-145.

Williams, E.M., Gordon, A.D., Richmond, B.G., 2012. Hand pressure distribution during Oldowan stone tool production. *J. Hum. Evol.* 62, 520-532.

Williams, E.M., Gordon, A.D., Richmond, B.G., 2014. Biomechanical strategies for accuracy and force generation during stone tool production. *J. Hum. Evol.* 72, 52-63.

CHAPTER 9: FRACTAL ANALYSIS RESULTS

9.1 Introduction

This chapter documents the results of the analyses of the fractal dimension values for the fossil material, as well as the results of the EMG experiments within a modal level framework. The computed fractal dimension values and raw fractals can be found in Appendices 2 and 3 respectively.

9.2 Modal Levels based on EMG Results

According to the EMG data presented in the previous chapter, peak muscle activity in the up-swing of Oldowan stone knapping can be categorised as follows:

Table 8. Muscle activity in the up-swing phase of stone knapping according to modal level.	
Up-swing Phase	
Modal Level	Muscle
Low (0–20% MVIC)	Latissimus dorsi, teres major, pectoralis major, anterior deltoid, subscapularis, infraspinatus, supraspinatus, rhomboid major, upper trapezius, proximal triceps brachii, distal triceps brachii, biceps brachii, wrist/finger extensors, wrist/finger flexors
Moderate (21–40% MVIC)	Lower trapezius
High (41–60% MVIC)	-
Very High (>60% MVIC)	-

In the up-swing, muscle recruitment is low and only one muscle, lower trapezius, experiences a moderate level of recruitment, experiencing a mean peak activation level of 26%MVIC (see Figure 4 in Chapter 8). Muscle recruitment is more marked in the down-swing phase:

Table 9. Muscle activity in the down-swing phase of stone knapping according to modal level.	
Down-swing Phase	
Modal Level	Muscle
Low (0–20% MVIC)	Anterior deltoid, upper trapezius, biceps brachii
Moderate (21–40% MVIC)	Latissimus dorsi, teres major, pectoralis major, subscapularis, infraspinatus, supraspinatus, rhomboid major, lower trapezius, proximal triceps brachii, distal triceps brachii, wrist/finger extensors, wrist/finger flexors
High (41–60% MVIC)	-
Very High (>60% MVIC)	-

In the down-swing, then, greatest muscle activity occurs only in the moderate range. Of the Moderate group, only lower trapezius (36% MVIC), teres major (33% MVIC), the wrist and finger extensors (33% MVIC), and pectoralis major (32% MVIC) exhibit mean peak EMG values above the 30% MVIC mark. The ranges of most other muscles peaked in the higher ranges of 22-29% MVIC. While muscle activity was generally only low-to-moderate across both phases of the knapping strike, muscle activity in the down-swing was markedly higher than in the up-swing (with the exception of lower trapezius that peaked in the moderate range for both phases).

Note that the clinical magnitude categories are used to classify muscle recruitment in very high-power activities like baseball pitching, football throwing, and the tennis serve (Escamilla and Andrews, 2009). Knapping is comparatively low-energy; when muscle recruitment is referred to as ‘high’ in the previous chapter, it is relative to the recruitment levels of the other muscles studied in the experiment.

9.3 Results of Fractal Analysis

9.3.1 Entheses for Analysis

The results of the EMG analyses indicate that some of the muscles with highest levels of recruitment find either their origins or insertions on the vertebral or axillary borders of the scapula. This presents an issue for the present analysis. While scapula specimens do indeed exist in the fossil record (e.g. STW 431, MH2, KNM-WT 15000, A.L. 288-1), the fragility of the scapula has meant that preservation of this element is uncommon and often poor. The corollary of this is that sample sizes for scapula entheses (and fractal complexity values) are too low to make meaningful comparisons between species, and this is additionally complicated by non-overlapping anatomical regions. For instance, the scapula of KNM-WT 15000 belongs to an immature individual and is not fully ossified and so must be discounted from inclusion in the analysis based on the exclusion criteria outlined in Chapter 6. The scapula of MH2 is more completely preserved, including the blade, spine, acromion, and vertebral border, and belongs to a mature individual. The lower trapezius inserts on the medial one-third of the scapula spine and MH2 is one of the only fossil specimens to preserve this region, so that no meaningful comparisons can be made for the complexity of this muscle insertion. Given the difficulty of low sample sizes and poor preservation and the importance of the elbow musculature in stone tool manufacture, the data collection for fractal analysis focused on muscles that insert on the humerus, radius, and ulna, as these elements preserve better in the fossil record. The following 14 entheses were analysed:

Table 10. Entheses included in fractal analysis.		
Muscle	Type	Enthesis Location
Biceps brachii	Insertion	Bicipital (radial) tuberosity of the radius
Brachialis	Insertion	Coronoid process of the ulna
Deltoid	Origin and Insertion	Origin: Acromion, the crest of the scapula spine, the lateral one-third of the clavicle Insertion: Deltoid tuberosity of the humerus
Infraspinatus	Insertion	Greater tubercle of the humerus
Extensor carpi radialis	Origin	Lateral epicondylar ridge of the humerus
Extensor muscles of the wrist and hand	Origin	Common origin on the lateral epicondyle of the humerus
Latissimus dorsi	Insertion	Crest of the lesser tuberosity of the humerus and bicipital (intertubercular groove)
Flexor muscles of the wrist and hand	Origin	Common origin on the medial epicondyle of the humerus
Flexor carpi ulnaris, pronator teres	Origin	Medial epicondylar “ridge” (superior surface of the medial epicondyle in a region analogous to the lateral epicondylar ridge)
Pectoralis major	Insertion	Crest of the greater tubercle of the humerus
Subscapularis	Insertion	Lesser tubercle of the humerus
Supinator	Origin	Lateral epicondyle of the humerus, supinator crest and fossa of the ulna
Supraspinatus	Insertion	Greater tubercle of the humerus
Triceps brachii (all heads)	Insertion	Common tendon on the proximal surface of the olecranon process of the ulna

9.3.2 Generalised Linear Mixed Models Analysis of *D*-values

The *D*-values of the muscle attachment sites were compared using a generalised linear mixed model (GLMM) analysis. A restricted maximum likelihood (REML) analysis was used to estimate the GLM model as, unlike maximum likelihood analysis, REML estimates for the variance parameters independent of the estimates for the fixed effects. This means that REML is unbiased random effects and takes into account the loss in degrees of freedom resulting from estimating fixed effects. The curves were clustered and analysed according to entheses, species, and genus.

9.3.2.1 REML variance components analysis (Estimation of the model)

Details of the REML analysis and model estimation are as follows:

Response variate: D_value

Fixed model: Constant + Enthesis + Species + Genus

Random model: Specimen_No

Number of units: 504

A test of fixed effects between the terms of the model (enthesis, species, and genus) shows significant differences ($p < 0.001$) in fractal dimension value or D -value between entheses, species, and genera.

Fixed term	Wald statistic	n.d.f.	F statistic	d.d.f.	F pr
Enthesis	50.58	13	3.87	203.8	<0.001
Species	36.79	7	5.25	32.1	<0.001
Genus	17.16	2	8.58	41.0	<0.001

9.3.2.2 Predicted means

As with an ANOVA, GLMM is an omnibus test statistic and cannot identify which specific levels within the clusters are significantly different from each other; it identifies only that at least two levels were different within those clusters/levels. To assess within-level differences, Fischer's least significant differences (LSD) for multiple comparisons was used to create confidence intervals for all pairwise differences between factor level predicted means. This test calculates the smallest significant difference (that is, the LSD) in pairwise comparisons of means between all factor levels. Significant differences between factor level means can then be determined based on whether the

difference between the two is greater than the LSD for that comparison. The following sections contain tables documenting the predicted means for Enthesis, Species, and Genus. High versus low values were determined based on rounding as variation in absolute D-values is a matter of a single decimal place for Enthesis, Species, and Genus. Those values that fell below 0.005 of the mean for a given category were determined as “low” and those above it “high”; e.g. In Table 12 below, most of the predicted mean D-values for Enthesis fell around 1.89, thus values below 1.895 were categorised as “low” and those above that value “high”.

9.3.2.2.1 Predicted means for Enthesis

Table 12. Predicted means for *D*-value and standard errors for Enthesis, sorted from lowest to highest value of PM. Highlighted rows indicate entheses with greatest mean *D*-value.

Enthesis	Predicted Mean	Standard Error
Supinator	1.880	0.009
Medial epicondyle	1.891	0.003
Pectoralis major	1.892	0.005
Lateral epicondyle	1.893	0.003
Biceps brachii	1.895	0.005
Supraspinatus	1.897	0.004
Infraspinatus	1.898	0.005
Subscapularis	1.898	0.004
Deltoid	1.899	0.005
Latissimus dorsi	1.899	0.005
Brachialis	1.904	0.003
Triceps brachii	1.905	0.003
Lateral epicondylar ridge	1.906	0.004
Medial epicondylar ridge	1.908	0.005

Average standard error is 0.004538, with a maximum value of 0.008836 and a minimum value of 0.003051. The entheses with the greatest mean *D*-value are (from lowest to highest): supraspinatus, infraspinatus, subscapularis, deltoid, latissimus dorsi, brachialis, triceps brachii, lateral epicondylar ridge, and medial epicondylar ridge.

9.3.2.2.2 Predicted means for Species

Predicted means for those enteses identified in the previous GLMM analyses were then analysed by species.

Species	Predicted Means	Standard Errors
<i>Au. sediba</i>	1.885	0.005
<i>H. habilis</i>	1.890	0.011
<i>Australopithecus sp.</i>	1.892	0.005
<i>Au. afarensis</i>	1.898	0.003
<i>H. ergaster</i>	1.898	0.003
<i>P. boisei</i>	1.898	0.003
<i>P. robustus</i>	1.898	0.006
<i>Au. anamensis</i>	1.900	0.009
<i>Homo aff. habilis</i>	1.902	0.008
<i>Au. africanus</i>	1.911	0.004

Average standard error is 0.005561, with a maximum value of 0.01091 and a minimum value of 0.002586. Species with the greatest predicted mean *D*-values were (from lowest to highest): *Au. afarensis*, *H. ergaster*, *P. boisei*, *P. robustus*, *Au. anamensis*, *Homo aff. habilis*, and *Au. africanus*.

9.3.2.2.3 Predicted means for Genus

Those results were then analysed by genus.

Genus	Predicted Mean	Standard Error
<i>Australopithecus</i>	1.903	0.003
<i>Homo</i>	1.898	0.004
<i>Paranthropus</i>	1.892	0.005

Average standard error is 0.003975, with a maximum value of 0.005053 and a minimum value of 0.002509. *Australopithecus* had the highest predicted mean *D*-value of the three genera included in this study.

9.3.2.3 Approximate least significant differences (5% level) of REML means

9.3.2.3.1 LSDs for Enthesis

For the following LSD comparisons, each entheses is allocated a number between 1 and 14 and the number beneath the LSD values indicates the entheses that the target entheses is being compared to. Asterisks indicate comparisons for which the LSD value is zero (comparisons between the same entheses).

Table 15. LSD calculations for entheses comparisons between Mm. biceps brachii (1), brachialis (2), and deltoid (3).

Enthesis	No.	LSDs		
Biceps brachii	1	*		
Brachialis	2	0.01013	*	
Deltoid	3	0.01270	0.01011	*
Infraspinatus	4	0.01248	0.00993	0.01190
Lateral epicondylar ridge	5	0.01123	0.00842	0.01055
Lateral epicondyle	6	0.01104	0.00802	0.01031
Latissimus dorsi	7	0.01312	0.01063	0.01178
Medial epicondylar ridge	8	0.01225	0.01002	0.01217
Medial epicondyle	9	0.01069	0.00793	0.01029
Pectoralis major	10	0.01267	0.01007	0.01139
Subscapularis	11	0.01178	0.00882	0.01111
Supinator	12	0.01909	0.01694	0.01885
Supraspinatus	13	0.01188	0.00920	0.01136
Triceps brachii	14	0.01048	0.00621	0.01053
	No.	1	2	3

Table 15 (contd.). LSD calculations for enthesis comparisons between infraspinatus (4), lateral epicondylar ridge (5), and lateral epicondyle (6).

Enthesis	No.	LSD		
Infraspinatus	4	*		
Lateral epicondylar ridge	5	0.01045	*	
Lateral epicondyle	6	0.01029	0.00822	*
Latissimus dorsi	7	0.01192	0.01100	0.01077
Medial epicondylar ridge	8	0.01230	0.01033	0.01058
Medial epicondyle	9	0.01025	0.00817	0.00723
Pectoralis major	10	0.01187	0.01072	0.01016
Subscapularis	11	0.01027	0.00931	0.00937
Supinator	12	0.01887	0.01813	0.01796
Supraspinatus	13	0.00994	0.00979	0.00964
Triceps brachii	14	0.01030	0.00884	0.00836
	No.	4	5	6

Table 15 (contd.). LSD calculations for enthesis comparisons between latissimus dorsi (7), medial epicondylar ridge (8), and medial epicondyle (9).

Enthesis	No.	LSD		
Latissimus dorsi	7	*		
Medial epicondylar ridge	8	0.01285	*	
Medial epicondyle	9	0.01079	0.01051	*
Pectoralis major	10	0.01129	0.01251	0.01040
Subscapularis	11	0.01089	0.01150	0.00935
Supinator	12	0.01919	0.01912	0.01792
Supraspinatus	13	0.01106	0.01163	0.00961
Triceps brachii	14	0.01105	0.01039	0.00827
	No.	7	8	9

Table 15 (contd.). LSD calculations for enthesis comparisons between pectoralis major (10), subscapularis (11), and supraspinatus (13).

Enthesis	No.	LSD		
Pectoralis major	10	*		
Subscapularis	11	0.01081	*	
Supinator	12	0.01875	0.01838	*
Supraspinatus	13	0.01107	0.00946	0.01859
Triceps brachii	14	0.01053	0.00938	0.01759
	No.	10	11	12

Table 15 (contd.). LSD calculations for enthesis comparisons between supraspinatus (13) and triceps brachii (14).

Enthesis	No.	LSD		
Supraspinatus	13	*		
Triceps brachii	14	0.00959	*	
	No.	13	14	

9.3.2.3.2 LSDs for Species

The following four tables present LSD calculations for species-level comparisons of predicted means following the same procedure as outlined in Section 9.3.2.5.1.

Table 16. LSD calculations for species comparisons between *Au. afarensis* (1), *Au. africanus* (2), and *Au. anamensis* (3).

Species	No.	LSD		
<i>Au. afarensis</i>	1	*		
<i>Au. africanus</i>	2	0.00729	*	
<i>Au. anamensis</i>	3	0.01741	0.01765	*
<i>Au. sediba</i>	4	0.00943	0.00965	0.01865
<i>Australopithecus sp.</i>	5	0.01023	0.01050	0.01899
<i>H. ergaster</i>	6	0.00000	0.00729	0.01741
<i>H. habilis</i>	7	0.02325	0.02497	0.02914
<i>Homo aff. habilis</i>	8	0.01698	0.01863	0.02384
<i>P. boisei</i>	9	0.00000	0.00729	0.01741
<i>P. robustus</i>	10	0.01386	0.01562	0.02206
	No.	1	2	3

Table 16 (contd.). LSD calculations for species comparisons between *Au. sediba* (4), *Australopithecus sp.* (5), and *H. ergaster* (6).

Species	No.	LSD		
<i>Au. sediba</i>	4	*		
<i>Australopithecus sp.</i>	5	0.01202	*	
<i>H. ergaster</i>	6	0.00943	0.01023	*
<i>H. habilis</i>	7	0.02479	0.02540	0.02325
<i>Homo aff. habilis</i>	8	0.01951	0.01995	0.01698
<i>P. boisei</i>	9	0.00943	0.01023	0.00000
<i>P. robustus</i>	10	0.01671	0.01726	0.01386
	No.	4	5	6

Table 16 (contd.). LSD calculations for species comparisons for *H. habilis* (7), *Homo aff. habilis* (8), and *P. boisei* (10).

Species	No.	LSD		
<i>H. habilis</i>	7	*		
<i>Homo aff. habilis</i>	8	0.02556	*	
<i>P. boisei</i>	9	0.02325	0.01698	*
<i>P. robustus</i>	10	0.02697	0.02173	0.01386
	No.	7	8	9

Table 16 (contd.). LSD calculation for species comparison for *P. robustus* (10).

Species	No.	LSD
<i>P. robustus</i>	10	*
	No.	10

9.3.2.3.3 LSDs for Genus

The following table presents LSD calculations for genus-level comparisons of predicted means following the same procedure as outlined in the previous sections.

Table 17. LSD calculations for genus comparisons.				
Genus	No.	LSD		
<i>Australopithecus</i>	1	*		
<i>Homo</i>	2	0.01083	*	
<i>Paranthropus</i>	3	0.01110	0.01366	*
	No.	1	2	3

9.3.2.4 Calculation and identification of significant differences

In order to determine where significant differences lie between entheses, species, and genera, the PMs of the *D*-values for each level in each cluster were subtracted from one another. This then can be compared with the LSDs for each pairwise comparison. In the following tables, the highlighted cells indicate muscles or muscle groups/species/genera whose differences in mean *D*-value are greater than their LSD scores, thereby indicating entheses/species/genera which differ significantly from one another. Zero values indicate comparisons that do not differ at all.

9.3.2.4.1 Significant differences between entheses

Table 18. Calculation of significant differences in enthesis-level PMs for *D*-values.

Enthesis		Supin.	ME	Pect.	LE	Biceps	Supra.	Infra.	Subscap.	Delt.	Lat.	Brach.	Triceps	LER	MER
	PM	1.880	1.891	1.892	1.893	1.895	1.897	1.898	1.898	1.899	1.899	1.904	1.905	1.906	1.908
Supin.	1.880	0	0.011	0.012	0.013	0.015	0.017	0.018	0.018	0.019	0.019	0.024	0.025	0.026	0.028
ME	1.891		0	0.001	0.002	0.004	0.006	0.007	0.007	0.008	0.008	0.013	0.014	0.015	0.017
Pect.	1.892			0	0.001	0.003	0.005	0.006	0.006	0.007	0.007	0.012	0.013	0.014	0.016
LE	1.893				0	0.002	0.004	0.005	0.005	0.006	0.006	0.011	0.012	0.013	0.015
Biceps	1.895					0	0.002	0.003	0.003	0.004	0.004	0.009	0.01	0.011	0.013
Supra.	1.897						0	0.001	0.001	0.002	0.002	0.007	0.008	0.009	0.011
Infra.	1.898							0	0	0.001	0.001	0.006	0.007	0.008	0.01
Subscap.	1.898								0	0.001	0.001	0.006	0.007	0.008	0.01
Delt.	1.899									0	0	0.005	0.006	0.007	0.009
Lat.	1.899										0	0.005	0.006	0.007	0.009
Brach.	1.904											0	0.001	0.002	0.004
Triceps	1.905												0	0.001	0.003
LER	1.906													0	0.002
MER	1.908														0

Abbreviations: Supin. = Supinator; ME = Medial epicondyle; Pect. = Pectoralis major; LE = Lateral epicondyle; Biceps = biceps brachii; Supra. = Supraspinatus; Infra. = Infraspinatus; Subscap. = Subscapularis; Delt. = Deltoid; Lat. = Latissimus dorsi; Brach. = Brachialis; Triceps = Triceps brachii; LER = Lateral epicondylar ridge; MER = Medial epicondylar ridge.

In terms of muscle attachment site robusticity, significant differences lie largely between the entheses with the five lowest PMs and those with the six highest PMs. The supinator insertion was significantly less complex than deltoid, brachialis, triceps brachii, lateral epicondylar ridge, and medial epicondylar ridge. The medial epicondyle, pectoralis major, and lateral epicondyle are significantly less complex than

brachialis, triceps brachii, lateral epicondylar ridge, and medial epicondylar ridge; biceps brachii is significantly less complex than the medial epicondylar ridge.

9.3.2.4.2 Significant differences between species

Table 19. Calculation of significant differences in species-level PMs for *D*-values.

Species		<i>Au. sediba</i>	<i>H. habilis</i>	<i>Au. sp.</i>	<i>Au. afarensis</i>	<i>H. ergaster</i>	<i>P. boisei</i>	<i>P. robustus</i>	<i>Au. anamensis</i>	<i>Homo aff. habilis</i>	<i>Au. africanus</i>
	PM	1.885	1.890	1.892	1.898	1.898	1.898	1.898	1.900	1.902	1.911
<i>Au. sediba</i>	1.885	0	0.005	0.007	0.013	0.013	0.013	0.013	0.015	0.017	0.026
<i>H. habilis</i>	1.890		0	0.002	0.008	0.008	0.008	0.008	0.01	0.012	0.021
<i>Au. sp.</i>	1.892			0	0.006	0.006	0.006	0.006	0.008	0.01	0.019
<i>Au. afarensis</i>	1.898				0	0	0	0	0.002	0.004	0.013
<i>H. ergaster</i>	1.898					0	0	0	0.002	0.004	0.013
<i>P. boisei</i>	1.898						0	0	0.002	0.004	0.013
<i>P. robustus</i>	1.898							0	0.002	0.004	0.013
<i>Au. anamensis</i>	1.900								0	0.002	0.011
<i>Homo aff. habilis</i>	1.902									0	0.009
<i>Au. africanus</i>	1.911										0

Between species comparisons of LSDs indicate that *Au. sediba* is significantly less complex in its mean *D*-value than *Au. afarensis*, *H. ergaster*, *P. boisei*, and *Au. africanus*. *Australopithecus africanus* is significantly more complex in its predicted mean *D*-values than all species except *H. habilis*, *P. robustus*, *Au. anamensis*, and *Homo* aff. *habilis*. *Homo ergaster* was significantly more complex than *Au. sediba* and significantly less complex than *Au. africanus*, but it did not differ from *H. habilis*, *H. aff. habilis*, *Australopithecus sp.*, *Au. afarensis*, *Au. anamensis*, or either of the Paranthropines.

9.3.2.4.3 Significant differences between genera

Table 20. Calculation of significant differences in species-level PMs for <i>D</i> -values.				
Genus		<i>Paranthropus</i>	<i>Homo</i>	<i>Australopithecus</i>
	PM	1.892	1.898	1.903
<i>Paranthropus</i>	1.892	0	0.006	0.011
<i>Homo</i>	1.898		0	0.005
<i>Australopithecus</i>	1.903			0

Genus-level comparisons of LSD scores indicate that *Australopithecus*, *Homo* and *Paranthropus* do not differ significantly from one another.

9.4 Summary

There are significant differences at two levels of analysis (entheses and species). Those entheses with greatest mean *D*-value/complexity scores are supraspinatus, infraspinatus, subscapularis, deltoid, latissimus dorsi, brachialis, triceps brachii, lateral epicondylar ridge, and medial epicondylar ridge. No significant differences were found between these entheses, indicating that they were all of similar degrees of complexity. Species with the greatest predicted mean *D*-values without significant differences were *Au. africanus*, *H. habilis*, *P. robustus*, *Au. anamensis*, and *Homo* aff. *habilis*. Of those

genera, there are no significant differences between *Paranthropus*, *Australopithecus*, and *Homo*.

CHAPTER TEN: DISCUSSION

10.1 Candidate Tool-Makers: Comparison of the Fractal Data with the EMG Data

The fractal complexity data collected and analysed in this study indicate that the muscles with high degrees of complexity, not differing significantly from each other, were supraspinatus, infraspinatus, subscapularis, deltoideus, latissimus dorsi, brachialis, triceps brachii, and the muscles of the lateral epicondylar ridge and medial epicondylar ridge; these entheses were all of similar degrees of complexity. When compared to the EMG data and the muscles with greatest levels of recruitment in Oldowan stone knapping, some of these entheses with greatest fractal complexity scores do indeed parallel the EMG data, and the overlap can be seen in Table 21.

Table 21. Entheses and muscles that exhibit high fractal complexity and muscle recruitment values.	
Highly complex entheses	Muscles with greatest %MVIC
Latissimus dorsi	Latissimus dorsi
Subscapularis	Subscapularis
Supraspinatus	Supraspinatus
Infraspinatus	Infraspinatus
Triceps brachii	Triceps brachii (proximal and distal)
Lateral epicondylar ridge	Wrist/finger extensors (Extensor carpi radialis)
Medial epicondylar ridge	Wrist/finger flexors (M. flexor carpi ulnaris, pronator teres)

There are significant differences at all levels of analysis (enthesis, species, and genera). At the species level, highest predicted mean *D*-values for these entheses were for *Au. africanus*, *Au. anamensis*, *P. robustus*, and *H. habilis/Homo* aff. *habilis*. *Au. sediba* is significantly less complex in its mean *D*-value than *Au. afarensis*, *H. ergaster*, *P. boisei*, and *Au. africanus*, making *Au. sediba* the species with the least complex entheses of all the species represented in the analysis. *H. ergaster* significantly differs only from the

two extremes of the fractal dimension values, *Au. sediba* on the low end and *Au. africanus* on the upper end. Prima facie these results would suggest that these species (*Au. africanus*, *Au. anamensis*, *P. robustus*, and *H. habilis/Homo* aff. *habilis*, and *H. ergaster*) are the probable candidates for the tool-making guild. There were no significant differences between *Australopithecus*, *Homo*, and *Paranthropus*

The reconstruction of activity patterns in past populations, including fossil populations, is highly complex. While bone is one of the more enduring tissues of the body, its plasticity and responsiveness – and the variedness of those responses – to both internal and external stimuli means that it is difficult to concretely attribute osteological changes to one cause over another (see Chapter 2). This problem is compounded by the nature of the evidence: palaeoanthropologists must necessarily deal with populations represented by fragmentary evidence, difficult age and sex determinations, and small sample sizes. While the results indicated here are highly significant ($p < 0.001$), their meaningfulness must be interrogated.

10.2 Interrogating the Candidates: The Morphology and Archaeology of Tool Use Compared

In order to evaluate the results of the analyses presented in this dissertation, we must compare the “candidate tool-makers” listed in the previous section with the other lines of evidence for tool behaviours (both morphological and archaeological) outlined in Chapter 3. Important questions to answer include: How do the enthesal data compare with what is inferred about the tool capacities of fossil hominins from other aspects of morphology? What does the archaeological record tell us? This section will compare other lines of evidence with the results presented in the previous chapter, and it is

organised by taxon. This will be followed by a summary of conclusions and an assessment of the strength of the evidence in its totality.

10.2.1 *Australopithecus africanus*

As is the case with other *Australopithecus* species, *Au. africanus* is not associated with stone tools. Overall, the external morphology of the upper limb in *Australopithecus africanus* appears to be quite primitive, maintaining few of the derived features characterising the upper limbs of later species associated with morphological commitment to tool behaviours (see Chapter 3 for details). Sts 7 (Broom et al., 1950) preserves one of the more complete scapular specimens attributed to *Au. africanus* and this specimen, much like other scapulae attributed to *Australopithecus*, maintains a glenoid fossa with a cranial orientation, suggesting that this species likely retained an upper limb committed at least in part to arboreal locomotion and climbing (Arias-Martorell et al., 2015, Vrba, 1979). This accords with the morphology of the Sts 7 coracoid process, which Vrba (1979) has interpreted to reflect a climbing shoulder. The humerus of Sts 7, by comparison, is reportedly more human-like in many respects (such as humeral head shape and bicipital groove depth: Broom et al., 1950), though damage to the specimen makes evaluating its morphology somewhat difficult. Humeral torsion in Sts 7 is, again, firmly on the primitive spectrum with an estimated value of 126° (Larson, 1996). The arms of *Au africanus* were long relative to the legs, indicating a primitive pattern of limb proportions (McHenry and Berger, 1998). Aspects of the hand morphology are less equivocal about tool use than the rest of the upper limb: *Au. africanus* exhibits basically human-like manual proportions, including a long thumb, though relative metacarpal breadth remained primitive (Green and Gordon, 2008). Ricklan (Ricklan, 1990, 1987) argued that manual remains from Sterkfontain Member 4

demonstrate an enhanced facility for precision pad-to-pad grips as well as a saddle-shaped trapeziometacarpal joint that would have facilitated thumb-to-finger opposition. *Au africanus* also appears to maintain a third metacarpal styloid process which would have stabilised the palm during hard-hammer percussion (Marzke and Marzke, 1987). Despite this, the phalanges are relatively curved (Ricklan, 1987), and the STW 618 scaphoid is primitive in its morphology, suggesting that the wrist did not habitually experience the kind of strong internal or transverse loading that would be expected in the hand of a habitual tool user (Kibii et al., 2011).

Most telling perhaps is the work of Skinner et al. (2015), who investigated trabecular orientation in the metacarpals of *Au. africanus*, *P. robustus*, *H. neanderthalensis*, early and recent *H. sapiens*, and great apes. Trabecular bone density and orientation has been demonstrated to be responsive to loading directions associated with differences in joint posture during locomotion and tool use in modern humans and great apes (Barak et al., 2011, Tsegai et al., 2013). While there is some minor variation between specimens, Skinner et al. (2015) have shown that the trabecular bone in the metacarpals of *Au. africanus* (StW 418, SK 84, SKX 5020) is orientated and distributed in a manner consistent with forceful precision grips – that is, a hand used in the habitual manufacture and use of stone tools. These results accord with the evidence from manual proportions and the trapeziometacarpal joint orientation, suggesting that tool manufacture and use did indeed form a selective pressure in the hand of *Au. africanus*.

Cumulatively, the evidence from the upper limb of *Au. africanus* describes a species that maintained a significant component of arborealism in its locomotor repertoire, but there is nonetheless strong evidence to suggest that tool manufacture or use served an important role. Indeed, the morphology of the hand is not inconsistent with these

behaviours, despite its primitive aspects; the hand of *Au. africanus* was certainly capable of forceful and precise opposition of the fingers and thumb in a manner that would facilitate tool behaviours.

STW 53 is a partial cranium recovered from Member 5 of the Sterkfontein Formation (Tobias, 1978), dating to either 2.6-2.0 Ma (Kuman and Clarke, 2000) or 1.8–1.5 million years (Herries and Shaw, 2011). It has been variously attributed to *Au. africanus* (Clarke, 2006, Kuman and Clarke, 2000, Wolpoff, 1996, Clarke, 2008, Clarke, 2013, Berger et al., 2010), *Homo habilis* (Hughes and Tobias, 1977, Tobias, 1991, Clarke, 1985, Kimbel et al., 1997), or as the type specimen of a separate species *Homo gautengensis* (Curnoe, 2010). While STW 53 itself is not associated with artefacts (Kuman and Clarke, 2000), the Member 5 sediments do contain artefacts from both Oldowan and Acheulean technological complexes (Herries and Shaw, 2011). If STW 53 reveals itself to be *Au. africanus*, it is possible that at least some of the stone tools from Member 5 were made by *Au. africanus*. As the evidence presently stands, the results of my analysis would appear to support the interpretation of *Au. africanus* as a tool-maker and user, providing yet more evidence of morphological commitment to tool use in a fossil hominin not considered by some (e.g. Robinson and Mason, 1962) to have been capable of it. This would place one of the first tool-capable species some half a million years prior to the first evidence of the Oldowan Technological Complex, raising the question of whether the tool culture of this species would demonstrate an Oldowan- (or even Acheulean-) level understanding of fracture mechanics or something more primitive like that of the Lomekwian. Future investigations into the muscle recruitment patterns of other forms of tool manufacture may help answer this question.

10.2.2 *Australopithecus anamensis*

At present, there is no functional morphological research on whether *Au. anamensis* was capable of making or using stone tools, and this is due largely to the limited sample of specimens attributed to it. *Australopithecus anamensis* is known from Kanapoi and Allia Bay in Kenya and dated to 4.17 – 4.07 million years (Leakey et al., 1998). This is a very early date, and if *Au. anamensis* was indeed a tool-maker, it would push the date for tool-making behaviour some 800,000 years earlier than the oldest and most primitive technological complex, the Lomekwian (Harmand et al., 2015). In terms of morphology, the humeral specimen KNM-KP 271 is not notably different from modern humans except in its large size and robusticity, and bears many similarities to other *Australopithecus* humeral specimens (see Chapter 7, Section 7.2.4), such that it is difficult to distinguish KNM-KP 271 from specimens of *Au. afarensis* (Lague and Jungers, 1996, Lague, 2015). While it was not possible to include it in this analysis (the specimen was unavailable at the time of visiting the institution), there is a radius attributed to *Au. anamensis*, KNM-ER 20419 (Ward et al., 2001); this radius is relatively long and is interpreted by Ward et al. (2001) to indicate that *Au. anamensis* maintained ape-like limb proportions, similar again to *Au. afarensis*. The Kanapoi hypodigm also includes two manual specimens including a capitate (KNM-KP 31724) and a proximal phalanx (KNM-KP 30503). The capitate is larger than the *Au. afarensis* capitates from Hadar or *Au. africanus* capitates from Sterkfontein, and maintains a laterally orientated facet for the second metacarpal that would not have permitted the kind of rotation inferred for later *Australopithecus* and early *Homo* (Leakey et al., 1998). The proximal phalanx appears similarly large compared to that of Hadar *Au. afarensis*, with pronounced phalangeal curvature and attachments for the flexor

musculature of the hand (Ward et al., 2001). Overall, the picture of *Au. anamensis* is of a markedly ape-like fossil hominin with primitive limb proportions indicative of an upper limb used predominantly in support during arboreal locomotion or other climbing behaviours. The morphology of the capitate articulations suggests that *Au. anamensis* would not have been able to cup the hands such as would be required by forceful precision grips and therefore tool behaviours (see Chapter 3, Section 3.3.1). Similarly, considering that phalangeal curvature is strongly influenced by mechanical loading and function (Richmond, 1998, Richmond, 2003), the curvature of the KNM-KP 30503 phalanx is suggestive of a significant climbing component in the locomotor repertoire. While the morphological evidence is limited, it is unlikely then that *Au. anamensis* was making stone tools, despite having the enthesal development that might place in among the toolmaking candidates.

10.2.3 *Paranthropus robustus*

Fortunately, evidence of tool manufacture and use is somewhat less equivocal (though far from certain) in *Paranthropus robustus*. Swartkrans and Drimolen, like Sterkfontein, preserve ample evidence of tool manufacture and use in the form of stone (at Swartkrans: Kuman, 1998, Kuman and Clarke, 2000) and bone tools (at both Swartkrans and Drimolen: Backwell and d'Errico, 2008, Backwell and d'Errico, 2001, Brain, 1970, Brain et al., 1988, Clarke et al., 1970, Robinson, 1959, d'Errico and Backwell, 2009, d'Errico and Backwell, 2003, d'Errico et al., 2001), though the associations between fossil hominin species and the artefacts remains tenuous (Kuman and Clarke, 2000). The Swartkrans bone tools derive from Members 1-3 and date from 1.8-1.0 million years (Brain, 1993); the Drimolen bone tools have been dated to ca 1.5-2.0 million years (Backwell and d'Errico, 2008); and the Sterkfontein Member 5 stone

and single bone tool, as mentioned earlier, have been dated to 1.40-1.07 million years (Herries and Shaw, 2011). At all three sites, the co-occurrence of *Homo* and *Paranthropus robustus* is well-established, though the abundant remains of *Paranthropus* from Drimolen have led Backwell and d'Errico (2008) to conclude that *Paranthropus robustus* was the species which made and used the Drimolen bone tools. Similarly, the majority of hominin material from Swartkrans is attributed to *P. robustus* (Keyser et al., 2000, Brain, 1993), potentially implicating that species as also the maker of the Swartkrans bone tools. Candidates for the maker of the Sterkfontein tools (bone and stone alike) are less clear. Given that Drimolen is the only site where stone tools have not been found (two presumed stone artefacts have been found but their status as tools is uncertain; Backwell and d'Errico, 2008), and *P. robustus* remains comprise the preponderance of fossil hominin material from the same site, it is possible that bone tools there at least can be accredited to *P. robustus*.

But what about morphology? The manual remains attributed to *P. robustus* from Swartkrans Member 1 – including a pollical metacarpal, a complete pollical distal phalanx, and an assortment of proximal, intermediate and distal phalanges – do not appear indicate regular climbing or suspensory behaviours in the locomotor repertoire of this species (Susman, 1988a, Susman, 1988b); Susman (1988a) interpreted the Swartkrans manual remains attributed to *P. robustus* as largely human-like with well-developed thumb musculature, indicative of the ability to bring the thumb into opposition with the fingers and forceful precision gripping respectively (see Chapter 3, Section 3.3.1). The distal pollical phalanx is broad and flat much like OH 7 (Napier, 1962b) with an expanded apical tuft. The functional implications of this are great, as it implies buttressing for a similarly fleshy finger pad. The phalanges themselves are short and straight (Susman, 1988a), indicating that climbing was unlikely to have been a

prominent part of their behavioural ecology, and differentiating *P. robustus* from other australopiths from South Africa (*Au. afarensis*, *Au. sediba*; see Chapter 3, Section 3.4.1). In Susman's (1988a) view, these features indicated enhanced ability for precision grip but a limited potential for power grasping ability. As mentioned previously, like other authors (see Chapter 3; Hamrick and Inouye, 1995, Marzke, 1997) I have been sceptical of Susman's interpretation (see Chapter 3), and the species attribution of the Swartkrans manual material have also been called into question (Trinkaus and Long, 1990).

The results of the present analyses, however, suggest that *P. robustus* may have indeed been making stone tools, if the Swartkrans manual remains do indeed belong to *P. robustus*: the enthesal complexity analysis, manual morphology, and archaeological evidence may collectively support the interpretation of *P. robustus* as at least one of the manufacturers of the Swartkrans and Sterkfontein Oldowan stone tools. (If the manual remains represent *Homo* instead, as has been suggested by others (e.g. Trinkaus and Long, 1990), the evidence would then implicate *Homo* sp. rather than *Paranthropus* as the probable manufacturer of the Swartkrans and Sterkfontein stone tools). Given the presence of bone tools at Drimolen and the absence of any other fossil hominin taxa aside from *P. robustus* at this site, at the very least it is highly likely that *P. robustus* was using bone as a tool in activities like foraging in termite mounds, extracting tubers, and processing fruits (d'Errico and Backwell, 2009) at both Drimolen and Swartkrans, though this does not preclude stone tool behaviours. How muscle recruitment patterns differ in these behaviours from Oldowan stone tool manufacture remains a question to be answered.

10.2.4 *Homo habilis/Homo aff. habilis*

This section discusses the material attributed to *Homo habilis* and *Homo aff. habilis* collectively, as the results of the fractal analyses indicate that they are not significantly different from one another, despite the *H. aff. habilis* material having higher overall *D*-values. Of the specimens included in this study, the specimen attributed to *H. habilis* is the OH 48 clavicle from Bed I, Olduvai Gorge in Tanzania (Leakey et al., 1964a), and the specimens attributed to *H. aff. habilis* are SK 24600 and SK 24601 from Swartkrans in South Africa (Susman et al., 2001, Lague, 2015). SK 24600 and SK 24601 are of particular interest because they derive from Swartkrans Member 1, placing them at 1.8 million years (Grine, 1988), and were initially described by (Susman et al., 2001) as belonging to *P. robustus*. The OH 48 clavicle similarly dates to 1.8 million years (Wood, 1974). Insofar as taxonomic debates are a concern, this analysis did not find any significant differences between the *H. habilis*, *H. aff. habilis*, or *P. robustus* material, indicating that there is no enthesal morphology basis for differentiating these species. While Lague (2015) referred the Swartkrans specimens to *H. aff. habilis* in his analysis of humeral diaphyseal form, his analysis did not refute the hypothesis (Grine et al., 1993, Grine et al., 2009) that the South African material characterises a species not represented in the east African material. Curnoe (2010) has referred the Swartkrans *Homo* material to his species *Homo gautengensis*, of which the Sterkfontein Member 5 specimen STW 53 (see above) is the type specimen. The assumption of conspecificity for the South African and east African material on this basis is not well supported, especially given the recent discovery of a new *Homo* species, *Homo naledi*, in close geographic proximity to the Swartkrans site, although its date is so far unclear. The inclusion of *H. naledi* in future expansions of the present study may help improve the

resolution of the enthesal complexity analyses at the species level (as would the inclusion of *H. naledi* in further studies of humeral diaphyseal cross-sectional shape).

While the enthesal complexity evidence presented here suggests that *H. habilis* may have been a tool-maker, other lines of morphological evidence speak strongly to *H. habilis* having been a proficient and habitual climber. The shoulder, as represented by OH 48 and KNM-ER 3735 (not included in this study because it is too poorly preserved), indicates a shoulder positioned high on the thorax like that of extant arboreal apes, and therefore overarm suspensory behaviours being an important locomotor strategy (Napier, 1965a, Oxnard, 1969a, Leakey et al., 1989). The manual remains attributed to *H. habilis* (but see Chapter 3, Section 3.4.4 for a discussion of the taxonomic allocation of these hand bones) tell a similar story: the articular facet for the first metacarpal on the trapezium of OH 7 is flat relative to modern humans, and is very different from the markedly curved morphology exhibited by chimpanzees and *Au. afarensis* (Marzke et al., 2002, cited in Marzke, 2013). This feature has been interpreted by Marzke (2013) as characterising a hand with reduced stability in forceful pinch grips, particularly between the first and second digits. The articular facet of the second metacarpal similarly would not have facilitated axial rotation of the second digit such as is required for securely cupping the hand around objects and conforming the palm to irregular shapes (such as a hammerstone; Napier, 1962b). In this regard, the hand of *H. habilis* is primitive compared to australopith specimens such as *Au. africanus* or *Au. afarensis*, both of which species appear more human-like in their configuration (Tocheri et al., 2003). The pollical distal phalanx of OH 7 may or may not exhibit an expanded apical tuft similar to modern humans (Napier, 1962b), though the functional significance of this is unclear (Shrewsbury et al., 2003) and the fossil may have been a

misidentified hallucal distal phalanx (Susman and Creel, 1979). In terms of the fingers, the intermediate phalanges associated with OH 7 are markedly curved and robust, features that are considered to be consistent with climbing in *H. habilis* (Moyà-Solà et al., 2008, Napier, 1962b, Susman and Creel, 1979). Susman and Stern (1982) argued strongly that the robusticity and phenotypic plasticity of the bones reflect actual arboreal behaviour rather than primitive retentions, and Ruff (2009) similarly concluded that *H. habilis* maintained a significant component of arboreal behaviour in their locomotor repertoire. This accords with the relatively long upper limb exhibited by OH 62 (Johanson et al., 1987), but contradicts the enthesal complexity data if these are indeed detecting tool manufacture behaviours.

Collectively, the balance of morphological evidence suggests that the hand and upper limb of *H. habilis* represent morphological commitment to climbing behaviours (Susman and Creel, 1979, Susman and Stern, 1982, Susman and Stern, 1979, Tocheri et al., 2003). This is a somewhat startling contradiction given that *H. habilis* a) is contemporaneous with some of the first discovered stone tools (Leakey, 1971a); b) has historically been considered to be their manufacturer (Leakey et al., 1964a), despite not being directly associated with the tools themselves and despite the contemporaneous presence of *Paranthropus boisei* remains at Olduvai (Leakey et al., 1964a); and c) would appear to maintain patterns of enthesal development potentially indicative of tool behaviours. In fact, Leakey et al. (1964a) attributed the manufacture of the Bed I Oldowan stone tools purely on inferences about cognitive complexity from the cranial capacity of *H. habilis*: *H. habilis* had a larger brain than *P. boisei* therefore, according to Leakey et al. (1964a), it and not *P. boisei* made the Olduvai stone tools.

The picture is further complicated by the discovery of skeletal material and earlier stone tools from the Hata Member of the Bouri Formation and Gona, both in Ethiopia and dated to 2.6 and 2.5 million years (Asfaw et al., 1999, de Heinzelin et al., 1999, Semaw et al., 1997, Semaw et al., 2003). While the origin of *Homo cf. habilis* has been pushed back to 2.34 Ma by the discovery of a maxillary fragment from Hadar in Ethiopia (Kimbel et al., 1997, Kimbel et al., 1996), cut marks and percussion scars have been found on the zooarchaeological material discovered at Bouri Formation in proximity to fossil remains attributed *Australopithecus garhi*, a small-brained australopith and the only taxon presently recognised at Bouri (Asfaw et al., 1999; de Heinzelin et al., 1999). Even so, if *Au. garhi* was indeed making the Bouri stone tools, no tools were found with the cut-marked bone and they do not occur in close association with the *Au. garhi* remains. At the very least, the implication of the Bouri finds and others (e.g. McPherron et al. (2010) for a discussion of cut-marked bone from 3.4 million years ago: but see Domínguez-Rodrigo et al. (2011)) is that cranial capacity is likely a poor indicator of cultural complexity in the case of stone tool manufacture.

The archaeological evidence for stone tool manufacture in the case of *H. habilis* then is unclear. The upper limb and hand of *H. habilis* signify a creature committed to a mostly arboreal lifestyle rather than manipulation or tool manufacture. While the enthesal data place *H. habilis* as one of the more fractally complex species in terms of their muscle attachment sites, and this pattern mirrors those muscles highly recruited by stone tool manufacture, the morphological evidence suggests that arboreality was an important locomotor strategy in this species, and it is difficult to conclude with any certainty whether the pattern being observed in the enthesal data is truly the result of tool manufacture or of a more generalised pattern of upper limb use.

10.2.5 *Homo ergaster*

Homo ergaster is considered to be a very strong candidate for one of the first stone tool manufacturers. Its appearance at approximately 1.9-1.5 million years ago marked a period of technocultural transition between the Oldowan and the Acheulean technological complexes characterised by the intentional bifacial modification of large core tools (Roche et al., 2009). This arrival of *H. ergaster* in the fossil record also signalled an expansion of the numbers of stone tool sites, particularly in the east African Rift Valley, after 2.0-1.9 million years ago. *H. ergaster* has been associated with Acheulean stone tools at both Kokiselei, west of Lake Turkana in Kenya, and the Konso Formation in Ethiopia (Beyene et al., 2013, Lepre et al., 2011); the Acheulean represents a technological advance over the Oldowan. Linking tool use in *H. ergaster* with the archaeological record suffers from the same difficulties as any other fossil hominin: while the tools and the fossils are contemporaneous with one another, rarely are they found in strong association. This is compounded in *H. ergaster*, which is considered to be the first fossil species to move out of Africa and yet the oldest non-African fossil sites contain only Oldowan stone tools (Gabunia et al., 2000, de Lumley et al., 2005, Swisher et al., 1994). Despite this, the overlapping geographic and temporal origins for both the species and the Acheulean tool complex (Klein, 2009), the increase in cranial capacity signified by *H. ergaster*, and the concomitant extinction of many other fossil hominin taxa, including other species of *Homo* (Spoor et al., 2007), all link the development of the Acheulean with the arrival of *H. ergaster*.

Morphologically, *H. ergaster* – while not fully modern – is a committed biped with an enhanced ability for fine manual dexterity and powerful precision grasping. The shoulders of KNM-WT 15000 and the related Dmanisi specimens are characterised by a

human-like degree of sigmoid curvature (Voisin, 2008, Larson, 2007, 2013, Jashashvili, 2005), but they remain relatively short and somewhat inferiorly inflected at their lateral extremity, evincing a shoulder that is situated higher on the thorax like *Pan* (Voisin, 2006a, Larson, 2013, Voisin, 2006b). The glenoid fossa no longer faces cranially, the scapular spine is orientated more horizontally, and the proportions of the supra- and infraspinous fossae approach a more human-like condition (Green and Alemseged, 2012). Humeral morphology on balance appears to be quite modern, although *H. ergaster* maintains low humeral torsion, making this species more similar to other australopith humeri in this regard (Lordkipanidze et al., 2007, Larson, 2007, Walker and Leakey, 1993). Thus, *H. ergaster* maintained a more australopith-like than human-like upper limb morphology (Stern and Susman, 1983) with, however, a fairly modern-looking scapula which sat on a more barrel-shaped rib cage than earlier fossil hominins (Jellema et al., 1993). Moving distally, the only manual remains that might be attributed to *H. ergaster* are the Dmanisi distal manual phalanges (D3480 and D2679) (though, of course, the taxonomic status of the fossil hominin remains from this site remain an open question; Lordkipanidze et al., 2007, Dembo et al., 2015), and a single third metacarpal, KNM-WT 51260 recovered from sediments dating to 1.42 million years in Kenya (Ward et al., 2014). KNM-WT 512560 preserves a styloid process which is less salient and a capitate-second metacarpal joint which is less obliquely orientated than that seen in Neandertals.

The association of this species with complex forms of tool manufacture places this morphology in the context of increased reliance on sophisticated manipulatory behaviours. While it is folly to link a single morphological feature to a particular behaviour, the basically modern appearance of KNM-WT 51260 suggests that *H.*

ergaster already possessed the complex of features characteristic of modern human hands. The shoulder had undergone one of the first significant structural reorganisations indicative of increasing morphological commitment to tool behaviours. Thus there are strong indications, both morphological and behavioural, that *H ergaster* was committed to sophisticated forms of stone tool manufacture and use, and this conclusion is supported by the enthesal data presented here.

10.3 Interpretation of the Results: Limitations and Caveats

Enthesal development might be one of the most sensitive markers for comparing species (Drapeau, 2008b), but it is difficult to say with confidence whether differences in enthesal complexity between species of fossil hominin reflect specific and habitual patterns of muscle recruitment (that is, activities) or species-level differences in the way that bone reacts to particular types of stress exerted across the enthesis (e.g. different types of muscle contraction). While there does appear to be some (non-statistical) correlation between the muscle attachments with greatest fractal complexity and those muscles which are more highly recruited during stone tool manufacture, the presence of fossil hominins with strong evidence of commitment to climbing behaviours – at least one of which predates the earliest evidence for stone tool manufacture by 800,000 years and the Oldowan by nearly 1.5 million years – would indicate that the pattern of behaviour being detected is unlikely to be solely tool manufacture.

The nature of the skeletal evidence must be considered: *Au. africanus* is very well-represented in the sample compared to species like *H. ergaster*, for instance. *Homo ergaster* – almost certainly a dedicated tool-maker and tool-user – may appear less complex than other species simply because there is not enough evidence to provide a truly representative mean *D*-value for the species for a given enthesis, especially when

compared to species such as *Au. africanus* for which appropriate skeletal evidence is relatively more abundant. In addition to sample sizes, not every enthesis was represented for every species due to preservation or the availability of the specimens (none of the Dmanisi *H. cf. ergaster* specimens were included in the analysis as access to this material is highly restricted); in the case of *H. ergaster*, proximal humeral entheses were not represented at all. Rather than detecting a signal for tool manufacture, the fractal dimension values may better reflect a more generalised pattern of robusticity attributable to other factors, such as climbing or specialised feeding behaviours, perhaps like digging in termite mounds as has been suggested for *P. robustus* (Backwell and d'Errico, 2001, d'Errico et al., 2001, Backwell and d'Errico, 2008, d'Errico and Backwell, 2009). This would fit with recent work by Williams-Hatala et al. (2016) on hand musculature and enthesal morphology, which found no correlation between behaviourally-influenced aspects of muscle architecture and enthesal morphology in modern human hands.

It is possible that the presence of at least three species with some of the most compelling skeletal and archaeological evidence for tool manufacture and use – *H. ergaster*, *Au. africanus*, and *P. robustus* – at the top of the list of candidate tool-makers appears to be coincidental, but it may yet be telling: enthesal complexity studies may not be able to differentiate specific behaviours very well at the enthesis-level, but this does not strictly mean that there is not a signal to detect. This study suffered from limitations resulting principally from difficulty accessing specimens and fossil preservation, and as such there a number of ways in which it could be improved. In order to control for as many variables as possible, the exclusion criteria for fossil specimens were very conservative, and this meant that many of the more complete fossil hominin upper limb specimens were excluded from the analysis; this limited sample

sizes (e.g. KNM-WT 15000). This issue was compounded when certain specimens were not available for analysis. The sample size could be greatly improved by the inclusion of, for instance, the *Au. garhi*, *Homo naledi*, *Homo floresiensis*, and Dmanisi material. Digital collection procedures such as 3D laser surface scans would have been a great benefit to the study. Laser scanning would have afforded greater accuracy when computing *D*-values for entheses and has the advantage of limiting the handling and exposure of the fossils to metal instruments, ensuring that no damage occurs to the specimen. It also was not possible to consider the effects of laterality in this project. In order to preserve decent sample sizes, both left and right side were included in the analysis and it is unclear at this point how bilateral asymmetry would affect the results. Future expansions on this project would benefit from a consideration of laterality and handedness as factors in the analysis, as well as higher resolution collection procedures and an expanded sample.

10.4 Summary

While analysis of enthesal complexity in the upper limb did indeed identify species with strong ancillary evidence for tool manufacture and use, the inclusion of *Au. anamensis*, a species dated 1.5 million years earlier than the first Oldowan stone tools and 800,000 years earlier than the earliest evidence for any stone tool behaviour, suggests that the utility of enthesal complexity studies to detect stone tool behaviours in the fossil record is limited. Comparison of the enthesal complexity results with multiple lines of evidence drawn from morphology and the archaeological record were inconclusive, despite the highly significant results presented in Chapter 9.

CHAPTER 11: CONCLUSION

11.1 Summary of Findings

This investigation asked a number of basic questions about the biomechanics of the hominin upper limb that have yet to be explored in any detail in the literature:

- What is the role of the shoulder and upper arm muscles in stone tool behaviours?
- What are the skeletal markers of stone tool manufacture at the shoulder girdle, if any?
- Can these markers be readily identified in fossil hominins?
- What does this reveal about the functional morphology of the shoulder in fossil hominins?

The aim of this project therefore was to provide one of the first complete biomechanical reports of the upper limb during basic stone tool manufacture behaviours with a view to identifying which the shoulder and elbow muscles strongly and repeatedly recruited during stone knapping. These data were then used to test whether patterns of development at muscle and ligament attachment sites on bone (that is, entheses) may be a means by which to identify tool manufacture behaviours in fossil populations, as the makers of the first stone tools have yet to be identified.

This project was divided into two parts. The first involved detailed biomechanical assessment of the upper limb during Oldowan stone tool manufacture; to that end, I investigated upper limb kinetics and kinematics, in addition to the normal activation patterns of 15 shoulder and elbow muscles using intramuscular and surface

electromyography (EMG) in 16 novices during Oldowan stone knapping. The results demonstrate that the motion of the knapping arm in stone tool manufacture is a dynamic three-dimensional flexion-extension motion. The shoulder and elbow musculature is active primarily to produce acceleration of the arm segments to generate the strike force. In line with previous studies, the segments of the upper limb moved in a coordinated proximal-to-distal sequence. This motion originated with the shoulder proximally in the up-swing phase and was transmitted through to the distal limb segments (the wrist and hammerstone) in the down-swing phase. The up-swing phase in this way can be characterised as a “cocking” phase, as it is in this phase that the arm and shoulder are prepared for forceful extension of the arm and movement of the hammerstone toward the objective tool stone. The down-swing phase is the phase in which greatest muscle recruitment occurs in order to generate torque and accelerate the hammerstone toward the tool stone, and to that end the principle strike force-generating muscles of the down-swing are *Mm. latissimus dorsi*, *teres major*, and *triceps brachii*. *Pectoralis major* works during this phase to decelerate the rapidly extending arm to improve strike accuracy. The rotator cuff (*supraspinatus*, *infraspinatus*, and *subscapularis*) works in a direct-specific manner to dynamically stabilise the humeral head against flexion and extension torques during the knapping strike. Contra to previous studies, the wrist flexor and extensor musculature, rather than producing specific motion of the wrist, appears to be highly recruited to stabilise the elbow and wrist against reactive forces from hammerstone impact.

The second part of this study examined enthesal complexity in the upper limbs of 10 species of fossil hominins in order to determine whether any patterns of complexity might be observed that mirror the muscles most highly recruited by basic stone

knapping (as revealed by the EMG analysis). If so, then it may be possible to use this as a means by which to identify the first tool-makers. The ability of the manufacturers of the Oldowan stone tools to effectively and, presumably, efficiently flake basalt cobbles and other materials (as indicated by the archaeological record) strongly suggests that these fossil hominins were capable of achieving speed, kinematic, kinetic, and muscle recruitment values similar to those documented in this study in modern humans. The fractal complexity data indicate that the muscles with high degrees of complexity without significant differences among them were supraspinatus, infraspinatus, subscapularis, deltoideus, latissimus dorsi, brachialis, triceps brachii, and the muscles of the lateral epicondylar ridge and medial epicondylar ridge; these entheses were all of similar degrees of complexity. When compared to the EMG data, the entheses with greatest fractal complexity scores do indeed parallel the muscles with greatest levels of recruitment in Oldowan stone knapping. Based on analysis of species-level differences in predicted mean *D*-values for these entheses, the species identified as potential members of the tool-making guild are *Au. africanus*, *Au. anamensis*, *P. robustus*, *H. habilis*/*Homo* aff. *habilis*, and *H. ergaster*.

While the correlation of enthesal complexity with muscle recruitment data in these species is highly suggestive, the results should nonetheless be viewed with caution. *Australopithecus anamensis* and *Homo habilis* are two fossil hominins for which there is significant morphological evidence suggestive of commitment to climbing behaviours. *Homo habilis* has historically been linked with the first stone tool assemblages at Olduvai dated to approximately 1.8-1.7 million years based on its enlarged brain and assumptions about how cognitive capacities relate to encephalisation quotients (see Chapter 10), but aside from contemporaneity there is very little

convincing evidence linking this species, rather than the contemporaneous *Paranthropus boisei*, with stone tool manufacture. *Australopithecus anamensis* also exhibits morphological commitment to arboreality and predates the earliest evidence for stone tool manufacture (the Lomekwian) by 800,000 years and the Oldowan by nearly 1.5 million years. In addition to the nature of preservation in the fossil record, this would indicate that the pattern or behaviour being detected by the enthesal complexity data is unlikely to be solely tool manufacture, if indeed its detecting tool manufacture at all. Despite this, the presence of at least three probable tool-makers in the list of candidate species as identified by the complexity analysis is compelling. If there is indeed a specific functional signal to detect, significant improvements must be made in order to improve the resolution and sensitivity of enthesal complexity studies such as this in the future.

11.2 Directions for Future Study

A number of suggestions can be made for directions for future study both in this project and in similar projects on enthesal complexity in fossil hominins. In addition to the specific improvements suggested in Chapter 10, Section 10.4, for this project (increased sample size through inclusion of previously unavailable material and taxa, digital collection procedures etc.), studies such as these would benefit from more detailed assessments of the diagnostic sensitivity of enthesal complexity and its relationship to handedness and laterality. The addition of extant great ape enthesal data would also be beneficial for use as reference populations with known locomotor and tool behaviour, and this could be extended to a comparison of extant stone tool using species such as West African chimpanzees (see Chapter 3) with other populations. Unanswered questions include: do the entheses of upper limb muscles differ significantly by side in

modern humans? What about in fossil hominins? Can this be used to indicate handedness in fossil taxa? It would also be fruitful to explore the relationship of different morphological configurations at the shoulder with patterns of muscle recruitment during stone knapping through biomechanical modelling. Are the muscle recruitment patterns of fossil hominins likely to differ from those of modern humans during stone knapping as a result of differences in gross configuration of the shoulder and upper limb? Do differences in skeletal morphology significantly alter muscle recruitment strategies? And finally, do muscle recruitment patterns differ between technological complexes in response to the different technical requirements of their production? How does expertise factor into this, especially for the muscles of the shoulder and elbow?

The evidence presented in this thesis indicates that the question of the first tool-makers is likely solvable. It is hoped that this study and discoveries in other disciplines will excite others to continue research and inquiries into the issues surrounding biomechanics of the upper limb in stone tool manufacture and the morphological indicators of tool behaviours.

LIST OF REFERENCES

- AIELLO, L. & DEAN, C. 2002a. CHAPTER SEVENTEEN - THE HOMINOID ARM. In: DEAN, L. A. (ed.) *An Introduction to Human Evolutionary Anatomy*. San Diego: Academic Press.
- AIELLO, L. & DEAN, C. 2002b. CHAPTER SIXTEEN - BONES, MUSCLES AND MOVEMENTS OF THE UPPER LIMB. In: DEAN, L. A. (ed.) *An Introduction to Human Evolutionary Anatomy*. San Diego: Academic Press.
- AIELLO, L. C., WOOD, B., KEY, C. & LEWIS, M. 1999. Morphological and taxonomic affinities of the Olduvai ulna (OH 36). *American Journal of Physical Anthropology*, 109, 89-110.
- AL-OUMAOUI, I., JIMÉNEZ-BROBEIL, S. & DU SOUICH, P. 2004. Markers of activity patterns in some populations of the Iberian Peninsula. *International Journal of Osteoarchaeology*, 14, 343-359.
- ALBA, D. M., MOYÀ-SOLÀ, S. & KÖHLER, M. 2003. Morphological affinities of the *Australopithecus afarensis* hand on the basis of manual proportions and relative thumb length. *Journal of Human Evolution*, 44, 225-254.
- ALCOCK, J. 1972. The Evolution of the Use of Tools by Feeding Animals. *Evolution*, 26, 464-473.
- ALEMSEGED, Z., COPPENS, Y. & GERAADS, D. 2002. Hominid cranium from Omo: Description and taxonomy of Omo-323-1976-896. *American Journal of Physical Anthropology*, 117, 103-112.
- ALEMSEGED, Z., SPOOR, F., KIMBEL, W. H., BOBE, R., GERAADS, D., REED, D. & WYNN, J. G. 2006. A juvenile early hominin skeleton from Dikika, Ethiopia. *Nature*, 443, 296-301.
- ALMÉCIJA, S. & ALBA, D. M. 2014. On manual proportions and pad-to-pad precision grasping in *Australopithecus afarensis*. *Journal of Human Evolution*, 73, 88-92.
- ALMÉCIJA, S., MOYÀ-SOLÀ, S. & ALBA, D. M. 2010. Early origin for human-like precision grasping: A comparative study of pollical distal phalanges in fossil hominins. *PLoS ONE*, 5, 1-10.
- ALVES-CARDOSO, F. & HENDERSON, C. Y. 2010. Enthesopathy formation in the humerus: Data from known age-at-death and known occupation skeletal collections. *American Journal of Physical Anthropology*, 141, 550-560.
- AMIS, A. A., DOWSON, D. & WRIGHT, V. 1979. Muscle strengths and musculoskeletal geometry of the upper limb. *Journal of Engineering in Medicine*, 8, 41-48.
- ANDERSON, D., NORDHEIM, E., BOESCH, C. & MOERMOND, T. 2002. Factors influencing fission-fusion grouping in chimpanzees in the Tai National Park, Cote d'Ivoire. In: BOESCH, C., HOHMANN, G. & MARCHANT, L. (eds.) *Behavioural Diversity in Chimpanzees and Bonobos*. Cambridge, UK: Cambridge University Press.
- ANDREWS, P. 1985. Family group systematics and evolution among Catarrhine primates. In: DELSON, E. (ed.) *Ancestors: The Hard Evidence*. New York: Alan R. Liss.
- ARIAS-MARTORELL, J., POTAU, J. M., BELLO-HELLEGOUARCH, G. & PÉREZ-PÉREZ, A. 2015. Like father, like son: Assessment of the morphological affinities of A.L. 288-1 (*A. afarensis*), Sts 7 (*A. africanus*) and Omo 119-73-

- 2718 (*Australopithecus sp.*) through a three-dimensional shape analysis of the shoulder joint. *PLoS ONE*, 10, 1-28.
- ARSUAGA, J. L., MARTINEZ, I., GARCIA, A. & LORENZO, C. 1997. The Sima de los Huesos crania (Sierra de Atapuerca, Spain): A comparative study. *Journal of Human Evolution*, 33, 219-281.
- ASFAW, B., WHITE, T., LOVEJOY, O., LATIMER, B., SIMPSON, S. & SUWA, G. 1999. *Australopithecus garhi*: A new species of early hominid from Ethiopia. *Science*, 284, 629-635.
- BACKWELL, L. & D'ERRICO, F. 2008. Early hominid bone tools from Drimolen, South Africa. *Journal of Archaeological Science*, 35, 2880-2894.
- BACKWELL, L. R. & D'ERRICO, F. 2001. Evidence of termite foraging by Swartkrans early hominids. *Proceedings of the National Academy of Sciences*, 98, 1358-1363.
- BARAK, M. M., LIEBERMAN, D. E. & HUBLIN, J.-J. 2011. A Wolff in sheep's clothing: Trabecular bone adaptation in response to changes in joint loading orientation. *Bone*, 49, 1141-1151.
- BASMAJIAN, J. V. & DELUCA, C. J. 1985. *Muscles Alive: Their functions revealed by electromyography*, Baltimore, Williams & Wilkins.
- BEATTY, H. 1951. A note on the behavior of the chimpanzee. *Journal of Mammalogy*, 32, 118.
- BECK, B. B. 1980. *Animal tool behaviour: The use and manufacture of tools by animals*, New York, N.Y., Garland STPM Publishing.
- BENJAMIN, M., EVANS, E. J. & COPP, L. 1986. The histology of tendon attachments to bone in man. *Journal of Anatomy*, 149, 89-100.
- BENJAMIN, M., KUMAI, T., MILZ, S., BOSZCZYK, B. M., BOSZCZYK, A. A. & RALPHS, J. R. 2002. The skeletal attachment of tendons—tendon 'entheses'. *Comparative Biochemistry and Physiology Part A: Molecular & Integrative Physiology*, 133, 931-945.
- BENJAMIN, M. & MCGONAGLE, D. 2001. The anatomical basis for disease localisation in seronegative spondyloarthropathy at entheses and related sites. *Journal of Anatomy*, 199, 503-526.
- BENJAMIN, M. & MCGONAGLE, D. 2009. Entheses: Tendon and ligament attachment sites. *Scandinavian Journal of Medicine & Science in Sports*, 19, 520-527.
- BENJAMIN, M. & RALPHS, J. R. 1995. Functional and developmental anatomy of tendons and ligaments. In: GORDON, S. L., BLAIR, S. J. & FINE, L. J. (eds.) *Repetitive Motion Disorders of the Upper Extremity*. Rosemont: American Academy of Orthopaedic Surgeons.
- BENJAMIN, M. & RALPHS, J. R. 1998. Fibrocartilage in tendons and ligaments — an adaptation to compressive load. *Journal of Anatomy*, 193, 481-494.
- BENJAMIN, M., TOUMI, H., RALPHS, J. R., BYDDER, G., BEST, T. M. & MILZ, S. 2006. Where tendons and ligaments meet bone: Attachment sites ('entheses') in relation to exercise and/or mechanical load. *Journal of Anatomy*, 208, 471-90.
- BERGER, L. R. 1994. *Functional Morphology of the Hominoid Shoulder, Past and Present*. Doctor of Philosophy, University of Witwatersrand.
- BERGER, L. R., DE RUITER, D. J., CHURCHILL, S. E., SCHMID, P., CARLSON, K. J., DIRKS, P. H. G. M. & KIBII, J. M. 2010. *Australopithecus sediba*: A new species of *Homo*-like Australopithecine from South Africa. *Science*, 328, 195-204.

- BERGER, L. R., HAWKS, J., DE RUITER, D. J., CHURCHILL, S. E., SCHMID, P., WILLIAMS, S. A., DESILVA, J. M., KIVELL, T. L., SKINNER, M. M., MUSIBA, C. M., CAMERON, N., HOLLIDAY, T. W., HARCOURT-SMITH, W., ACKERMANN, R. R., BASTIR, M., BOGIN, B., BOLTER, D. R., BROPHY, J. K., COFRAN, Z. D., CONGDON, K. A., DEANE, A. S., DELEZENE, L. K., DEMBO, M., DRAPEAU, M. S., ELLIOTT, M., FEUERRIEGEL, E. M., GARCIA-MARTINEZ, D., GARVIN, H. M., GREEN, D. J., GURTOV, A., IRISH, J. D., KRUGER, A., LAIRD, M. F., MARCHI, D., MEYER, M. R., NALLA, S., NEGASH, E. W., ORR, C. M., RADOVCIC, D., SCOTT, J. E., SCHROEDER, L., THROCKMORTON, Z., TOCHERI, M. W., VANSICKLE, C., WALKER, C. S., WEI, P. & ZIPFEL, B. 2015. *Homo naledi*, a new species of the genus *Homo* from the Dinaledi Chamber, South Africa. *eLife*, 4, 1-35.
- BERGER, L. R., KEYSER, A. W. & TOBIAS, P. V. 1993. Gladysvale: First early hominid site discovered in South Africa since 1948. *American Journal of Physical Anthropology*, 92, 107-111.
- BERMÚDEZ DE CASTRO, J. M., ARSUAGA, J. L., CARBONELL, E., ROSAS, A., MARTÍNEZ, I. & MOSQUERA, M. 1997. A hominid from the Lower Pleistocene of Atapuerca, Spain: Possible ancestor to Neandertals and modern humans. *Science*, 276, 1392-1395.
- BESICOVITCH, A. S. 1929. On linear sets of points of fractional dimension. *Mathematische Annalen*, 101, 161-193.
- BEYENE, Y., KATOH, S., WOLDEGABRIEL, G., HART, W. K., UTO, K., SUDO, M., KONDO, M., HYODO, M., RENNE, P. R., SUWA, G. & ASFAW, B. 2013. The characteristics and chronology of the earliest Acheulean at Konso, Ethiopia. *Proceedings of the National Academy of Sciences*, 110, 1584-1591.
- BIERMANN, H. 1957. Die Knochenbildung im Bereich periosteal-diaphysärer Sehnen- und Bandansätze. *Zeitschrift für Zellforschung und mikroskopische Anatomie*, 46, 635-671.
- BIRO, D., INOUE-NAKAMURA, N., TONOOKA, R., YAMAKOSHI, G., SOUSA, C. & MATSUZAWA, T. 2003. Cultural innovation and transmission of tool use in wild chimpanzees: Evidence from field experiments. *Animal Cognition*, 6, 213-223.
- BIRO, D., SOUSA, C. & MATSUZAWA, T. 2006. Ontogeny and cultural propagation of tool use by wild chimpanzees at Bossou, Guinea: Case studies in nut cracking and leaf folding. In: MATSUZAWA, T., TOMONAGA, M. & TANAKA, M. (eds.) *Cognitive Development in Chimpanzees*. Springer Tokyo.
- BIRYUKOVA, E. V. & BRIL, B. 2008. Organization of goal-directed action at a high level of motor skill: The case of stone knapping in India. *Motor Control*, 12, 181-209.
- BIRYUKOVA, E. V., BRIL, B., DIETRICH, G., ROBY-BRAMI, A., KULIKOV, M. A. & MOLCHANOV, P. E. 2005. The organization of arm kinematic synergies: The case of stone-bead knapping in Khambhat. In: ROUX, V. & BRIL, B. (eds.) *Stone Knapping: The Necessary Conditions for a Uniquely Hominin Behaviour*. Cambridge, England: McDonald Institute for Archaeological Research.
- BIRYUKOVA, E. V., BRIL, B., FROLOV, A. A. & KOULIKOV, M. A. 2015. Movement kinematics as an index of the level of motor skill: The case of Indian craftsmen stone knapping. *Motor Control*, 19, 34-59.

- BLAND, Y. S. & ASHHURST, D. E. 1997. Fetal and postnatal development of the patella, patellar tendon and suprapatella in the rabbit; changes in the distribution of the fibrillar collagens. *Journal of Anatomy*, 190, 327-342.
- BLUMENSCHINE, R. J., MASAO, F. T., TACTIKOS, J. C. & EBERT, J. I. 2008. Effects of distance from stone source on landscape-scale variation in Oldowan artifact assemblages in the Paleo-Olduvai Basin, Tanzania. *Journal of Archaeological Science*, 35, 76-86.
- BLUMENSCHINE, R. J. & PETERS, C. R. 1998. Archaeological predictions for hominid land use in the Paleo-Olduvai Basin, Tanzania, during lowermost Bed II times. *Journal of Human Evolution*, 34, 565-607.
- BOESCH, C. & BOESCH-ACHERMANN, H. 2000. *The chimpanzees of the Tai forest: behavioural ecology and evolution*, Oxford University Press Oxford.
- BOESCH, C. & BOESCH, H. 1983. Optimisation of nut-cracking with natural hammers by wild chimpanzees. *Behaviour*, 83, 265-286.
- BOESCH, C. & BOESCH, H. 1990. Tool use and tool making in wild chimpanzees. *Folia Primatologica*, 54, 86-99.
- BOETTCHER, C. E., GINN, K. A. & CATHERS, I. 2008. Standard maximum isometric voluntary contraction tests for normalizing shoulder muscle EMG. *Journal of Orthopaedic Research*, 26, 1591-1597.
- BOULLE, E.-L. 2001. Osteological features associated with ankle hyperdorsiflexion. *International Journal of Osteoarchaeology*, 11, 345-349.
- BRAIN, C. K. 1970. New finds at the Swartkrans australopithecine site. *Nature*, 225, 1112-1119.
- BRAIN, C. K. 1993. *Swartkrans: A cave's chronicle of early man*, Transvaal Museum.
- BRAIN, C. K. 2007. Fifty years of fun with fossils: Some cave taphonomy-related ideas and concepts that emerged between 1953 and 2003. In: PICKERING, T. R., SCHICK, K. D. & TOTH, N. P. (eds.) *Breathing life into fossils: taphonomic studies in honor of C.K. (Bob) Brain*. Gosport: Stone Age Institute Press.
- BRAIN, C. K., CHURCHER, C. S., CLARK, J. D., GRINE, F. E., SHIPMAN, P., SUSMAN, R. L., TURNER, A. & WATSON, V. 1988. New evidence of early hominids, their culture and environment from the Swartkrans cave, South Africa. *South African Journal of Science*, 84, 828-835.
- BRAUN, D. R., HARRIS, J. W. K. & MAINA, D. N. 2009a. Oldowan raw material procurement and use: Evidence from the Koobi Fora Formation. *Archaeometry*, 51, 26-42.
- BRAUN, D. R., PLUMMER, T., FERRARO, J. V., DITCHFIELD, P. & BISHOP, L. C. 2009b. Raw material quality and Oldowan hominin toolstone preferences: Evidence from Kanjera South, Kenya. *Journal of Archaeological Science*, 36, 1605-1614.
- BRAUN, D. R., TACTIKOS, J. C., FERRARO, J. V. & HARRIS, J. W. K. 2005. Flake recovery rates and inferences of Oldowan hominin behavior: A response to Kimura 1999, 2002. *Journal of Human Evolution*, 48, 525-531.
- BRAUN, D. R., TACTIKOS, J. C., FERRARO, J. V. & HARRIS, J. W. K. 2006. Archaeological inference and Oldowan behavior. *Journal of Human Evolution*, 51, 106-108.
- BRICKLEY, M. & RACHEL, I. 2008. Chapter 3 - Background to bone biology and mineral metabolism. In: BRICKLEY, M. & RACHEL, I. (eds.) *The Bioarchaeology of Metabolic Bone Disease*. San Diego: Academic Press.

- BRIL, B., REIN, R., NONAKA, T., WENBAN-SMITH, F. & DIETRICH, G. 2010. The role of expertise in tool use: Skill differences in functional action adaptations to task constraints. *Journal of Experimental Psychology: Human Perception and Performance*, 36, 825-39.
- BRIL, B., ROUX, V. & DIETRICH, G. 2005. Stone knapping: Khambhat (India), a unique opportunity? In: ROUX, V. & BRIL, B. (eds.) *Stone Knapping: The Necessary Conditions for a Uniquely Hominin Behaviour*. Cambridge, England: McDonald Institute for Archaeological Research.
- BROOM, R. 1938. Further evidence on the structure of the South African Pleistocene anthropoids. *Nature*, 142, 897-899.
- BROOM, R., ROBINSON, J. T. & SCHEPERS, G. W. H. 1950. Sterkfontein ape-men *Plesianthropus*. *Transvaal Museum Memoires*, 4.
- BROOM, R. & SCHEPERS, G. W. H. 1946. The South African fossil ape men: The Australopithecinae. *Transvaal Museum Memoires*, 2, 1-272.
- BROWN, B., WALKER, A., WARD, C. V. & LEAKEY, R. E. 1993. New *Australopithecus boisei* calvaria from East Lake Turkana, Kenya. *American Journal of Physical Anthropology*, 91, 137-159.
- BROWN, F. H., MCDOUGALL, I. & GATHOGO, P. N. 2007. Age ranges of *Australopithecus* Species, Kenya, Ethiopia, and Tanzania. In: REED, K. E., FLEAGLE, J. & LEAKEY, R. (eds.) *The Paleobiology of Australopithecus*. London: Springer.
- BRUMM, A., AZIZ, F., VAN DEN BERGH, G. D., MORWOOD, M. J., MOORE, M. W., KURNIAWAN, I., HOBBS, D. R. & FULLAGAR, R. 2006. Early stone technology on Flores and its implications for *Homo floresiensis*. *Nature*, 441, 624-628.
- BUNN, H. T. 1983. Evidence of the diet and subsistence patterns of Plio-Pleistocene hominids at Koobi Fora, Kenya, and Olduvai Gorge, Tanzania. In: CLUTTON-BROCK, J. & GRIGSON, C. (eds.) *Animals and Archaeology: Hunters and Their Prey*. Oxford: BAR Publishing.
- BUNN, H. T. & KROLL, E. M. 1986. Systematic butchery by Plio/Pleistocene hominids at Olduvai Gorge, Tanzania [and Comments and Reply]. *Current Anthropology*, 27, 431-452.
- BUSH, M. E., LOVEJOY, C. O., JOHANSON, D. C. & COPPENS, Y. 1982. Hominid carpal, metacarpal, and phalangeal bones recovered from the Hadar formation: 1974-1977 collections. *American Journal of Physical Anthropology*, 57, 651-677.
- CAPASSO, L., KENNEDY, K. & WILCZAK, C. 1999. *Atlas of Occupational Markers on Human Remains*, Teramo, Edigrafital S.P.A.
- CARBONELL, E., BERMUDEZ DE CASTRO, J. M., PARES, J. M., PEREZ-GONZALEZ, A., CUENCA-BESCOS, G., OLLE, A., MOSQUERA, M., HUGUET, R., VAN DER MADE, J., ROSAS, A., SALA, R., VALLVERDU, J., GARCIA, N., GRANGER, D. E., MARTINON-TORRES, M., RODRIGUEZ, X. P., STOCK, G. M., VERGES, J. M., ALLUE, E., BURJACHS, F., CACERES, I., CANALS, A., BENITO, A., DIEZ, C., LOZANO, M., MATEOS, A., NAVAZO, M., RODRIGUEZ, J., ROSELL, J. & ARSUAGA, J. L. 2008. The first hominin of Europe. *Nature*, 452, 465-469.
- CARLSON, K. J., STOUT, D., JASHASHVILI, T., DE RUITER, D. J., TAFFOREAU, P., CARLSON, K. & BERGER, L. R. 2011. The endocast of MH1, *Australopithecus sediba*. *Science*, 333, 1402-1407.

- CARNEY, J., HILL, A., MILLER, J. A. & WALKER, A. 1971. Late australopithecine from Baringo District, Kenya. *Nature*, 230, 509-514.
- CARR, J. R. & WARDNER, J. B. 1987. Rock mass classification using fractal dimension. *The 28th U.S. Symposium on Rock Mechanics (USRMS), 29 June-1 July*. Tucson, Arizona: American Rock Mechanics Association.
- CARRETERO, J. M., ARSUAGA, J. L. & LORENZO, C. 1997. Clavicles, scapulae and humeri from the Sima de los Huesos site (Sierra de Atapuerca, Spain). *Journal of Human Evolution*, 33, 357-408.
- CARRETERO, J. M., LORENZO, C. & ARSUAGA, J. L. 1999. Axial and appendicular skeleton of *Homo antecessor*. *Journal of Human Evolution*, 37, 459-499.
- CASPARI, R. & LEE, S.-H. 2004. Older age becomes common late in human evolution. *Proceedings of the National Academy of Sciences of the United States of America*, 101, 10895-10900.
- CHAMAY, A. & TSCHANTZ, P. 1972. Mechanical influences in bone remodeling. Experimental research on Wolff's law. *Journal of Biomechanics*, 5, 173-180.
- CHAO, E. Y., OPGRANDE, J. D. & AXMEAR, F. E. 1976. Three-dimensional force analysis of finger joints in selected isometric hand functions. *Journal of Biomechanics*, 9, 387-396.
- CHAPMAN, N. E. M. 1997. Evidence for Spanish influence on activity induced musculoskeletal stress markers at Pecos Pueblo. *International Journal of Osteoarchaeology*, 7, 497-506.
- CHEN, X., MACICA, C., NASIRI, A., JUDEX, S. & BROADUS, A. E. 2007. Mechanical regulation of PTHrP expression in entheses. *Bone*, 41, 752-759.
- CHEN, X., MACICA, C. M., DREYER, B. E., HAMMOND, V. E., HENS, J. R., PHILBRICK, W. M. & BROADUS, A. E. 2006. Initial characterization of PTH-related protein gene-driven lacZ expression in the mouse. *Journal of Bone and Mineral Research*, 21, 113-123.
- CHEN, Y. M. & BOHRER, S. P. 1990. Coracoclavicular and coracoacromial ligament calcification and ossification. *Skeletal Radiology*, 19, 263-266.
- CHURCHILL, S. E. 1994. *Human Upper Body Evolution in the Eurasian Later Pleistocene*. Doctor of Philosophy, University of New Mexico.
- CHURCHILL, S. E. 1996. Particulate versus integrated evolution of the upper body in late Pleistocene humans: A test of two models. *American Journal of Physical Anthropology*, 100, 559-583.
- CHURCHILL, S. E. 2001. Hand morphology, manipulation, and tool use in Neandertals and early modern humans of the Near East. *Proceedings of the National Academy of Sciences*, 98, 2953-2955.
- CHURCHILL, S. E., HOLLIDAY, T. W., CARLSON, K. J., JASHASHVILI, T., MACIAS, M. E., MATHEWS, S., SPARLING, T. L., SCHMID, P., DE RUITER, D. J. & BERGER, L. R. 2013. The upper limb of *Australopithecus sediba*. *Science*, 340.
- CHURCHILL, S. E. & MORRIS, A. G. 1998. Muscle marking morphology and labour intensity in prehistoric Khoisan foragers. *International Journal of Osteoarchaeology*, 8, 390-411.
- CHURCHILL, S. E., PEARSON, O. M., GRINE, F. E., TRINKAUS, E. & HOLLIDAY, T. W. 1996. Morphological affinities of the proximal ulna from Klasies River main site: Archaic or modern? *Journal of Human Evolution*, 31, 213-237.

- CHURCHILL, S. E. & TRINKAUS, E. 1990. Neandertal scapular glenoid morphology. *American Journal of Physical Anthropology*, 83, 147-160.
- CIOCHON, R. L. & CORRUCINI, R. S. 1976. Shoulder joint of Sterkfontein *Australopithecus*. *South African Journal of Science*, 72, 80-82.
- CLARKE, R. J. 1985. *Australopithecus* and early *Homo* in southern Africa. In: DELSON, E. (ed.) *Ancestors: The Hard Evidence*. New York Alan R. Liss.
- CLARKE, R. J. 1999. Discovery of complete arm and hand of the 3.3 million-year-old *Australopithecus* skeleton. *South African Journal of Science*, 95, 477.
- CLARKE, R. J. 2002. Newly revealed information on the Sterkfontein Member 2 *Australopithecus* skeleton: news & views. *South African Journal of Science*, 98, 523-526.
- CLARKE, R. J. 2006. A deeper understanding of the stratigraphy of Sterkfontein fossil hominid site. *Transactions of the Royal Society of South Africa*, 61, 111-120.
- CLARKE, R. J. 2008. Latest information on Sterkfontein's *Australopithecus* skeleton and a new look at *Australopithecus*. *South African Journal of Science*, 104, 443-449.
- CLARKE, R. J. 2013. *Australopithecus* from Sterkfontein Caves, South Africa. In: REED, K. E., FLEAGLE, J. & LEAKEY, R. E. (eds.) *The Paleobiology of Australopithecus*. New York: Springer.
- CLARKE, R. J., HOWELL, F. C. & BRAIN, C. K. 1970. New finds at the Swartkrans australopithecine site (contd): More evidence of an advanced hominid at Swartkrans. *Nature*, 225, 1219-1222.
- CLAUDEPIERRE, P. & VOISIN, M.-C. 2005. The entheses: Histology, pathology, and pathophysiology. *Joint Bone Spine*, 72, 32-37.
- COPPENS, Y. 1978. Evolution of the hominids and of their environment during the Plio-Pleistocene in the lower Omo Valley, Ethiopia. In: BISHOP, W. W. (ed.) *Geological background to fossil man*. Edinburgh: Scottish Academic Press.
- COPPENS, Y. 1980. The differences between *Australopithecus* and *Homo*: Preliminary conclusions from the Omo research expedition's studies. In: KONIGSSON, L.-K. (ed.) *Current argument on early man*. Oxford: Pergamon.
- COPPENS, Y. & SAKKA, M. 1983. Un nouveau crane d'australopitheque: evolutive morphogenese du cranie et anthropogenese. In: SAKKA, M. (ed.) *Morphologie evolutive, morphogenèse du crâne et origine de l'homme*. Paris: CNRS.
- CORBETTA, D. 2005. Dynamic interactions between posture, handedness, bimanual coordination in human infants: Why stone knapping might be a uniquely hominin behaviour. In: ROUX, V. & BRIL, B. (eds.) *Stone Knapping: The Necessary Conditions for a Uniquely Hominin Behaviour*. Cambridge, England: McDonald Institute for Archaeological Research.
- COTTERELL, B. & KAMMINGA, J. 1987. The formation of flakes. *American Antiquity*, 52, 675-708.
- CURNOE, D. 2010. A review of early *Homo* in southern Africa focusing on cranial, mandibular and dental remains, with the description of a new species (*Homo gautengensis* sp. nov.). *HOMO - Journal of Comparative Human Biology*, 61, 151-177.
- D'ERRICO, F. & BACKWELL, L. 2009. Assessing the function of early hominin bone tools. *Journal of Archaeological Science*, 36, 1764-1773.
- D'ERRICO, F. & BACKWELL, L. R. 2003. Possible evidence of bone tool shaping by Swartkrans early hominids. *Journal of Archaeological Science*, 30, 1559-1576.

- D'ERRICO, F., BACKWELL, L. R. & BERGER, L. 2001. Bone tool use in termite foraging by early hominids and its impact on our understanding of early hominid behaviour. *South African Journal of Science*, 97, 71-75.
- D'ERRICO, F. & HENSHILWOOD, C. S. 2007. Additional evidence for bone technology in the southern African Middle Stone Age. *Journal of Human Evolution*, 52, 142-163.
- DAPENA, J., ANDERST, W. J. & TOTH, N. 2006. The biomechanics of the arm swing in Oldowan stone flaking. In: TOTH, N. & SCHICK, K. (eds.) *The Oldowan: Case Studies Into the Earliest Stone Age*. Gosport: Stone Age Institute Press.
- DART, R. A. 1925. *Australopithecus africanus*: The Man-Ape of South Africa. *Nature*, 115, 195-199.
- DART, R. A. 1948. The Makapansgat proto-human *Australopithecus prometheus*. *American Journal of Physical Anthropology*, 6, 259-284.
- DART, R. A. 1961. Further information about how *Australopithecus* made bone tools and utensils. *South African Journal of Science*, 57, 127-134.
- DAY, M. 1978. Hominid postcranial material from Bed I, Olduvai Gorge. In: ISAAC, G. L. & MCCOWAN, E. R. (eds.) *Human Origins: Louis Leakey and the East African evidence*. Menlo Park: W.A. Benjamin.
- DAY, M. H. 1986. *Guide to Fossil Man*, London, Cassell.
- DAY, M. H. & LEAKEY, R. E. F. 1974. New evidence of the genus *Homo* from East Rudolf, Kenya (III). *American Journal of Physical Anthropology*, 41, 367-380.
- DE HEINZELIN, J., CLARK, J. D., WHITE, T., HART, W., RENNE, P., WOLDEGABRIEL, G., BEYENE, Y. & VRBA, E. S. 1999. Environment and behavior of 2.5-million-year-old Bouri hominids. *Science*, 284, 625-629.
- DE LUMLEY, H., NIORADZÉ, M., BARSKY, D., CAUCHE, D., CELIBERTI, V., NIORADZÉ, G., NOTTER, O., ZVANIA, D. & LORDKIPANIDZE, D. 2005. Les industries lithiques préoldowayennes du début du Pléistocène inférieur du site de Dmanissi en Géorgie. *L'Anthropologie*, 109, 1-182.
- DEBICKI, D. B., GRIBBLE, P. L., WATTS, S. & HORE, J. 2004. Kinematics of wrist joint flexion in overarm throws made by skilled subjects. *Experimental Brain Research*, 154, 382-394.
- DELAGNES, A. & ROCHE, H. 2005. Late Pliocene hominid knapping skills: The case of Lokalalei 2C, West Turkana, Kenya. *Journal of Human Evolution*, 48, 435-472.
- DEMBO, M., MATZKE, N. J., MOOERS, A. Ø. & COLLARD, M. 2015. Bayesian analysis of a morphological supermatrix sheds light on controversial fossil hominin relationships. *Proceedings of the Royal Society of London B: Biological Sciences*, 282, 1-9.
- DIEZ-MARTÍN, F., SÁNCHEZ, P., DOMÍNGUEZ-RODRIGO, M., MABULLA, A. & BARBA, R. 2009. Were Olduvai hominins making butchering tools or battering tools? Analysis of a recently excavated lithic assemblage from BK (Bed II, Olduvai Gorge, Tanzania). *Journal of Anthropological Archaeology*, 28, 274-289.
- DIOGO, R., RICHMOND, B. G. & WOOD, B. 2012. Evolution and homologies of primate and modern human hand and forearm muscles, with notes on thumb movements and tool use. *Journal of Human Evolution*, 63, 64-78.
- DOLGO-SABUROFF, B. 1929. Ober ursprung und insertion der skelettmuskeln. *Anatomischer Anzeiger*, 68, 80-87.

- DOMÍNGUEZ-RODRIGO, M. 2009. Are all Oldowan sites palimpsests? If so, what can they tell us about hominid carnivory? *In: HOVERS, E. & BRAUN, D. (eds.) Interdisciplinary Approaches to the Oldowan.* Springer Netherlands.
- DOMÍNGUEZ-RODRIGO, M., PICKERING, T. R., BAQUEDANO, E., MABULLA, A., MARK, D. F., MUSIBA, C., BUNN, H. T., URIBELARREA, D., SMITH, V., DIEZ-MARTIN, F., PÉREZ-GONZÁLEZ, A., SÁNCHEZ, P., SANTONJA, M., BARBONI, D., GIDNA, A., ASHLEY, G., YRAVEDRA, J., HEATON, J. L. & ARRIAZA, M. C. 2013. First partial skeleton of a 1.34-Million-Year-Old *Paranthropus boisei* from Bed II, Olduvai Gorge, Tanzania. *PLoS ONE*, 8, 1-10.
- DOMÍNGUEZ-RODRIGO, M., PICKERING, T. R. & BUNN, H. T. 2010. Configurational approach to identifying the earliest hominin butchers. *Proceedings of the National Academy of Sciences*, 107, 20929-20934.
- DOMÍNGUEZ-RODRIGO, M., PICKERING, T. R. & BUNN, H. T. 2011. Reply to McPherron et al.: Doubting Dikika is about data, not paradigms. *Proceedings of the National Academy of Sciences*, 108, E117.
- DOSCHAK, M. R. & ZERNICKE, R. F. 2005. Structure, function and adaptation of bone-tendon and bone-ligament complexes. *Journal of Musculoskeletal Neuronal Interaction*, 5, 35-40.
- DRAPEAU, M. S. M. 2004. Functional anatomy of the olecranon process in hominoids and Plio-Pleistocene hominins. *American Journal of Physical Anthropology*, 124, 297-314.
- DRAPEAU, M. S. M. 2008a. Articular morphology of the proximal ulna in extant and fossil hominoids and hominins. *Journal of Human Evolution*, 55, 86-102.
- DRAPEAU, M. S. M. 2008b. Enthesis bilateral asymmetry in humans and African apes. *HOMO - Journal of Comparative Human Biology*, 59, 93-109.
- DRAPEAU, M. S. M., WARD, C. V., KIMBEL, W. H., JOHANSON, D. C. & RAK, Y. 2005. Associated cranial and forelimb remains attributed to *Australopithecus afarensis* from Hadar, Ethiopia. *Journal of Human Evolution*, 48, 593-642.
- DUBUC, B., QUINIOU, J. F., ROQUES-CARMES, C., TRICOT, C. & ZUCKER, S. W. 1989. Evaluating the fractal dimension of profiles. *Physical Review A*, 39, 1500-1512.
- DUTOIR, O. 1986. Enthesopathies (lesions of muscular insertions) as indicators of the activities of neolithic Saharan populations. *American Journal of Physical Anthropology*, 71, 221-224.
- ESHED, V., GOPHER, A., GALILI, E. & HERSHKOVITZ, I. 2004. Musculoskeletal stress markers in Natufian hunter-gatherers and Neolithic farmers in the Levant: The upper limb. *American Journal of Physical Anthropology*, 123, 303-315.
- ETTER, H. F. 1973. Terrestrial adaptations in the hands of Cercopithecinae. *Folia primatologica*, 20, 331-50.
- EVANS, F. G. & KRAHL, V. E. 1945. The torsion of the humerus: A phylogenetic survey from fish to man. *American Journal of Anatomy*, 76, 303-337.
- FALCONER, K. 2003. *Fractal Geometry*, New York, Wiley.
- FEUERRIEGEL, E. M., GREEN, D. J., WALKER, C. S., SCHMID, P., BERGER, L., HAWKS, J. & CHURCHILL, S. E. [Submitted]. The Upper limb of *Homo naledi*. *Journal of Human Evolution*.
- FOUCART, J., BRIL, B., HIRATA, S., MORIMURA, N., HOUKI, C., UENO, Y. & MATSUZAWA, T. 2005. A preliminary analysis of nut-cracking movements in a captive chimpanzee: Adaptation to the properties of tools and nuts. *Stone*

- Knapping: The necessary conditions for a uniquely hominin behaviour.* Cambridge, UK: McDonald Institute for Archaeological Research.
- FRANÇOIS, R. J., BRAUN, J. & KHAN, M. A. 2001. Entheses and enthesitis: A histopathologic review and relevance to spondyloarthritides. *Current Opinion in Rheumatology*, 13, 255-264.
- FROST, H. M. 2001. From Wolff's law to the Utah paradigm: Insights about bone physiology and its clinical applications. *The Anatomical Record*, 262, 398-419.
- FUJIOKA, H., WANG, G.-J., MIZUNO, K., BALIAN, G. & HURWITZ, S. R. 1997. Changes in the expression of type-X collagen in the fibrocartilage of rat Achilles tendon attachment during development. *Journal of Orthopaedic Research*, 15, 675-681.
- GABUNIA, L., VEKUA, A., LORDKIPANIDZE, D., SWISHER, C. C., FERRING, R., JUSTUS, A., NIORADZE, M., TVALCHRELIDZE, M., ANTÓN, S. C., BOSINSKI, G., JÖRIS, O., LUMLEY, M.-A.-D., MAJSURADZE, G. & MOUSKHELISHVILI, A. 2000. Earliest Pleistocene hominid cranial remains from Dmanisi, Republic of Georgia: Taxonomy, geological setting, and age. *Science*, 288, 1019-1025.
- GALATZ, L., ROTHERMICH, S., VANDERPLOEG, K., PETERSEN, B., SANDELL, L. & THOMOPOULOS, S. 2007. Development of the supraspinatus tendon-to-bone insertion: Localized expression of extracellular matrix and growth factor genes. *Journal of Orthopaedic Research*, 25, 1621-1628.
- GALIS, F., VAN ALPHEN, J. J. M. & METZ, J. A. J. 2001. Why five fingers? Evolutionary constraints on digit numbers. *Trends in Ecology & Evolution*, 16, 637-646.
- GAO, J., MESSNER, K., RALPHS, J. R. & BENJAMIN, M. 1996. An immunohistochemical study of enthesis development in the medial collateral ligament of the rat knee joint. *Anatomy and Embryology*, 194, 399-406.
- GENIN, G. M., KENT, A., BIRMAN, V., WOPENKA, B., PASTERIS, J. D., MARQUEZ, P. J. & THOMOPOULOS, S. 2009. Functional grading of mineral and collagen in the attachment of tendon to bone. *Biophysical Journal*, 97, 976-985.
- GINN, K., HALAKI, M. & CATHERS, I. 2011. Revision of the shoulder normalisation tests is required to include rhomboid major and teres major. *Journal of Orthopaedic Research*, 29, 1846-1849.
- GOODALL, J. 1964. Tool-using and aimed throwing in a community of free-living chimpanzees. *Nature*, 201, 1264-1266.
- GOWLETT, J. A. J., HARRIS, J. W. K., WALTON, D. & WOOD, B. A. 1981. Early archaeological sites, hominid remains and traces of fire from Chesowanja, Kenya. *Nature*, 294, 125-129.
- GREEN, D. J. 2013. Ontogeny of the hominoid scapula: The influence of locomotion on morphology. *American Journal of Physical Anthropology*, 152, 239-260.
- GREEN, D. J. & ALEMSEGED, Z. 2012. *Australopithecus afarensis* scapular ontogeny, function, and the role of climbing in human evolution. *Science*, 338, 514-517.
- GREEN, D. J. & GORDON, A. D. 2008. Metacarpal proportions in *Australopithecus africanus*. *Journal of Human Evolution*, 54, 705-719.
- GRINE, F. E. 1988. New craniodental fossils of *Paranthropus* from the Swartkrans formation and their significance in 'robust' Australopithecine evolution. *In:*

- GRINE, F. E. (ed.) *Evolutionary history of the 'robust' Australopithecines*. New York: Aldine.
- GRINE, F. E., DEMES, B., JUNGERS, W. L. & COLE, T. M. 1993. Taxonomic affinity of the early *Homo* cranium from Swartkrans, South Africa. *American Journal of Physical Anthropology*, 92, 411-426.
- GRINE, F. E., SMITH, H. F., HEESY, C. P. & SMITH, E. J. 2009. Phenetic affinities of Plio-Pleistocene *Homo* fossils from South Africa: Molar cusp proportions. In: GRINE, F. E., FLEAGLE, J. G. & LEAKEY, R. E. (eds.) *The first humans*. Dordrecht: Springer Netherlands.
- GRINE, F. E. & SUSMAN, R. L. 1991. Radius of *Paranthropus robustus* from Member 1, Swartkrans Formation, South Africa. *American Journal of Physical Anthropology*, 84, 229-248.
- GRUBER, A. 1969. A functional definition of primate tool making. *Man*, 4, 573-579.
- HAILE-SELASSIE, Y., LATIMER, B. M., ALENE, M., DEINO, A. L., GIBERT, L., MELILLO, S. M., SAYLOR, B. Z., SCOTT, G. R. & LOVEJOY, C. O. 2010. An early *Australopithecus afarensis* postcranium from Woranso-Mille, Ethiopia. *Proceedings of the National Academy of Sciences*, 107, 12121-12126.
- HAINES, R. W. & MOHIUDDIN, A. 1968. Metaplastic bone. *Journal of Anatomy*, 103, 527-538.
- HALL, K. R. L. 1963. Tool-using performances as indicators of behavioural adaptability. *Current Anthropology*, 4, 479-494.
- HAMRICK, M. & INOUE, S. 1995. Thumbs, tools, and early humans. *Science*, 268, 586-587.
- HAMRICK, M. W., CHURCHILL, S. E., SCHMITT, D. & HYLANDER, W. L. 1998. EMG of the human flexor pollicis longus muscle: Implications for the evolution of hominid tool use. *Journal of Human Evolution*, 34, 123-136.
- HARCOURT-SMITH, W. E. H., THROCKMORTON, Z., CONGDON, K. A., ZIPFEL, B., DEANE, A. S., DRAPEAU, M. S. M., CHURCHILL, S. E., BERGER, L. R. & DESILVA, J. M. 2015. The foot of *Homo naledi*. *Nature Communications*, 6, 1-8.
- HARMAND, S. 2009. Variability in raw material selectivity at the Late Pliocene sites of Lokalalei, West Turkana, Kenya. In: HOVERS, E. & BRAUN, D. (eds.) *Interdisciplinary Approaches to the Oldowan*. Springer Netherlands.
- HARMAND, S., LEWIS, J. E., FEIBEL, C. S., LEPRE, C. J., PRAT, S., LENOBLE, A., BOES, X., QUINN, R. L., BRENET, M., ARROYO, A., TAYLOR, N., CLEMENT, S., DAVER, G., BRUGAL, J.-P., LEAKEY, L., MORTLOCK, R. A., WRIGHT, J. D., LOKORODI, S., KIRWA, C., KENT, D. V. & ROCHE, H. 2015. 3.3-million-year-old stone tools from Lomekwi 3, West Turkana, Kenya. *Nature*, 521, 310-315.
- HAUSDORFF, F. 1918. Dimension und äußeres Maß. *Mathematische Annalen*, 79, 157-179.
- HAWKEY, D. E. & MERBS, C. F. 1995. Activity-induced musculoskeletal stress markers (MSM) and subsistence strategy changes among ancient Hudson Bay Eskimos. *International Journal of Osteoarchaeology*, 5, 324-338.
- HEMS, T. & TILLMANN, B. 2000. Tendon entheses of the human masticatory muscles. *Anatomy and Embryology*, 202, 201-8.
- HENDERSON, C. Y. 2008. When hard work is disease: The interpretation of enthesopathies. In: BRICKLEY, M. & SMITH, M. (eds.) *Proceedings of the*

- eighth annual conference of the British association for biological anthropology and osteoarchaeology*. Oxford: British Archaeological Reports.
- HENDERSON, C. Y. 2012. Technical note: Quantifying the size and shape of entheses. *Anthropological Science*, 121, 63-73.
- HENDERSON, C. Y. 2013. Do diseases cause enthesal changes at fibrous entheses? *International Journal of Paleopathology*, 3, 64-69.
- HENDERSON, C. Y., MARIOTTI, V., PANY-KUCERA, P., PERRÉARD-LOPRENO, G., VILLOTTE, S. & WILCZAK, C. 2012. The effect of age on enthesal changes at some fibrocartilaginous entheses. *81th Annual Meeting of the American Association of Physical Anthropologists*. Portland, Oregon.
- HERRIES, A. I. R. & SHAW, J. 2011. Palaeomagnetic analysis of the Sterkfontein palaeocave deposits: Implications for the age of the hominin fossils and stone tool industries. *Journal of Human Evolution*, 60, 523-539.
- HOVERS, E. 2012. Invention, re-invention and innovation: The makings of Oldowan lithic technology. In: ELIAS, S. (ed.) *Origins of Human Innovation and Creativity*. Oxford, UK: Elsevier.
- HOWELL, F. C. 1978. Hominidae. In: MAGLIO, V. J. & COOKE, H. B. S. (eds.) *Evolution of African mammals*. Cambridge: Harvard University Press.
- HOWELL, F. C. & COPPENS, Y. 1976. An Overview of Hominidae from the Omo Succession, Ethiopia. In: COPPENS, Y., HOWELL, F. C., ISAAC, G. L. & LEAKEY, R. E. F. (eds.) *Earliest Man and Environments in the Lake Rudolf Basin*. Chicago: University of Chicago Press.
- HOWELL, F. C., HAESAERTS, P. & DE HEINZELIN, J. 1987. Depositional environments, archeological occurrences and hominids from Members E and F of the Shungura Formation (Omo basin, Ethiopia). *Journal of Human Evolution*, 16, 665-700.
- HOWELL, F. C. & WOOD, B. A. 1974. Early hominid ulna from the Omo basin, Ethiopia. *Nature*, 249, 174-176.
- HUGHES, A. R. & TOBIAS, P. V. 1977. A fossil skull probably of the genus *Homo* from Sterkfontein, Transvaal. *Nature*, 265, 310-312.
- INMAN, V. T., SAUNDERS, J. B. D. M. & ABBOTT, L. C. 1944. Observations on the function of the shoulder joint. *Journal of Bone and Joint Surgery*, 26A, 1-30.
- ISAAC, G. L. & ISAAC, B. 1997. *Koobi Fora Research Project: Plio-Pleistocene Archaeology*, Oxford, Clarendon.
- IVANOVA, G. P. 2005. The Biomechanics of the Complex Coordinated Stroke In: ROUX, V. & BRIL, B. (eds.) *Stone Knapping: The Necessary Conditions for a Uniquely Hominin Behaviour*. Cambridge, England: McDonald Institute for Archaeological Research.
- JAHREN, A. H., TOTH, N., SCHICK, K., CLARK, J. D. & AMUNDSON, R. G. 1997. Determining stone tool use: Chemical and morphological analyses of residues on experimentally manufactured stone tools. *Journal of Archaeological Science*, 24, 245-250.
- JASHASHVILI, T. 2005. *A hominid upper limb remains from the Palaeolithic site of Dmanisi, a morphometric comparison to taxonomic units and functional interpretation*. PhD, University of Ferrara.
- JELLEMA, L. M., LATIMER, B. & WALKER, A. 1993. The Rib Cage. In: WALKER, A. & LEAKEY, R. E. (eds.) *The Nariokotome Homo erectus skeleton*. Cambridge: Harvard University Press.

- JOHANSON, D. C., LOVEJOY, C. O., KIMBEL, W. H., WHITE, T. D., WARD, S. C., BUSH, M. E., LATIMER, B. M. & COPPENS, Y. 1982. Morphology of the Pliocene partial hominid skeleton (A.L. 288-1) from the Hadar formation, Ethiopia. *American Journal of Physical Anthropology*, 57, 403-451.
- JOHANSON, D. C., MASAO, F. T., ECK, G., WHITE, T. D., WALTER, R. C., KIMBEL, W. H., ASFAW, B., MANEGA, P., NDESSOKIA, P. & SUWA, G. 1987. New partial skeleton of *Homo habilis* from Olduvai Gorge, Tanzania. *Nature*, 327, 205-209.
- JOLLY, C. J. 1966. The evolution of the baboons. In: VAGTBORG, H. (ed.) *The baboon in medical research*. Austin, Texas: Texas University Press.
- JOLLY, C. J. 1970. The seed-eaters: A new model of hominid differentiation based on a baboon analogy. *Man*, 5, 5-26.
- JOLLY, C. J. 1972. The classification and natural history of *Theropithecus* (*Simopithecus*) (Andrews, 1916), baboons of the African Plio-Pleistocene. *Bulletin of the British Museum of Natural History. Geology*, 22, 3-123.
- JONES, F. 1982. *Structure and function as seen in the foot*, London, Bailliere, Tindall & Cox.
- JUDE, J. 1993. *Manipulative behavior of Hamadryas baboons*. Senior thesis, Arizona State University.
- JUDEX, S. & CARLSON, K. J. 2009. Is bone's response to mechanical signals dominated by gravitational loading? *Medicine & Science in Sports & Exercise*, 41, 2037-2043.
- JUNNO, J.-A., NIINIMÄKI, S., NISKANEN, M., NUNEZ, M. & TUUKKANEN, J. 2011. Cross sectional properties of the human radial tuberosity. *HOMO - Journal of Comparative Human Biology*, 62, 459-465.
- JURMAIN, R. 1999. *Stories from the Skeleton: Behavioral Reconstruction in Human Osteology*, London, Taylor and Francis.
- JURMAIN, R., CARDOSO, F. A., HENDERSON, C. & VILLOTTE, S. 2012. Bioarchaeology's Holy Grail: The reconstruction of activity. *A Companion to Paleopathology*. Oxford, UK: Wiley-Blackwell.
- JURMAIN, R. & VILLOTTE, S. 2010. Terminology. Entheses in medical literature and physical anthropology: A brief review. *Workshop in Musculoskeletal Stress Markers (MSM): limitations and achievements in the reconstruction of past activity patterns, July 2-3, 2009*. University of Coimbra: CIAS – Centro de Investigação em Antropologia e Saúde.
- KACKI, S. & VILLOTTE, S. 2006. Maladie hyperostotique et mode de vie: Intérêt d'une démarche bio-archéologique - Exemple du couvent des Soeurs Grises de Beauvais (Oise), XVe-XVIIIe siècles. *Bulletins et Mémoires de la Société d'Anthropologie de Paris*, 12, 55-64.
- KEELEY, L. H. & TOTH, N. 1981. Microwear polishes on early stone tools from Koobi Fora, Kenya. *Nature*, 293, 464-465.
- KENNEDY, K. 1989. Skeletal markers of occupational stress. In: ISCAN, M. & KENNEDY, K. (eds.) *Reconstruction of life from the skeleton*. New York: Alan R. Liss.
- KENNEDY, K. A. R. 1998. Markers of occupational stress: Conspectus and prognosis of research. *International Journal of Osteoarchaeology*, 8, 305-310.
- KEY, A. J. M. & DUNMORE, C. J. 2015. The evolution of the hominin thumb and the influence exerted by the non-dominant hand during stone tool production. *Journal of Human Evolution*, 78, 60-69.

- KEYSER, A. W., MENTER, C. G., MOGGI-CECCHI, J., PICKERING, P. R. & BERGER, L. R. 2000. Drimolen: A new hominid-bearing site in Gauteng, South Africa. *South African Journal of Science*, 96, 193-197.
- KHAN, K. M., BONAR, F., DESMOND, P. M., COOK, J. L., YOUNG, D. A., VISENTINI, P. J., FEHRMANN, M. W., KISS, Z. S., O'BRIEN, P. A., HARCOURT, P. R., DOWLING, R. J., O'SULLIVAN, R. M., CRICHTON, K. J., TRESS, B. M. & WARK, J. D. 1996. Patellar tendinosis (jumper's knee): Findings at histopathologic examination, US, and MR imaging. Victorian Institute of Sport Tendon Study Group. *Radiology*, 200, 821-827.
- KIBII, J. M., CLARKE, R. J. & TOCHERI, M. W. 2011. A hominin scaphoid from Sterkfontein, Member 4: Morphological description and first comparative phenetic 3D analyses. *Journal of Human Evolution*, 61, 510-517.
- KIMBEL, W. H. 1988. Identification of a partial cranium of *Australopithecus afarensis* from the Koobi Fora Formation, Kenya. *Journal of Human Evolution*, 17, 647-656.
- KIMBEL, W. H., JOHANSON, D. C. & RAK, Y. 1997. Systematic assessment of a maxilla of *Homo* from Hadar, Ethiopia. *American Journal of Physical Anthropology*, 103, 235-262.
- KIMBEL, W. H., WALTER, R. C., JOHANSON, D. C., REED, K. E., ARONSON, J. L., ASSEFA, Z., MAREAN, C. W., ECK, G. G., BOBE, R., HOVERS, E., RAK, Y., VONDRA, C., YEMANE, T., YORK, D., CHEN, Y., EVENSEN, N. M. & SMITH, P. E. 1996. Late Pliocene *Homo* and Oldowan tools from the Hadar Formation (Kada Hadar Member), Ethiopia. *Journal of Human Evolution*, 31, 549-561.
- KIMURA, Y. 1999. Tool-using strategies by early hominids at Bed II, Olduvai Gorge, Tanzania. *Journal of Human Evolution*, 37, 807-831.
- KIMURA, Y. 2002. Examining time trends in the Oldowan technology at Beds I and II, Olduvai Gorge. *Journal of Human Evolution*, 43, 291-321.
- KIVELL, T. L. 2011. A comparative analysis of the hominin triquetrum (SKX 3498) from Swartkrans, South Africa. *South African Journal of Science*, 107, 1-10.
- KIVELL, T. L., DEANE, A. S., TOCHERI, M. W., ORR, C. M., SCHMID, P., HAWKS, J., BERGER, L. R. & CHURCHILL, S. E. 2015. The hand of *Homo naledi*. *Nature Communications*, 6, 1-9.
- KIVELL, T. L., KIBII, J. M., CHURCHILL, S. E., SCHMID, P. & BERGER, L. R. 2011. *Australopithecus sediba* hand demonstrates mosaic evolution of locomotor and manipulative abilities. *Science*, 333, 1411-1417.
- KLEIN, R. 2009. *The Human Career: Human Biological and Cultural Origins* Chicago, University Chicago Press.
- KLINKENBERG, B. 1994. A review of methods used to determine the fractal dimension of linear features. *Mathematical Geology*, 26, 23-46.
- KLINKENBERG, B. & GOODCHILD, M. F. 1992. The fractal properties of topography: A comparison of methods. *Earth Surface Processes and Landforms*, 17, 217-234.
- KNESE, K. H. & BIERMANN, H. 1958. Die Knochenbildung an Sehnen- und Bandansätzen im Bereich ursprünglich chondraler Apophysen. *Zeitschrift für Zellforschung und mikroskopische Anatomie*, 49, 142-187.
- KORTLANDT, A. 1986. The use of stone tools by wild-living Chimpanzees and earliest hominids. *Journal of Human Evolution*, 15, 77-132.

- KRAHL, V. E. 1947. The torsion of the humerus: Its localization, cause and duration in man. *American Journal of Anatomy*, 80, 275-319.
- KRAHL, V. E. & EVANS, F. G. 1945. Humeral torsion in man. *American Journal of Physical Anthropology*, 3, 229-253.
- KRAMER, A. 1986. Hominid-pongid distinctiveness in the Miocene-Pliocene fossil record: The Lothagam mandible. *American Journal of Physical Anthropology*, 70, 457-473.
- KRANTZ, G. 1960. Evolution of the human hand and the great hand-axe tradition. *Kroeber Anthropological Society Papers*, 23, 114-129.
- KUMAN, K. 1998. The earliest South African industries. In: PETRAGLIA, M. D. & KORISSETAR, R. (eds.) *Early Hominid Behaviour in Global Context: The Rise and Diversity of the the Lower Palaeolithic Record*. London: Routledge.
- KUMAN, K. & CLARKE, R. J. 2000. Stratigraphy, artefact industries and hominid associations for Sterkfontein, Member 5. *Journal of Human Evolution*, 38, 827-847.
- LAGUE, M. R. 2015. Taxonomic identification of Lower Pleistocene fossil hominins based on distal humeral diaphyseal cross-sectional shape. *PeerJ*, 3, 1-31.
- LAGUE, M. R. & JUNGERS, W. L. 1996. Morphometric variation in Plio-Pleistocene hominid distal humeri. *American Journal of Physical Anthropology*, 101, 401-427.
- LAI, P. & LOVELL, N. C. 1992. Skeletal markers of occupational stress in the Fur Trade: A case study from a Hudson's Bay Company Fur Trade post. *International Journal of Osteoarchaeology*, 2, 221-234.
- LARSEN, C. 1997. *Bioarchaeology: Interpreting behavior from the human skeleton*, Cambridge, Cambridge University Press.
- LARSEN, C. 2000. *Skeletons in our closet: revealing our past through bioarchaeology*, Princeton, Princeton University Press.
- LARSON, S. G. 1988. Subscapularis function in gibbons and chimpanzees: Implications for interpretation of humeral head torsion in hominoids. *American Journal of Physical Anthropology*, 76, 449-462.
- LARSON, S. G. 1996. Estimating humeral torsion on incomplete fossil anthropoid humeri. *Journal of Human Evolution*, 31, 239-258.
- LARSON, S. G. 2007. Evolutionary transformation of the hominin shoulder. *Evolutionary Anthropology*, 16, 172-187.
- LARSON, S. G. 2009. Evolution of the Hominin Shoulder: Early *Homo*. In: GRINE, F. E. F., JOHN G.; LEAKEY, RICHARD E. (ed.) *The First Humans: Origin and Early Evolution of the Genus Homo*. Dordrecht: Springer.
- LARSON, S. G. 2013. Shoulder morphology in early hominin evolution. In: REED, K. E., FLEAGLE, J. G. & LEAKEY, R. E. (eds.) *The paleobiology of Australopithecus*. Springer.
- LARSON, S. G., JUNGERS, W. L., MORWOOD, M. J., SUTIKNA, T., JATMIKO, SAPTOMO, E. W., DUE, R. A. & DJUBIANTONO, T. 2007. *Homo floresiensis* and the evolution of the hominin shoulder. *Journal of Human Evolution*, 53, 718-731.
- LE GROS CLARK, W. E. 1959. *The Antecedents of Man*, Edinburgh, Edinburgh University Press.
- LEAKEY, L. S., TOBIAS, P. V. & NAPIER, J. R. 1964a. A new species of the genus *Homo* from Olduvai Gorge. *Nature*, 202, 7-9.
- LEAKEY, L. S. B. 1959. A new fossil skull from Olduvai. *Nature*, 184, 491-493.

- LEAKEY, L. S. B. 1960. Recent discoveries at Olduvai Gorge. *Nature*, 188, 1050-1052.
- LEAKEY, L. S. B. & LEAKEY, M. D. 1964. Recent discoveries of fossil hominids in Tanganyika, at Olduvai and near Lake Natron. *Nature*, 202, 5-7.
- LEAKEY, L. S. B., TOBIAS, P. V. & NAPIER, J. R. 1964b. A new species of the genus *Homo* from Olduvai Gorge. *Nature*, 202, 7-9.
- LEAKEY, M. D. 1971a. *Olduvai Gorge*, London, Cambridge University Press.
- LEAKEY, M. D. 1971b. *Olduvai Gorge: Excavations in beds I & II 1960-1963*, Cambridge, Cambridge University Press.
- LEAKEY, M. D. 1978. Olduvai fossil hominids: Their stratigraphic positions and associations. In: JOLLY, C. J. (ed.) *Early Hominids of Africa*. London: Duckworth.
- LEAKEY, M. G., FEIBEL, C. S., MCDUGALL, I. & WALKER, A. 1995. New four-million-year-old hominid species from Kanapoi and Allia Bay, Kenya. *Nature*, 376, 565-571.
- LEAKEY, M. G., FEIBEL, C. S., MCDUGALL, I., WARD, C. & WALKER, A. 1998. New specimens and confirmation of an early age for *Australopithecus anamensis*. *Nature*, 393, 62-66.
- LEAKEY, R. E. F. 1971c. Further evidence of Lower Pleistocene hominids from East Rudolf, North Kenya. *Nature*, 231, 241-245.
- LEAKEY, R. E. F. 1973. Further evidence of Lower Pleistocene hominids from East Rudolf, North Kenya, 1972. *Nature*, 242, 170-173.
- LEAKEY, R. E. F., MUNGAI, J. M. & WALKER, A. C. 1971. New australopithecines from East Rudolf, Kenya. *American Journal of Physical Anthropology*, 35, 175-186.
- LEAKEY, R. E. F., MUNGAI, J. M. & WALKER, A. C. 1972. New australopithecines from East Rudolf, Kenya (II). *American Journal of Physical Anthropology*, 36, 235-251.
- LEAKEY, R. E. F. & WALKER, A. 1988. New *Australopithecus boisei* specimens from east and west Lake Turkana, Kenya. *American Journal of Physical Anthropology*, 76, 1-24.
- LEAKEY, R. E. F., WALKER, A., WARD, C. V. & GRAUSZ, H. M. 1989. A partial skeleton of a gracile hominid from the Upper Burgi Member of the Koobi Fora Formation, East Lake Turkana, Kenya. In: GIACOBINI, G. (ed.) *Hominidae: Proceedings of the 2nd International Congress of Human Paleontology*, Turin. Milan: Jaka Books.
- LEMORINI, C., PLUMMER, T. W., BRAUN, D. R., CRITTENDEN, A. N., DITCHFIELD, P. W., BISHOP, L. C., HERTEL, F., OLIVER, J. S., MARLOWE, F. W., SCHOENINGER, M. J. & POTTS, R. 2014. Old stones' song: Use-wear experiments and analysis of the Oldowan quartz and quartzite assemblage from Kanjera South (Kenya). *Journal of Human Evolution*, 72, 10-25.
- LEPRE, C. J., ROCHE, H., KENT, D. V., HARMAND, S., QUINN, R. L., BRUGAL, J.-P., TEXIER, P.-J., LENOBLE, A. & FEIBEL, C. S. 2011. An earlier origin for the Acheulian. *Nature*, 477, 82-85.
- LEWIS, O. J. 1973. The hominoid os capitatum, with special reference to the fossil bones from Sterkfontein and Olduvai Gorge. *Journal of Human Evolution*, 2, 1-11.
- LEWIS, O. J. 1977. Joint remodelling and the evolution of the human hand. *Journal of Anatomy*, 123, 157-201.

- LIEBOVITCH, L. S. & TOTH, T. 1989. A fast algorithm to determine fractal dimensions by box counting. *Physics Letters A*, 141, 386-390.
- LIEVERSE, A. R., BAZALIISKII, V. I., GORIUNOVA, O. I. & WEBER, A. W. 2009. Upper limb musculoskeletal stress markers among middle Holocene foragers of Siberia's Cis-Baikal region. *American Journal of Physical Anthropology*, 138, 458-472.
- LORDKIPANIDZE, D., JASHASHVILI, T., VEKUA, A., DE LEÓN, M. S. P., ZOLLIKOFER, C. P. E., RIGHTMIRE, P. G., PONTZER, H., FERRING, R., OMS, O., TAPPEN, M., BUKHSIANIDZE, M., AGUSTI, J., KAHLKE, R., KILADZE, G., MARTINEZ-NAVARRO, B., MOUSKHELISHVILI, A., NIORADZE, M. & ROOK, L. 2007. Postcranial evidence from early *Homo* from Dmanisi, Georgia. *Nature*, 449, 305-310.
- LORENZO, C., ARSUAGA, J. L. & CARRETERO, J. M. 1999. Hand and foot remains from the Gran Dolina Early Pleistocene site (Sierra de Atapuerca, Spain). *Journal of Human Evolution*, 37, 501-522.
- LOVEJOY, C. O., JOHANSON, D. C. & COPPENS, Y. 1982. Hominid upper limb bones recovered from the Hadar formation: 1974-1977 collections. *American Journal of Physical Anthropology*, 57, 637-649.
- LOVEJOY, C. O., SIMPSON, S. W., WHITE, T. D., ASFAW, B. & SUWA, G. 2009. Careful climbing in the Miocene: The forelimbs of *Ardipithecus ramidus* and humans are primitive. *Science*, 326, 70, 70e1-70e8.
- LU, H. H. & THOMOPOULOS, S. 2013. Functional attachment of soft tissues to bone: Development, healing, and tissue engineering. *Annual Review of Biomedical Engineering*, 15, 201-226.
- MAGA, M., KAPPELMAN, J., RYAN, T. M. & KETCHAM, R. A. 2006. Preliminary observations on the calcaneal trabecular microarchitecture of extant large-bodied hominoids. *American Journal of Physical Anthropology*, 129, 410-417.
- MAGNUSSON, S. P. & KJAER, M. 2003. Region-specific differences in Achilles tendon cross-sectional area in runners and non-runners. *European Journal of Applied Physiology*, 90, 549-553.
- MANDELBROT, B. B. 1967. How long is the coast of Britain? Statistical self-similarity and fractional dimension. *Science*, 156, 636-638.
- MANDELBROT, B. B. 1983. *The Fractal Geometry of Nature*, New York, Henry Holt and Company.
- MANDELBROT, B. B. 1985. Self-affine fractals and fractal dimension. *Physica Scripta*, 32, 257.
- MANN, R. W. & HUNT, D. R. 2005. *Photographic Regional Atlas of Bone Disease*, Springfield, IL, Charles C. Thomas.
- MARCHI, D., WALKER, C. S., WEI, P., HOLLIDAY, T. W., CHURCHILL, S. E., BERGER, L. R. & DESILVA, J. M. 2016. Thigh and leg remains of *Homo naledi*. *American Journal of Physical Anthropology*, 159, 218-219.
- MARIOTTI, V., FACCHINI, F. & BELCASTRO, M. G. 2004. Enthesopathies-- Proposal of a standardized scoring method and applications. *Collegium Anthropologicum*, 28, 145-59.
- MARIOTTI, V., FACCHINI, F. & GIOVANNA BELCASTRO, M. 2007. The study of entheses: Proposal of a standardised scoring method for twenty-three entheses of the postcranial skeleton. *Coll Antropol*, 31, 291-313.

- MARTIN, L. B. 1986. Relationships among extant and extinct great apes and humans. In: WOOD, B. A., MARTIN, L. B. & ANDREWS, P. (eds.) *Major Topics in Primate and Human Evolution*. Cambridge: Cambridge University Press.
- MARZKE, M. W. 1983. Joint functions and grips of the *Australopithecus afarensis* hand, with special reference to the region of the capitate. *Journal of Human Evolution*, 12, 197-211.
- MARZKE, M. W. 1997. Precision grips, hand morphology, and tools. *American Journal of Physical Anthropology*, 102, 91-110.
- MARZKE, M. W. 2005. Who made stone tools? In: ROUX, V. & BLANDINE, B. (eds.) *Stone Knapping: The Necessary Conditions for a Uniquely Hominin Behaviour*. Cambridge, England: McDonald Institute for Archaeological Research.
- MARZKE, M. W. 2013. Tool making, hand morphology and fossil hominins. *Philosophical Transactions of the Royal Society of London B: Biological Sciences*, 368, 1-8.
- MARZKE, M. W. & MARZKE, R. F. 1987. The third metacarpal styloid process in humans: Origin and functions. *American Journal of Physical Anthropology*, 73, 415-431.
- MARZKE, M. W. & MARZKE, R. F. 2000. Evolution of the human hand: Approaches to acquiring, analysing and interpreting the anatomical evidence. *Journal of Anatomy*, 197, 121-140.
- MARZKE, M. W., MARZKE, R. F., LINSCHIED, R. L., SMUTZ, P., STEINBERG, B., REECE, S. & AN, K. N. 1999. Chimpanzee thumb muscle cross sections, moment arms and potential torques, and comparisons with humans. *American Journal of Physical Anthropology*, 110, 163-178.
- MARZKE, M. W. & SHACKLEY, M. S. 1986. Hominid hand use in the Pliocene and Pleistocene: Evidence from experimental archaeology and comparative morphology. *Journal of Human Evolution*, 15, 439-460.
- MARZKE, M. W., TOCHERI, M. W., STEINBERG, B., FEMIANI, J. D., REECE, S. P., LINSCHIED, R. L., ORR, C. M. & MARZKE, R. F. 2010. Comparative 3D quantitative analyses of trapeziometacarpal joint surface curvatures among living catarrhines and fossil hominins. *American Journal of Physical Anthropology*, 141, 38-51.
- MARZKE, M. W., TOTH, N., SCHICK, K., REECE, S., STEINBERG, B., HUNT, K., LINSCHIED, R. L. & AN, K. N. 1998. EMG study of hand muscle recruitment during hard hammer percussion manufacture of Oldowan tools. *American Journal of Physical Anthropology*, 105, 315-332.
- MARZKE, M. W. & WULLSTEIN, K. L. 1996. Chimpanzee and human grips: A new classification with a focus on evolutionary morphology. *International Journal of Primatology*, 17, 117-139.
- MARZKE, M. W., WULLSTEIN, K. L. & VIEGAS, S. F. 1992. Evolution of the power ("squeeze") grip and its morphological correlates in hominids. *American Journal of Physical Anthropology*, 89, 283-298.
- MATSUZAWA, T. 1994. Field experiments on use of stone tools by chimpanzees in the wild. In: WRANGHAM, R. W., MCGREW, W. C., DE WAAL, F. B. M. & HELTNE, P. G. (eds.) *Chimpanzee Cultures*. Cambridge: Harvard University Press.
- MATSUZAWA, T., BIRO, D., HUMLE, T., INOUE-NAKAMURA, N. & TONOOKA, R. 2001. Emergence of culture in wild chimpanzees: Education by master-

- apprenticeship. In: MATSUZAWA, T. (ed.) *Primate Origins of Human Cognition and Behavior*. Tokyo: Springer.
- MATYAS, J. R., ANTON, M. G., SHRIVE, N. G. & FRANK, C. B. 1995. Stress governs tissue phenotype at the femoral insertion of the rabbit MCL. *Journal of Biomechanics*, 28, 147-157.
- MAYS, S. 2000. Age-dependent cortical bone loss in women from 18th and early 19th Century London. *American Journal of Physical Anthropology*, 112, 349-361.
- MCCROSSIN, M. L., BENEFIT, B. R., GITAU, S. N., PALMER, A. K. & BLUE, K. T. 1998. Fossil evidence for the origins of terrestriality among Old World higher primates. In: STRASSER, E., FLEAGLE, J., ROSENBERGER, A. L. & MCHENRY, H. M. (eds.) *Primate locomotion: Recent advances*. New York, N.Y.: Plenum Press.
- MCGREW, W. C. 2004. *The Cultured Chimpanzee: Reflections on Cultural Primatology*, Cambridge, MA, Cambridge University Press.
- MCHENRY, H. M. 1973. Early hominid humerus from East Rudolf, Kenya. *Science*, 180, 739-41.
- MCHENRY, H. M. 1983. The capitate of *Australopithecus afarensis* and *A. africanus*. *American Journal of Physical Anthropology*, 62, 187-198.
- MCHENRY, H. M. 1994. Early hominid postcrania: Phylogeny and function. In: CORRUCINI, R. S. & CIOCHON, R. L. (eds.) *Integrative paths to the past: paleoanthropological advances in honour of F. Clark Howell*. Englewood Cliffs, N.J.: Prentice Hall.
- MCHENRY, H. M. & BERGER, L. R. 1998. Body proportions of *Australopithecus afarensis* and *A. africanus* and the origin of the genus *Homo*. *Journal of Human Evolution*, 35, 1-22.
- MCHENRY, H. M., BROWN, C. C. & MCHENRY, L. J. 2007. Fossil hominin ulnae and the forelimb of *Paranthropus*. *American Journal of Physical Anthropology*, 134, 209-218.
- MCHENRY, H. M., CORRUCINI, R. S. & HOWELL, F. C. 1976. Analysis of an early hominid ulna from the Omo basin, Ethiopia. *American Journal of Physical Anthropology*, 44, 295-304.
- MCHENRY, H. M. & TEMERIN, L. A. 1979. The evolution of hominid bipedalism: Evidence from the fossil record. *Yearbook Of Physical Anthropology*, 22, 105-131.
- MCPHERRON, S. P., ALEMSEGED, Z., MAREAN, C. W., WYNN, J. G., REED, D., GERAADS, D., BOBE, R. & BEARAT, H. A. 2010. Evidence for stone-tool-assisted consumption of animal tissues before 3.39 million years ago at Dikika, Ethiopia. *Nature*, 466, 857-860.
- MENTER, C. G., KUYKENDALL, K. L., KEYSER, A. W. & CONROY, G. C. 1999. First record of hominid teeth from the Plio-Pleistocene site of Gondolin, South Africa. *Journal of Human Evolution*, 37, 299-307.
- MERCADER, J., PANGER, M. & BOESCH, C. 2002. Excavation of a chimpanzee stone tool site in the African rainforest. *Science*, 296, 1452-1455.
- MILELLA, M., GIOVANNA BELCASTRO, M., ZOLLIKOFER, C. P. E. & MARIOTTI, V. 2012. The effect of age, sex, and physical activity on enthesal morphology in a contemporary Italian skeletal collection. *American Journal of Physical Anthropology*, 148, 379-388.
- MINAR, C. J. & CROWN, P. L. 2001. Learning and craft production: An introduction. *Journal of Anthropological Research*, 57, 369-380.

- MOLNAR, P. 2006. Tracing prehistoric activities: Musculoskeletal stress marker analysis of a stone-age population on the Island of Gotland in the Baltic sea. *American Journal of Physical Anthropology*, 129, 12-23.
- MORGAN, T. J. H., UOMINI, N. T., RENDELL, L. E., CHOUINARD-THULY, L., STREET, S. E., LEWIS, H. M., CROSS, C. P., EVANS, C., KEARNEY, R., DE LA TORRE, I., WHITEN, A. & LALAND, K. N. 2015. Experimental evidence for the co-evolution of hominin tool-making teaching and language. *Nature Communications*, 6, 1-8.
- MOYÀ-SOLÀ, S., KÖHLER, M., ALBA, D. M. & ALMECIJA, S. 2008. Taxonomic attribution of the Olduvai hominid 7 manual remains and the functional interpretation of hand morphology in robust australopithecines. *Folia Primatologica*, 79, 215-50.
- MUSGRAVE, J. H. 1971. How dextrous was Neanderthal man? *Nature*, 233, 538-541.
- MYERS, T. W. 2001. *Anatomy Train: Myofascial Meridians for Manual and Movement Therapists*, Edinburgh, Churchill Livingstone.
- NAKAMA, L. H., KING, K. B., ABRAHAMSSON, S. & REMPEL, D. M. 2005. Evidence of tendon microtears due to cyclical loading in an in vivo tendinopathy model. *Journal of Orthopaedic Research*, 23, 1199-1205.
- NAPIER, J. R. 1956. The prehensile movements of the human hand. *Journal of Bone & Joint Surgery, British Volume*, 38-B, 902-913.
- NAPIER, J. R. 1960. Studies of the hands of living primates. *Proceedings of the Zoological Society of London*, 134, 647-657.
- NAPIER, J. R. 1962a. The evolution of the hand. *Scientific American*, 204, 2-9.
- NAPIER, J. R. 1962b. Fossil hand bones from Olduvai Gorge. *Nature*, 196, 409-411.
- NAPIER, J. R. 1965a. Comment on "New discoveries in Tanganyika: Their bearing on hominid evolution" by P.V. Tobias. *Current Anthropology*, 5, 402-403.
- NAPIER, J. R. 1965b. Evolution of the human hand. *Proceedings of the Royal Institution of Great Britain*, 40, 544-557.
- NAPIER, J. R. 1993. *Hands*, Princeton, N.J., Princeton University Press.
- NASCIMENTO, F. A., GATTO, L. A. M., LAGES, R. O., NETO, H. M., DEMARTINI, Z. & KOPPE, G. L. 2014. Diffuse idiopathic skeletal hyperostosis: A review. *Surgical Neurology International*, 5, S122-S125.
- NGUYEN, N. H., PAHR, D. H., GROSS, T., SKINNER, M. M. & KIVELL, T. L. 2014. Micro-finite element (FE) modeling of the siamang (*Symphalangus syndactylus*) third proximal phalanx: The functional role of curvature and the flexor sheath ridge. *Journal of Human Evolution*, 67, 60-75.
- NIEPEL, G. A. & SIT'AJ, S. 1979. Enthesopathy. *Clinics in Rheumatic disease*, 5, 857-872.
- NIEWOEHRNER, W. A. 2000. *The Functional Anatomy of Late Pleistocene and Recent Human Carpometacarpal and Metacarpo-phalangeal Articulations*. Ph. D., University of New Mexico.
- NIEWOEHRNER, W. A. 2001. Behavioral inferences from the Skhul/Qafzeh early modern human hand remains. *Proceedings of the National Academy of Sciences*, 98, 2979-2984.
- NIEWOEHRNER, W. A., WEAVER, A. H. & TRINKAUS, E. 1997. Neandertal capitate-metacarpal articular morphology. *American Journal of Physical Anthropology*, 103, 219-233.
- NIINIMÄKI, S. 2011. What do muscle marker ruggedness scores actually tell us? *International Journal of Osteoarchaeology*, 21, 292-299.

- NISHIDA, T. 1987. Local traditions and cultural transmission. *In: SMUTS, B., CHENEY, D., SEYFARTH, R., WRANGHAM, R. & STRUHSAKER, T. (eds.) Primate societies.* Chicago: University of Chicago Press.
- NISHIDA, T., MATSUSAKA, T. & MCGREW, W. 2009. Emergence, propagation or disappearance of novel behavioral patterns in the habituated chimpanzees of Mahale: A review. *Primates*, 50, 23-36.
- OREY, S. 1970. Gaussian sample functions and the Hausdorff dimension of level crossings. *Zeitschrift für Wahrscheinlichkeitstheorie und Verwandte Gebiete*, 15, 249-256.
- ORR, C. M., TOCHERI, M. W., BURNETT, S. E., AWE, R. D., SAPTOMO, E. W., SUTIKNA, T., JATMIKO, WASISTO, S., MORWOOD, M. J. & JUNGERS, W. L. 2013. New wrist bones of *Homo floresiensis* from Liang Bua (Flores, Indonesia). *Journal of Human Evolution*, 64, 109-129.
- OXNARD, C. E. 1963. Locomotor adaptations in the primate forelimb. *Symposia of the Zoological Society of London: The primates.* London: Zoological Society of London.
- OXNARD, C. E. 1968. The architecture of the shoulder in some mammals. *Journal of Morphology*, 126, 249-290.
- OXNARD, C. E. 1969a. Evolution of the human shoulder: Some possible pathways. *American Journal of Physical Anthropology*, 30, 319-332.
- OXNARD, C. E. 1969b. A note on the Olduvai clavicular fragment. *American Journal of Physical Anthropology*, 29, 429-432.
- PANGER, M. A., BROOKS, A. S., RICHMOND, B. G. & WOOD, B. 2002. Older than the Oldowan? Rethinking the emergence of hominin tool use. *Evolutionary Anthropology: Issues, News, and Reviews*, 11, 235-245.
- PARTRIDGE, T. C., GRANGER, D. E., CAFFEE, M. W. & CLARKE, R. J. 2003. Lower Pliocene hominid remains from Sterkfontein. *Science*, 300, 607-612.
- PATTERSON, B. & HOWELLS, W. W. 1967. Hominid humeral fragment from Early Pleistocene of Northwestern Kenya. *Science*, 156, 64-66.
- PAXTON, J. Z., BAAR, K. & GROVER, L. M. 2012. Current progress in enthesis repair: Strategies for interfacial tissue engineering. *Orthopedic & Muscular System: Current Research*, S1, 1-13.
- PAYNE, R. W., MURRAY, D. A., HARDING, S. A., BAIRD, D. B. & SOUTAR, D. M. 2015. GenStat for Windows. Hemel Hempstead: VSN International.
- PEITGEN, H.-O. & RICHTER, P. H. 1986. *The Beauty of Fractals*, New York, Springer.
- PELCIN, A. W. 1997. The formation of flakes: The role of platform thickness and exterior platform angle in the production of flake initiations and terminations. *Journal of Archaeological Science*, 24, 1107-1113.
- PELEGRIN, J. 2005. Remarks about archaeological techniques and methods of knapping: Elements of a cognitive approach to stone knapping. *In: ROUX, V. & BRIL, B. (eds.) Stone Knapping: The Necessary Conditions for a Uniquely Hominin Behaviour.* Cambridge, England: McDonald Institute for Archaeological Research.
- PELOSO, P. M. & BRAUN, J. 2004. Expanding the armamentarium for the spondyloarthropathies. *Arthritis Research & Therapy*, 6, S36-S43.
- PETERSON, J. & HAWKEY, D. E. 1998. Preface. *International Journal of Osteoarchaeology*, 8, 303-304.

- PFEIFER, P. 1984. Fractal dimension as working tool for surface-roughness problems. *Applications of Surface Science*, 18, 146-164.
- PICKERING, T. R. 2013. *Rough and Tumble: Aggression, Hunting, and Human Evolution*, University of California Press.
- PICKERING, T. R. & DOMÍNGUEZ-RODRIGO, M. 2006. The acquisition and use of large animal carcasses by Oldowan hominins in Eastern and Southern Africa: A selected review and assessment. In: TOTH, N. & SCHICK, K. (eds.) *The Oldowan: Case Studies Into the Earliest Stone Age*. Indiana: The Stone Age Institute.
- PICKERING, T. R., DOMÍNGUEZ-RODRIGO, M., EGELAND, C. P. & BRAIN, C. K. 2007. Carcass foraging by early hominids at Swartkrans Cave (South Africa): A new investigation of the zooarchaeology and taphonomy of Member 3. In: PICKERING, T. R., SCHICK, K. D. & TOTH, N. P. (eds.) *Breathing life into fossils: Taphonomic studies in honor of C.K. (Bob) Brain*. Godport, Indiana: Stone Age Institute Press.
- PICKERING, T. R., HEATON, J. L., CLARKE, R. J., SUTTON, M. B., BRAIN, C. K. & KUMAN, K. 2012. New hominid fossils from Member 1 of the Swartkrans formation, South Africa. *Journal of Human Evolution*, 62, 618-628.
- PICKFORD, M., JOHANSON, D. C., LOVEJOY, C. O., WHITE, T. D. & ARONSON, J. L. 1983. A hominid humeral fragment from the Pliocene of Kenya. *American Journal of Physical Anthropology*, 60, 337-346.
- PIEPER, H. G. 1998. Humeral torsion in the throwing arm of handball players. *American Journal of Sports Medicine*, 26, 247-53.
- PIGEON, P., YAHIA, L. H. & FELDMAN, A. G. 1996. Moment arms and lengths of human upper limb muscles as functions of joint angles. *Journal of Biomechanics*, 29, 1365-1370.
- PLUMMER, T. W., BISHOP, L. C., DITCHFIELD, P. W., FERRARO, J. V., KINGSTON, J. D., HERTEL, F. & BRAUN, D. R. 2009. The environmental context of Oldowan hominin activities at Kanjera South, Kenya. In: HOVERS, E. & BRAUN, D. (eds.) *Interdisciplinary Approaches to the Oldowan*. Springer Netherlands.
- PRAT, S., BRUGAL, J.-P., ROCHE, H. & TEXIER, P.-J. 2003. Nouvelles découvertes de dents d'hominidés dans le membre Kaitio de la formation de Nachukui (1,65-1,9 Ma), Ouest du lac Turkana (Kenya). *Comptes Rendus Palevol*, 2, 685-693.
- PRUETZ, J. D. & BERTOLANI, P. 2007. Savanna chimpanzees, *Pan troglodytes verus*, hunt with tools. *Current Biology*, 17, 412-417.
- PUTT, S. S. 2015. The origins of stone tool reduction and the transition to knapping: An experimental approach. *Journal of Archaeological Science: Reports*, 2, 51-60.
- QUINE, W. V. 1960. *Word and Object*, Cambridge, Harvard University Press.
- REAGAN, K. M., MEISTER, K., HORODYSKI, M. B., WERNER, D. W., CARRUTHERS, C. & WILK, K. 2002. Humeral retroversion and its relationship to glenohumeral rotation in the shoulder of college baseball players. *American Journal of Sports Medicine*, 30, 354-60.
- REED, K. E., KITCHING, J. W., GRINE, F. E., JUNGERS, W. L. & SOKOLOFF, L. 1993. Proximal femur of *Australopithecus africanus* from Member 4, Makapansgat, South Africa. *American Journal of Physical Anthropology*, 92, 1-15.

- REICHMISTER, J. P., REEDER, J. D. & MCCARTHY, E. 1996. Ossification of the coracoacromial ligament: Association with rotator cuff pathology of the shoulder. *Maryland medical journal*, 45, 849-52.
- REIN, R., NONAKA, T. & BRIL, B. 2014. Movement pattern variability in stone knapping: Implications for the development of percussive traditions. *PLoS ONE*, 9, 1-27.
- RESNICK, D. & NIWAYAMA, G. 1983. Enteses and enthesopathy. Anatomical, pathological, and radiological correlation. *Radiology*, 146, 1-9.
- RICHMOND, B. G. 1998. *Ontogeny and Biomechanics of Phalangeal Form in Primates*. PhD, Stony Brook University.
- RICHMOND, B. G. 2003. Early hominin locomotion and the ontogeny of phalangeal curvature in primates. *American Journal of Physical Anthropology*, 36 (Supplementary), 178-179.
- RICHMOND, B. G. 2007. Biomechanics of phalangeal curvature. *Journal of Human Evolution*, 53, 678-690.
- RICKLAN, D. E. 1987. Functional anatomy of the hand of *Australopithecus africanus*. *Journal of Human Evolution*, 16, 643-664.
- RICKLAN, D. E. 1990. The precision grip in *Australopithecus africanus*: Anatomical and behavioral correlates. In: SPERBER, G. H. (ed.) *From Apes to Angels: Essays in Anthropology in Honor of Phillip V. Tobias*. New York: Wiley-Liss.
- RIJKELIJKHUIZEN, J. M., BAAN, G. C., DE HAAN, A., DE RUITER, C. J. & HUIJING, P. A. 2005. Extramuscular myofascial force transmission for in situ rat medial gastrocnemius and plantaris muscles in progressive stages of dissection. *Journal of Experimental Biology*, 208, 129-140.
- RILEY, G. & TRINKAUS, E. 1989. Neandertal capitate-metacarpal 2 articular morphology and Neandertal manipulation (abstract). *American Journal of Physical Anthropology*, 78, 290.
- ROACH, N. T. & RICHMOND, B. G. 2015. Clavicle length, throwing performance and the reconstruction of the *Homo erectus* shoulder. *Journal of Human Evolution*, 80, 107-113.
- ROACH, N. T., VENKADESAN, M., RAINBOW, M. J. & LIEBERMAN, D. E. 2013. Elastic energy storage in the shoulder and the evolution of high-speed throwing in *Homo*. *Nature*, 498, 483-486.
- ROBB, J. 1994. Skeletal signs of activity in the Italian metal ages: Methodological and interpretative notes. *Human Evolution*, 9, 215-229.
- ROBB, J. E. 1998. The interpretation of skeletal muscle sites: A statistical approach. *International Journal of Osteoarchaeology*, 8, 363-377.
- ROBINSON, J. T. 1953. *Telanthropus* and its phylogenetic significance. *American Journal of Physical Anthropology*, 11, 445-501.
- ROBINSON, J. T. 1959. A Bone Implement from Sterkfontein. *Nature*, 184, 583-585.
- ROBINSON, J. T. 1965a. Comment on 'New discoveries in Tanganyika: Their bearing on hominid evolution' by P.V. Tobias. *Current Anthropology*, 6, 403-406.
- ROBINSON, J. T. 1965b. *Homo 'habilis'* and the Australopithecines. *Nature*, 205, 121-124.
- ROBINSON, J. T. 1972. *Early hominid posture and locomotion*, Chicago, University of Chicago Press.
- ROBINSON, J. T. 1978. Evidence for locomotor difference between gracile and robust early hominids from South Africa. In: JOLLY, C. J. (ed.) *Early Hominids of Africa*. New York: St. Martin's Press.

- ROBINSON, J. T. & MASON, R. J. 1962. Australopithecines and artefacts at Sterkfontein. *The South African Archaeological Bulletin*, 17, 87-126.
- ROCHE, H. 2005. From simple flaking to shaping: Stone-knapping evolution among early hominins. In: ROUX, V. & BRIL, B. (eds.) *Stone Knapping: The Necessary Conditions for a Uniquely Hominin Behaviour*. Cambridge, England: McDonald Institute for Archaeological Research.
- ROCHE, H., BLUMENSCHINE, R. J. & SHEA, J. J. 2009. Origins and adaptations of early *Homo*: What archeology tells us. In: GRINE, F. E., FLEAGLE, J. G. & LEAKEY, R. E. (eds.) *The First Humans – Origin and Early Evolution of the Genus Homo: Contributions from the Third Stony Brook Human Evolution Symposium and Workshop October 3 – October 7, 2006*. Dordrecht: Springer Netherlands.
- ROCHE, H., DELAGNES, A., BRUGAL, J. P., FEIBEL, C., KIBUNJIA, M., MOURRE, V. & TEXIER, P. J. 1999. Early hominid stone tool production and technical skill 2.34 Myr ago in West Turkana, Kenya. *Nature*, 399, 57-60.
- ROFFMAN, I., SAVAGE-RUMBAUGH, S., RUBERT-PUGH, E., RONEN, A. & NEVO, E. 2012. Stone tool production and utilization by bonobo-chimpanzees (*Pan paniscus*). *Proceedings of the National Academy of Sciences*, 109, 14500-14503.
- ROGOFF, B. 1990. *Apprenticeship in Thinking: Cognitive Development in Social Context*, Oxford, Oxford University Press.
- ROLIAN, C. & GORDON, A. D. 2013. Reassessing manual proportions in *Australopithecus afarensis*. *American Journal of Physical Anthropology*, 152, 393-406.
- ROLIAN, C. & GORDON, A. D. 2014. Response to Almécija and Alba (2014) – On manual proportions in *Australopithecus afarensis*. *Journal of Human Evolution*, 73, 93-97.
- ROLIAN, C., LIEBERMAN, D. E. & ZERMENO, J. P. 2011. Hand biomechanics during simulated stone tool use. *Journal of Human Evolution*, 61, 26-41.
- ROTHSCHILD, B. M., CALDERON, F. L., COPPA, A. & ROTHSCCHILD, C. 2000. First European exposure to syphilis: The Dominican Republic at the time of Columbian contact. *Clinical Infectious Diseases*, 31, 936-941.
- ROTHSCHILD, B. M., HERSHKOVITZ, I. & ROTHSCCHILD, C. 1995. Origin of jaws in the Pleistocene. *Nature*, 378, 343-344.
- ROUX, V. & BRIL, B. 2005. *Stone Knapping: The Necessary Conditions for a Uniquely Hominin Behaviour*, Cambridge, England, McDonald Institute for Archaeological Research.
- ROUX, V. & DAVID, E. 2005. Planning abilities as a dynamic perceptual-motor skill: An actualist study of different levels of expertise involved in stone knapping. In: ROUX, V. & BRIL, B. (eds.) *Stone Knapping: The Necessary Conditions for a Uniquely Hominin Behaviour*. Cambridge, England: McDonald Institute for Archaeological Research.
- RUFF, C. 2009. Relative limb strength and locomotion in *Homo habilis*. *American Journal of Physical Anthropology*, 138, 90-100.
- RUFF, C., HOLT, B. & TRINKAUS, E. 2006. Who's afraid of the big bad Wolff?: "Wolff's law" and bone functional adaptation. *American Journal of Physical Anthropology*, 129, 484-498.
- RUFF, C. B. & BURGESS, M. L. 2015. How much more would KNM-WT 15000 have grown? *Journal of Human Evolution*, 80, 74-82.

- RYAN, T. M. & SHAW, C. N. 2012. Unique suites of trabecular bone features characterize locomotor behavior in human and non-human anthropoid primates. *PLoS ONE*, 7, 1-11.
- RYAN, T. M. & VAN RIETBERGEN, B. 2005. Mechanical significance of femoral head trabecular bone structure in *Loris* and *Galago* evaluated using micromechanical finite element models. *American Journal of Physical Anthropology*, 126, 82-96.
- SAHNOUNI, M., SCHICK, K. & TOTH, N. 1997. An experimental investigation into the nature of faceted limestone “spheroids” in the Early Palaeolithic. *Journal of Archaeological Science*, 24, 701-713.
- SAKELLARIOU, M., NAKOS, B. & MITSAKAKI, C. 1991. On the fractal character of rock surfaces. *International Journal of Rock Mechanics and Mining Sciences & Geomechanics Abstracts*, 28, 527-533.
- SANTOS, A. L., ALVES-CARDOSO, F., ASSIS, S. & VILLOTTE, S. 2011. The Coimbra Workshop in musculoskeletal stress markers (MSM): An annotated review. *Antropologia Portuguesa*, 28, 135-161.
- SCHICK, K. & TOTH, N. 1993. *Making Silent Stones Speak: Human Evolution and the Dawn of Technology*, New York, Simon & Schuster.
- SCHICK, K. D., TOTH, N., GARUFI, G., SAVAGE-RUMBAUGH, E. S., RUMBAUGH, D. & SEVCIK, R. 1999. Continuing investigations into the stone tool-making and tool-using capabilities of a Bonobo (*Pan paniscus*). *Journal of Archaeological Science*, 26, 821-832.
- SCHMID, P. 1983. Eine Rekonstruktion des Skelettes von A.L. 288-1 (Hadar) und deren Konsequenzen. *Folia Primatologica*, 40, 283-306.
- SCHMID, P., CHURCHILL, S. E., NALLA, S., WEISSEN, E., CARLSON, K. J., DE RUITER, D. J. & BERGER, L. R. 2013. Mosaic morphology in the thorax of *Australopithecus sediba*. *Science*, 340, 1-5.
- SCHNEIDER, H. 1956. Zur Struktur der Sehnenansatzonen. *Zeitschrift für Anatomie und Entwicklungsgeschichte*, 119, 431-456.
- SCHWEITZER, M. E. & KARASICK, D. 2000. MR Imaging of disorders of the Achilles tendon. *American Journal of Roentgenology*, 175, 613-625.
- SELTMAN, H. J. 2015. Mixed models. *Experimental Design and Analysis*. Online: CMU Statistics.
- SEMAW, S. 2000. The world’s oldest stone artefacts from Gona, Ethiopia: Their implications for understanding stone technology and patterns of human evolution between 2.6–1.5 million years ago. *Journal of Archaeological Science*, 27, 1197-1214.
- SEMAW, S., RENNE, P., HARRIS, J. W. K., FEIBEL, C. S., BERNOR, R. L., FESSEHA, N. & MOWBRAY, K. 1997. 2.5-million-year-old stone tools from Gona, Ethiopia. *Nature*, 385, 333-336.
- SEMAW, S., ROGERS, M. J., QUADE, J., RENNE, P. R., BUTLER, R. F., DOMINGUEZ-RODRIGO, M., STOUT, D., HART, W. S., PICKERING, T. & SIMPSON, S. W. 2003. 2.6-Million-year-old stone tools and associated bones from OGS-6 and OGS-7, Gona, Afar, Ethiopia. *Journal of Human Evolution*, 45, 169-177.
- SENU, B. 1978. *Contribution a L'etude de l'humerus et des articulations chez les hominides du Plio-Pleistocene*. Doctor of Philosophy, Pierre-and-Marie-Curie University.

- SENUT, B. 1980. New data on the humerus and its joints in Plio-Pleistocene hominids. *Collegium Anthropologicum*, 4, 87-93.
- SENUT, B. 1981. L'humérus et ses articulations chez les hominidés plio-pléistocènes. *Cahiers de Paléontologie (Paléoanthropologie)*. Paris: Éditions du Centre National de la Recherche Scientifique.
- SENUT, B. 1983. Les Hominides Plio-Pleistocenes: Essai taxonomique et phylogenetique a partir de certains os longs. *Bulletins et mémoires de la Société d'Anthropologie de Paris*, 10, 325-334.
- SHAW, H. M., VAZQUEZ, O. T., MCGONAGLE, D., BYDDER, G., SANTER, R. M. & BENJAMIN, M. 2008. Development of the human Achilles tendon enthesis organ. *Journal of Anatomy*, 213, 718-24.
- SHREWSBURY, M. M., MARZKE, M. W., LINSCHIED, R. L. & REECE, S. P. 2003. Comparative morphology of the pollical distal phalanx. *American Journal of Physical Anthropology*, 121, 30-47.
- SKINNER, M. M., STEPHENS, N. B., TSEGAI, Z. J., FOOTE, A. C., NGUYEN, N. H., GROSS, T., PAHR, D. H., HUBLIN, J.-J. & KIVELL, T. L. 2015. Human-like hand use in *Australopithecus africanus*. *Science*, 347, 395-399.
- SKUBALSKA-RAFAJŁOWICZ, E. 2005. A new method of estimation of the box-counting dimension of multivariate objects using space-filling curves. *Nonlinear Analysis: Theory, Methods & Applications*, 63, e1281-e1287.
- SMITH JR, T. G., MARKS, W. B., LANGE, G. D., SHERIFF JR, W. H. & NEALE, E. A. 1989. A fractal analysis of cell images. *Journal of Neuroscience Methods*, 27, 173-180.
- SMITSMAN, A. W., COX, R. F. A. & BONGERS, R. M. 2005. Action dynamics in tool use. In: ROUX, V. & BRIL, B. (eds.) *Stone Knapping: The Necessary Conditions for a Uniquely Hominin Behaviour*. Cambridge, England: McDonald Institute for Archaeological Research.
- SOLAN, M. & DAY, M. H. 1992. The Baringo (Kapthurin) ulna. *Journal of Human Evolution*, 22, 307-313.
- SPOOR, F., LEAKEY, M. G., GATHOGO, P. N., BROWN, F. H., ANTON, S. C., MCDUGALL, I., KIARIE, C., MANTHI, F. K. & LEAKEY, L. N. 2007. Implications of new early *Homo* fossils from Ileret, east of Lake Turkana, Kenya. *Nature*, 448, 688-691.
- STEEN, S. L. & LANE, R. W. 1998. Evaluation of habitual activities among two Alaskan Eskimo populations based on musculoskeletal stress markers. *International Journal of Osteoarchaeology*, 8, 341-353.
- STERN, J. T. & SUSMAN, R. L. 1983. The locomotor anatomy of *Australopithecus afarensis*. *American Journal of Physical Anthropology*, 60, 279-317.
- STIRLAND, A. J. 1998. Musculoskeletal evidence for activity: Problems of evaluation. *International Journal of Osteoarchaeology*, 8, 354-362.
- STONER, B. P. & TRINKAUS, E. 1981. Getting a grip on the Neandertals: Were they all thumbs? (abstract). *American Journal of Physical Anthropology*, 54, 281-282.
- STOUFFER, D. C., BUTLER, D. L. & HOSNY, D. 1985. The relationship between crimp pattern and mechanical response of human patellar tendon-bone units. *Journal of Biomechanical Engineering*, 107, 158-165.
- STOUT, D. 2002. Skill and cognition in stone tool production: An ethnographic case study from Irian Jaya. *Current Anthropology*, 43, 693-722.

- STOUT, D., QUADE, J., SEMAW, S., ROGERS, M. J. & LEVIN, N. E. 2005. Raw material selectivity of the earliest stone toolmakers at Gona, Afar, Ethiopia. *Journal of Human Evolution*, 48, 365-380.
- STOUT, D., SEMAW, S., ROGERS, M. J. & CAUCHE, D. 2010. Technological variation in the earliest Oldowan from Gona, Afar, Ethiopia. *Journal of Human Evolution*, 58, 474-491.
- SUSMAN, R. L. 1979. Comparative and functional morphology of hominoid fingers. *American Journal of Physical Anthropology*, 50, 215-236.
- SUSMAN, R. L. 1988a. Hand of *Paranthropus robustus* from Member 1, Swatkrans: Fossil evidence for tool behavior. *Science*, 240, 781-784.
- SUSMAN, R. L. 1988b. New postcranial remains from the Swartkrans and their bearing on the functional morphology and behavior of *Paranthropus robustus*. In: GRINE, F. E. (ed.) *Evolutionary History of the "Robust" Australopithecines*. New York: Aldine de Gruyter.
- SUSMAN, R. L. 1989. New hominid fossils from the Swartkrans formation (1979–1986 excavations): Postcranial specimens. *American Journal of Physical Anthropology*, 79, 451-474.
- SUSMAN, R. L. 1991. Who made the Oldowan tools? Fossil evidence for tool behavior in Plio-Pleistocene hominids. *Journal of Anthropological Research*, 47, 129-151.
- SUSMAN, R. L. 1994. Fossil evidence for early hominid tool use. *Science*, 265, 1570-3.
- SUSMAN, R. L. 1998. Hand function and tool behavior in early hominids. *Journal of Human Evolution*, 35, 23-46.
- SUSMAN, R. L. & CREEL, N. 1979. Functional and morphological affinities of the subadult hand (O.H. 7) from Olduvai Gorge. *American Journal of Physical Anthropology*, 51, 311-332.
- SUSMAN, R. L., DE RUITER, D. & BRAIN, C. K. 2001. Recently identified postcranial remains of *Paranthropus* and early *Homo* from Swartkrans Cave, South Africa. *Journal of Human Evolution*, 41, 607-629.
- SUSMAN, R. L. & STERN, J. T. 1982. Functional morphology of *Homo habilis*. *Science*, 217, 931-4.
- SUSMAN, R. L. & STERN, J. T. J. 1979. Telemetered electromyography of flexor digitorum profundus and flexor digitorum superficialis in *Pan troglodytes* and implications for interpretation of the O.H. 7 hand. *American Journal of Physical Anthropology*, 50, 565-574.
- SWISHER, C. C., CURTIS, G. H., JACOB, T., GETTY, A. G., SUPRIJO, A. & WIDIASMORO 1994. Age of the earliest known hominids in Java, Indonesia. *Science*, 263, 1118-1121.
- TAIEB, M., JOHANSON, D. C. & COPPENS, Y. 1975. Expédition internationale de l'Afar, Éthiopie (3^{ème} campagne 1974) découverte d'Hominidés Plio-Pléistocènes à Hadar. *Comptes Rendus de l'Académie des Sciences*, 281, 1297-1300.
- THACKERAY, J. F., DE RUITER, D. J., BERGER, L. R. & VAN DER MERVE, N. J. 2001. Hominid fossils from Kromdraai: A revised list of specimens discovered since 1938. *Annals of the Transvaal Museum*, 38, 43-56.
- THOMOPOULOS, S., GENIN, G. M. & GALATZ, L. M. 2010. The development and morphogenesis of the tendon-to-bone insertion - what development can teach us about healing. *Journal of Musculoskeletal & Neuronal Interactions*, 10, 35-45.

- THOMOPOULOS, S., KIM, H.-M., ROTHERMICH, S. Y., BIEDERSTADT, C., DAS, R. & GALATZ, L. M. 2007. Decreased muscle loading delays maturation of the tendon enthesis during postnatal development. *Journal of Orthopaedic Research*, 25, 1154-1163.
- THOMOPOULOS, S., WILLIAMS, G. R., GIMBEL, J. A., FAVATA, M. & SOSLOWSKY, L. J. 2003. Variation of biomechanical, structural, and compositional properties along the tendon to bone insertion site. *Journal of Orthopaedic Research*, 21, 413-419.
- THORPE, S. K. S., CROMPTON, R. H., GUNTHER, M. M., KER, R. F. & MCNEILL ALEXANDER, R. 1999. Dimensions and moment arms of the hind- and forelimb muscles of common chimpanzees (*Pan troglodytes*). *American Journal of Physical Anthropology*, 110, 179-199.
- THORPE, W. H. 1963. *Learning and Instinct in Animals*, London, Methuen & Co.
- TOBIAS, P. V. 1965. New Discoveries in Tanganyika: Their bearing on hominid evolution. *Current Anthropology*, 6, 391-411.
- TOBIAS, P. V. 1971. *The Brain in Hominid Evolution*, New York, Columbia University Press.
- TOBIAS, P. V. 1978. The earliest Transvaal members of the genus *Homo* with another look at some problems of hominid taxonomy and systematics. *Zeitschrift fur Morphologie und Anthropologie*, 69, 225-265.
- TOBIAS, P. V. 1989. The Gradual Appraisal of *Homo habilis*. In: GIACOBINI, G. (ed.) *Hominidae: Proceedings of the Second International Congress of Human Palaeontology*. Milano: Jaca Books.
- TOBIAS, P. V. 1991. *Olduvai Gorge: The Skulls, Endocasts and Teeth of Homo habilis*, Cambridge, Cambridge University Press.
- TOCHERI, M. W. 2007. *Three-dimensional riddles of the radial wrist: derived carpal and carpometacarpal joint morphology in the genus Homo and the implications for understanding the evolution of stone tool-related behaviours in hominins*. PhD, Arizona State University.
- TOCHERI, M. W., MARZKE, M. W., LIU, D., BAE, M., JONES, G. P., WILLIAMS, R. C. & RAZDAN, A. 2003. Functional capabilities of modern and fossil hominid hands: Three-dimensional analysis of trapezia. *American Journal of Physical Anthropology*, 122, 101-112.
- TOCHERI, M. W., ORR, C. M., JACOFISKY, M. C. & MARZKE, M. W. 2008. The evolutionary history of the hominin hand since the last common ancestor of *Pan* and *Homo*. *Journal of Anatomy*, 212, 544-562.
- TOCHERI, M. W., ORR, C. M., LARSON, S. G., SUTIKNA, T., JATMIKO, SAPTOMO, E. W., DUE, R. A., DJUBIANTONO, T., MORWOOD, M. J. & JUNGERS, W. L. 2007. The primitive wrist of *Homo floresiensis* and its implications for hominin evolution. *Science*, 317, 1743-1745.
- TOCHERI, M. W., RAZDAN, A., WILLIAMS, R. C. & MARZKE, M. W. 2005. A 3D quantitative comparison of trapezium and trapezoid relative articular and nonarticular surface areas in modern humans and great apes. *Journal of Human Evolution*, 49, 570-586.
- TOTH, N. 1985. The Oldowan reassessed: A close look at early stone artifacts. *Journal of Archaeological Science*, 12, 101-120.
- TOTH, N. 1987. Behavioral inferences from early stone artifact assemblages: An experimental model. *Journal of Human Evolution*, 16, 763-787.

- TOTH, N. & SCHICK, K. 2009. The Oldowan: The tool making of early hominins and Chimpanzees compared. *Annual Review of Anthropology*, 38, 289-305.
- TOTH, N., SCHICK, K. & SEMAW, S. 2006. A comparative study of the stone tool-making skills of *Pan*, *Australopithecus*, and *Homo sapiens*. In: TOTH, N. & SCHICK, K. (eds.) *The Oldowan: Case Studies into the Earliest Stone Age*. Gosport: Stone Age Institute Press.
- TOTH, N., SCHICK, K. D., SAVAGE-RUMBAUGH, E. S., SEVCIK, R. A. & RUMBAUGH, D. M. 1993. *Pan* the tool-maker: Investigations into the stone tool-making and tool-using capabilities of a Bonobo (*Pan paniscus*). *Journal of Archaeological Science*, 20, 81-91.
- TOUSSAINT, M., MACHO, G. A., TOBIAS, P. V., PARTRIDGE, T. C. & HUGHES, A. R. 2003. The third partial skeleton of a Pliocene hominin (Stw 431) from Sterkfontein, South Africa. *South African Journal of Science*, 99, 215-223.
- TRINKAUS, E. 1977. A functional interpretation of the axillary border of the Neanderthal scapula. *Journal of Human Evolution*, 6, 231-234.
- TRINKAUS, E. 1983. *The Shanidar Neandertals*, New York, Academic Press.
- TRINKAUS, E. 1989. Neandertal upper limb morphology and manipulation. In: GIACOBINI, G. (ed.) *Hominidae*. Milano: Jaca Books.
- TRINKAUS, E. & LONG, J. C. 1990. Species attribution of the Swartkrans member 1 first metacarpals: SK 84 and SKX 5020. *American Journal of Physical Anthropology*, 83, 419-424.
- TRINKAUS, E. & VILLEMEUR, I. 1991. Mechanical advantages of the Neanderthal thumb in flexion: A test of an hypothesis. *American Journal of Physical Anthropology*, 84, 249-60.
- TSEGAI, Z. J., KIVELL, T. L., GROSS, T., NGUYEN, N. H., PAHR, D. H., SMAERS, J. B. & SKINNER, M. M. 2013. Trabecular bone structure correlates with hand posture and use in hominoids. *PLoS ONE*, 8, 1-14.
- TUTTLE, R. H. 1992. Hands from Newt to Napier. In: MATANO, S., TUTTLE, R. H., ISHIDA, H. & GOODMAN, M. (eds.) *Topics in Primatology*. Tokyo: University of Tokyo Press.
- TUTTLE, R. H. & BASMAJIAN, J. V. 1974. Electromyography of brachial muscles in *Pan gorilla* and hominoid evolution. *American Journal of Physical Anthropology*, 41, 71-90.
- UBELAKER, D. H. 1979. Skeletal evidence for kneeling in prehistoric Ecuador. *American Journal of Physical Anthropology*, 51, 679-685.
- VAN DER MADE, J. 1999. Ungulates from Atapuerca TD6. *Journal of Human Evolution*, 37, 389-413.
- VAN LAWICK-GOODALL, J. 1970. Tool-using in primates and other vertebrates. In: LEHRMAN, D. S., HINDE, R. A. & SHAW, E. (eds.) *Advances in the Study of Behaviour*. New York: Academic Press.
- VANDERMEERSCH, B. & TRINKAUS, E. 1995. The postcranial remains of the Régourdou 1 Neandertal: the shoulder and arm remains. *Journal of Human Evolution*, 28, 439-476.
- VILLOTTE, S. 2006. Connaissances médicales actuelles, cotation des enthésopathies: Nouvelle méthode. *Bulletins et Mémoires de la Société d'Anthropologie de Paris*, 18, 65-85.
- VILLOTTE, S. 2012. Practical protocol for scoring the appearance of some fibrocartilaginous entheses on the human skeleton. Bordeaux, France: Université Bordeaux. Available online:

- http://www.academia.edu/1427191/Practical_protocol_for_scoring_the_appearance_of_some_fibrocartilaginous_entheses_on_the_human_skeleton
- VILLOTTE, S., CASTEX, D., COUALLIER, V., DUTOUR, O., KNÜSEL, C. J. & HENRY-GAMBIER, D. 2010. Enthesopathies as occupational stress markers: Evidence from the upper limb. *American Journal of Physical Anthropology*, 142, 224–234.
- VLČEK, E. 1975. Morphology of the first metacarpal of Neandertal individuals from the Crimea. *Bulletins et Mémoires de la Société d'anthropologie de Paris*, 257–276.
- VOISIN, J.-L. 2004. Clavicule: Approche architecturale de l'épaule et réflexions sur le statut systématique des néandertaliens. *Comptes Rendus Palevol*, 3, 133–142.
- VOISIN, J.-L. 2006a. Clavicule, a neglected bone: Morphology and relation to arm movements and shoulder architecture in primates. *Anatomical Record*, 288, 944–53.
- VOISIN, J.-L. 2006b. Krapina and other Neanderthal clavicles: A peculiar morphology? *Periodicum Biologorum*, 108, 331–339.
- VOISIN, J.-L. 2008. The Omo I hominin clavicle: Archaic or modern? *Journal of Human Evolution*, 55, 438–444.
- VRBA, E. 1982. Biostratigraphy and chronology, based particularly on Bovidae, of southern hominid-associated assemblages: Makapansgat, Sterkfontein, Taung, Kromdraai, Swartkrans; also Elandsfontein (Saldanha), Broken Hill (now Kabwe) and Cave of Hearths. In: DE LUMLEY, M.-A. (ed.) *L'Homo erectus et la place de l'homme de Tautavel parmi les hominidés fossiles: Congrès international de paléontologie humaine, 1er Congrès, Nice, 16-21 octobre 1982*. Paris: Institut de paléontologie humaine.
- VRBA, E. S. 1979. A new study of the scapula of *Australopithecus africanus* from Sterkfontein. *American Journal of Physical Anthropology*, 51, 117–129.
- WALKER, A. & LEAKEY, R. E. 1993. The Postcranial Bones. In: LEAKEY, R. & WALKER, A. (eds.) *The Nariokotome Homo erectus Skeleton*. Cambridge: Harvard University Press.
- WARD, C. V. 2013. Postural and locomotor adaptations of *Australopithecus species*. In: REED, K. E., FLEAGLE, J. & LEAKEY, R. E. (eds.) *The Paleobiology of Australopithecus*. Springer Verlag.
- WARD, C. V. 2014. Taxonomic affinity of the Pliocene hominin fossils from Fejej, Ethiopia. *Journal of Human Evolution*, 73, 98–102.
- WARD, C. V., LEAKEY, M. G. & WALKER, A. 2001. Morphology of *Australopithecus anamensis* from Kanapoi and Allia Bay, Kenya. *Journal of Human Evolution*, 41, 255–368.
- WARD, C. V., MANTHI, F. K. & PLAVCAN, J. M. 2013. New fossils of *Australopithecus anamensis* from Kanapoi, West Turkana, Kenya (2003–2008). *Journal of Human Evolution*, 65, 501–524.
- WARD, C. V., TOCHERI, M. W., PLAVCAN, J. M., BROWN, F. H. & MANTHI, F. K. 2014. Early Pleistocene third metacarpal from Kenya and the evolution of modern human-like hand morphology. *Proceedings of the National Academy of Sciences*, 111, 121–124.
- WASHBURN, S. L. 1971. The study of human evolution. In: DOLHINOW, P. & SARICH, V. (eds.) *Background for Man*. Boston: Brown & Co.
- WASHBURN, S. L. 1974. Human evolution: Science or game. *Yearbook of Physical Anthropology*, 17, 67–70.

- WASHBURN, S. L. 1978. The evolution of man. *Scientific American*, 293, 194-208.
- WEISS, E. 2003. Understanding muscle markers: Aggregation and construct validity. *American Journal of Physical Anthropology*, 121, 230-240.
- WEISS, E. 2004. Understanding muscle markers: Lower limbs. *American Journal of Physical Anthropology*, 125, 232-238.
- WEISS, E. 2007. Muscle markers revisited: Activity pattern reconstruction with controls in a central California Amerind population. *American Journal of Physical Anthropology*, 133, 931-940.
- WEISS, E. 2012. Examining activity patterns and biological confounding factors: Differences between fibrocartilaginous and fibrous musculoskeletal stress markers. *International Journal of Osteoarchaeology*, 25, 1-8.
- WEISS, E., CORONA, L. & SCHULTZ, B. 2012. Sex differences in musculoskeletal stress markers: Problems with activity pattern reconstructions. *International Journal of Osteoarchaeology*, 22, 70-80.
- WHEELER, W. M. 1930. *Demons in the Dust*, New York, W. W. Norton & Co.
- WHITE, T. D., SUWA, G. & ASFAW, B. 1994. *Australopithecus ramidus*, a new species of early hominid from Aramis, Ethiopia. *Nature*, 371, 306-312.
- WHITE, T. D., SUWA, G., SIMPSON, S. & ASFAW, B. 2000. Jaws and teeth of *Australopithecus afarensis* from Maka, Middle Awash, Ethiopia. *American Journal of Physical Anthropology*, 111, 45-68.
- WHITEN, A., GOODALL, J., MCGREW, W. C., NISHIDA, T., REYNOLDS, V., SUGIYAMA, Y., TUTIN, C. E. G., WRANGHAM, R. W. & BOESCH, C. 2001. Charting cultural variation in chimpanzees. *Behaviour*, 138, 1481-1516.
- WHITEN, A., SCHICK, K. & TOTH, N. 2009. The evolution and cultural transmission of percussive technology: Integrating evidence from palaeoanthropology and primatology. *Journal of Human Evolution*, 57, 420-435.
- WILCZAK, C. A. 1998. Consideration of sexual dimorphism, age, and asymmetry in quantitative measurements of muscle insertion sites. *International Journal of Osteoarchaeology*, 8, 311-325.
- WILLIAMS-HATALA, E. M., HATALA, K. G., HILES, S. & RABEY, K. N. 2016. Morphology of muscle attachment sites in the modern human hand does not reflect muscle architecture. *Scientific Reports*, 6, 1-8.
- WILLIAMS, E. M., GORDON, A. D. & RICHMOND, B. G. 2010. Upper limb kinematics and the role of the wrist during stone tool production. *American Journal of Physical Anthropology*, 143, 134-45.
- WILLIAMS, E. M., GORDON, A. D. & RICHMOND, B. G. 2012. Hand pressure distribution during Oldowan stone tool production. *Journal of Human Evolution*, 62, 520-532.
- WILLIAMS, E. M., GORDON, A. D. & RICHMOND, B. G. 2014. Biomechanical strategies for accuracy and force generation during stone tool production. *Journal of Human Evolution*, 72, 52-63.
- WILLIAMS, S. A., GARCIA-MARTINEZ, D., MEYER, M. R., NALLA, S., SCHMID, P., HAWKS, J., CHURCHILL, S. E., BERGER, L. R. & BASTIR, M. 2016. The axial skeleton and scaling of the trunk in *Homo naledi*. *American Journal of Physical Anthropology*, 159, 335-336.
- WOLFE, S. W., CRISCO, J. J., ORR, C. M. & MARZKE, M. W. 2006. The dart-throwing motion of the wrist: Is it unique to humans? *Journal of Hand Surgery (American Volume)*, 31, 1429-1437.
- WOLPOFF, M. H. 1996. *Human Evolution*, New York, Knopf.

- WOO, S. L.-Y., MAYNARD, J. & BUTLER, D. 1988. Ligament, tendon, and joint capsule insertions to bone. *In*: WOO, S. L.-Y. & BUCKWALTER, J. A. (eds.) *Injury and Repair of the Musculoskeletal Soft Tissues*. Illinois, IL: American Academy of Orthopaedic Surgeons.
- WOO, S. L., KUEI, S. C., AMIEL, D., GOMEZ, M. A., HAYES, W. C., WHITE, F. C. & AKESON, W. H. 1981. The effect of prolonged physical training on the properties of long bone: A study of Wolff's Law. *Journal of Bone and Joint Surgery (America)*, 63, 780-787.
- WOOD, B. & CONSTANTINO, P. 2007. *Paranthropus boisei*: Fifty years of evidence and analysis. *Yearbook of Physical Anthropology*, 50, 106-132.
- WOOD, B. A. 1974. Olduvai Bed I post-cranial fossils: A reassessment. *Journal of Human Evolution*, 3, 373-378.
- WOOD, B. A. 1991. *Koobi Fora Research Project: Hominid Cranial Remains*, Oxford, Clarendon Press.
- WOOD, J. W., MILNER, G. R., HARPENDING, H. C., WEISS, K. M., COHEN, M. N., EISENBERG, L. E., HUTCHINSON, D. L., JANKAUSKAS, R., CESNYS, G., ČESNYS, G., KATZENBERG, M. A., LUKACS, J. R., MCGRATH, J. W., ROTH, E. A., UBELAKER, D. H. & WILKINSON, R. G. 1992. The Osteological Paradox: Problems of inferring prehistoric health from skeletal samples [and Comments and Reply]. *Current Anthropology*, 33, 343-370.
- WYNN, T., HERNANDEZ-AGUILAR, R. A., MARCHANT, L. F. & MCGREW, W. C. 2011. "An ape's view of the Oldowan" revisited. *Evolutionary Anthropology: Issues, News, and Reviews*, 20, 181-197.
- ZUMWALT, A. 2005. A new method for quantifying the complexity of muscle attachment sites. *The Anatomical Record Part B: The New Anatomist*, 286B, 21-28.
- ZUMWALT, A. 2006. The effect of endurance exercise on the morphology of muscle attachment sites. *Journal of Experimental Biology*, 209, 444-454.
- ZUMWALT, A., RUFF, C. & WILCZAK, C. 2000. Primate muscle insertions: what does size tell you? (Abstract). *American Journal of Physical Anthropology*, 30, 331.

APPENDICES

APPENDIX 1: GLOSSARY OF TERMS

A glossary of anatomical terms and their definitions that appear in this dissertation.

Abduction	Drawing away from midline
Adduction	Drawing toward the midline
Anterior	Situated before or in front of (also Ventral)
Aponeurosis	Layers of flat broad tendons, very sparingly supplied with blood vessels and nerves (pl. aponeuroses). The Latissimus dorsi, for instance, arises from a broad aponeurosis that has its origin at the spinous processes of the T7-L5 vertebrae and the iliac crest.
Articulation	Connection between bones
Bipennate	Muscles consisting of a central tendon on which two rows of obliquely orientated fibres converge. Bipennate muscles are shaped similarly to a feather. (e.g. Rectus femoris)
Caudal	Below; farther from the head (also inferior)
Convergent	Muscle whose fibres are distributed over a broad origin but converge at one common insertion site (e.g. Pectoralis major)

Cranial	Upper; nearer to the head (also Superior)
Distal	Farthest from the axial skeleton (antonym to Proximal)
Dorsal	Toward the rear, back (also Posterior)
Enteseal development	A spectrum of normal (i.e. non-pathological) osseous changes at the site of attachment for a muscle or ligament (cf. Hawkey and Merbs, 1995). They are the physiological responses of the bone to mechanical loading and the transmission of forces during movement by the muscle or ligament which in turn engender a bony response at the enthesis. The extent of this response (i.e. degree of development) varies between individuals resulting in different morphologies that occur across a spectrum of expression. This is unlike enthesopathies which are either present or absent. Used synonymously in this dissertation with “enteseal complexity”.
Enteseal robusticity	See Enteseal development. “Enteseal robusticity” is occasionally and confusingly used in the bioarchaeological literature to denote enteseal <i>rugosity</i> or development. Robusticity in biology generally or morphology specifically refers to a pattern of generalised skeletal strength relative to a mechanically relevant measure of body size
Enthesis	The site of attachment, either origin or insertion, between muscle, tendon, or ligament and bone (pl. entheses). Entheses can be recognised on skeletal elements as irregularities in the

bone surface ranging from rugosity to marked ridges or grooves. They may also appear completely smooth and indistinguishable from the surrounding non-insertion bone depending on the degree of development (see Entheseal development). There are two types of entheses: fibrous and fibrocartilaginous.

Enthesopathy

Any pathological change/s to the appearance or biochemistry of an enthesis arising through the work of an abnormal condition. The aetiology of these changes may include trauma, hormonal, degenerative/age-related, genetic, disease, or dietary factors. This is the most common term in the clinical literature used for the description of these changes. Osseous markers of enthesopathy include enthesophytes or eroded areas and are characterised as a binary state. That is, unlike enthesal development/robusticity, enthesopathies are either present or absent and do not occur across a continuum of development (cf. Mariotti et al., 2007).

Enthesophyte

Pathological bony projections at an enthesis. They are differentiated from osteophytes, which are abnormal bony projections in joint spaces

Extension

Straightening

Fascia

Dense regular connective tissue that attach, stabilise, enclose, and separate muscles and other internal organs (pl. fasciae).

Fasciae are classified according to their anatomical location and function into three categories: superficial, deep (muscle), or visceral fascia.

Fascicle perimysium	A bundle of skeletal muscle fibres encapsulated by
Flexion	Bending or angulation
Fibrous enthesis	An enthesis where the tendon or ligament directly attaches to the bone
Fibrocartilaginous	An enthesis with an interface characterised by four transition zones: 1. A tendinous area with longitudinally oriented fibroblasts and a parallel arrangement of collagen fibres; 2. Fibrocartilaginous region where the structure of the cells changes to chondrocytes; 3. The “tidemark” or the transition from cartilaginous to calcified fibrocartilage; 4. Bone
Foramen	A small opening, orifice, or perforation (pl. foramina). Foramina in skeletal anatomy allow for the passage of muscles, nerves, arteries, veins, or other structures to one part of the body to another
Fossa	Shallow depression (pl. fossae)
Frontal	Vertical; at right angles to sagittal (also Coronal)
Fusiform	Spindle-shaped muscles with fibres that lay parallel to the length of the muscle (e.g. Pronator teres)

Head (of bone)	Enlarged round end of a long bone/knob generally located proximally
Inferior	Below; farther from the head (also Caudal)
Insertion	The (generally distal) area of attachment of a muscle to the bone, tendon, or other connective tissue that it moves by muscular contraction
Lateral	Farthest from the midline (antonym to Medial)
Ligament	Dense regular connective tissue which attaches bone to bone, and serves to hold structures together and keep them stable
Margin	Border
Medial	Nearer to midline (antonym to Lateral)
Midline	The imaginary line dividing the body into left and right sides
Multipennate	Muscles whose fibres are oriented at multiple angles along the force-generating axis (e.g. the Deltoid muscle)
MSM	Musculoskeletal stress markers. This term appears in the bioarchaeological literature to describe activity-related changes to entheses in archaeological populations
Neck (of bone)	Constriction of bone near the head
Origin	The site on the bone, typically proximal, from which the muscle arises. It generally has greater mass and is more stable during a contraction than the insertion site.

Pennate	Muscles whose fibres are arranged obliquely to the force-generating axis (pennation angle). They usually insert into a central tendon
Posterior	Toward the rear, back (also Dorsal)
Proximal	Nearest to the axial skeleton (antonym to Distal)
Rugosity	The quality of being rugose; roughness (see also Enteseal Robusticity)
Sagittal	Vertical plane or section dividing body into right and left (also Midline)
Superficial	Closer to the surface
Superior	Upper; nearer to the head (also Cranial)
Tendon	Dense regular connective tissue that connects muscle to bone
Transverse	At right angles to long axis, perpendicular to the sagittal and frontal planes (also horizontal)
Tubercle	Small bump
Unipennate	A pennate muscle which fibres are arranged all to one side of a central tendon, similar in shape to a feather quill (e.g. M. palmar interosseous)

APPENDIX 2: FRACTAL DIMENSION VALUES

Table containing fractal dimension (D) values for fossil entheses. Category O/I indicates whether an enthesis is an origin or an insertion, followed by axis, D -value, and standard deviation (s.d.) as calculated by Benoit fractal analysis software.

Specimen No.	Species	Institution	Element	Siding	Enthesis	O/I	Axis	D	s.d.
STW 113	Au. africanus	WITS	Ulna	Left	Brachialis	I	distal-x-axis	1.94	0.006
STW 113	Au. africanus	WITS	Ulna	Left	Brachialis	I	lat-y-axis	1.95	0.005
STW 113	Au. africanus	WITS	Ulna	Left	Brachialis	I	med-y-axis	1.95	0.005
STW 113	Au. africanus	WITS	Ulna	Left	Brachialis	I	prox-x-axis	1.91	0.010
STW 113	Au. africanus	WITS	Ulna	Left	Brachialis	I	x-axis	1.91	0.007
STW 113	Au. africanus	WITS	Ulna	Left	Brachialis	I	y-axis	1.93	0.006
STW 113	Au. africanus	WITS	Ulna	Left	Triceps brachii	I	med-y-axis	1.93	0.002
STW 113	Au. africanus	WITS	Ulna	Left	Triceps brachii	I	y-axis	1.94	0.003
STW 113	Au. africanus	WITS	Ulna	Left	Triceps brachii	I	distal-x-axis	1.93	0.003
STW 113	Au. africanus	WITS	Ulna	Left	Triceps brachii	I	lat-y-axis	1.91	0.006
STW 113	Au. africanus	WITS	Ulna	Left	Triceps brachii	I	prox-x-axis	1.94	0.010
STW 113	Au. africanus	WITS	Ulna	Left	Triceps brachii	I	x-axis	1.94	0.004
STW 328	Au. africanus	WITS	Humerus	Right	Med. epicondylar ridge	O	distal-x-axis	1.91	0.003
STW 328	Au. africanus	WITS	Humerus	Right	Med. epicondylar ridge	O	lat-y-axis	1.95	0.002
STW 328	Au. africanus	WITS	Humerus	Right	Med. epicondylar ridge	O	med-y-axis	1.95	0.007
STW 328	Au. africanus	WITS	Humerus	Right	Med. epicondylar ridge	O	prox-x-axis	1.92	0.004
STW 328	Au. africanus	WITS	Humerus	Right	Med. epicondylar ridge	O	x-axis	1.90	0.003
STW 328	Au. africanus	WITS	Humerus	Right	Med. epicondylar ridge	O	y-axis	1.94	0.003
STW 339	Au. africanus	WITS	Humerus	Right	Supraspinatus	I	distal-x-axis	1.94	0.006
STW 339	Au. africanus	WITS	Humerus	Right	Supraspinatus	I	med-y-axis	1.93	0.015
STW 339	Au. africanus	WITS	Humerus	Right	Supraspinatus	I	prox-x-axis	1.94	0.006
STW 339	Au. africanus	WITS	Humerus	Right	Supraspinatus	I	x-axis	1.92	0.008

STW 339	Au. africanus	WITS	Humerus	Right	Supraspinatus	I	y-axis	1.93	0.006
STW 339	Au. africanus	WITS	Humerus	Right	Supraspinatus	I	lat-y-axis	1.92	0.002
STW 380	Au. africanus	WITS	Ulna	Right	Brachialis	I	distal-x-axis	1.91	0.004
STW 380	Au. africanus	WITS	Ulna	Right	Brachialis	I	lat-y-axis	1.94	0.011
STW 380	Au. africanus	WITS	Ulna	Right	Brachialis	I	med-y-axis	1.95	0.003
STW 380	Au. africanus	WITS	Ulna	Right	Brachialis	I	prox-x-axis	1.90	0.007
STW 380	Au. africanus	WITS	Ulna	Right	Brachialis	I	x-axis	1.92	0.007
STW 380	Au. africanus	WITS	Ulna	Right	Brachialis	I	y-axis	1.94	0.013
STW 380	Au. africanus	WITS	Ulna	Right	Triceps brachii	I	med-y-axis	1.95	0.007
STW 380	Au. africanus	WITS	Ulna	Right	Triceps brachii	I	prox-x-axis	1.92	0.003
STW 380	Au. africanus	WITS	Ulna	Right	Triceps brachii	I	distal-x-axis	1.94	0.011
STW 380	Au. africanus	WITS	Ulna	Right	Triceps brachii	I	lat-y-axis	1.93	0.009
STW 380	Au. africanus	WITS	Ulna	Right	Triceps brachii	I	x-axis	1.94	0.006
STW 380	Au. africanus	WITS	Ulna	Right	Triceps brachii	I	y-axis	1.94	0.040
STW 398	Au. africanus	WITS	Ulna	Left	Triceps brachii	I	distal-x-axis	1.92	0.006
STW 398	Au. africanus	WITS	Ulna	Left	Triceps brachii	I	lat-y-axis	1.92	0.008
STW 398	Au. africanus	WITS	Ulna	Left	Triceps brachii	I	med-y-axis	1.91	0.012
STW 398	Au. africanus	WITS	Ulna	Left	Triceps brachii	I	prox-x-axis	1.92	0.005
STW 398	Au. africanus	WITS	Ulna	Left	Triceps brachii	I	x-axis	1.89	0.009
STW 398	Au. africanus	WITS	Ulna	Left	Triceps brachii	I	y-axis	1.92	0.009
STW 528	Au. africanus	WITS	Radius	Left	Biceps brachii	I	distal-x-axis	1.90	0.007
STW 528	Au. africanus	WITS	Radius	Left	Biceps brachii	I	lat-y-axis	1.90	0.006
STW 528	Au. africanus	WITS	Radius	Left	Biceps brachii	I	med-y-axis	1.90	0.006
STW 528	Au. africanus	WITS	Radius	Left	Biceps brachii	I	x-axis	1.91	0.005
STW 528	Au. africanus	WITS	Radius	Left	Biceps brachii	I	y-axis	1.92	0.011
STW 528	Au. africanus	WITS	Radius	Left	Biceps brachii	I	prox-x-axis	1.90	0.005
STW 571	Au. africanus	WITS	Ulna	Right	Brachialis	I	distal-x-axis	1.93	0.007
STW 571	Au. africanus	WITS	Ulna	Right	Brachialis	I	lat-y-axis	1.94	0.013

STW 571	Au. africanus	WITS	Ulna	Right	Brachialis	I	med-y-axis	1.94	0.003
STW 571	Au. africanus	WITS	Ulna	Right	Brachialis	I	prox-x-axis	1.93	0.006
STW 571	Au. africanus	WITS	Ulna	Right	Brachialis	I	x-axis	1.94	0.009
STW 571	Au. africanus	WITS	Ulna	Right	Brachialis	I	y-axis	1.94	0.006
STW 571	Au. africanus	WITS	Humerus	Left	Subscapularis	I	distal-x-axis	1.91	0.005
STW 571	Au. africanus	WITS	Humerus	Left	Subscapularis	I	lat-y-axis	1.94	0.009
STW 571	Au. africanus	WITS	Humerus	Left	Subscapularis	I	med-y-axis	1.94	0.006
STW 571	Au. africanus	WITS	Humerus	Left	Subscapularis	I	prox-x-axis	1.92	0.005
STW 571	Au. africanus	WITS	Humerus	Left	Subscapularis	I	x-axis	1.93	0.015
STW 571	Au. africanus	WITS	Humerus	Left	Subscapularis	I	y-axis	1.93	0.003
STW 150	Au. africanus	WITS	Humerus	Left	Lat. epicondylar ridge	O	distal-x-axis	1.91	0.006
STW 150	Au. africanus	WITS	Humerus	Left	Lat. epicondylar ridge	O	lat-y-axis	1.94	0.010
STW 150	Au. africanus	WITS	Humerus	Left	Lat. epicondylar ridge	O	med-y-axis	1.93	0.008
STW 150	Au. africanus	WITS	Humerus	Left	Lat. epicondylar ridge	O	prox-x-axis	1.94	0.005
STW 150	Au. africanus	WITS	Humerus	Left	Lat. epicondylar ridge	O	x-axis	1.91	0.005
STW 150	Au. africanus	WITS	Humerus	Left	Lat. epicondylar ridge	O	y-axis	1.93	0.008
STW 150	Au. africanus	WITS	Humerus	Left	Med.epicondylar ridge	O	distal-x-axis	1.93	0.002
STW 150	Au. africanus	WITS	Humerus	Left	Med.epicondylar ridge	O	lat-y-axis	1.95	0.005
STW 150	Au. africanus	WITS	Humerus	Left	Med.epicondylar ridge	O	med-y-axis	1.94	0.006
STW 150	Au. africanus	WITS	Humerus	Left	Med.epicondylar ridge	O	prox-x-axis	1.93	0.007
STW 150	Au. africanus	WITS	Humerus	Left	Med.epicondylar ridge	O	x-axis	1.93	0.003
STW 150	Au. africanus	WITS	Humerus	Left	Med.epicondylar ridge	O	y-axis	1.93	0.009
STW 431	Au. africanus	WITS	Radius	Right	Biceps brachii	I	distal-x-axis	1.89	0.008
STW 431	Au. africanus	WITS	Radius	Right	Biceps brachii	I	lat-y-axis	1.91	0.006
STW 431	Au. africanus	WITS	Radius	Right	Biceps brachii	I	med-y-axis	1.92	0.006
STW 431	Au. africanus	WITS	Radius	Right	Biceps brachii	I	prox-x-axis	1.91	0.006
STW 431	Au. africanus	WITS	Radius	Right	Biceps brachii	I	x-axis	1.91	0.006
STW 431	Au. africanus	WITS	Radius	Right	Biceps brachii	I	y-axis	1.94	0.002

STW 432a	Au. africanus	WITS	Ulna	Right	Brachialis	I	distal-x-axis	1.90	0.006
STW 432a	Au. africanus	WITS	Ulna	Right	Brachialis	I	lat-y-axis	1.94	0.004
STW 432a	Au. africanus	WITS	Ulna	Right	Brachialis	I	med-y-axis	1.92	0.004
STW 432a	Au. africanus	WITS	Ulna	Right	Brachialis	I	prox-x-axis	1.89	0.008
STW 432a	Au. africanus	WITS	Ulna	Right	Brachialis	I	x-axis	1.94	0.011
STW 432a	Au. africanus	WITS	Ulna	Right	Brachialis	I	y-axis	1.92	0.004
STW 432a	Au. africanus	WITS	Ulna	Right	Triceps brachii	I	y-axis	1.92	0.010
STW 432a	Au. africanus	WITS	Ulna	Right	Triceps brachii	I	distal-x-axis	1.92	0.007
STW 432a	Au. africanus	WITS	Ulna	Right	Triceps brachii	I	lat-y-axis	1.95	0.006
STW 432a	Au. africanus	WITS	Ulna	Right	Triceps brachii	I	prox-x-axis	1.93	0.004
STW 432a	Au. africanus	WITS	Ulna	Right	Triceps brachii	I	x-axis	1.93	0.009
STW 432a	Au. africanus	WITS	Ulna	Right	Triceps brachii	I	med-y-axis	1.93	0.008
STW 433	Au. africanus	WITS	Humerus	Right	Lat. epicondylar ridge	O	distal-x-axis	1.88	0.004
STW 433	Au. africanus	WITS	Humerus	Right	Lat. epicondylar ridge	O	lat-y-axis	1.93	0.001
STW 433	Au. africanus	WITS	Humerus	Right	Lat. epicondylar ridge	O	med-y-axis	1.95	0.005
STW 433	Au. africanus	WITS	Humerus	Right	Lat. epicondylar ridge	O	prox-x-axis	1.90	0.013
STW 433	Au. africanus	WITS	Humerus	Right	Lat. epicondylar ridge	O	x-axis	1.91	0.003
STW 433	Au. africanus	WITS	Humerus	Right	Lat. epicondylar ridge	O	y-axis	1.94	0.004
STW 433	Au. africanus	WITS	Humerus	Right	Lateral epicondyle	O	distal-x-axis	1.88	0.010
STW 433	Au. africanus	WITS	Humerus	Right	Lateral epicondyle	O	med-y-axis	1.90	0.010
STW 433	Au. africanus	WITS	Humerus	Right	Lateral epicondyle	O	prox-x-axis	1.91	0.010
STW 433	Au. africanus	WITS	Humerus	Right	Lateral epicondyle	O	x-axis	1.92	0.003
STW 433	Au. africanus	WITS	Humerus	Right	Lateral epicondyle	O	y-axis	1.91	0.005
STW 433	Au. africanus	WITS	Humerus	Right	Lateral epicondyle	O	lat-y-axis	1.91	0.009
STW 433	Au. africanus	WITS	Humerus	Right	Medial epicondyle	O	distal-x-axis	1.89	0.009
STW 433	Au. africanus	WITS	Humerus	Right	Medial epicondyle	O	prox-x-axis	1.90	0.007
STW 433	Au. africanus	WITS	Humerus	Right	Medial epicondyle	O	x-axis	1.89	0.010
STW 433	Au. africanus	WITS	Humerus	Right	Medial epicondyle	O	y-axis	1.90	0.010

STW 433	Au. africanus	WITS	Humerus	Right	Medial epicondyle	O	lat-y-axis	1.92	0.005
STW 433	Au. africanus	WITS	Humerus	Right	Medial epicondyle	O	med-y-axis	1.94	0.007
STW 434	Au. africanus	WITS	Scapula	Right	Teres major	O	distal-x-axis	1.90	0.004
STW 434	Au. africanus	WITS	Scapula	Right	Teres major	O	lat-y-axis	1.91	0.008
STW 434	Au. africanus	WITS	Scapula	Right	Teres major	O	med-y-axis	1.91	0.007
STW 434	Au. africanus	WITS	Scapula	Right	Teres major	O	prox-x-axis	1.92	0.004
STW 434	Au. africanus	WITS	Scapula	Right	Teres major	O	x-axis	1.91	0.007
STW 434	Au. africanus	WITS	Scapula	Right	Teres major	O	y-axis	1.90	0.007
UW 88-38	Au. sediba	WITS	Clavicle	Right	Deltoid	O	distal-x-axis	1.92	0.004
UW 88-38	Au. sediba	WITS	Clavicle	Right	Deltoid	O	lat-y-axis	1.89	0.002
UW 88-38	Au. sediba	WITS	Clavicle	Right	Deltoid	O	med-y-axis	1.89	0.002
UW 88-38	Au. sediba	WITS	Clavicle	Right	Deltoid	O	prox-x-axis	1.91	0.007
UW 88-38	Au. sediba	WITS	Clavicle	Right	Deltoid	O	x-axis	1.92	0.005
UW 88-38	Au. sediba	WITS	Clavicle	Right	Deltoid	O	y-axis	1.87	0.003
UW 88-57	Au. sediba	WITS	Humerus	Right	Infraspinatus	I	lat-y-axis	1.88	0.011
UW 88-57	Au. sediba	WITS	Humerus	Right	Infraspinatus	I	med-y-axis	1.87	0.009
UW 88-57	Au. sediba	WITS	Humerus	Right	Infraspinatus	I	prox-x-axis	1.91	0.002
UW 88-57	Au. sediba	WITS	Humerus	Right	Infraspinatus	I	x-axis	1.91	0.006
UW 88-57	Au. sediba	WITS	Humerus	Right	Infraspinatus	I	y-axis	1.87	0.003
UW 88-57	Au. sediba	WITS	Humerus	Right	Infraspinatus	I	distal-x-axis	1.90	0.007
UW 88-57	Au. sediba	WITS	Humerus	Right	Lat. epicondylar ridge	O	ant-y-axis	1.91	0.005
UW 88-57	Au. sediba	WITS	Humerus	Right	Lat. epicondylar ridge	O	distal-x-axis	1.87	0.004
UW 88-57	Au. sediba	WITS	Humerus	Right	Lat. epicondylar ridge	O	post-y-axis	1.93	0.008
UW 88-57	Au. sediba	WITS	Humerus	Right	Lat. epicondylar ridge	O	prox-x-axis	1.89	0.002
UW 88-57	Au. sediba	WITS	Humerus	Right	Lat. epicondylar ridge	O	x-axis	1.89	0.009
UW 88-57	Au. sediba	WITS	Humerus	Right	Lat. epicondylar ridge	O	y-axis	1.93	0.010
UW 88-57	Au. sediba	WITS	Humerus	Right	Lateral epicondyle	O	ant-y-axis	1.89	0.004
UW 88-57	Au. sediba	WITS	Humerus	Right	Lateral epicondyle	O	distal-x-axis	1.88	0.004

UW 88-57	Au. sediba	WITS	Humerus	Right	Lateral epicondyle	O	post-y-axis	1.88	0.010
UW 88-57	Au. sediba	WITS	Humerus	Right	Lateral epicondyle	O	prox-x-axis	1.86	0.003
UW 88-57	Au. sediba	WITS	Humerus	Right	Lateral epicondyle	O	x-axis	1.87	0.007
UW 88-57	Au. sediba	WITS	Humerus	Right	Lateral epicondyle	O	y-axis	1.89	0.006
UW 88-57	Au. sediba	WITS	Humerus	Right	Latissimus dorsi	I	distal-x-axis	1.86	0.004
UW 88-57	Au. sediba	WITS	Humerus	Right	Latissimus dorsi	I	lat-y-axis	1.94	0.007
UW 88-57	Au. sediba	WITS	Humerus	Right	Latissimus dorsi	I	med-y-axis	1.92	0.003
UW 88-57	Au. sediba	WITS	Humerus	Right	Latissimus dorsi	I	prox-x-axis	1.88	0.002
UW 88-57	Au. sediba	WITS	Humerus	Right	Latissimus dorsi	I	x-axis	1.88	0.002
UW 88-57	Au. sediba	WITS	Humerus	Right	Latissimus dorsi	I	y-axis	1.91	0.006
UW 88-57	Au. sediba	WITS	Humerus	Right	Medial epicondyle	O	ant-y-axis	1.87	0.005
UW 88-57	Au. sediba	WITS	Humerus	Right	Medial epicondyle	O	distal-x-axis	1.86	0.002
UW 88-57	Au. sediba	WITS	Humerus	Right	Medial epicondyle	O	post-y-axis	1.90	0.005
UW 88-57	Au. sediba	WITS	Humerus	Right	Medial epicondyle	O	prox-x-axis	1.88	0.003
UW 88-57	Au. sediba	WITS	Humerus	Right	Medial epicondyle	O	x-axis	1.92	0.006
UW 88-57	Au. sediba	WITS	Humerus	Right	Medial epicondyle	O	y-axis	1.90	0.005
UW 88-57	Au. sediba	WITS	Humerus	Right	Subscapularis	I	distal-x-axis	1.89	0.010
UW 88-57	Au. sediba	WITS	Humerus	Right	Subscapularis	I	lat-y-axis	1.90	0.009
UW 88-57	Au. sediba	WITS	Humerus	Right	Subscapularis	I	med-y-axis	1.92	0.004
UW 88-57	Au. sediba	WITS	Humerus	Right	Subscapularis	I	prox-x-axis	1.87	0.003
UW 88-57	Au. sediba	WITS	Humerus	Right	Subscapularis	I	x-axis	1.86	0.008
UW 88-57	Au. sediba	WITS	Humerus	Right	Subscapularis	I	y-axis	1.90	0.003
UW 88-57	Au. sediba	WITS	Humerus	Right	Supraspinatus	I	distal-x-axis	1.91	0.003
UW 88-57	Au. sediba	WITS	Humerus	Right	Supraspinatus	I	lat-y-axis	1.87	0.008
UW 88-57	Au. sediba	WITS	Humerus	Right	Supraspinatus	I	med-y-axis	1.89	0.004
UW 88-57	Au. sediba	WITS	Humerus	Right	Supraspinatus	I	x-axis	1.89	0.010
UW 88-57	Au. sediba	WITS	Humerus	Right	Supraspinatus	I	y-axis	1.88	0.004
UW 88-57	Au. sediba	WITS	Humerus	Right	Supraspinatus	I	prox-x-axis	1.89	0.012

UW 88-62	Au. sediba	WITS	Ulna	Right	Brachialis	I	distal-x-axis	1.89	0.007
UW 88-62	Au. sediba	WITS	Ulna	Right	Brachialis	I	lat-y-axis	1.94	0.004
UW 88-62	Au. sediba	WITS	Ulna	Right	Brachialis	I	med-y-axis	1.91	0.003
UW 88-62	Au. sediba	WITS	Ulna	Right	Brachialis	I	prox-x-axis	1.89	0.005
UW 88-62	Au. sediba	WITS	Ulna	Right	Brachialis	I	x-axis	1.89	0.009
UW 88-62	Au. sediba	WITS	Ulna	Right	Brachialis	I	y-axis	1.88	0.011
UW 88-62	Au. sediba	WITS	Ulna	Right	Triceps brachii	I	prox-x-axis	1.89	0.013
UW 88-62	Au. sediba	WITS	Ulna	Right	Triceps brachii	I	med-y-axis	1.89	0.010
UW 88-62	Au. sediba	WITS	Ulna	Right	Triceps brachii	I	distal-x-axis	1.88	0.005
UW 88-62	Au. sediba	WITS	Ulna	Right	Triceps brachii	I	x-axis	1.89	0.010
UW 88-62	Au. sediba	WITS	Ulna	Right	Triceps brachii	I	y-axis	1.90	0.007
UW 88-62	Au. sediba	WITS	Ulna	Right	Triceps brachii	I	lat-y-axis	1.89	0.013
UW 88-101	Au. sediba	WITS	Humerus	Left	Infraspinatus	I	distal-x-axis	1.89	0.001
UW 88-101	Au. sediba	WITS	Humerus	Left	Infraspinatus	I	lat-y-axis	1.91	0.009
UW 88-101	Au. sediba	WITS	Humerus	Left	Infraspinatus	I	med-y-axis	1.90	0.011
UW 88-101	Au. sediba	WITS	Humerus	Left	Infraspinatus	I	prox-x-axis	1.87	0.009
UW 88-101	Au. sediba	WITS	Humerus	Left	Infraspinatus	I	x-axis	1.89	0.006
UW 88-101	Au. sediba	WITS	Humerus	Left	Infraspinatus	I	y-axis	1.91	0.008
UW 88-101	Au. sediba	WITS	Humerus	Left	Subscapularis	I	distal-x-axis	1.87	0.002
UW 88-101	Au. sediba	WITS	Humerus	Left	Subscapularis	I	lat-y-axis	1.89	0.007
UW 88-101	Au. sediba	WITS	Humerus	Left	Subscapularis	I	med-y-axis	1.89	0.003
UW 88-101	Au. sediba	WITS	Humerus	Left	Subscapularis	I	prox-x-axis	1.87	0.005
UW 88-101	Au. sediba	WITS	Humerus	Left	Subscapularis	I	x-axis	1.89	0.005
UW 88-101	Au. sediba	WITS	Humerus	Left	Subscapularis	I	y-axis	1.89	0.008
UW 88-101	Au. sediba	WITS	Humerus	Left	Supraspinatus	I	distal-x-axis	1.87	0.003
UW 88-101	Au. sediba	WITS	Humerus	Left	Supraspinatus	I	lat-y-axis	1.90	0.005
UW 88-101	Au. sediba	WITS	Humerus	Left	Supraspinatus	I	med-y-axis	1.87	0.005
UW 88-101	Au. sediba	WITS	Humerus	Left	Supraspinatus	I	prox-x-axis	1.87	0.005

UW 88-101	Au. sediba	WITS	Humerus	Left	Supraspinatus	I	x-axis	1.89	0.004
UW 88-101	Au. sediba	WITS	Humerus	Left	Supraspinatus	I	y-axis	1.89	0.004
AL 288-1m	Au. afarensis	NME	Humerus	Right	Lat. epicondylar ridge	O	lat-y-axis	1.93	0.003
AL 288-1m	Au. afarensis	NME	Humerus	Right	Lat. epicondylar ridge	O	distal-x-axis	1.90	0.002
AL 288-1m	Au. afarensis	NME	Humerus	Right	Lat. epicondylar ridge	O	med-y-axis	1.95	0.005
AL 288-1m	Au. afarensis	NME	Humerus	Right	Lat. epicondylar ridge	O	prox-x-axis	1.92	0.007
AL 288-1m	Au. afarensis	NME	Humerus	Right	Lat. epicondylar ridge	O	x-axis	1.93	0.009
AL 288-1m	Au. afarensis	NME	Humerus	Right	Lat. epicondylar ridge	O	y-axis	1.93	0.004
AL 288-1m	Au. afarensis	NME	Humerus	Right	Subscapularis	I	distal-x-axis	1.90	0.004
AL 288-1m	Au. afarensis	NME	Humerus	Right	Subscapularis	I	lat-y-axis	1.92	0.006
AL 288-1m	Au. afarensis	NME	Humerus	Right	Subscapularis	I	med-y-axis	1.91	0.010
AL 288-1m	Au. afarensis	NME	Humerus	Right	Subscapularis	I	prox-x-axis	1.91	0.006
AL 288-1m	Au. afarensis	NME	Humerus	Right	Subscapularis	I	x-axis	1.92	0.003
AL 288-1m	Au. afarensis	NME	Humerus	Right	Subscapularis	I	y-axis	1.92	0.003
AL 288-1n	Au. afarensis	NME	Ulna	Right	Brachialis	I	distal-x-axis	1.91	0.007
AL 288-1n	Au. afarensis	NME	Ulna	Right	Brachialis	I	lat-y-axis	1.92	0.008
AL 288-1n	Au. afarensis	NME	Ulna	Right	Brachialis	I	med-y-axis	1.93	0.007
AL 288-1n	Au. afarensis	NME	Ulna	Right	Brachialis	I	prox-x-axis	1.88	0.007
AL 288-1n	Au. afarensis	NME	Ulna	Right	Brachialis	I	x-axis	1.88	0.009
AL 288-1n	Au. afarensis	NME	Ulna	Right	Brachialis	I	y-axis	1.93	0.007
AL 288-1n	Au. afarensis	NME	Ulna	Right	Triceps brachii	I	y-axis	1.92	0.006
AL 288-1n	Au. afarensis	NME	Ulna	Right	Triceps brachii	I	med-y-axis	1.92	0.004
AL 288-1n	Au. afarensis	NME	Ulna	Right	Triceps brachii	I	distal-x-axis	1.91	0.003
AL 288-1n	Au. afarensis	NME	Ulna	Right	Triceps brachii	I	lat-y-axis	1.92	0.002
AL 288-1n	Au. afarensis	NME	Ulna	Right	Triceps brachii	I	prox-x-axis	1.92	0.004
AL 288-1n	Au. afarensis	NME	Ulna	Right	Triceps brachii	I	x-axis	1.92	0.004
AL 288-1p	Au. afarensis	NME	Radius	Right	Biceps brachii	I	distal-x-axis	1.89	0.013
AL 288-1p	Au. afarensis	NME	Radius	Right	Biceps brachii	I	lat-y-axis	1.91	0.005

AL 288-1p	Au. afarensis	NME	Radius	Right	Biceps brachii	I	med-y-axis	1.93	0.009
AL 288-1p	Au. afarensis	NME	Radius	Right	Biceps brachii	I	prox-x-axis	1.89	0.009
AL 288-1p	Au. afarensis	NME	Radius	Right	Biceps brachii	I	x-axis	1.90	0.007
AL 288-1p	Au. afarensis	NME	Radius	Right	Biceps brachii	I	y-axis	1.91	0.008
AL 288-1r	Au. afarensis	NME	Humerus	Left	Lateral epicondyle	O	distal-x-axis	1.92	0.002
AL 288-1r	Au. afarensis	NME	Humerus	Left	Lateral epicondyle	O	lat-y-axis	1.91	0.012
AL 288-1r	Au. afarensis	NME	Humerus	Left	Lateral epicondyle	O	med-y-axis	1.89	0.010
AL 288-1r	Au. afarensis	NME	Humerus	Left	Lateral epicondyle	O	prox-x-axis	1.89	0.005
AL 288-1r	Au. afarensis	NME	Humerus	Left	Lateral epicondyle	O	x-axis	1.91	0.011
AL 288-1r	Au. afarensis	NME	Humerus	Left	Lateral epicondyle	O	y-axis	1.93	0.004
AL 288-1r	Au. afarensis	NME	Humerus	Left	Pectoralis major	I	distal-x-axis	1.90	0.004
AL 288-1r	Au. afarensis	NME	Humerus	Left	Pectoralis major	I	lat-y-axis	1.92	0.006
AL 288-1r	Au. afarensis	NME	Humerus	Left	Pectoralis major	I	med-y-axis	1.92	0.004
AL 288-1r	Au. afarensis	NME	Humerus	Left	Pectoralis major	I	prox-x-axis	1.90	0.004
AL 288-1r	Au. afarensis	NME	Humerus	Left	Pectoralis major	I	x-axis	1.90	0.002
AL 288-1r	Au. afarensis	NME	Humerus	Left	Pectoralis major	I	y-axis	1.92	0.008
AL 288-1t	Au. afarensis	NME	Ulna	Left	Brachialis	I	med-y-axis	1.94	0.005
AL 288-1t	Au. afarensis	NME	Ulna	Left	Brachialis	I	distal-x-axis	1.93	0.003
AL 288-1t	Au. afarensis	NME	Ulna	Left	Brachialis	I	lat-y-axis	1.93	0.008
AL 288-1t	Au. afarensis	NME	Ulna	Left	Brachialis	I	prox-x-axis	1.92	0.005
AL 288-1t	Au. afarensis	NME	Ulna	Left	Brachialis	I	x-axis	1.89	0.011
AL 288-1t	Au. afarensis	NME	Ulna	Left	Brachialis	I	y-axis	1.93	0.006
AL 137-48a	Au. afarensis	NME	Humerus	Right	Medial epicondyle	O	prox-x-axis	1.88	0.012
AL 137-48a	Au. afarensis	NME	Humerus	Right	Medial epicondyle	O	ant-y-axis	1.88	0.009
AL 137-48a	Au. afarensis	NME	Humerus	Right	Medial epicondyle	O	distal-x-axis	1.90	0.009
AL 137-48a	Au. afarensis	NME	Humerus	Right	Medial epicondyle	O	post-y-axis	1.89	0.005
AL 137-48a	Au. afarensis	NME	Humerus	Right	Medial epicondyle	O	x-axis	1.90	0.004
AL 137-48a	Au. afarensis	NME	Humerus	Right	Medial epicondyle	O	y-axis	1.89	0.006

AL 322-1	Au. afarensis	NME	Humerus	Left	Lat. epicondylar ridge	O	post-y-axis	1.92	0.005
AL 322-1	Au. afarensis	NME	Humerus	Left	Lat. epicondylar ridge	O	distal-x-axis	1.91	0.002
AL 322-1	Au. afarensis	NME	Humerus	Left	Lat. epicondylar ridge	O	ant-y-axis	1.92	0.003
AL 322-1	Au. afarensis	NME	Humerus	Left	Lat. epicondylar ridge	O	prox-x-axis	1.88	0.003
AL 322-1	Au. afarensis	NME	Humerus	Left	Lat. epicondylar ridge	O	x-axis	1.89	0.004
AL 322-1	Au. afarensis	NME	Humerus	Left	Lat. epicondylar ridge	O	y-axis	1.92	0.006
AL 322-1	Au. afarensis	NME	Humerus	Left	Lateral epicondyle	O	ant-y-axis	1.93	0.006
AL 322-1	Au. afarensis	NME	Humerus	Left	Lateral epicondyle	O	distal-x-axis	1.88	0.003
AL 322-1	Au. afarensis	NME	Humerus	Left	Lateral epicondyle	O	post-y-axis	1.90	0.007
AL 322-1	Au. afarensis	NME	Humerus	Left	Lateral epicondyle	O	x-axis	1.88	0.007
AL 322-1	Au. afarensis	NME	Humerus	Left	Lateral epicondyle	O	y-axis	1.89	0.013
AL 322-1	Au. afarensis	NME	Humerus	Left	Lateral epicondyle	O	prox-x-axis	1.87	0.006
AL 322-1	Au. afarensis	NME	Humerus	Left	Medial epicondyle	O	post-y-axis	1.91	0.005
AL 322-1	Au. afarensis	NME	Humerus	Left	Medial epicondyle	O	ant-y-axis	1.90	0.007
AL 322-1	Au. afarensis	NME	Humerus	Left	Medial epicondyle	O	distal-x-axis	1.88	0.005
AL 322-1	Au. afarensis	NME	Humerus	Left	Medial epicondyle	O	prox-x-axis	1.88	0.011
AL 322-1	Au. afarensis	NME	Humerus	Left	Medial epicondyle	O	x-axis	1.91	0.005
AL 322-1	Au. afarensis	NME	Humerus	Left	Medial epicondyle	O	y-axis	1.90	0.009
AL 333-107	Au. afarensis	NME	Humerus	Right	Infraspinatus	I	x-axis	1.91	0.008
AL 333-107	Au. afarensis	NME	Humerus	Right	Infraspinatus	I	lat-y-axis	1.90	0.007
AL 333-107	Au. afarensis	NME	Humerus	Right	Infraspinatus	I	med-y-axis	1.91	0.004
AL 333-107	Au. afarensis	NME	Humerus	Right	Infraspinatus	I	prox-x-axis	1.92	0.009
AL 333-107	Au. afarensis	NME	Humerus	Right	Infraspinatus	I	y-axis	1.90	0.005
AL 333-107	Au. afarensis	NME	Humerus	Right	Infraspinatus	I	distal-x-axis	1.91	0.004
AL 333-109	Au. afarensis	NME	Humerus	Left	Deltoid	I	distal-x-axis	1.92	0.002
AL 333-109	Au. afarensis	NME	Humerus	Left	Deltoid	I	lat-y-axis	1.89	0.005
AL 333-109	Au. afarensis	NME	Humerus	Left	Deltoid	I	med-y-axis	1.90	0.003
AL 333-109	Au. afarensis	NME	Humerus	Left	Deltoid	I	prox-x-axis	1.91	0.003

AL 333-109	Au. afarensis	NME	Humerus	Left	Deltoid	I	y-axis	1.89	0.003
AL 333-109	Au. afarensis	NME	Humerus	Left	Deltoid	I	x-axis	1.91	0.003
AL 333-109	Au. afarensis	NME	Humerus	Left	Latissimus dorsi	I	distal-x-axis	1.89	0.005
AL 333-109	Au. afarensis	NME	Humerus	Left	Latissimus dorsi	I	lat-y-axis	1.93	0.003
AL 333-109	Au. afarensis	NME	Humerus	Left	Latissimus dorsi	I	med-y-axis	1.92	0.004
AL 333-109	Au. afarensis	NME	Humerus	Left	Latissimus dorsi	I	prox-x-axis	1.87	0.010
AL 333-109	Au. afarensis	NME	Humerus	Left	Latissimus dorsi	I	x-axis	1.89	0.005
AL 333-109	Au. afarensis	NME	Humerus	Left	Latissimus dorsi	I	y-axis	1.91	0.008
AL 333-109	Au. afarensis	NME	Humerus	Left	Pectoralis major	I	prox-x-axis	1.89	0.006
AL 333-109	Au. afarensis	NME	Humerus	Left	Pectoralis major	I	distal-x-axis	1.89	0.007
AL 333-109	Au. afarensis	NME	Humerus	Left	Pectoralis major	I	lat-y-axis	1.90	0.003
AL 333-109	Au. afarensis	NME	Humerus	Left	Pectoralis major	I	med-y-axis	1.89	0.007
AL 333-109	Au. afarensis	NME	Humerus	Left	Pectoralis major	I	y-axis	1.92	0.004
AL 333-109	Au. afarensis	NME	Humerus	Left	Pectoralis major	I	x-axis	1.90	0.007
AL 333W-36	Au. afarensis	NME	Ulna	Left	Brachialis	I	x-axis	1.89	0.003
AL 333W-36	Au. afarensis	NME	Ulna	Left	Brachialis	I	y-axis	1.91	0.005
AL 333W-36	Au. afarensis	NME	Ulna	Left	Brachialis	I	lat-y-axis	1.93	0.003
AL 333W-36	Au. afarensis	NME	Ulna	Left	Brachialis	I	med-y-axis	1.91	0.004
AL 333W-36	Au. afarensis	NME	Ulna	Left	Brachialis	I	distal-x-axis	1.92	0.007
AL 333W-36	Au. afarensis	NME	Ulna	Left	Brachialis	I	prox-x-axis	1.86	0.007
AL 333W-36	Au. afarensis	NME	Ulna	Left	Supinator	I	y-axis	1.91	0.005
AL 333W-36	Au. afarensis	NME	Ulna	Left	Supinator	I	post-y-axis	1.89	0.003
AL 333W-36	Au. afarensis	NME	Ulna	Left	Supinator	I	distal-x-axis	1.87	0.007
AL 333W-36	Au. afarensis	NME	Ulna	Left	Supinator	I	prox-x-axis	1.86	0.003
AL 333W-36	Au. afarensis	NME	Ulna	Left	Supinator	I	x-axis	1.86	0.006
AL 333W-36	Au. afarensis	NME	Ulna	Left	Supinator	I	ant-y-axis	1.91	0.005
AL 333x-6	Au. afarensis	NME	Clavicle	Right	Deltoid	O	x-axis	1.91	0.009
AL 333x-6	Au. afarensis	NME	Clavicle	Right	Deltoid	O	distal-x-axis	1.92	0.006

AL 333x-6	Au. afarensis	NME	Clavicle	Right	Deltoid	O	lat-y-axis	1.88	0.009
AL 333x-6	Au. afarensis	NME	Clavicle	Right	Deltoid	O	med-y-axis	1.87	0.008
AL 333x-6	Au. afarensis	NME	Clavicle	Right	Deltoid	O	prox-x-axis	1.91	0.003
AL 333x-6	Au. afarensis	NME	Clavicle	Right	Deltoid	O	y-axis	1.87	0.009
AL 438-1a	Au. afarensis	NME	Ulna	Left	Brachialis	I	distal-x-axis	1.92	0.003
AL 438-1a	Au. afarensis	NME	Ulna	Left	Brachialis	I	lat-y-axis	1.90	0.015
AL 438-1a	Au. afarensis	NME	Ulna	Left	Brachialis	I	y-axis	1.91	0.003
AL 438-1a	Au. afarensis	NME	Ulna	Left	Brachialis	I	med-y-axis	1.91	0.004
AL 438-1a	Au. afarensis	NME	Ulna	Left	Brachialis	I	prox-x-axis	1.87	0.003
AL 438-1a	Au. afarensis	NME	Ulna	Left	Brachialis	I	x-axis	1.92	0.006
AL 438-1a	Au. afarensis	NME	Ulna	Left	Triceps brachii	I	med-y-axis	1.89	0.004
AL 438-1a	Au. afarensis	NME	Ulna	Left	Triceps brachii	I	distal-x-axis	1.89	0.003
AL 438-1a	Au. afarensis	NME	Ulna	Left	Triceps brachii	I	lat-y-axis	1.90	0.002
AL 438-1a	Au. afarensis	NME	Ulna	Left	Triceps brachii	I	prox-x-axis	1.91	0.004
AL 438-1a	Au. afarensis	NME	Ulna	Left	Triceps brachii	I	x-axis	1.89	0.007
AL 438-1a	Au. afarensis	NME	Ulna	Left	Triceps brachii	I	y-axis	1.92	0.003
AL 438-1c	Au. afarensis	NME	Humerus	Right	Pectoralis major	I	distal-x-axis	1.88	0.005
AL 438-1c	Au. afarensis	NME	Humerus	Right	Pectoralis major	I	prox-x-axis	1.87	0.006
AL 438-1c	Au. afarensis	NME	Humerus	Right	Pectoralis major	I	lat-y-axis	1.91	0.002
AL 438-1c	Au. afarensis	NME	Humerus	Right	Pectoralis major	I	med-y-axis	1.91	0.002
AL 438-1c	Au. afarensis	NME	Humerus	Right	Pectoralis major	I	y-axis	1.95	0.007
AL 438-1c	Au. afarensis	NME	Humerus	Right	Pectoralis major	I	x-axis	1.85	0.004
L40-19	P. boisei	NME	Ulna	Right	Brachialis	I	y-axis	1.91	0.012
L40-19	P. boisei	NME	Ulna	Right	Brachialis	I	distal-x-axis	1.88	0.010
L40-19	P. boisei	NME	Ulna	Right	Brachialis	I	lat-y-axis	1.93	0.008
L40-19	P. boisei	NME	Ulna	Right	Brachialis	I	med-y-axis	1.89	0.010
L40-19	P. boisei	NME	Ulna	Right	Brachialis	I	prox-x-axis	1.88	0.009
L40-19	P. boisei	NME	Ulna	Right	Brachialis	I	x-axis	1.91	0.008

L40-19	P. boisei	NME	Ulna	Right	Triceps brachii	I	distal-x-axis	1.92	0.005
L40-19	P. boisei	NME	Ulna	Right	Triceps brachii	I	lat-y-axis	1.91	0.001
L40-19	P. boisei	NME	Ulna	Right	Triceps brachii	I	med-y-axis	1.89	0.008
L40-19	P. boisei	NME	Ulna	Right	Triceps brachii	I	prox-x-axis	1.91	0.005
L40-19	P. boisei	NME	Ulna	Right	Triceps brachii	I	x-axis	1.91	0.003
L40-19	P. boisei	NME	Ulna	Right	Triceps brachii	I	y-axis	1.91	0.004
Omo 119-1973-2718	Australopithecus sp.	NME	Humerus	Left	Latissimus dorsi	I	distal-x-axis	1.89	0.007
Omo 119-1973-2718	Australopithecus sp.	NME	Humerus	Left	Latissimus dorsi	I	lat-y-axis	1.93	0.005
Omo 119-1973-2718	Australopithecus sp.	NME	Humerus	Left	Latissimus dorsi	I	med-y-axis	1.91	0.006
Omo 119-1973-2718	Australopithecus sp.	NME	Humerus	Left	Latissimus dorsi	I	prox-x-axis	1.86	0.010
Omo 119-1973-2718	Australopithecus sp.	NME	Humerus	Left	Latissimus dorsi	I	x-axis	1.86	0.005
Omo 119-1973-2718	Australopithecus sp.	NME	Humerus	Left	Latissimus dorsi	I	y-axis	1.93	0.003
Omo 119-1973-2718	Australopithecus sp.	NME	Humerus	Left	Pectoralis major	I	distal-x-axis	1.87	0.009
Omo 119-1973-2718	Australopithecus sp.	NME	Humerus	Left	Pectoralis major	I	lat-y-axis	1.91	0.002
Omo 119-1973-2718	Australopithecus sp.	NME	Humerus	Left	Pectoralis major	I	med-y-axis	1.91	0.006
Omo 119-1973-2718	Australopithecus sp.	NME	Humerus	Left	Pectoralis major	I	prox-x-axis	1.89	0.007
Omo 119-1973-2718	Australopithecus sp.	NME	Humerus	Left	Pectoralis major	I	x-axis	1.85	0.008
Omo 119-1973-2718	Australopithecus sp.	NME	Humerus	Left	Pectoralis major	I	y-axis	1.90	0.008

Omo 119-1973-2718	Australopithecus sp.	NME	Humerus	Left	Subscapularis	I	prox-x-axis	1.87	0.009
Omo 119-1973-2718	Australopithecus sp.	NME	Humerus	Left	Subscapularis	I	x-axis	1.93	0.007
Omo 119-1973-2718	Australopithecus sp.	NME	Humerus	Left	Subscapularis	I	distal-x-axis	1.90	0.007
Omo 119-1973-2718	Australopithecus sp.	NME	Humerus	Left	Subscapularis	I	lat-y-axis	1.91	0.008
Omo 119-1973-2718	Australopithecus sp.	NME	Humerus	Left	Subscapularis	I	med-y-axis	1.89	0.003
Omo 119-1973-2718	Australopithecus sp.	NME	Humerus	Left	Subscapularis	I	y-axis	1.91	0.005
Omo 119-1973-2718	Australopithecus sp.	NME	Humerus	Left	Supraspinatus	I	distal-x-axis	1.91	0.007
Omo 119-1973-2718	Australopithecus sp.	NME	Humerus	Left	Supraspinatus	I	lat-y-axis	1.90	0.006
Omo 119-1973-2718	Australopithecus sp.	NME	Humerus	Left	Supraspinatus	I	med-y-axis	1.92	0.006
Omo 119-1973-2718	Australopithecus sp.	NME	Humerus	Left	Supraspinatus	I	prox-x-axis	1.88	0.004
Omo 119-1973-2718	Australopithecus sp.	NME	Humerus	Left	Supraspinatus	I	x-axis	1.91	0.006
Omo 119-1973-2718	Australopithecus sp.	NME	Humerus	Left	Supraspinatus	I	y-axis	1.91	0.004
Omo 119-1973-2718	Australopithecus sp.	NME	Humerus	Left	Teres major	I	med-y-axis	1.91	0.002
Omo 119-1973-2718	Australopithecus sp.	NME	Humerus	Left	Teres major	I	distal-x-axis	1.88	0.004
Omo 119-1973-2718	Australopithecus sp.	NME	Humerus	Left	Teres major	I	prox-x-axis	1.84	0.003
Omo 119-	Australopithecus	NME	Humerus	Left	Teres major	I	lat-y-axis	1.92	0.003

1973-2718	sp.								
Omo 119-1973-2718	Australopithecus sp.	NME	Humerus	Left	Teres major	I	y-axis	1.94	0.007
Omo 119-1973-2718	Australopithecus sp.	NME	Humerus	Left	Teres major	I	x-axis	1.90	0.006
OH 36	P. boisei	NMT	Ulna	Right	Brachialis	I	distal-x-axis	1.87	0.009
OH 36	P. boisei	NMT	Ulna	Right	Brachialis	I	lat-y-axis	1.93	0.006
OH 36	P. boisei	NMT	Ulna	Right	Brachialis	I	med-y-axis	1.90	0.014
OH 36	P. boisei	NMT	Ulna	Right	Brachialis	I	prox-x-axis	1.89	0.009
OH 36	P. boisei	NMT	Ulna	Right	Brachialis	I	x-axis	1.89	0.009
OH 36	P. boisei	NMT	Ulna	Right	Brachialis	I	y-axis	1.90	0.007
OH 48	H. habilis	NMT	Clavicle	Left	Deltoid	O	distal-x-axis	1.90	0.004
OH 48	H. habilis	NMT	Clavicle	Left	Deltoid	O	lat-y-axis	1.89	0.004
OH 48	H. habilis	NMT	Clavicle	Left	Deltoid	O	med-y-axis	1.88	0.002
OH 48	H. habilis	NMT	Clavicle	Left	Deltoid	O	prox-x-axis	1.89	0.010
OH 48	H. habilis	NMT	Clavicle	Left	Deltoid	O	x-axis	1.90	0.006
OH 48	H. habilis	NMT	Clavicle	Left	Deltoid	O	y-axis	1.89	0.003
KNM-BK 66	H. ergaster	KNM	Ulna	Right	Brachialis	I	distal-x-axis	1.92	0.007
KNM-BK 66	H. ergaster	KNM	Ulna	Right	Brachialis	I	lat-y-axis	1.93	0.010
KNM-BK 66	H. ergaster	KNM	Ulna	Right	Brachialis	I	med-y-axis	1.89	0.007
KNM-BK 66	H. ergaster	KNM	Ulna	Right	Brachialis	I	prox-x-axis	1.90	0.003
KNM-BK 66	H. ergaster	KNM	Ulna	Right	Brachialis	I	x-axis	1.90	0.005
KNM-BK 66	H. ergaster	KNM	Ulna	Right	Brachialis	I	y-axis	1.89	0.005
KNM-BK 66	H. ergaster	KNM	Ulna	Right	Triceps brachii	I	med-y-axis	1.90	0.003
KNM-BK 66	H. ergaster	KNM	Ulna	Right	Triceps brachii	I	prox-x-axis	1.90	0.005
KNM-BK 66	H. ergaster	KNM	Ulna	Right	Triceps brachii	I	y-axis	1.88	0.005
KNM-BK 66	H. ergaster	KNM	Ulna	Right	Triceps brachii	I	distal-x-axis	1.89	0.005
KNM-BK 66	H. ergaster	KNM	Ulna	Right	Triceps brachii	I	lat-y-axis	1.91	0.007

KNM-BK 66	H. ergaster	KNM	Ulna	Right	Triceps brachii	I	x-axis	1.92	0.008
KNM-ER 739	Australopithecus sp.	KNM	Humerus	Right	Deltoid	I	distal-x-axis	1.90	0.011
KNM-ER 739	Australopithecus sp.	KNM	Humerus	Right	Deltoid	I	lat-y-axis	1.92	0.004
KNM-ER 739	Australopithecus sp.	KNM	Humerus	Right	Deltoid	I	med-y-axis	1.92	0.002
KNM-ER 739	Australopithecus sp.	KNM	Humerus	Right	Deltoid	I	prox-x-axis	1.89	0.010
KNM-ER 739	Australopithecus sp.	KNM	Humerus	Right	Deltoid	I	x-axis	1.89	0.011
KNM-ER 739	Australopithecus sp.	KNM	Humerus	Right	Deltoid	I	y-axis	1.92	0.004
KNM-ER 739	Australopithecus sp.	KNM	Humerus	Right	Lat. epicondylar ridge	O	distal-x-axis	1.89	0.004
KNM-ER 739	Australopithecus sp.	KNM	Humerus	Right	Lat. epicondylar ridge	O	lat-y-axis	1.90	0.004
KNM-ER 739	Australopithecus sp.	KNM	Humerus	Right	Lat. epicondylar ridge	O	med-y-axis	1.91	0.004
KNM-ER 739	Australopithecus sp.	KNM	Humerus	Right	Lat. epicondylar ridge	O	prox-x-axis	1.92	0.008
KNM-ER 739	Australopithecus sp.	KNM	Humerus	Right	Lat. epicondylar ridge	O	x-axis	1.91	0.004
KNM-ER 739	Australopithecus sp.	KNM	Humerus	Right	Lat. epicondylar ridge	O	y-axis	1.91	0.001
KNM-ER 739	Australopithecus sp.	KNM	Humerus	Right	Lateral epicondyle	O	ant-y-axis	1.94	0.010
KNM-ER 739	Australopithecus sp.	KNM	Humerus	Right	Lateral epicondyle	O	distal-x-axis	1.91	0.006
KNM-ER 739	Australopithecus sp.	KNM	Humerus	Right	Lateral epicondyle	O	post-y-axis	1.90	0.006

KNM-ER 739	Australopithecus sp.	KNM	Humerus	Right	Lateral epicondyle	O	prox-x-axis	1.89	0.011
KNM-ER 739	Australopithecus sp.	KNM	Humerus	Right	Lateral epicondyle	O	x-axis	1.89	0.010
KNM-ER 739	Australopithecus sp.	KNM	Humerus	Right	Lateral epicondyle	O	y-axis	1.94	0.002
KNM-ER 739	Australopithecus sp.	KNM	Humerus	Right	Med. epicondylar ridge	O	ant-y-axis	1.92	0.003
KNM-ER 739	Australopithecus sp.	KNM	Humerus	Right	Med. epicondylar ridge	O	distal-x-axis	1.89	0.009
KNM-ER 739	Australopithecus sp.	KNM	Humerus	Right	Med. epicondylar ridge	O	post-y-axis	1.92	0.004
KNM-ER 739	Australopithecus sp.	KNM	Humerus	Right	Med. epicondylar ridge	O	prox-x-axis	1.90	0.003
KNM-ER 739	Australopithecus sp.	KNM	Humerus	Right	Med. epicondylar ridge	O	x-axis	1.89	0.005
KNM-ER 739	Australopithecus sp.	KNM	Humerus	Right	Med. epicondylar ridge	O	y-axis	1.94	0.005
KNM-ER 739	Australopithecus sp.	KNM	Humerus	Right	Medial epicondyle	O	ant-y-axis	1.91	0.004
KNM-ER 739	Australopithecus sp.	KNM	Humerus	Right	Medial epicondyle	O	distal-x-axis	1.90	0.002
KNM-ER 739	Australopithecus sp.	KNM	Humerus	Right	Medial epicondyle	O	lat-y-axis	1.88	0.005
KNM-ER 739	Australopithecus sp.	KNM	Humerus	Right	Medial epicondyle	O	prox-x-axis	1.89	0.006
KNM-ER 739	Australopithecus sp.	KNM	Humerus	Right	Medial epicondyle	O	x-axis	1.89	0.009
KNM-ER 739	Australopithecus sp.	KNM	Humerus	Right	Medial epicondyle	O	y-axis	1.90	0.010
KNM-ER	P. boisei	KNM	Humerus	Right	Lateral epicondyle	O	ant-y-axis	1.89	0.011

1504									
KNM-ER 1504	<i>P. boisei</i>	KNM	Humerus	Right	Lateral epicondyle	O	distal-x-axis	1.88	0.005
KNM-ER 1504	<i>P. boisei</i>	KNM	Humerus	Right	Lateral epicondyle	O	post-y-axis	1.89	0.005
KNM-ER 1504	<i>P. boisei</i>	KNM	Humerus	Right	Lateral epicondyle	O	prox-x-axis	1.85	0.002
KNM-ER 1504	<i>P. boisei</i>	KNM	Humerus	Right	Lateral epicondyle	O	x-axis	1.88	0.004
KNM-ER 1504	<i>P. boisei</i>	KNM	Humerus	Right	Lateral epicondyle	O	y-axis	1.89	0.007
KNM-ER 1504	<i>P. boisei</i>	KNM	Humerus	Right	Medial epicondyle	O	distal-x-axis	1.89	0.007
KNM-ER 1504	<i>P. boisei</i>	KNM	Humerus	Right	Medial epicondyle	O	ant-y-axis	1.89	0.007
KNM-ER 1504	<i>P. boisei</i>	KNM	Humerus	Right	Medial epicondyle	O	post-y-axis	1.89	0.009
KNM-ER 1504	<i>P. boisei</i>	KNM	Humerus	Right	Medial epicondyle	O	prox-x-axis	1.89	0.003
KNM-ER 1504	<i>P. boisei</i>	KNM	Humerus	Right	Medial epicondyle	O	x-axis	1.88	0.010
KNM-ER 1504	<i>P. boisei</i>	KNM	Humerus	Right	Medial epicondyle	O	y-axis	1.89	0.011
KNM-KP 271	<i>Au. anamensis</i>	KNM	Humerus	Left	Lateral epicondyle	O	ant-y-axis	1.91	0.003
KNM-KP 271	<i>Au. anamensis</i>	KNM	Humerus	Left	Lateral epicondyle	O	distal-x-axis	1.91	0.002
KNM-KP 271	<i>Au. anamensis</i>	KNM	Humerus	Left	Lateral epicondyle	O	post-y-axis	1.91	0.002
KNM-KP 271	<i>Au. anamensis</i>	KNM	Humerus	Left	Lateral epicondyle	O	prox-x-axis	1.89	0.007
KNM-KP 271	<i>Au. anamensis</i>	KNM	Humerus	Left	Lateral epicondyle	O	x-axis	1.91	0.012
KNM-KP 271	<i>Au. anamensis</i>	KNM	Humerus	Left	Lateral epicondyle	O	y-axis	1.89	0.012
KNM-KP 271	<i>Au. anamensis</i>	KNM	Humerus	Left	Medial epicondyle	O	x-axis	1.89	0.007

KNM-KP 271	Au. anamensis	KNM	Humerus	Left	Medial epicondyle	O	ant-y-axis	1.88	0.005
KNM-KP 271	Au. anamensis	KNM	Humerus	Left	Medial epicondyle	O	distal-x-axis	1.89	0.007
KNM-KP 271	Au. anamensis	KNM	Humerus	Left	Medial epicondyle	O	post-y-axis	1.88	0.006
KNM-KP 271	Au. anamensis	KNM	Humerus	Left	Medial epicondyle	O	prox-x-axis	1.89	0.006
KNM-KP 271	Au. anamensis	KNM	Humerus	Left	Medial epicondyle	O	y-axis	1.95	0.006
SK 18b	H. ergaster	Ditsong	Ulna	Left	Brachialis	I	lat-y-axis	1.92	0.001
SK 18b	H. ergaster	Ditsong	Ulna	Left	Brachialis	I	med-y-axis	1.93	0.006
SK 18b	H. ergaster	Ditsong	Ulna	Left	Brachialis	I	prox-x-axis	1.89	0.006
SK 18b	H. ergaster	Ditsong	Ulna	Left	Brachialis	I	x-axis	1.90	0.005
SK 18b	H. ergaster	Ditsong	Ulna	Left	Brachialis	I	y-axis	1.91	0.004
SK 18b	H. ergaster	Ditsong	Ulna	Left	Brachialis	I	distal-x-axis	1.87	0.006
SK 2045	H. ergaster	Ditsong	Radius	Right	Biceps brachii	I	distal-x-axis	1.90	0.009
SK 2045	H. ergaster	Ditsong	Radius	Right	Biceps brachii	I	lat-y-axis	1.91	0.006
SK 2045	H. ergaster	Ditsong	Radius	Right	Biceps brachii	I	med-y-axis	1.90	0.005
SK 2045	H. ergaster	Ditsong	Radius	Right	Biceps brachii	I	prox-x-axis	1.89	0.009
SK 2045	H. ergaster	Ditsong	Radius	Right	Biceps brachii	I	x-axis	1.90	0.004
SK 2045	H. ergaster	Ditsong	Radius	Right	Biceps brachii	I	y-axis	1.93	0.006
SK 24601	Homo aff. habilis	Ditsong	Radius	Left	Biceps brachii	I	distal-x-axis	1.89	0.005
SK 24601	Homo aff. habilis	Ditsong	Radius	Left	Biceps brachii	I	lat-y-axis	1.92	0.003
SK 24601	Homo aff. habilis	Ditsong	Radius	Left	Biceps brachii	I	med-y-axis	1.91	0.003
SK 24601	Homo aff. habilis	Ditsong	Radius	Left	Biceps brachii	I	prox-x-axis	1.88	0.008
SK 24601	Homo aff. habilis	Ditsong	Radius	Left	Biceps brachii	I	x-axis	1.90	0.003
SK 24601	Homo aff. habilis	Ditsong	Radius	Left	Biceps brachii	I	y-axis	1.90	0.004

SKX 8761	<i>P. robustus</i>	Ditsong	Ulna	Left	Triceps brachii	I	distal-x-axis	1.90	0.004
SKX 8761	<i>P. robustus</i>	Ditsong	Ulna	Left	Triceps brachii	I	lat-y-axis	1.91	0.008
SKX 8761	<i>P. robustus</i>	Ditsong	Ulna	Left	Triceps brachii	I	med-y-axis	1.89	0.012
SKX 8761	<i>P. robustus</i>	Ditsong	Ulna	Left	Triceps brachii	I	prox-x-axis	1.90	0.005
SKX 8761	<i>P. robustus</i>	Ditsong	Ulna	Left	Triceps brachii	I	x-axis	1.91	0.007
SKX 8761	<i>P. robustus</i>	Ditsong	Ulna	Left	Triceps brachii	I	y-axis	1.89	0.010
SKX 24600	<i>Homo. aff. habilis</i>	Ditsong	Humerus	Left	Medial epicondyle	O	ant-y-axis	1.88	0.009
SKX 24600	<i>Homo. aff. habilis</i>	Ditsong	Humerus	Left	Medial epicondyle	O	distal-x-axis	1.93	0.006
SKX 24600	<i>Homo. aff. habilis</i>	Ditsong	Humerus	Left	Medial epicondyle	O	post-y-axis	1.89	0.008
SKX 24600	<i>Homo. aff. habilis</i>	Ditsong	Humerus	Left	Medial epicondyle	O	prox-x-axis	1.89	0.013
SKX 24600	<i>Homo. aff. habilis</i>	Ditsong	Humerus	Left	Medial epicondyle	O	x-axis	1.90	0.005
SKX 24600	<i>Homo. aff. habilis</i>	Ditsong	Humerus	Left	Medial epicondyle	O	y-axis	1.89	0.001
SKX 34805	<i>Homo ergaster</i>	Ditsong	Humerus	Right	Med. epicondylar ridge	O	ant-y-axis	1.90	0.009
SKX 34805	<i>Homo ergaster</i>	Ditsong	Humerus	Right	Med. epicondylar ridge	O	distal-x-axis	1.90	0.005
SKX 34805	<i>Homo ergaster</i>	Ditsong	Humerus	Right	Med. epicondylar ridge	O	post-y-axis	1.92	0.005
SKX 34805	<i>Homo ergaster</i>	Ditsong	Humerus	Right	Med. epicondylar ridge	O	prox-x-axis	1.91	0.003
SKX 34805	<i>Homo ergaster</i>	Ditsong	Humerus	Right	Med. epicondylar ridge	O	x-axis	1.89	0.006
SKX 34805	<i>Homo ergaster</i>	Ditsong	Humerus	Right	Med. epicondylar ridge	O	y-axis	1.92	0.003
STS 7	<i>Au. africanus</i>	Ditsong	Humerus	Right	Infraspinatus	I	distal-x-axis	1.90	0.009
STS 7	<i>Au. africanus</i>	Ditsong	Humerus	Right	Infraspinatus	I	lat-y-axis	1.89	0.008
STS 7	<i>Au. africanus</i>	Ditsong	Humerus	Right	Infraspinatus	I	med-y-axis	1.93	0.012
STS 7	<i>Au. africanus</i>	Ditsong	Humerus	Right	Infraspinatus	I	prox-x-axis	1.90	0.014
STS 7	<i>Au. africanus</i>	Ditsong	Humerus	Right	Infraspinatus	I	x-axis	1.87	0.004

STS 7	Au. africanus	Ditsong	Humerus	Right	Infraspinatus	I	y-axis	1.90	0.013
STS 7	Au. africanus	Ditsong	Humerus	Right	Supraspinatus	I	distal-x-axis	1.89	0.008
STS 7	Au. africanus	Ditsong	Humerus	Right	Supraspinatus	I	lat-y-axis	1.90	0.007
STS 7	Au. africanus	Ditsong	Humerus	Right	Supraspinatus	I	med-y-axis	1.89	0.005
STS 7	Au. africanus	Ditsong	Humerus	Right	Supraspinatus	I	prox-x-axis	1.90	0.002
STS 7	Au. africanus	Ditsong	Humerus	Right	Supraspinatus	I	x-axis	1.90	0.006
STS 7	Au. africanus	Ditsong	Humerus	Right	Supraspinatus	I	y-axis	1.90	0.005
TM 1517	P. robustus	Ditsong	Humerus	Right	Lateral epicondyle	O	ant-y-axis	1.86	0.008
TM 1517	P. robustus	Ditsong	Humerus	Right	Lateral epicondyle	O	distal-x-axis	1.92	0.006
TM 1517	P. robustus	Ditsong	Humerus	Right	Lateral epicondyle	O	post-y-axis	1.89	0.006
TM 1517	P. robustus	Ditsong	Humerus	Right	Lateral epicondyle	O	prox-x-axis	1.88	0.008
TM 1517	P. robustus	Ditsong	Humerus	Right	Lateral epicondyle	O	x-axis	1.88	0.005
TM 1517	P. robustus	Ditsong	Humerus	Right	Lateral epicondyle	O	y-axis	1.91	0.002
TM 1517e	P. robustus	Ditsong	Ulna	Right	Triceps brachii	I	distal-x-axis	1.89	0.005
TM 1517e	P. robustus	Ditsong	Ulna	Right	Triceps brachii	I	lat-y-axis	1.92	0.003
TM 1517e	P. robustus	Ditsong	Ulna	Right	Triceps brachii	I	med-y-axis	1.89	0.014
TM 1517e	P. robustus	Ditsong	Ulna	Right	Triceps brachii	I	prox-x-axis	1.90	0.005
TM 1517e	P. robustus	Ditsong	Ulna	Right	Triceps brachii	I	y-axis	1.91	0.003
TM 1517e	P. robustus	Ditsong	Ulna	Right	Triceps brachii	I	x-axis	1.89	0.004
TM 1517f	P. robustus	Ditsong	Humerus	Right	Medial epicondyle	O	ant-y-axis	1.89	0.002
TM 1517f	P. robustus	Ditsong	Humerus	Right	Medial epicondyle	O	distal-x-axis	1.87	0.009
TM 1517f	P. robustus	Ditsong	Humerus	Right	Medial epicondyle	O	post-y-axis	1.90	0.002
TM 1517f	P. robustus	Ditsong	Humerus	Right	Medial epicondyle	O	prox-x-axis	1.89	0.006
TM 1517f	P. robustus	Ditsong	Humerus	Right	Medial epicondyle	O	x-axis	1.89	0.005
TM 1517f	P. robustus	Ditsong	Humerus	Right	Medial epicondyle	O	y-axis	1.87	0.010

APPENDIX 3: RAW FRACTAL AXES

Catalogue No.: AL 137 - 48A .

Institution: JME .

Species:

Siding: R

Element: Hum .

Enthesis: *medial epicondyle* .

Origin/Insertion: 

PD (y axis) length:

Y axis interval:

ML (x axis) length

X axis interval:

Y AXIS

~~Ant~~
~~MED~~ Y AXIS

~~Post~~
~~LAT~~ Y AXIS



X AXIS

PROX X AXIS

DIST X AXIS



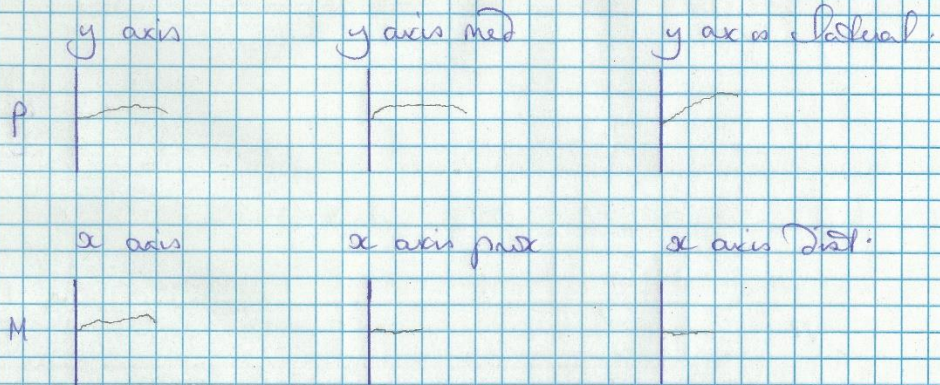
Al. 288-1m right humerus

Subscapularis insertion

Note: while humeral head on the whole distended, the lesser tuberosity + Subscapular insertion is intact.

y axis length: 18.27 mm.

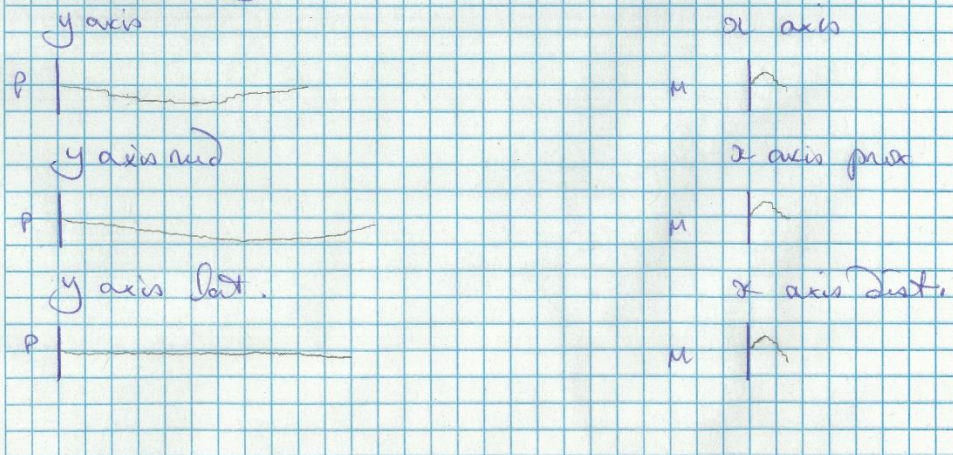
z axis length: 12.46 mm.



Supracoracoid ~~ridge~~ (lateral) signs of Brachioradialis

y axis length: 66.69 mm

z axis length: 50.5 mm



AL 288-1N. Right whorl.

Brachialis insecta (w/ Pronator dorus).

y axis length: 29.43 mm.

x axis length: 6.90 mm

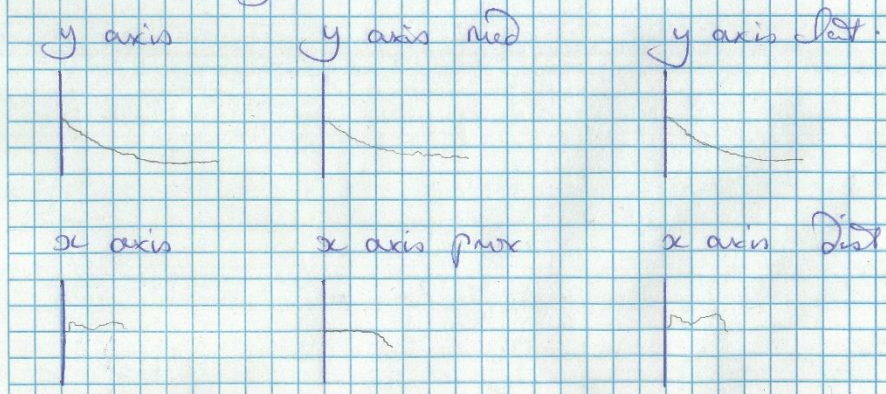


AL 288-1T

Brachialis insecta (w/ Pronator dorus)

y axis length: 27.45 mm.

x axis length: 8.43 mm.



AL 288-12 Right ~~prox~~ ulna.

Triceps brachii insertion:

y axis length: 18.11 mm.

x axis length: 14.46 mm.

y axis

y axis med

y axis lat.

P

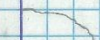


x axis

x axis ~~prox~~

x axis ~~prox~~

M



AL 288-13

Biceps brachii insertion on radial tuberosity

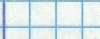
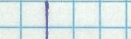
y axis length: 7.07 mm.

x axis length: 9.16 mm.

y axis

y axis med

y axis lat.



x axis

x axis prox

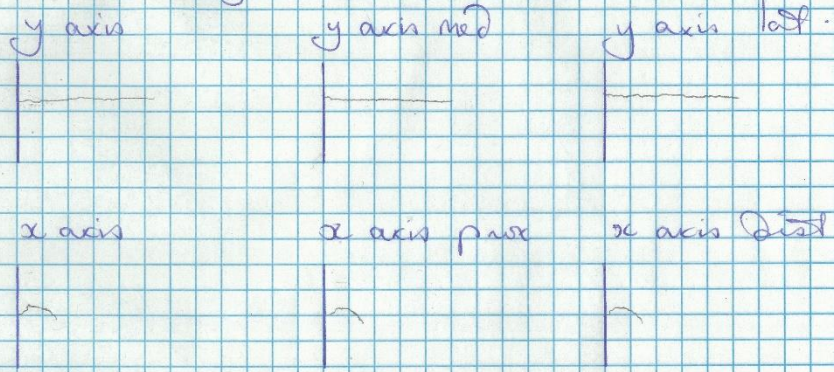
x axis dist.



AL 288-1r *A. afaensis*. Left humerus.
 Insertion for Pectoralis major.

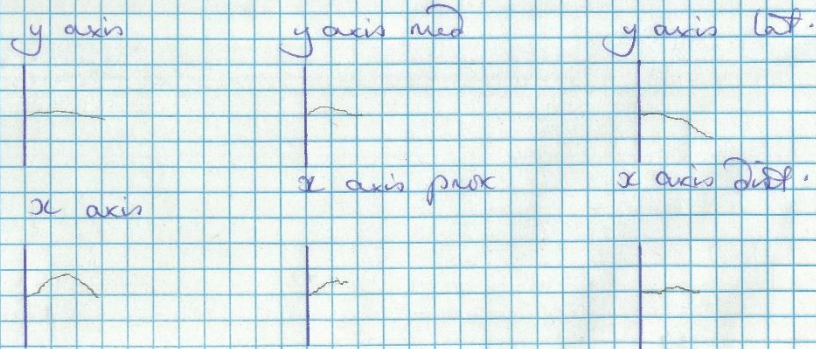
Note: two cracks slightly alter the topography of the insertion site - will be controlled by aligning pins w/ existing contours.

y axis length: ~~30.27~~ ~~30.27~~ mm - 30.37 mm
 x axis length: 3.57 mm



humeral condyle given wrist flexors.

y axis length: 13.73 mm. x axis length: 9.18 mm



Catalogue No.: Ah 322-1

Institution: JME

Species: afan-

Element: Hum.

Siding: L

Origin/Insertion: O.

Enthesis: lat epi crest*

PD (y axis) length:

Y axis interval:

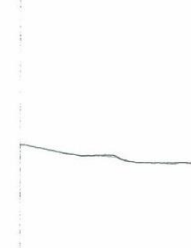
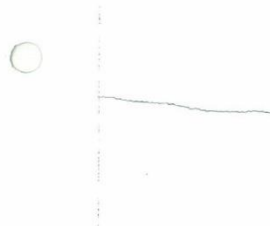
ML (x axis) length

X axis interval:

Y AXIS

ANT.
MED Y AXIS

POST.
LAT Y AXIS



X AXIS


PROX X AXIS

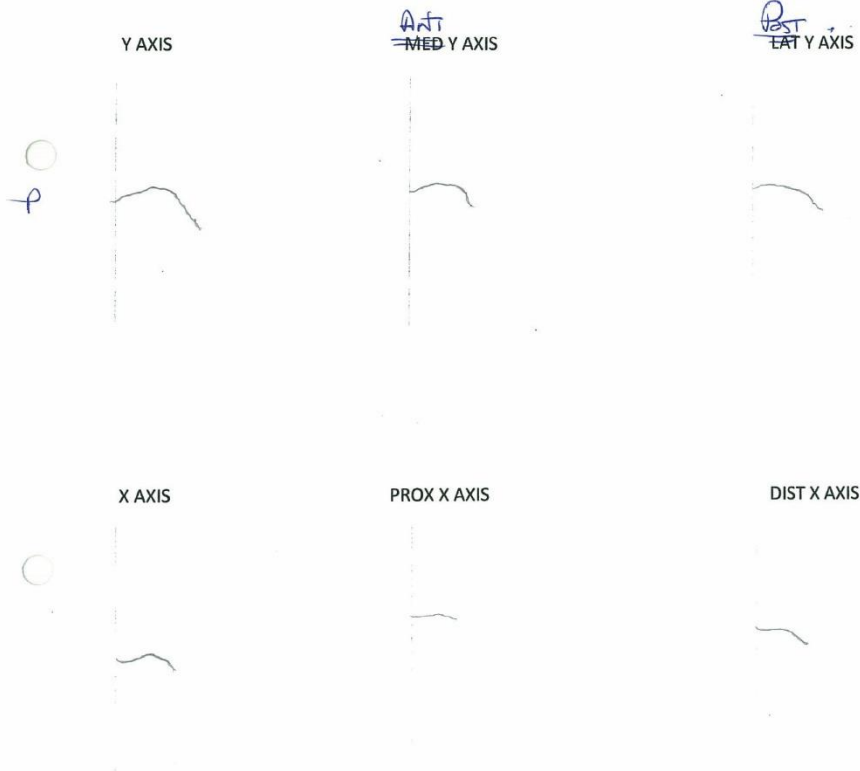
DIST X AXIS



* brachioradialis
~~Extensor carpi radialis longus~~

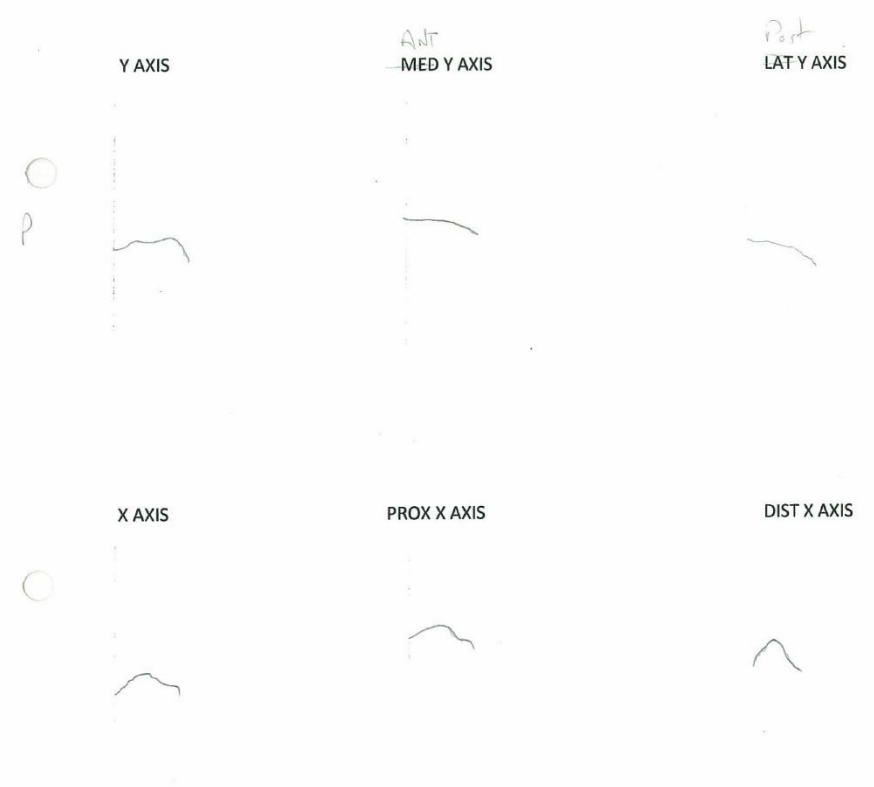
Catalogue No.: AL 302-1
Species: *cat. afaensis*
Siding: L
Enthesis: *lat. epicondyle*
PD (y axis) length:
ML (x axis) length

Institution: JMC
Element: *Hum.*
Origin/Insertion: 
Y axis interval:
X axis interval:



Catalogue No.: *Am 322-1*
Species: *Am. farensis*
Siding: *L.*
Enthesis: *Med. epicondyle*
PD (y axis) length:
ML (x axis) length

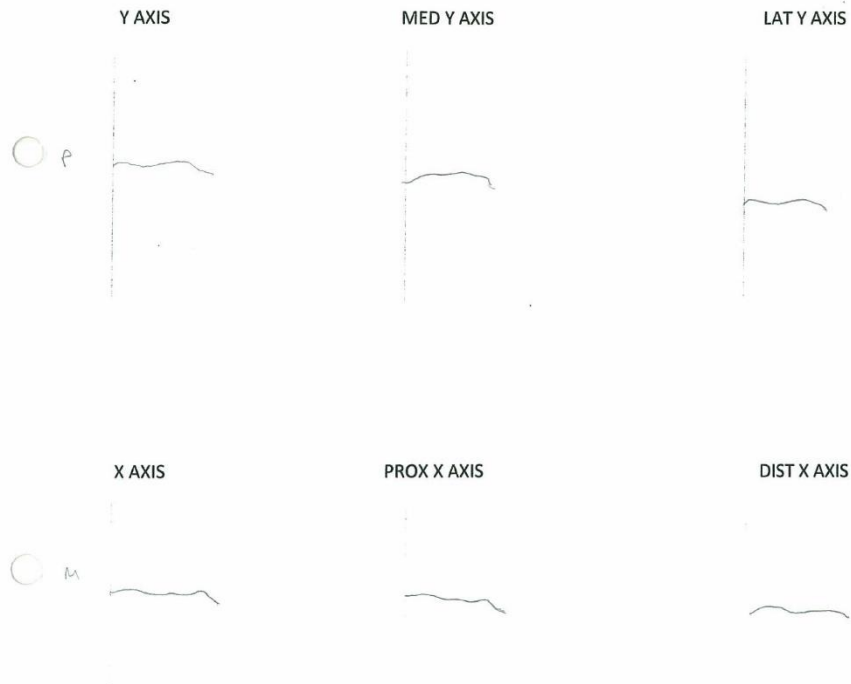
Institution: *JME*
Element: *Humerus (Dist.)*
Origin/Insertion: *Origin*
Y axis interval:
X axis interval:



Catalogue No.: AL ³³³⁻¹⁰⁷ ~~138~~
Species: *A. ofarensis*
Siding: right
Enthesis: *Infusparacten*
PD (y axis) length: 19.1
ML (x axis) length: 20.7

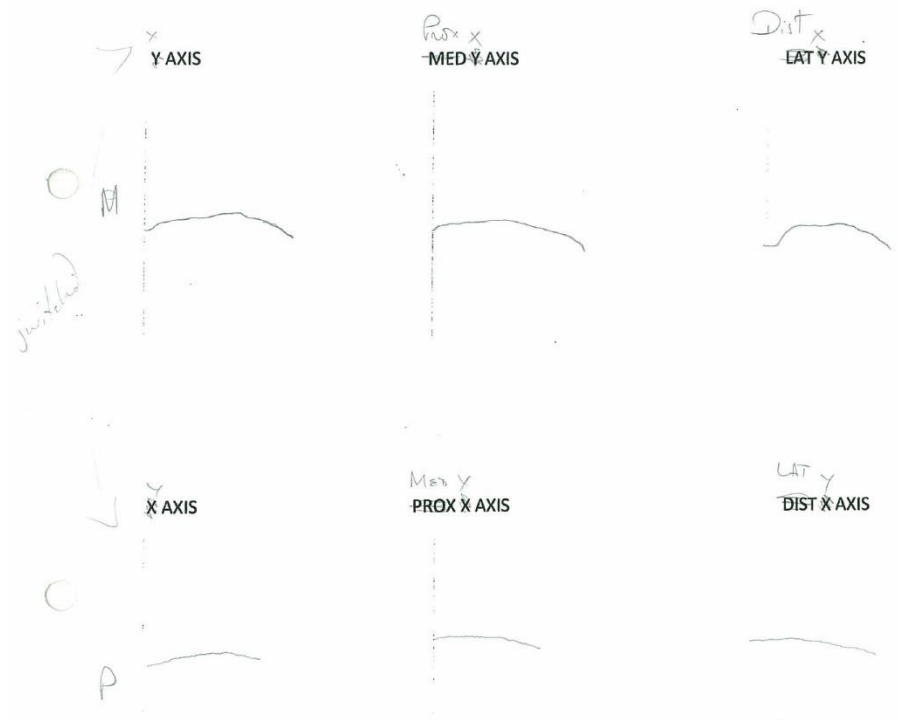
Institution: JME

Element: *Humerus*
Origin/Insertion: *Insect*
Y axis interval: 6.36
X axis interval: 6.9



Catalogue No.: AL 333-109
 Species: *Ch. aeneus*
 Siding: left?
 Enthesis: Deltoid
 PD (y axis) length: 22.1
 ML (x axis) length: 28.9 mm

Institution: JME
 Element: Humerus
 Origin/Insertion: Isert
 Y axis interval: 7.36
 X axis interval: 9.63



Catalogue No.: *Alw 333-109*

Institution: *LME*

Species: *Au. africanus*

Siding: *left*

Element: *Humerus*

Enthesis: *head, Darsi*

Origin/Insertion: *Insert*

PD (y axis) length: *31.3*

Y axis interval: *10.4*

ML (x axis) length: *9.2*

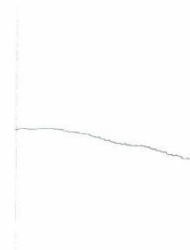
X axis interval: *3.06*

Y AXIS

MED Y AXIS

LAT Y AXIS

○
P



X AXIS

PROX X AXIS

DIST X AXIS

○



Catalogue No.: Ah 333-109

Institution: LME

Species: *A. afaensis*

Siding: left

Element: Humerus

Enthesis: Pectoralis major

Origin/Insertion: Insert

PD (y axis) length: 30.2 mm

Y axis interval: 10 mm

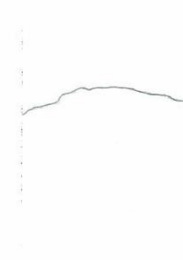
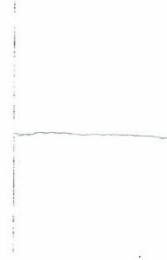
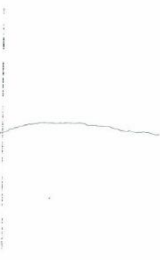
ML (x axis) length: 15.7 mm

X axis interval: 5.2 mm

Y AXIS

MED Y AXIS

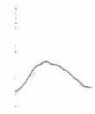
LAT Y AXIS



X AXIS

PROX X AXIS

DIST X AXIS



Catalogue No.: AL 333W-36

Institution: NME

Species:

Siding: L

Element: ULNA

Enthesis: Brachialis -

Origin/Insertion: I -

PD (y axis) length:

Y axis interval:

ML (x axis) length

X axis interval:



Catalogue No.: AL 333W-36

Institution: SME

Species:

Siding: L
Enthesis: *Syrinacta crest*

Element: Ulna

Origin/Insertion:

PD (y axis) length:

Y axis interval:

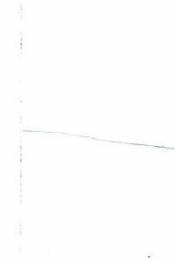
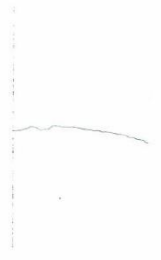
ML (x axis) length

X axis interval:

Y AXIS

ANT
MED Y AXIS

POST
ANT Y AXIS



X AXIS

PROX X AXIS

DIST X AXIS



Catalogue No.: *Al 333x-6*

Institution: *JME*

Species:

Siding: *R*

Element: *Claw*

Enthesis: *Deltoid*

Origin/Insertion: *O*

PD (y axis) length:

Y axis interval:

ML (x axis) length

X axis interval:

Y AXIS

MED Y AXIS

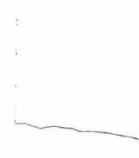
LAT Y AXIS



X AXIS

PROX X AXIS

DIST X AXIS



Catalogue No.: AL 438-1a

Institution: JME

Species: *An. afaensis*

Siding:

Element: Ulna

Enthesis: ~~Symphysis~~ *h. Breghia's*

Origin/Insertion: Insert

PD (y axis) length: 22.6

Y axis interval: 7.53

ML (x axis) length: 15.9

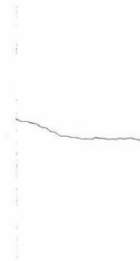
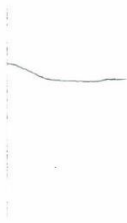
X axis interval: 5.3

Y AXIS

MED Y AXIS

LAT Y AXIS

O
P



X AXIS

PROX X AXIS

DIST X AXIS

O



Catalogue No.: AL 438-1a

Institution: JME

Species: *du. afanensis*

Siding: L.

Element: Ulna

Enthesis: *Triceps brachii*

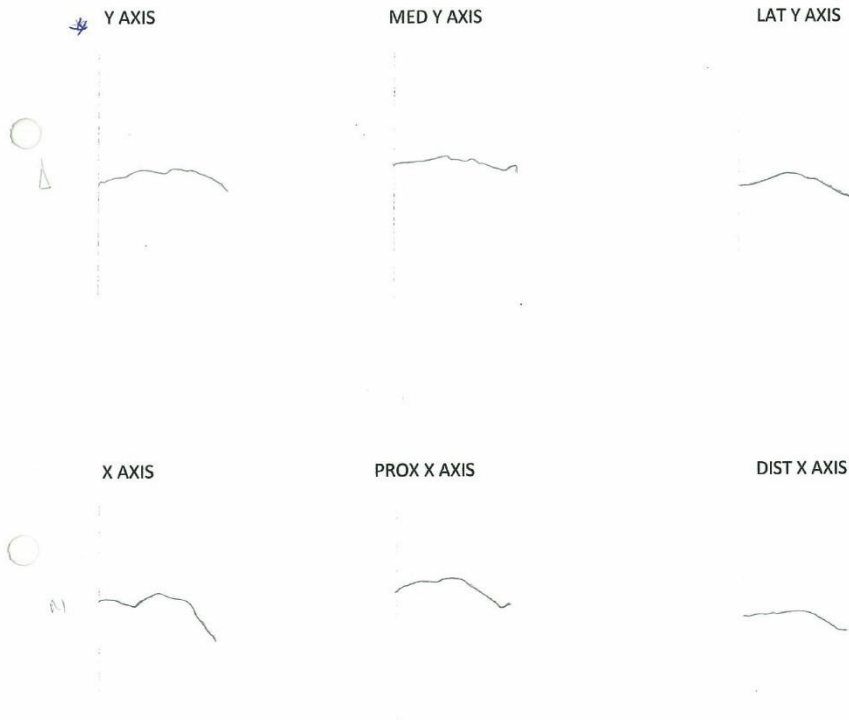
Origin/Insertion: Insect

AP PD (y axis) length: 25

Y axis interval: 8.3

ML (x axis) length: 22.4

X axis interval: 7.46



Note: This ulna has two large foramina in the center of it. Not daphnomic damage so I'm taking it anyway, but leveling the foramina. Refer to photos of specimen. Profiles of foramina marked w/ star.

Catalogue No.: AL 438-1c

Species: *A. cf. areolaris*

Siding: R.

Enthesis: Pect. maj

PD (y axis) length:

ML (x axis) length

Institution: JME

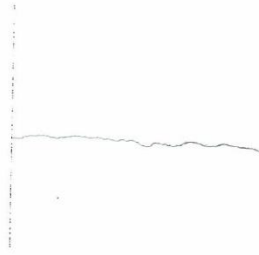
Element: Humerus

Origin/insertion: D.

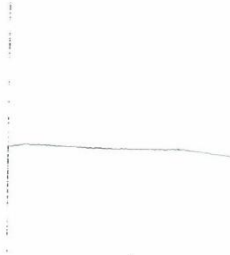
Y axis interval:

X axis interval:

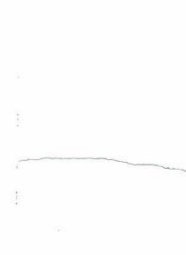
Y AXIS



MED Y AXIS



LAT Y AXIS



X AXIS



PROX X AXIS



DIST X AXIS



Catalogue No.: KDM-BK 66

Species: *H. egaseter*

Siding: R

Enthesis: Brachialis

PD (y axis) length:

ML (x axis) length

Institution: NMC

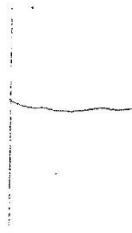
Element: Ulna

Origin/insertion: P.

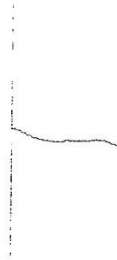
Y axis interval:

X axis interval:

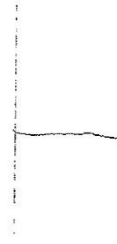
Y AXIS



MED Y AXIS



LAT Y AXIS



X AXIS



PROX X AXIS



DIST X AXIS



Catalogue No.: KNM-BK 66.

Species: *H. ergaster*

Siding: R.

Enthesis: *Triceps brachii*

~~AP~~
PD (y axis) length:

ML (x axis) length

Institution: DMK.

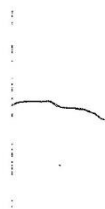
Element: *Ulna*

Origin/Insertion: *1*

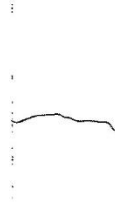
Y axis interval:

X axis interval:

Y AXIS



MED Y AXIS



LAT Y AXIS



X AXIS



PROX X AXIS



DIST X AXIS



Catalogue No.: KLM-EE 739.

Institution: JMK

Species: *du. bairdi*

Siding: 2

Element: Humerus -

Enthesis: *Deltoid tuberosity*

Origin/Insertion: I

PD (y axis) length:

Y axis interval:

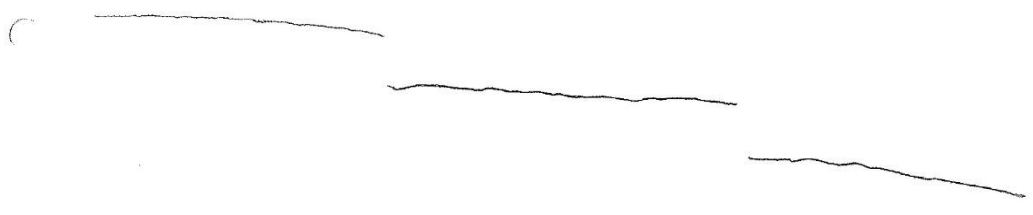
ML (x axis) length

X axis interval:

Y AXIS

MED Y AXIS

LAT Y AXIS



X AXIS

PROX X AXIS

DIST X AXIS



Catalogue No.: KNM-ER 739

Species: *Au. boisei*

Siding: R

Enthesis: lat epi crest

PD (y axis) length:

ML (x axis) length

Institution: NMK

Element: humerus

Origin/Insertion: O

Y axis interval:

X axis interval:

Y AXIS

~~MED~~ Y AXIS

~~EAT~~ Y AXIS



X AXIS

PROX X AXIS

DIST X AXIS



Catalogue No.: KUM-ER 737

Species: *Ch. basei*

Siding: R

Enthesis: lat epicoyle

PD (y axis) length:

ML (x axis) length

Institution: JUK

Element: humerus -

Origin/Insertion: O

Y axis interval:

X axis interval:

Y AXIS

Ant
MED Y AXIS

Post
LAT Y AXIS



X AXIS

PROX X AXIS

DIST X AXIS



Catalogue No.: KLM-EE 239

Institution: NMU

Species: *Ad. borealis*

Siding: R.

Element: Humerus

Enthesis: Med. epi. crest

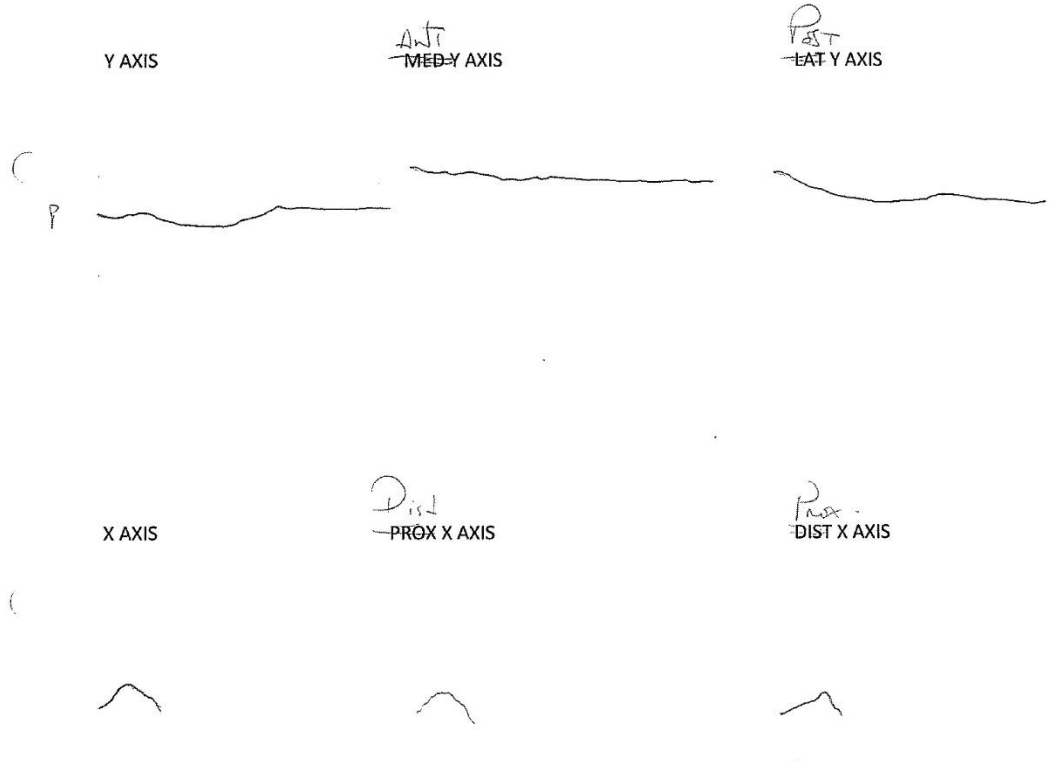
Origin/Insertion: O

PD (y axis) length:

Y axis interval:

ML (x axis) length

X axis interval:



Medial epicondyle crest has an anterior curvature Distally

Catalogue No.: KNM-EE 739

Species: *Can. bairdi*

Siding: R

Enthesis: Med. epicondyle.

PD (y axis) length:

ML (x axis) length

Institution: LMC

Element: Humerus -

Origin/Insertion: O.

Y axis interval:

X axis interval:

Y AXIS

ANT.
MEDI Y AXIS

LAT Y AXIS



X AXIS

PROX X AXIS

DIST X AXIS



Catalogue No.: KJM-ER 150L

Institution: NMK

Species:

Siding: *H. lat.*

Element: *Humerus*

Enthesis: ~~H. lat.~~ *epi.*

Origin/Insertion:

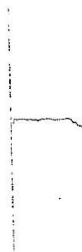
PD (y axis) length:

Y axis interval:

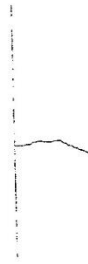
ML (x axis) length

X axis interval:

Y AXIS



MED Y AXIS



LAT Y AXIS



X AXIS



PROX X AXIS



DIST X AXIS



Catalogue No.: KNM-ER 1504

Institution: JMK

Species:

Siding: R

Element: Humerus

Enthesis: ~~IMPD~~ epicondyle

Origin/Insertion:

PD (y axis) length:

Y axis interval:

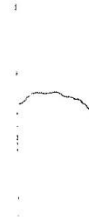
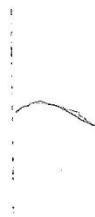
ML (x axis) length

X axis interval:

Y AXIS

MED Y AXIS

LAT Y AXIS



X AXIS

PROX X AXIS

DIST X AXIS



Catalogue No.: KNM-KP 271


Institution: JMK

Species:

Siding: L

Element: Humerus

Enthesis: lateral epicondyle

Origin/Insertion: 

PD (y axis) length:

Y axis interval:

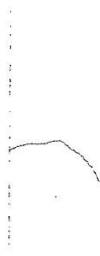
ML (x axis) length

X axis interval:

Y AXIS

^{Med}
MED Y AXIS

^{Post}
POST Y AXIS



X AXIS

PROX X AXIS

DIST X AXIS



Catalogue No.: KMM-KP 251


Institution: JMK

Species:

Siding: L.

Element: Humerus

Enthesis: Medial epicondyle

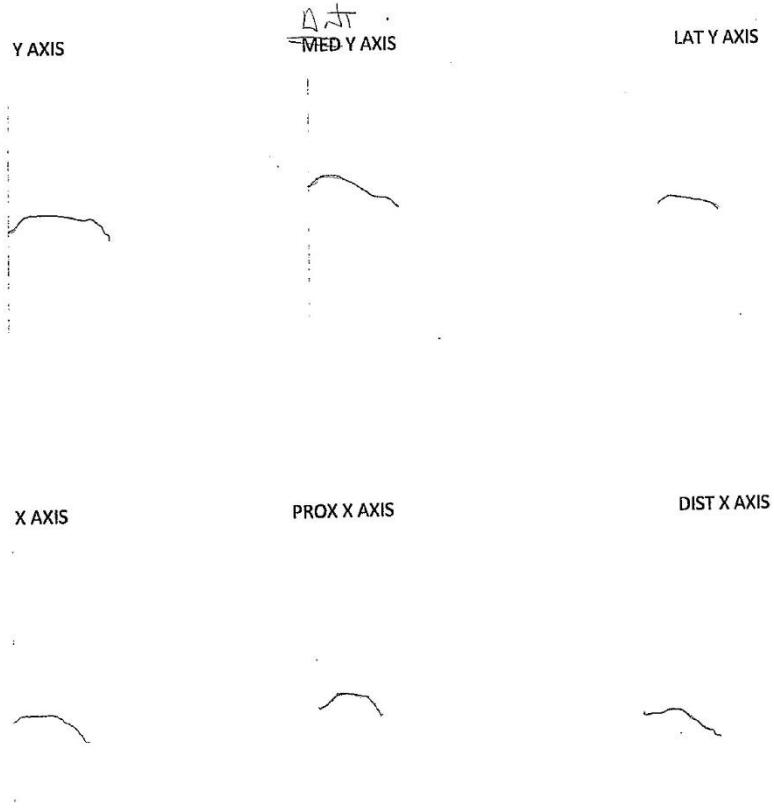
Origin/Insertion: 

PD (y axis) length:

Y axis interval:

ML (x axis) length

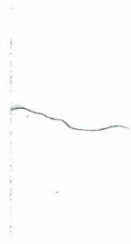
X axis interval:



Catalogue No.: W40-19.
Species: Boisei
Siding: Right.
Enthesis: Brachialia.
PD (y axis) length: 23.1.
ML (x axis) length 16.5

Institution: JME
Element: Ulna
Origin/Insertion: I
Y axis interval: 7.7
X axis interval: 5.5

Y AXIS



MED Y AXIS



LAT Y AXIS



X AXIS



PROX X AXIS



DIST X AXIS



Catalogue No.: 640-19.

Species: Boisei

Siding: h.

Enthesis: Triceps.

PD (y axis) length: 18.5

ML (x axis) length: 26.0

Institution: JME.

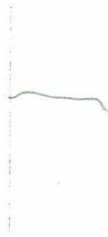
Element: Ulna.

Origin/Insertion: I.

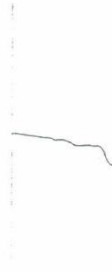
Y axis interval: 6.16

X axis interval: 8.7

Y AXIS



MED Y AXIS



LAT Y AXIS



X AXIS



PROX X AXIS



DIST X AXIS



Catalogue No.: 01136

Species: *H. erectus?* *Panathrop.*

Siding: *R.*

Enthesis: *Brachialis.*

PD (y axis) length:

ML (x axis) length

Institution: *NMT.*

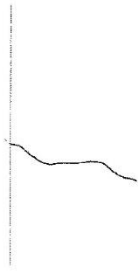
Element: *ULNA.*

Origin/Insertion: *Insert.*

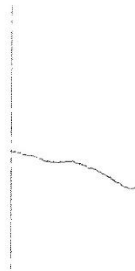
Y axis interval:

X axis interval:

Y AXIS



MED Y AXIS



LAT Y AXIS



X AXIS



PROX X AXIS



DIST X AXIS



Catalogue No.: OH 48
Species: *Homo habilis*
Siding:
Enthesis: *Deloid*

Institution: NMT

Element: *Clavicle*

Origin/Insertion: *O*

PD (y axis) length:

Y axis interval:

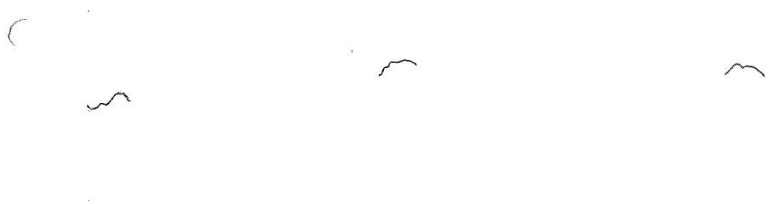
ML (x axis) length

X axis interval:

Y AXIS

MED Y AXIS

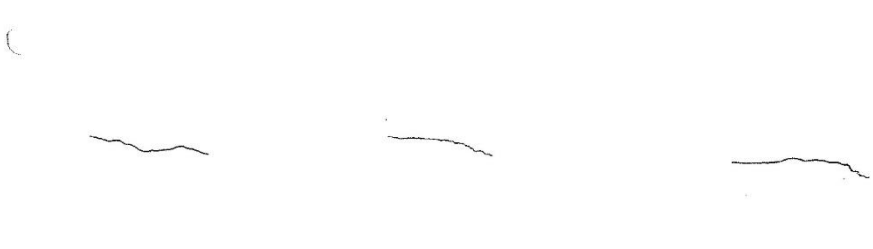
LAT Y AXIS



X AXIS

PROX X AXIS

DIST X AXIS



Catalogue No.: Omo 119 .

Institution: NME -

Species: *Africanus* . cf .

Siding:

Element:

Enthesis: Last Dorsi .

Origin/Insertion: I

PD (y axis) length: 41.3

Y axis interval: 13.73..

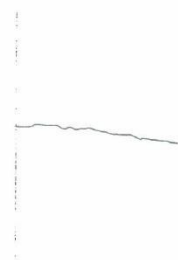
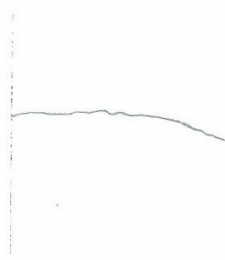
ML (x axis) length 7.9

X axis interval: 2.63

Y AXIS

MED Y AXIS

LAT Y AXIS



X AXIS

PROX X AXIS

DIST X AXIS



Catalogue No.: Ono 19.
Species: *A. cf. africanus*.
Siding: 6.
Enthesis: Pect. Maj.
PD (y axis) length: 34.3
ML (x axis) length: 10.

Institution: JME.
Element: Humerus.
Origin/Insertion: Insert.
Y axis interval: 11.43.
X axis interval: 3.33.

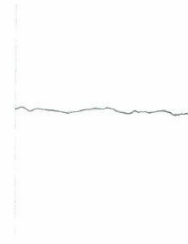
Y AXIS



MED Y AXIS



LAT Y AXIS



X AXIS



PROX X AXIS



DIST X AXIS



Catalogue No.: OMO 119-
Species: An. cf. african.
Siding: left -
Enthesis: Supraspinatus
PD (y axis) length: 17.5
ML (x axis) length: 11.8

Institution: JME.
Element: Humerus,
Origin/Insertion: Inset
Y axis interval: 5.83
X axis interval: 3.93

Y AXIS

MED Y AXIS

LAT Y AXIS

X AXIS

PROX X AXIS

DIST X AXIS

Catalogue No.: OMO 119-1973-2718.

Institution: JME.

Species: *Au. cf. africanus*.

Siding: Left.

Element: Humerus.

Enthesis: Subscapularis.

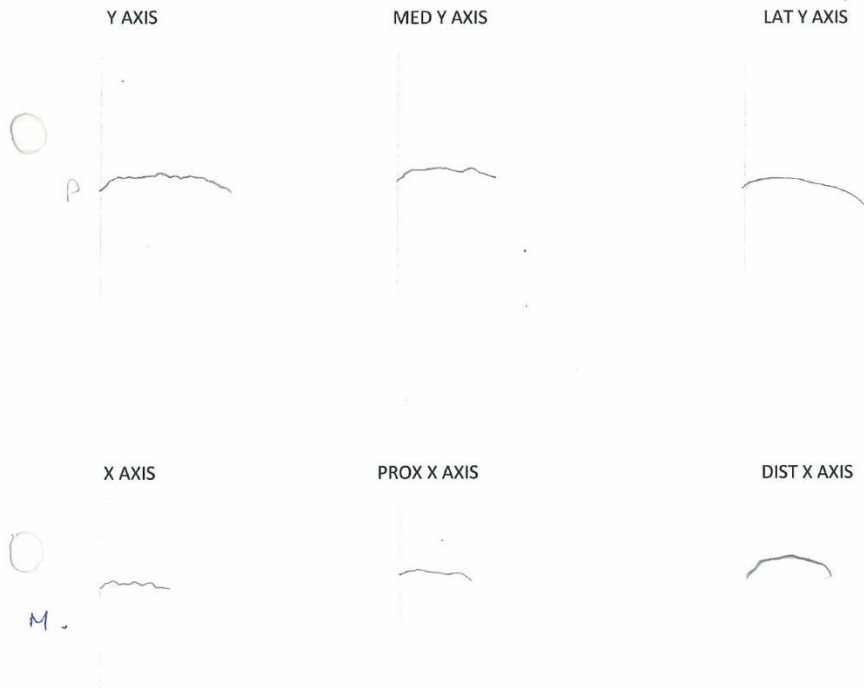
Origin/Insertion: Insert.

PD (y axis) length: 27.6 mm.

Y axis interval: 9.2 mm.

ML (x axis) length: 13.9 mm.

X axis interval: 4.6 mm.



Catalogue No.: OMO 119-1973-2718 Institution: JME.

Species: *Aef africanus*

Siding:

Element:

Enthesis: *Teres major*

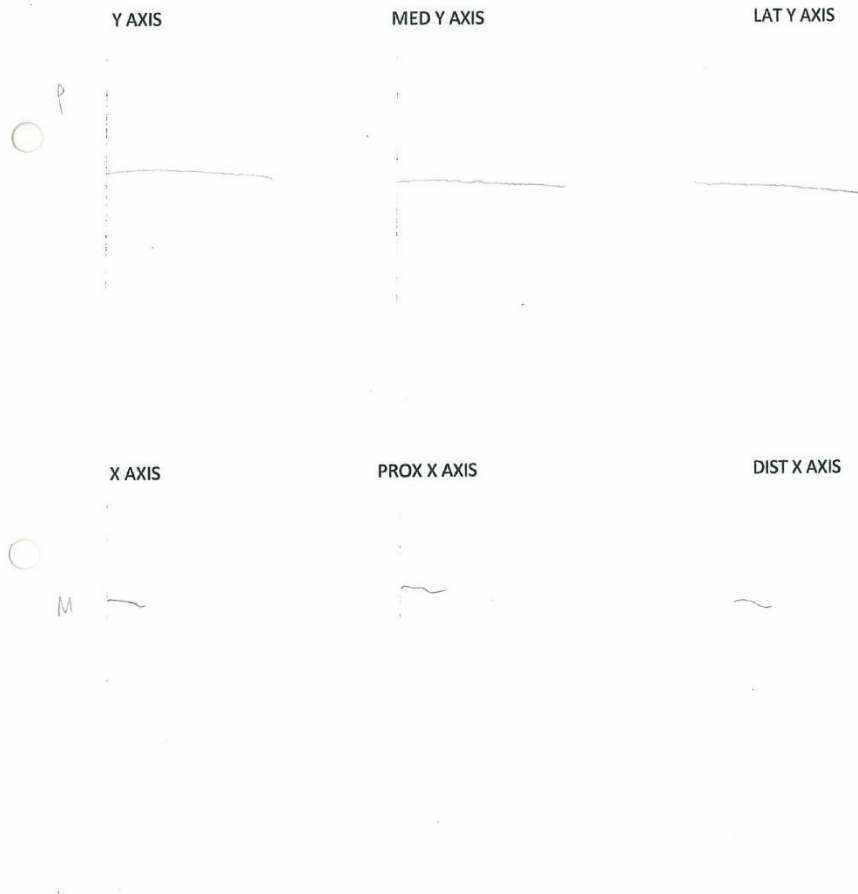
Origin/Insertion: INSECT.

PD (y axis) length: 31.3 mm.

Y axis interval: 10.4 mm.

ML (x axis) length: 4.5 mm.

X axis interval: 1.5 mm.



Catalogue No.: OMO 119-1973-2718

Institution: JME.

Species: *A. cf. africanus*

Siding:

Element:

Enthesis: *Triceps brachii* (lat.)

Origin/Insertion: ORIGIN.

PD (y axis) length: 64.4.

Y axis interval: 21.46 mm

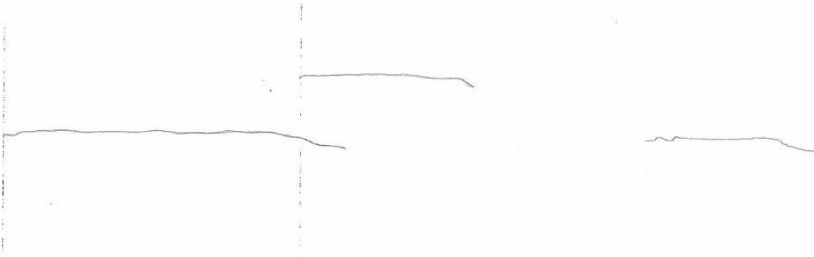
ML (x axis) length 10.9

X axis interval: 3.63.

Y AXIS

MED Y AXIS

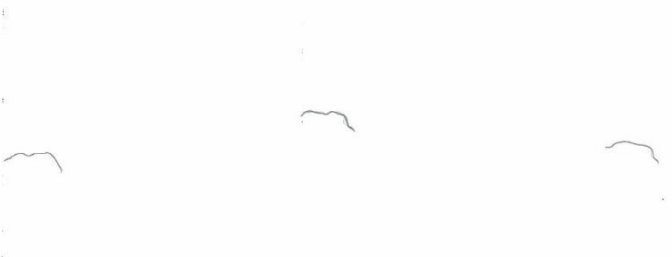
LAT Y AXIS



X AXIS

PROX X AXIS

DIST X AXIS



Catalogue No.: OMO 141-1972-23

Institution: JME

Species:

Siding: L.

Element: ULNA.

Enthesis: Brachialis

Origin/Insertion: I

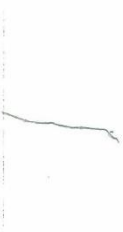
PD (y axis) length: 23.1.

Y axis interval: 7.7.

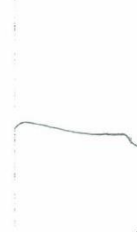
ML (x axis) length: 12.3

X axis interval: 4.1.

Y AXIS



MED Y AXIS



LAT Y AXIS



X AXIS



PROX X AXIS



DIST X AXIS



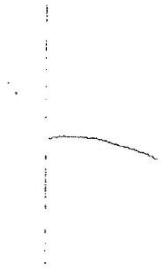
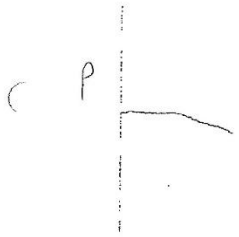
Catalogue No.: Slc 18b
Species: *H. ergasdesfora*
Siding: L?
Enthesis: *Breclialis*
PD (y axis) length:
ML (x axis) length:

Institution: Didsay
Element: *Radiis*
Origin/Insertion: *f.*
Y axis interval:
X axis interval:

Y AXIS

MED Y AXIS

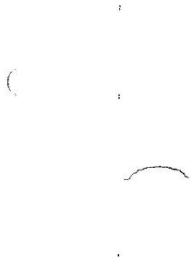
LAT Y AXIS



X AXIS

PROX X AXIS

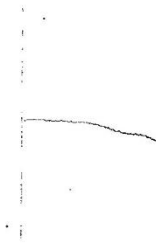
DIST X AXIS



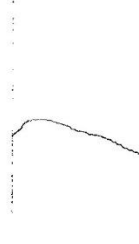
Catalogue No.: SK 2045
Species: ?
Siding: R.
Enthesis: Biceps.
PD (y axis) length:
ML (x axis) length

Institution: Didsbury.
Element: Radius.
Origin/Insertion: f.
Y axis interval:
X axis interval:

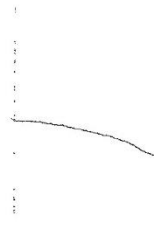
Y AXIS



MED Y AXIS



LAT Y AXIS



X AXIS



PROX X AXIS



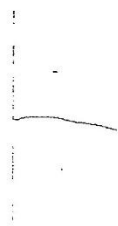
DIST X AXIS



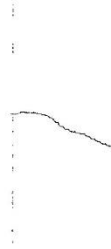
Catalogue No.: SK 94601
Species: *P. robustus*
Siding: L.
Enthesis: Biceps brachii
PD (y axis) length:
ML (x axis) length

Institution: Ditsong
Element: Radial
Origin/Insertion: P.
Y axis interval:
X axis interval:

Y AXIS



MED Y AXIS



LAT Y AXIS



X AXIS



PROX X AXIS



DIST X AXIS



Catalogue No.: SKX 8761.

Species: ?

Siding: L.

Enthesis: *Triceps brachii*

PD (y axis) length:

ML (x axis) length

Institution: *Ditson*

Element: *Una*

Origin/Insertion: *p.*

Y axis interval:

X axis interval:

Y AXIS

MED Y AXIS

LAT Y AXIS



X AXIS

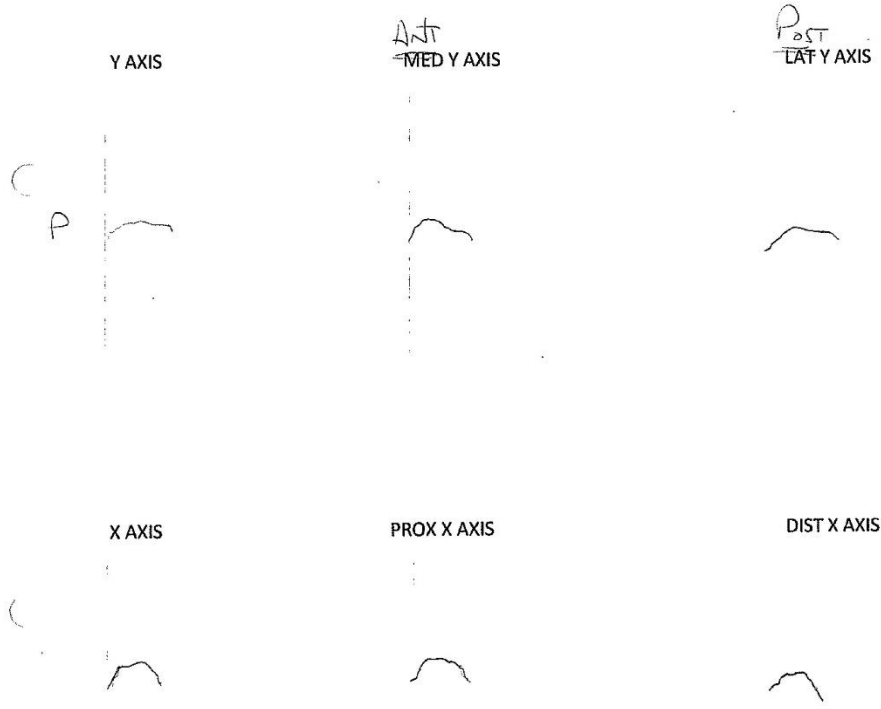
PROX X AXIS

DIST X AXIS



Catalogue No.: Skx 24600
Species: *P. robustus*
Siding: L.
Enthesis: Medial epicondyle
PD (y axis) length:
ML (x axis) length

Institution: Ditsay
Element: Humerus
Origin/Insertion: O
Y axis interval:
X axis interval:



Catalogue No.: SLX 37805 -

Institution: Ditsay -

Species: ?

Siding: R.

Element: humerus -

Enthesis: Med. epi. crest*

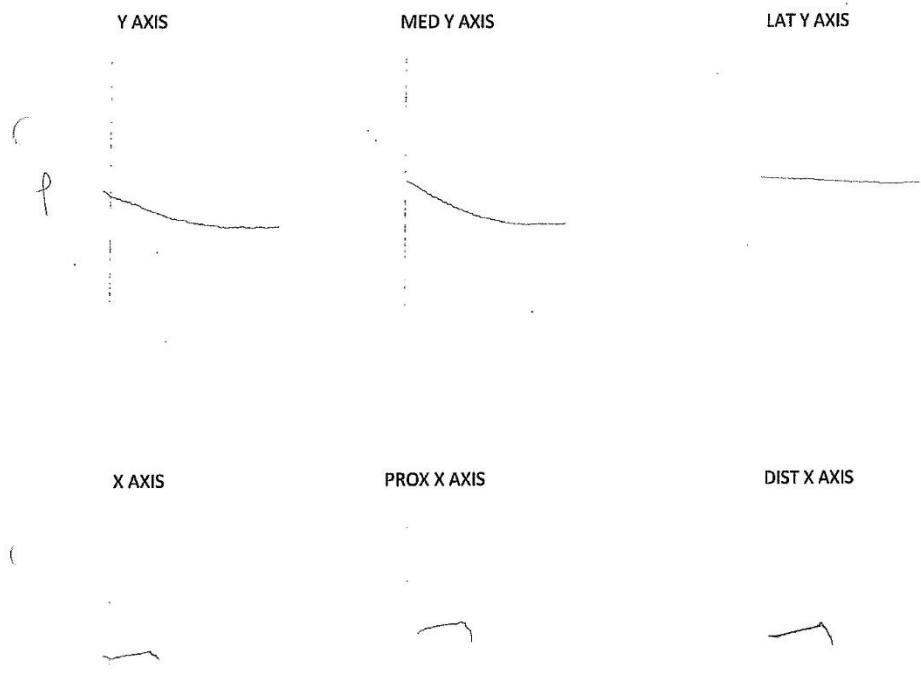
Origin/Insertion:

PD (y axis) length:

Y axis interval:

ML (x axis) length

X axis interval:

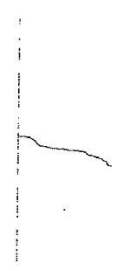


*Bardialis origin

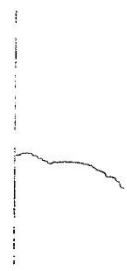
Catalogue No.: 87
Species: *A. africanus*
Siding: R
Enthesis: *Subscapularis*
PD (y axis) length:
ML (x axis) length

Institution: Ditsong -
Element: humerus -
Origin/insertion: S.
Y axis interval:
X axis interval:

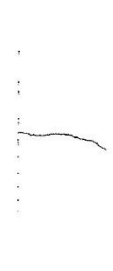
Y AXIS



MED Y AXIS



LAT Y AXIS



X AXIS



PROX X AXIS

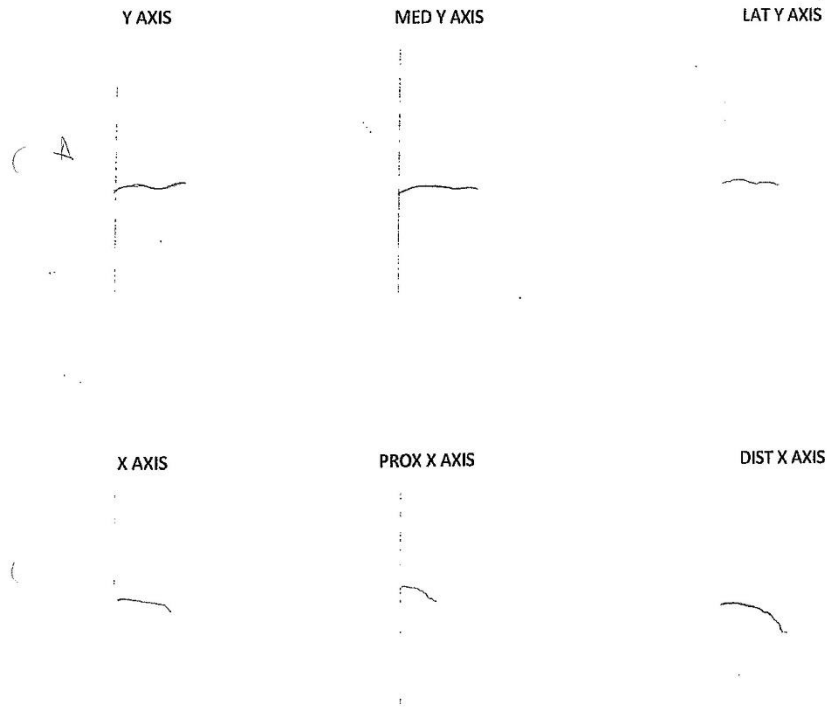


DIST X AXIS



Catalogue No.: Sets 7
Species: *A. africanus*
Siding: R.
Enthesis: Synspondylar
PD (y axis) length:
ML (x axis) length

Institution: Ditsong
Element: humerus
Origin/insertion: P.
Y axis interval:
X axis interval:



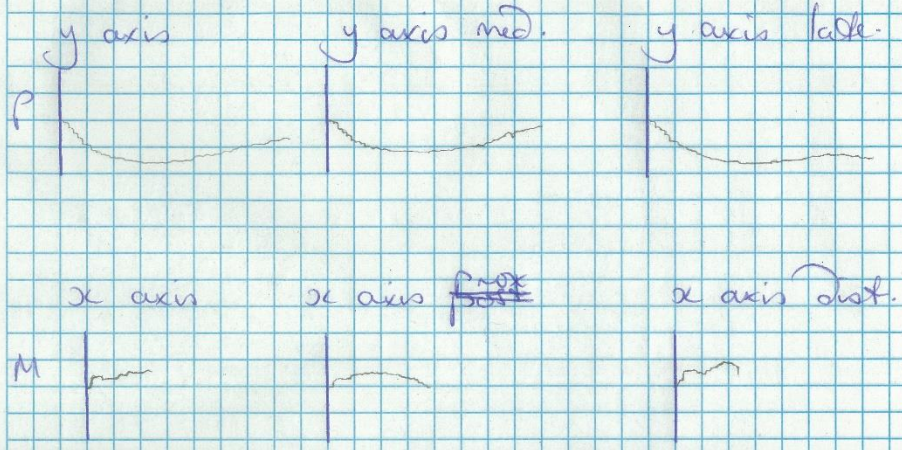
Set 113. left prox ulna

A. africanus.

Attachment for the brachialis.

y axis length: 33.34 mm

x axis length: 18.45 mm



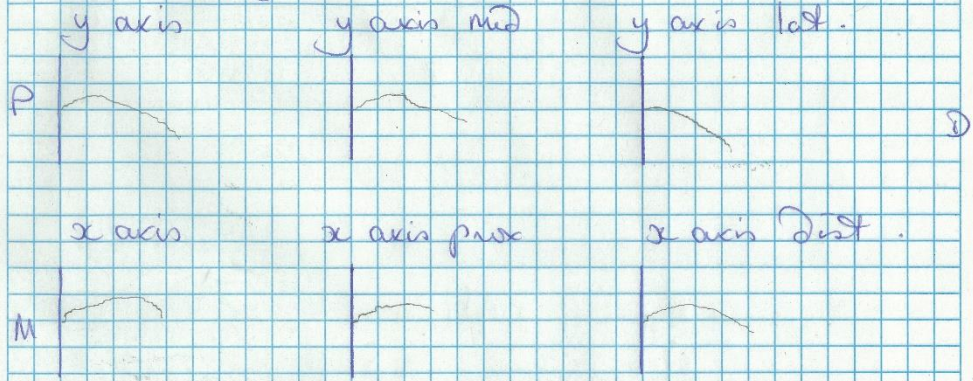
Set 11.3 - left prox uba.

A. africanus.

Insertion for *biceps brachii*

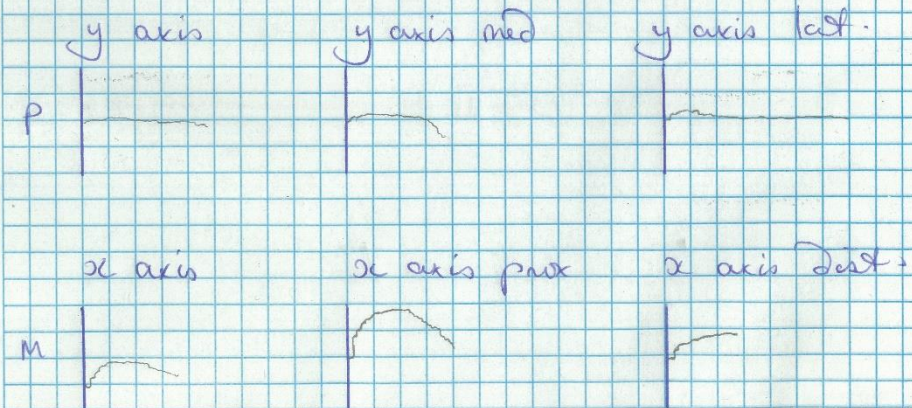
Superior Surface.

y axis length: 23.34 mm
x axis length:



Posterior Surface.

y axis length: 23.56 mm.
x axis length: 16.22 mm.



Stw 150 left Distal humerus (A. africanus)

lateral supracondylar ridge attachment for
 extensor carpi radialis (longus, brachioradialis,
 extensor carpi radialis brevis.)

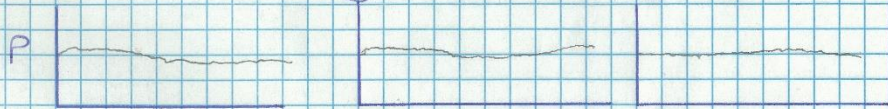
Proximodistal axis (y) length: 46.66 mm.

Mediolateral axis (x) length: 5.77 mm.

y axis .

y axis ~~med~~.

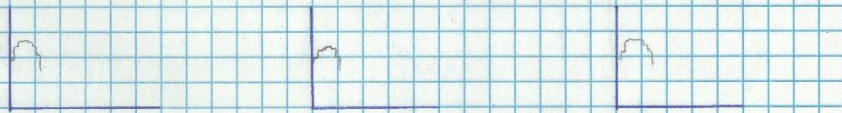
y axis Dist



x axis .

x axis prox

x axis Dist.



Dist b/d x axes: 11.66 mm.

Dist b/d y axes: 14.4 mm.

INCOMPLETE ENTHESES.

Pa no: 384. + 382.
 (and RAS)

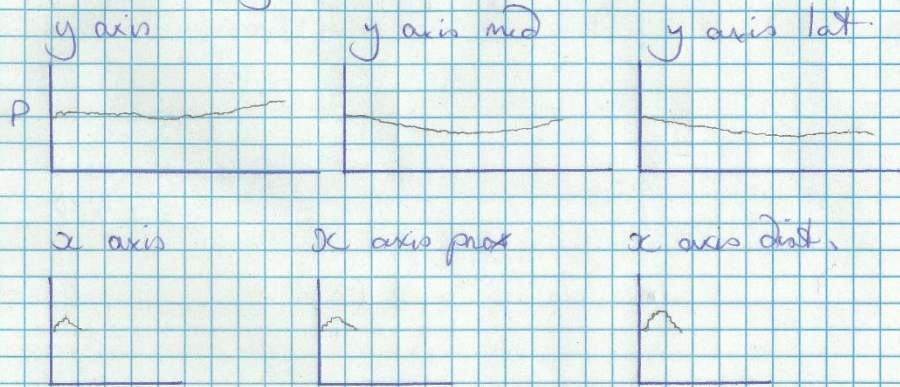
Stw 150 left distal humerus.

Medial supracondylar ridge (attachment for flexor of the wrist flexor).

INCOMPLETE ENTHESES

FR Nos: 382 + ~~384~~ 385
 (ant-LHS) (top edge) (top edge - distal is left)

y axis length: 39.39 mm
 x axis length: 4.99 mm



Dist b/t y axes: ~~9.84~~ mm

Dist between x axes: 9.84 mm

Where the entheses can't be defined clearly, the approximate limits of the same entheses in MHS were drawn.

Stw 328 Right Distal humerus.

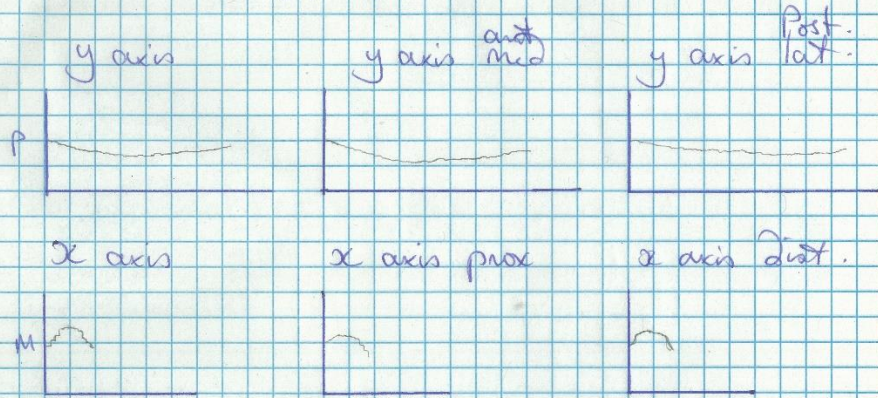
Medial supracondylar ridge.

y axis length: 38.98 mm

x axis length: 7.90 mm

INCOMPLETE ENTHESES.

FR No. 401, 403, 407



Dist b/t y axes: 1.975 mm

Dist b/t x axis: 9.74 mm

$\alpha = 19.49$ mm of y'

Stw 339 right prox. humerus.

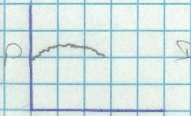
A. africanus.

~~Stw~~ Insetin for *Supra-spinatus*.

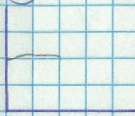
Proximal (y) axis length: 13.21 mm.

Medial (x) axis length: 15.17 mm.

y axis



y axis med.



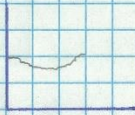
y axis lateral.



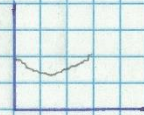
x axis



x axis prox



x axis Dist.



Dist. b/w y axes: 3.79 mm.

Dist. b/w x axes: 3.30 mm.

Spec 380. Right prox ulna *A. africanus*.

Triceps brachii insertion — Posterior Surface.

y axis length: 33.47 mm.

x axis length: 13.77 mm.

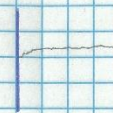
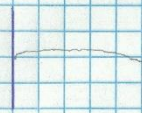
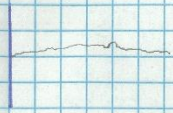
Superior Surface
too damaged.

y axis

y axis med

y axis lateral.

P

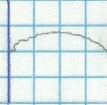


x axis

x axis prox

x axis dist

M



Brachialis insertion ~~on the~~

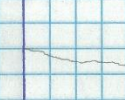
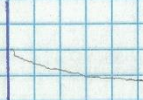
y axis length: ~~21.52~~ ^{25.60} mm.

x axis length: 9.83 mm.

y axis

y axis med

y axis lat.



x axis

x axis prox

x axis dist



Sdw 398 left prox uba. A oficams.

Brachialis insectis.

INCOMPLETE ENTHESES. Buphen. Dicyphysis of midpoint of suberoticas uba.

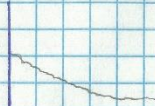
y axis length: 2803 mm.

x axis length: 7.33 mm.

y axis



y axis mid



y axis distal.



x axis



x axis prox



x axis distal.

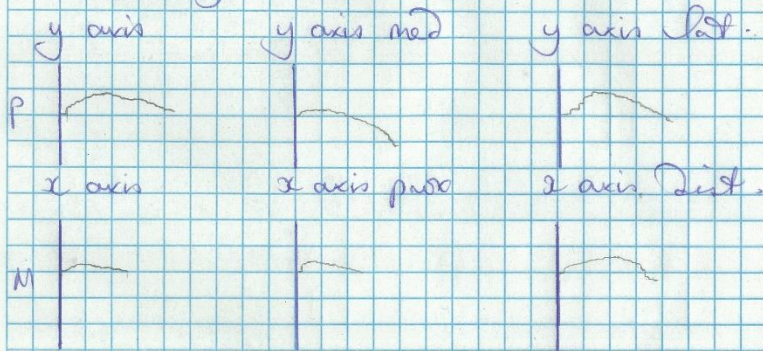


Stn 398 left prox uba *A. africanus*.

Triceps brachii insertion.

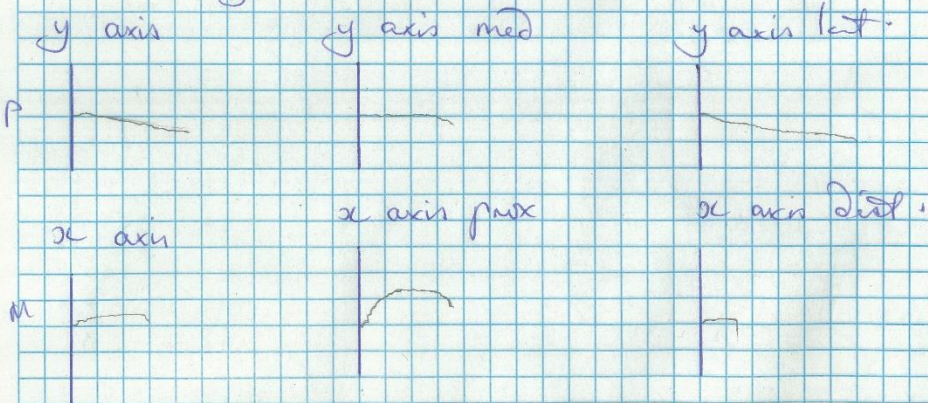
Superior Surface — Damage to M + L sides of process resulting x axis being taken completely.
∴ x axis only positive.

y axis length: 21.62 mm
x axis length: 10.83 mm



Posterior Surface.

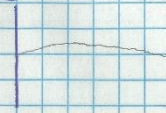
y axis length: 20.04 mm.
x axis length: 13.20 mm.



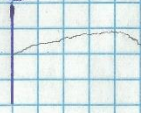
Setw 431 Radire (Pux, Right?)

Biceps brachii insertion
y axis length: 24.4 mm
x axis length: 9.93 mm

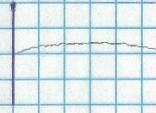
y axis



y axis med



y axis lat.



x axis



x axis prox.



x axis dist.



Stw 432a Pux uban.

Triceps brachii inserta.

y axis length: 26.67 mm.

x axis length: 44.84 mm.

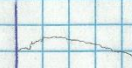
y axis



x axis



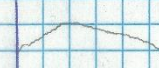
y axis med



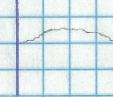
x axis pux



y axis lat.



x axis dist.

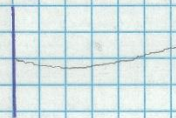


Braehialis ~~ins~~ inserta. (as PT) - Damaged.

y axis length: 31.39 mm.

x axis length: 9.91 mm.

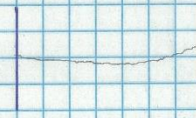
y axis



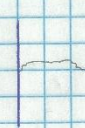
x axis



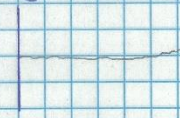
y axis med



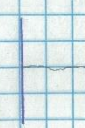
x axis pux



y axis lat.



x axis dist.

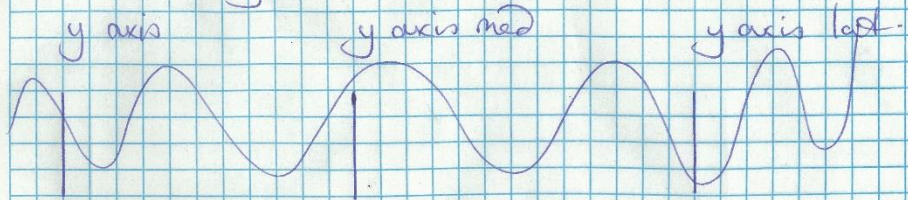


Stw 433.

lateral supracondylar ridge.

y axis length: 67.19 mm.

x axis length:



x axis

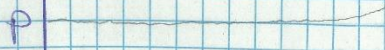
x axis prox.

x axis Dist.



y axis

y axis medial.



y axis lateral.



Stw 433 Right humerus (distal)

Medial condyle origin of wrist flexors.

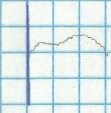
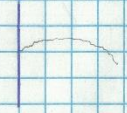
y axis length: 15.66 mm.

x axis length: 10.03 mm.

y axis

y axis med/post

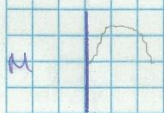
y axis lat/ant.



x axis

x axis prox

x axis Dist.



Lateral condyle.

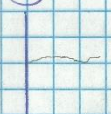
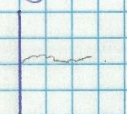
y axis length: 18.86 mm.

x axis length: 15.68 mm.

y axis

y axis med/post

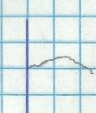
y axis lat/ant.



x axis

x axis prox

x axis Dist.



Stw 434 Scapula fragment Acilay-Bodur

Origin dens major.

y axis length: ~~9.97~~ mm. 8.38 mm.

x axis length: 10.54 mm.

y axis



y axis mid



y axis lateral.



x axis



x axis prox



x axis dist.



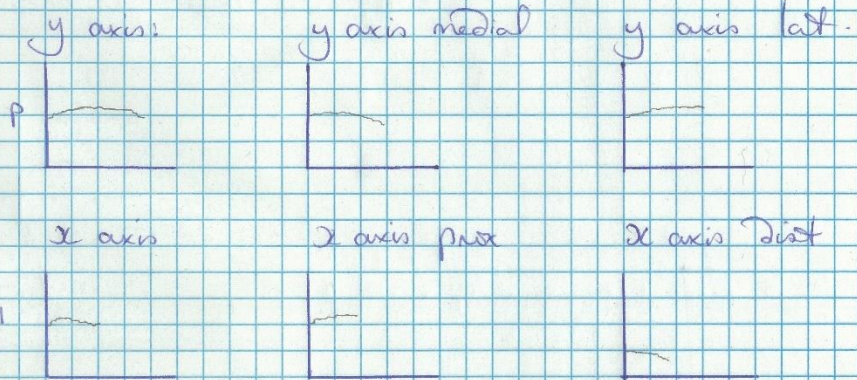
Setw 517. - left humeral head.

Subscapularis insertion on lesser tuberosity.

INCOMPLETE - Missing Superior-most Section.

y axis length: 17.23 mm.

x axis length: 8.06 mm



y axis ph. nr 452.

Sew 528

Radial Diaphysis (left)

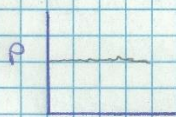
Insertion for the short head Biceps Brachii at radial tuberosity

Note: Proximal $\frac{1}{4}$ of Rt missing; lengths will only pertain to existing surfaces + proximal x axis will not be drawn.

Proximodistal (y) axis length: 19.78 mm. ~~Distal~~

Mediolateral (x) axis length: 12.76 mm.

y axis



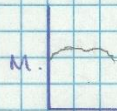
y axis medial



y axis lateral



x axis



x axis distal



Distal dist y axis: 3.19 mm

Distal dist x axis: 6.593 mm

Estimated of total endhesis length (y axis): 26.373 mm

Mediolateral axis drawn at approx midpoint of endhesis based on est. y axis.

Let us assume that 19.78 mm represents $\frac{3}{4}$ of total complete endhesis length in y axis.

$$19.78 / 3 = 6.593 \text{ mm.}$$

$$19.78 + 6.593 \text{ mm}$$

$$= 26.373 \text{ mm est total y axis.}$$

Midpoint (actual) for x axis .:

$$19.78 - 6.593$$

$$= 13.187 \text{ mm of y axis.}$$

Sdw 571. Right prox ulna A. africanus.
Brachialis insertion.

INCOMPLETE ENTHESES: distal most end missing in
Similar pattern to Sdw 378.
Inner surface of depression also

y axis length: 27.12mm

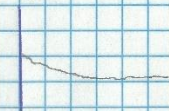
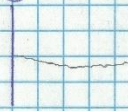
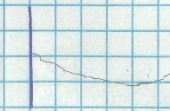
x axis length: 4.89mm

y axis

y axis med

y axis dist.

P

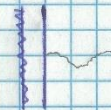
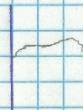
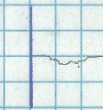


x axis

x axis prox

x axis dist.

M



Catalogue No.: TM 1517

Species: *P. robustus*

Siding: R.

Enthesis: Lateral epicondyle

PD (y axis) length:

ML (x axis) length

Institution: D. Tsing

Element: humerus

Origin/insertion: O

Y axis interval:

X axis interval:

Y AXIS

~~ANT~~
MED Y AXIS

~~POST~~
LAT Y AXIS



X AXIS

PROX X AXIS

DIST X AXIS



Catalogue No.: TM 157e.

Species: *P. robustus*

Siding: L

Enthesis: *Triceps brachii*

PD (y axis) length:

ML (x axis) length

Institution: Didsbury

Element: Ulna

Origin/Insertion: P.

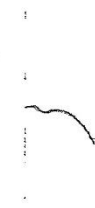
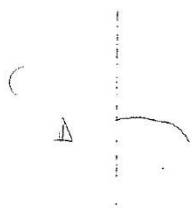
Y axis interval:

X axis interval:

Y AXIS

MED Y AXIS

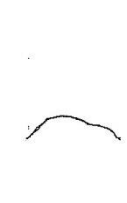
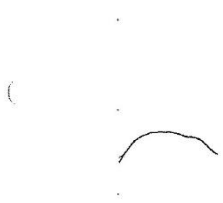
LAT Y AXIS




X AXIS

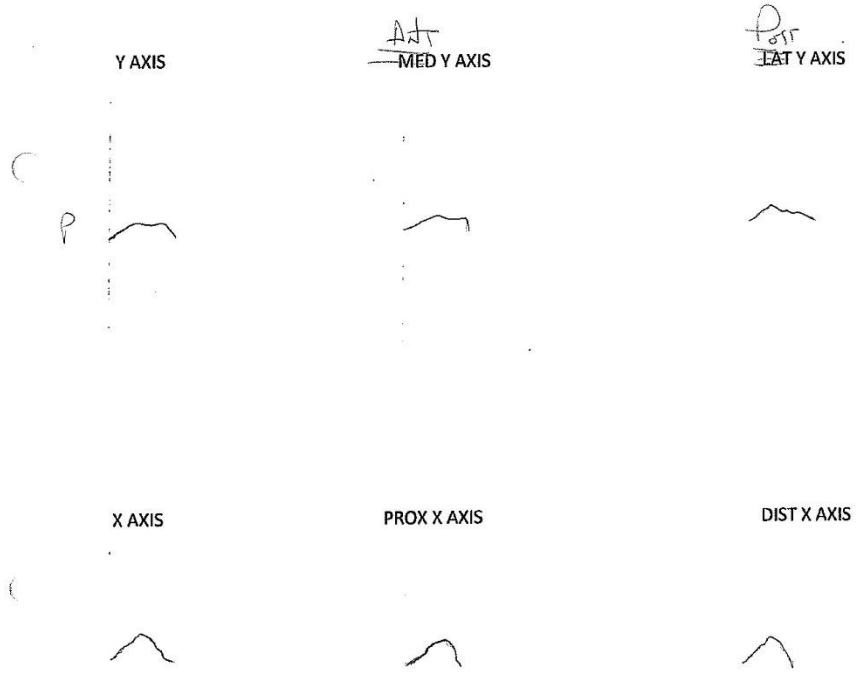
PROX X AXIS

DIST X AXIS



Catalogue No.: TM 1517 f.
Species: *P. robustus*
Siding: R.
Enthesis: Medial epicondyle
PD (y axis) length:
ML (x axis) length:

Institution: D. Hay
Element: humerus
Origin/Insertion: 
Y axis interval:
X axis interval:



Catalogue No.: UW 88-38/MH2


Institution: Wits

Species: *Au Scabi*

Siding: *R.*

Element: *clavich*

Enthesis: *Deltoid Scar*

Origin/Insertion: 

PD (y axis) length:

Y axis interval:

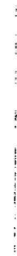
ML (x axis) length

X axis interval:

Y AXIS

MED Y AXIS

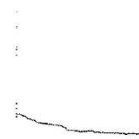
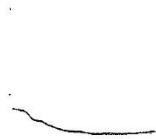
LAT Y AXIS



X AXIS

PROX X AXIS

DIST X AXIS



Catalogue No.: UN 88-57 / MH2
Species: *An. Seiden*
Siding: 2.
Enthesis: *Infundibularis*
PD (y axis) length:
ML (x axis) length

Institution: *Witz*
Element: *Humerus*
Origin/Insertion: *l.*
Y axis interval:
X axis interval:

Y AXIS

MED Y AXIS

LAT Y AXIS

X AXIS

PROX X AXIS

DIST X AXIS

DN 88-57/MH2 Witz.

basal epicyclar crest

y-axis

Ant-y

Post-y



(

x-axis

Prox-x

Distal-x



(

UW 88-57/MHZ With
hostal episcopy O.

Y-axis Ant-Y Pot-Y

— — —

X-axis Pax-x Dist-x .

— — —

Pect major
Sanjago . * *Pteris major* insert
Same as *lat Darsi* .

Catalogue No.: UN 88-57/MH2 .

Institution: Witz .

Species: *An. Deidre*

Siding: 2

Element: *humans* .

Enthesis: ~~*Pect major lat Darsi*~~

Origin/Insertion: *l.*

PD (y axis) length:

Y axis interval:

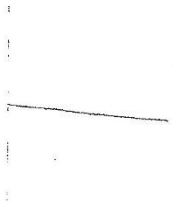
ML (x axis) length

X axis interval:

Y AXIS

MED Y AXIS

LAT Y AXIS



X AXIS

PROX X AXIS

DIST X AXIS



VW 88-57/MH2. Witz.
Andia^f episcopa O.

Y-axis

Ant Y

Post Y.



X-axis

Post-X

Dist-X



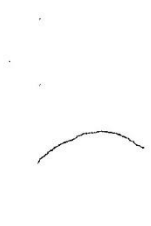
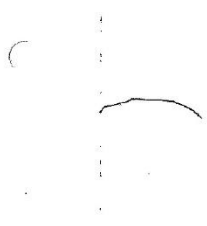
Catalogue No.: *UN88-57/M42*
Species: *An. sediba*
Siding: *R.*
Enthesis: *Subcap.*
PD (y axis) length:
ML (x axis) length

Institution: *Wits.*
Element: *Humerus.*
Origin/Insertion: *L.*
Y axis interval:
X axis interval:

Y AXIS

MED Y AXIS

LAT Y AXIS



X AXIS

PROX X AXIS

DIST X AXIS



Catalogue No.: UW88-57/MH2
Species: *At. fediba*
Siding: R.
Enthesis: *Supraspinatus*
PD (y axis) length:
ML (x axis) length

Institution: Witz

Medial epicondyle
cross bridge

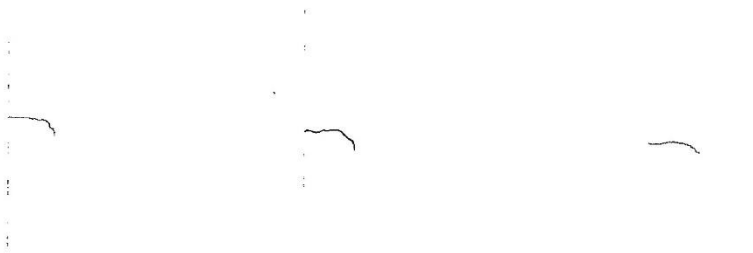
Element: *humerus*
Origin/Insertion: *l*

Y axis interval:
X axis interval:

Y AXIS

MED Y AXIS

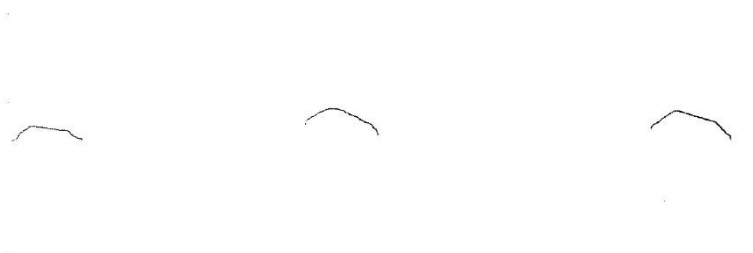
LAT Y AXIS



X AXIS

PROX X AXIS

DIST X AXIS



UW 88-62/MH12 Witz.

R. ulna.

Brachialis insert.

y-axis

Med-y

Lat-y



x-axis

Prox-x

Distal-x



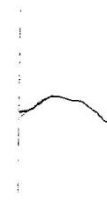
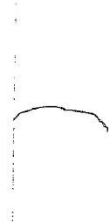
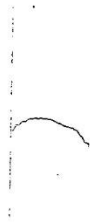
Catalogue No.: JN 88-62/M412
Species: An. quadricornis
Siding: R.
Enthesis: Triceps brachii
PD (y axis) length:
ML (x axis) length

Institution: Widy.
Element: An.
Origin/Insertion: P.
Y axis interval:
X axis interval:

Y AXIS

MED Y AXIS

LAT Y AXIS



X AXIS

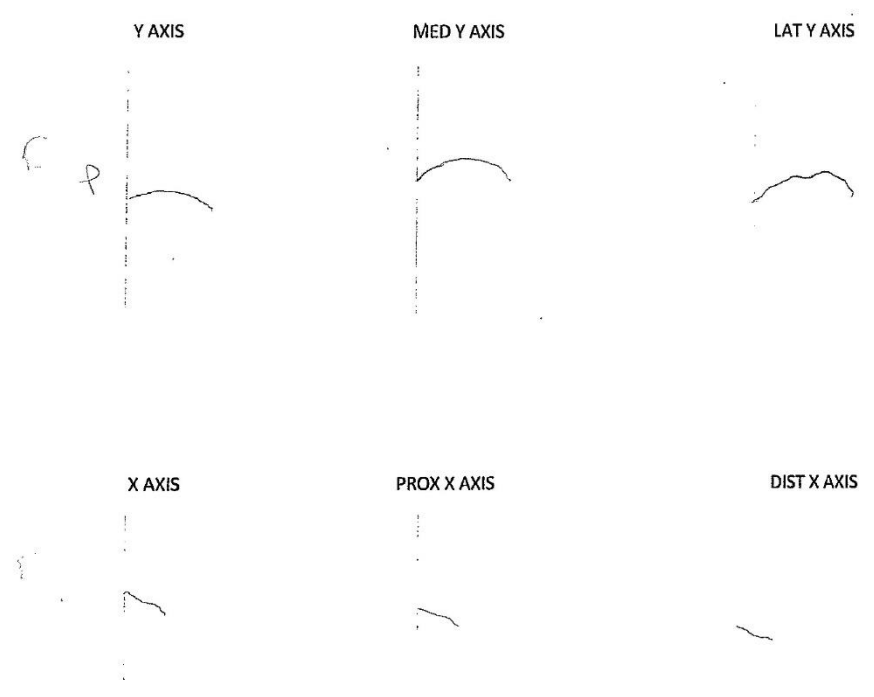
Ant
-PROX X AXIS

Post
-DIST X AXIS



Catalogue No.: UW ~~88~~ 101 / M42
Species: *Stu. badibu*
Siding: *k*
Enthesis: *Subscap.*
PD (y axis) length:
ML (x axis) length

Institution: *Wig.*
Element: *humeral head*
Origin/Insertion: *p.*
Y axis interval:
X axis interval:



UW88-101/M42. Witz.
h. humeral head
Supraspinatus Insert.

y-axis	Med-y	Lat-y
—	—	—
x-axis	Prox-x	Dist-x
—	—	—

UW88-101/M42.
h. humeral head.
Infraspinatus Insert.

y-axis	Med-y	Lat-y
—	—	—
x-axis	Prox-x	Dist-x
—	—	—